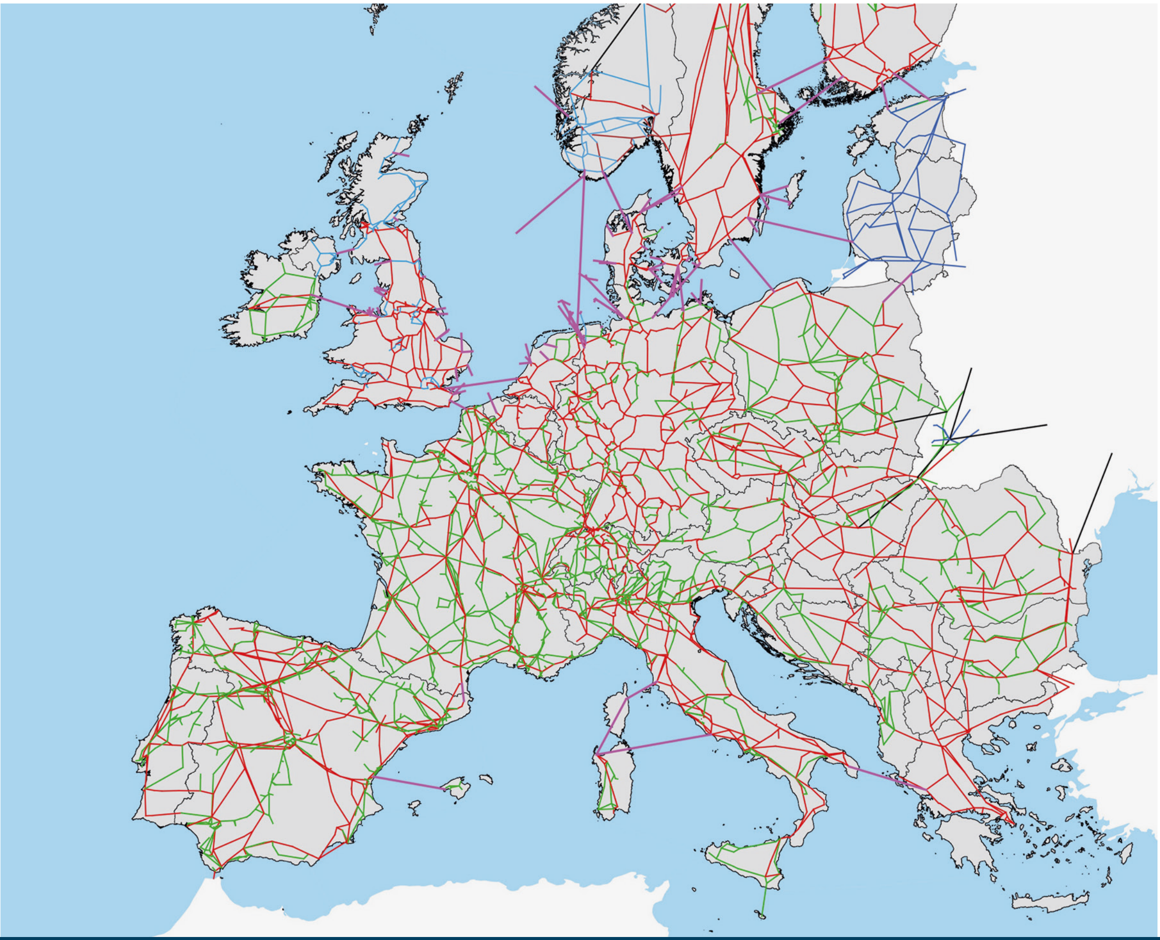

Integration of Renewable Energy Sources into the Future European Power System Using a Verified Dispatch Model with High Spatiotemporal Resolution

Chloi Syranidou

Energie & Umwelt / Energy & Environment
Band / Volume 507
ISBN 978-3-95806-494-2

Mitglied der Helmholtz-Gemeinschaft

JÜLICH
Forschungszentrum

Schriften des Forschungszentrums Jülich
Reihe Energie & Umwelt / Energy & Environment Band / Volume 507

Forschungszentrum Jülich GmbH
Institut für Energie- und Klimaforschung
Techno-ökonomische Systemanalyse (IEK-3)

Integration of Renewable Energy Sources into the Future European Power System Using a Verified Dispatch Model with High Spatiotemporal Resolution

Chloi Syranidou

Schriften des Forschungszentrums Jülich
Reihe Energie & Umwelt / Energy & Environment Band / Volume 507

ISSN 1866-1793 ISBN 978-3-95806-494-2

Bibliografische Information der Deutschen Nationalbibliothek.
Die Deutsche Nationalbibliothek verzeichnet diese Publikation in der Deutschen Nationalbibliografie; detaillierte Bibliografische Daten sind im Internet über http://dnb.d-nb.de abrufbar.

Herausgeber und Vertrieb:	Forschungszentrum Jülich GmbH Zentralbibliothek, Verlag 52425 Jülich Tel.: +49 2461 61-5368 Fax: +49 2461 61-6103 zb-publikation@fz-juelich.de www.fz-juelich.de/zb
Umschlaggestaltung:	Grafische Medien, Forschungszentrum Jülich GmbH
Druck:	Grafische Medien, Forschungszentrum Jülich GmbH
Copyright:	Forschungszentrum Jülich 2020

Schriften des Forschungszentrums Jülich
Reihe Energie & Umwelt / Energy & Environment, Band / Volume 507

D 82 (Diss. RWTH Aachen University, 2019)

ISSN 1866-1793
ISBN 978-3-95806-494-2

Vollständig frei verfügbar über das Publikationsportal des Forschungszentrums Jülich (JuSER) unter www.fz-juelich.de/zb/openaccess.

This is an Open Access publication distributed under the terms of the Creative Commons Attribution License 4.0, which permits unrestricted use, distribution, and reproduction in any medium, provided the original work is properly cited.

Integration Erneuerbarer Energiequellen In Das Zukünftige Europäische Stromnetz Unter Verwendung Eines Verifizierten Übertragungsnetz-Modells Mit Hoher Räumzeitlicher Auflösung

von Chloi Syranidou

Kurzfassung

Die Anforderungen zur Reduzierung der Treibhausgasemissionen des Stromsektors in Europa werden zu einem deutlichen Anstieg der Erzeugung aus variablen erneuerbaren Energiequellen (VRES) führen. Das Vorhandensein solcher Technologien kann erhebliche Herausforderungen für den Betrieb und die Struktur des bestehenden Übertragungsnetzes darstellen. Unter diesem Aspekt wird in dieser Arbeit die Integration von VRES in das zukünftige europäische Stromsystem bis zum Jahr 2050 untersucht.

Die oben beschriebenen Herausforderungen führen auch zu Herausforderungen bei der Modellierung des Stromversorgungssystems. Daher werden sowohl die numerische Modellierung als auch der bestehende europäische Rahmen des Netzbetriebs ausführlich beschrieben, einschließlich der entsprechenden Literatur. In dieser Arbeit wird eine neuartige mehrstufige Methodik für die Erzeugungsdisposition vorgestellt, die die Übertragungsbeschränkungen respektiert und einen flexiblen Nachfragebetrieb beinhaltet, um das gesamte europäische Stromsystem zu modellieren. Die Endentwicklung des Modells wird durch die Bestimmung der Randbedingungen und technischen Parameter des Systems in Bezug auf Netzinfrastruktur, Erzeugung und Nachfrage in hoher räumlich-zeitlicher Auflösung abgeschlossen. Das daraus resultierende Modell wird für das Jahr 2015 unter historischen Bedingungen verifiziert und bildet die Grundlage für die Umsetzung aller europäischen Zukunftsszenarien.

Das zukünftige Stromnetz wird für die Jahre 2030, 2040 und 2050 im Hinblick auf die VRES-Integration und die entsprechenden Auswirkungen der Nachfrageflexibilität analysiert. Es stellt sich fest, dass die Hauptnetzüberlastung zwischen Nord- und Ostseeraum und Mitteleuropa auftritt. Diese Stauung ist für die Mehrheit der daraus resultierenden VRES-Abregelung verantwortlich, die mit der Windkraft zusammenhängen. Der Gesamtbetrag der Abregelung für den Referenzfall beträgt 88 TWh für Deutschland und 729 TWh für Europa, woraus der Schluss gezogen wird, dass die geeignetsten Standorte zur Nutzung der entsprechenden Abregelungsenergie in Westdänemark und Westirland liegen. Was die Auswirkungen der Nachfrageflexibilität betrifft, so ist festzustellen, dass die Gesamtauswirkungen relativ gering sind (Reduzierung der VRES-Kürzungen um 7,6%), weshalb mehr Flexibilitätsoptionen in Betracht gezogen werden sollten. Darüber hinaus wird festgestellt, dass die VRES-Integration eher auf die Dauer der Verlagerung als auf die verfügbare Flexibilität reagiert, insbesondere, wenn saisonale Flexibilität erlaubt ist. Weiterhin wird gezeigt, dass die räumliche Verlagerung ebenfalls sehr vorteilhaft sein kann (27% Reduktion). Allerdings kann die Lastverlagerung nicht die einzige Lösung für ihre Verringerung sein, sondern es können auch weitere Alternativen erforderlich sein. Betrachtet man alle Szenarien für 2050, so stellt man fest, dass die durchschnittliche Anzahl der VRES-Kürzungen 592 TWh beträgt und sich dieser Wert von 2030 bis 2050 alle 10 Jahre etwa verdoppelt. Schließlich wird gezeigt, dass die Höhe der räumlichen Auflösung für die Darstellung des Übertragungsnetzes eine wichtige Rolle bei der VRES-Integration spielt, bei der selbst Modelle mit 100-200 Knoten die Gesamtkürzungen um die Hälfte unterschätzen können.

INTEGRATION OF RENEWABLE ENERGY SOURCES INTO THE FUTURE EUROPEAN POWER SYSTEM USING A VERIFIED DISPATCH MODEL WITH HIGH SPATIOTEMPORAL RESOLUTION

by Chloi Syranidou

ABSTRACT

The requirements for reducing the greenhouse gas emissions of the power sector in Europe will result in a significant increase of generation from variable renewable energy sources (VRES). The presence of such technologies may pose significant challenges to the traditional operation and structure of the existing transmission grid. In this thesis, the integration of VRES into the future European power system is investigated until the year 2050.

The introduced challenges translate to challenges of modeling the power system as well. Hence, the numerical modeling as well as the existing European framework of power system operation is described in detail, including the corresponding literature. In this thesis, a novel multi-level methodology for the generation dispatch that respects transmission constraints and includes flexible demand operation is introduced to model the pan-European power system. The final development of the model is completed via the determination of the system's boundary conditions and technical parameters with respect to grid infrastructure, generation and demand in high spatiotemporal resolution. The resulting model is verified for the year 2015 against historical conditions and forms the basis for the implementation of all future European scenarios.

The future power system is analyzed for the years 2030, 2040 and 2050 with respect to VRES integration and the impact of demand flexibility. It is found that the main grid congestion occurs between the North and Baltic Sea regions and Central Europe. This congestion becomes responsible for the majority of the resulting VRES curtailments, which are related to wind generation. The total amount of curtailments for the reference case is 88 TWh for Germany and 729 TWh for Europe, out of which it is concluded that the most suitable locations for exploiting the corresponding curtailment energy occurs in western Denmark and western Ireland. Regarding the impact of demand flexibility, it is found that the overall impact is relatively small (7.6% reduction in VRES curtailments) and therefore more flexibility options should be considered. Moreover, it is found that VRES integration is more sensitive to the shifting duration rather than to the available flexibility especially when seasonal flexibility is allowed, while also it is shown that shifting in space can also become very beneficial (27% reduction). However load shifting cannot constitute the only solution for their mitigation but further alternatives may be required as well. Examining all scenarios for 2050, it is found that the average amount of VRES curtailments becomes 592 TWh and that this value approximately doubles every 10 years from 2030 to 2050. Finally, it is shown that the level of the spatial resolution for the transmission grid representation plays a significant role with respect to VRES integration, where even models with 100-200 nodes can underestimate the total curtailments by half.

Acknowledgements

Above all, I would like to express my gratitude to Univ.-Prof. Dr.-Ing. Detleft Stolten for trusting me with this difficult task and supervising my progress. I am also thankful for supporting me from the beginning during my transition, which was crucial for my well-being and successful completion of my dissertation. For the same reasons, I would also like to thank Dr.-Ing. Martin Robinius, whom I additionally thank for sharing his scientific knowledge and insight as well as valuable advice in all aspects of a researcher's work.

I also thank Univ.-Prof. Dr.-Ing. Armin Schnettler and Univ.-Prof. Dr.-Ing Dirk Abel for ensuring the fairness of the examination process and the interesting discussions about transmission grid modeling.

Many thanks to Dr.-Ing. Peter Markewitz and Dr.-Ing. Jochen Linssen for successively supervising my doctoral thesis. Each of you offered different and valuable perspectives to my work, which led to interesting discussions and helped me identify and resolve several issues. I appreciate the time you invested in me and sharing your knowledge and experience. I also particularly appreciate your openness, availability and honest feedback. I always felt welcome to talk about anything, which made all discussions and feedback even more valuable. In addition, I would also like to thank Dr.-Ing Sebastian Schiebahn, who also offered valuable perspectives both scientifically as well as in terms of working life.

I want to give special thanks to my colleagues who shared the same office with me in the beginning of my thesis. These include Markus Reuss, Severin Ryberg, Lara Welder and Leander Kotzur. Although each one offered their unique contribution to the dynamic, overall you all participated in creating a safe, supportive and pleasant working environment, which lasted even after moving to new offices. I believe our group was one of the most important contributors for succeeding with my thesis. The way we analyzed each other's approaches and exchanged knowledge and ideas was very beneficial to all of us. I appreciate your genuine input and for being open to different ideas. I will definitely miss our discussions but also all the fun we have had together that extended besides the working environment. Moreover, I would also like to thank my following office mates, Simonas Cerniauskas, Eleonora Talpacci and Maximillian Hoffmann. We have also had a great collaboration and valuable exchanges. I hope our small elephant will pass to the next generation of researchers. Yuan Wang, thank you for all the deep and less deep discussions we shared. We definitely fulfilled the stereotype of a Greek and a Chinese debating about philosophy and life. Dilara Caglayan, thank you too for all the funny moments and debates, especially about food. They helped a lot in regulating my stress levels. Furthermore, I would like to thank all the other coworkers and group leaders. I have had valuable and interesting exchanges with all of you and I appreciate the kindness, openness and the warm environment that we developed together. I also appreciate everyone's acceptance of me as a trans woman, thus creating a secure and safe environment that was so crucial during those vulnerable times. Besides my science-related coworkers, I cannot forget to mention the equally supporting attitude and great collaboration I have had with all the other employees and PhD candidates in the institute especially to my colleagues Anke Clemens, Anne Schroeders, Madita Kaul, Ann-Katrin Steinke, Sandra Hoffmann, Wilma Fladung and Susanne Klatt.

I would also like to express my gratitude for the collaboration with my master students Konstantinos Karamanlis, Simon Dehmel and Christoph Pfister as well as my intern Khusbhu Saxena. I hope you all gained a lot from your experience, I definitely did and I appreciate having worked with all of you.

I also like give special thanks to Dr. Tom Brown and Dr. Jonas Hörsch, who, maybe unintentionally, have also contributed a lot to this thesis. I feel very lucky for having come across your open-source modeling framework, PyPSA, in the beginning of my work. It happened to be exactly what I was looking for implementing my model. Moreover, much of my knowledge of python, including the packages used by PyPSA, was gained by studying your code. Besides that, I also thank you for the very useful exchanges whenever we met. I also thank you for the powerplantmatching package, which was also very valuable for my dissertation and thank you for providing everything as open source. In that regard, I would like to express my gratitude to the whole openmod community. I have a gained a lot from the online and in person discussions regarding modeling, data, openstreetmap, licensing and many other interesting topics relevant to energy system modeling. You have all contributed to the realization of this dissertation and I deeply appreciate it.

I would also like to thank my parents for supporting me during my studies. They were proven to be very valuable in completing my thesis. In that regard, I would like to express my appreciation for the public and free educational systems in Greece and Germany for offering education of very high quality. That also includes my professors and supervisors in both study programs. In particular, I would like to mention Prof. Labridis, Prof. Tsiboukis and Dr. Milioudis from the Aristotle University of Thessaloniki and Prof. Behr and Prof. Lehnert from the RWTH Aachen University. Moreover, I cannot omit Dr. Michael Höh, who also took the initiative to introduce me to this project and the corresponding team. Without him, I might have not even started it.

I would also like to give special thanks to my ex-partner Zoi for enduring all the stress and long-working hours that come together with conducting a PhD. I deeply appreciate all of your support and for going through all of this together. There will always be a special place in my heart for you.

I also want to deeply thank my friend Emily. I wish I could have met you earlier and also gain more from your experience of doing a PhD. Nevertheless, your contribution to my mental health is immeasurable and our friendship will always be one of the most valuable things in my life.

Finally, I want to express my biggest gratitude to Chloi. You managed to accomplish a very difficult task under adverse circumstances and I am very proud of you. I am glad I could finally meet you and looking forward for your bright future.

Table of contents

1 Introduction

1.1 Motivation

The agreement of the European states to commit in reducing the anthropogenic emissions of greenhouse gases (GHG) in order to halt the rise of the atmospheric temperature may bear profound effects on the configuration and operation of their power systems. Although each individual system has followed a unique history in terms of generation mix and power grid evolution, the majority of them rely on a combination of thermal power plants based on fossil fuels or nuclear power and hydroelectricity. Thereby, due to the significant dependency on fossil fuels, the power sector constitutes one of the highest contributors in GHG emissions in Europe, as it is shown in figure 1-1.

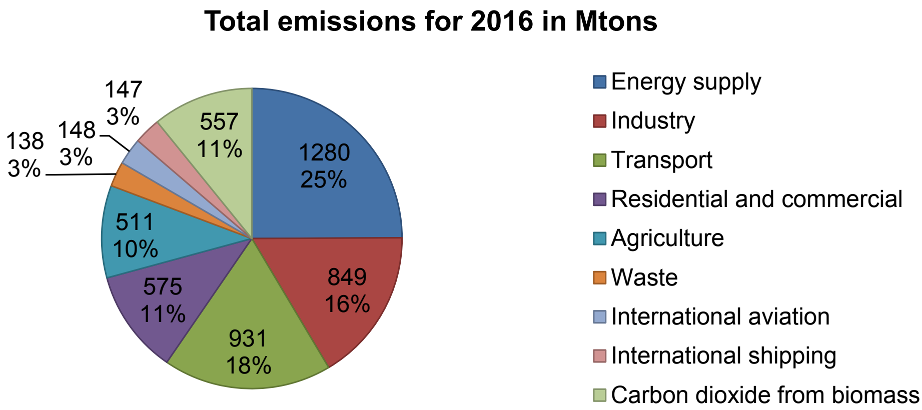

Figure 1-1 Total greenhouse gas emissions in million tons of CO_2 equivalent for 2016 in the EU-28 [1].

Decarbonizing the power supply would require the replacement of thermal generators based on burning fossil fuels with different technologies that rely on renewable energy sources (RES) such as hydroelectricity. However, due to the several limitations of developing hydro plants, like topography, further options must be considered among which wind turbines and photovoltaics (PV) constitute the primary candidates due to their high technology readiness level (TRL) and costs. Besides the replacement of fossil plants, an increase in generation capacity might also be required as well due to expected changes in the electricity demand side. Although an increase in energy efficiency might lead to considerable energy savings, the decarbonization of other energy sectors, e.g. transportation, might be realized via electrification, which could result in a net increase in electricity demand while also altering its behavior.

In contrast to the conventional thermal generation however, wind and PV technologies introduce several challenges in the traditional way of operating power systems due to the different characteristics of their primary energy source. For both of these technologies, the primary energy source cannot be stored or transferred, therefore electricity can only be generated when and where wind and solar energy is available. Hence, power supply becomes considerably less flexible in both time and space, which may result in dropping otherwise available energy because it cannot be consumed. This inflexible behavior of generation technologies depending on wind and solar sources distinguishes them from other more flexible renewable technologies, like hydro, and are therefore classified as variable RES (VRES). Avoiding such energy curtailments, which can be affected by the structure and operation of the power system, results in a higher utilization of the corresponding generation technologies and thus in a higher integration of renewable energy into the power system.

1.2 Scope of the thesis

Typically, designing a power system would aim to the maximum utilization of its assets, i.e. minimization of VRES generation curtailments would be sought. Nevertheless, eliminating such curtailments entirely does not usually constitute the most economic option due to the corresponding oversizing requirements that may lead to a reduction of the capacity specific utilization of these assets. Since such curtailments are therefore inherent to a system with high VRES shares, Power-to-X applications such as Power-to-Gas and Power-to-Heat may also become economically attractive as coupling pathways to decarbonize other energy sectors.

The goal of this thesis consists of analyzing the future European power system with regard to VRES integration, i.e. quantifying and investigating VRES curtailments. The greatest challenges for such an analysis include the high temporal and spatial dynamics that are involved in a system relying on wind and solar generation, the potential change in consumer behavior as well as the uncertainties of the future system design. Moreover, due to the wind flow patterns spanning on continental scale and the expected increase of power trading among the European countries, the examination of the whole interconnected European region is deemed mandatory.

In order to address the increased requirements for spatiotemporal dynamics in conjunction with the considerable scale of the investigated system, corresponding methodologies and assumptions need to be developed. Regarding spatial dynamics, one of the most crucial components consists of the sufficient modeling of the transmission grid. Since the geographical potential for solar and wind generation does not necessarily follow the existing demand centers and grid infrastructure, the role of the transmission grid may change significantly in this new setting and may also pose a limiting factor in RES integration. Besides the requirements for detailed modeling of the power system components, the behavior of the electricity demand may also become critical with regard to VRES integration, since new technologies and consumptions may allow more flexible consumption patterns.

In this study, a pan-European model is developed which can adequately address such challenges. Moreover, a verification of the selected approach is conducted against historical conditions. By applying this model it becomes possible to quantify the VRES curtailments and the impact of demand flexibility with high spatiotemporal resolution on pan-European scale. Such combination of high resolution and geographical extent can rarely be found in the literature for future systems. More specifically this study attempts to answer the following questions:

- Where will the future grid congestion appear?

- How much energy from VRES will be curtailed in the future and where will it be located?
- What is the impact of demand flexibility on reducing curtailments?

The thesis is divided into 8 chapters including the introduction. Chapter 2 introduces the fundamentals of power system modeling within the modern European market framework and presents the relative literature based on the corresponding review by Syranidis et al. [2]. In chapter 3 the developed methodology is described, whereas in chapter 4 the selected modeling approach and required data are verified against historical values. Chapter 5 describes the future European scenarios that are investigated. Chapter 6 presents the main results of this thesis including the analysis of the reference case as well as the impact of demand flexibility and other modeling parameters. These results are also compared to corresponding values from the literature. Finally, chapter 7 summarizes the content of the thesis and chapter 8 draws the main conclusions and outcome of the thesis. An overview of the whole structure is depicted in figure 1-2.

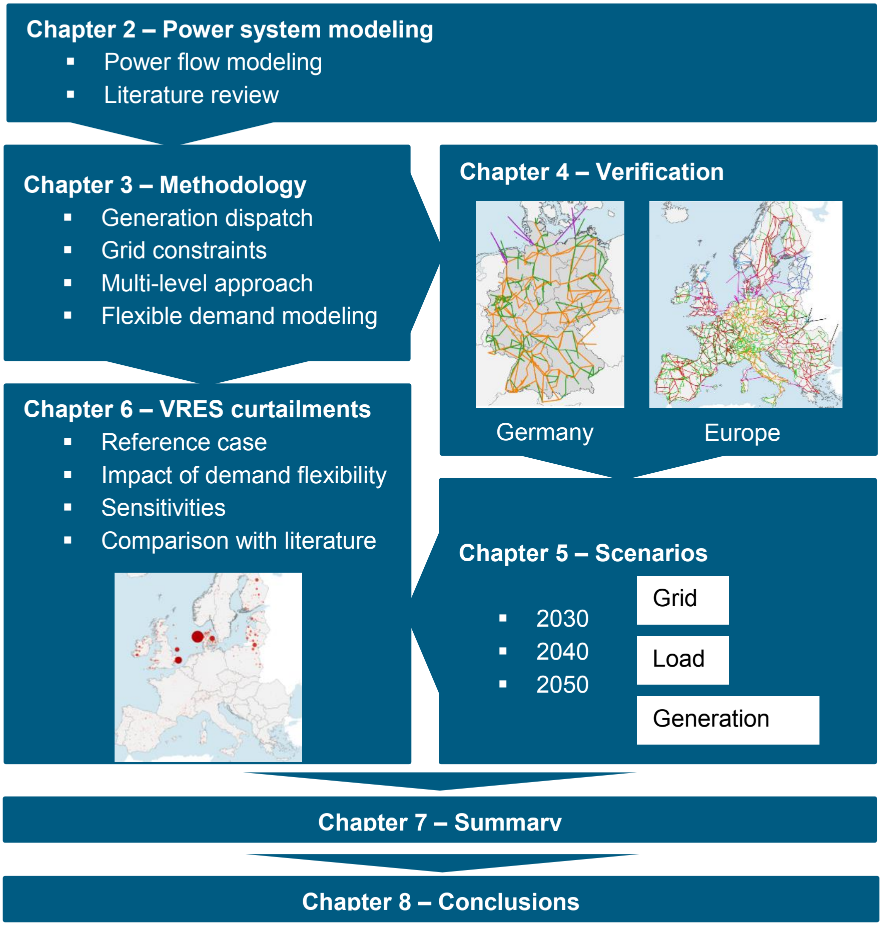

Figure 1-2 Structure overview of the thesis.

2 Power system modeling

Modeling of power systems typically involves the mathematical description of the various elements and their interactions with focus on the power and electrical variables. As the systems developed, the complexity of the corresponding models increased as well and could only be addressed with the significant advances in the computer science and optimization fields. Although the basic principles of power system operation are well established and known for many years, interest in their modeling has been growing recently due to the transitional phase they are currently undergoing. This transition, towards a carbon-free energy supply based on RES, requires a distributed generation model that stands in contrast to the hitherto vertical approach of power system operation. Moreover, the inflexible nature of the most dominant technologies, namely wind turbines and photovoltaics, in conjunction with their strong dependency on weather conditions require a detailed geographical representation of transmission systems, as well as the development of accurate models of power flows over them. Further complications to the modeling of power systems are imposed by the continuously changing market environment in Europe. The ongoing transition towards a closer collaboration between the otherwise independent systems within a deregulated market context introduces further challenges to power system modeling, as the system operation heavily relies on the corresponding market environment.

In this chapter, which content is largely based on the corresponding review by Syranidis et al. [2], theoretical aspects of power system modeling as well as its status quo are presented in a twofold manner. On the one hand, a comprehensive overview of the operation and control of power systems both in terms of theory and modeling is provided. Problem formulations, corresponding numerical approaches and underlying assumptions are presented, as well as related literature. On the other hand, an extensive review of the existing applications of power flow models in real systems is presented, key points of which are amalgamated into four tables based on the used methodology. The various approaches are compared and evaluated, providing valuable insights into the topic, as well as helping to establish future extension and improvement possibilities. In this chapter the complexities in modeling electrical power flows over transmission networks, especially those that arise from the non-linearity of the network constraints and the usually non-convex electricity markets, the passive nature of the grid elements and the lack of energy storage flexibility, are highlighted as well as how such complexities are tackled in the literature. In this way, a suitable method can be selected for the aim of the thesis.

2.1 Power system operation and control

2.1.1 Spatial hierarchy

Power systems are structured in a hierarchical way both spatially and temporally. Spatially, the electricity grid is usually divided into four different voltage levels, the low, medium, high and extra high voltage regimes. While there is no consensus on the limits between the different levels, IEC 60038 [6] standard is continuously gaining acceptance, where extra high voltage is typically considered beyond 220-245 kV. Although the same physical laws apply to the low voltage (distribution level) and high voltage (transmission level), the two areas are clearly distinguished in terms of research and modeling, since their goals differ substantially. The primary goal of a distribution network is to provide unconstrained access to power over the entirety of a region, whereas the transmission network attempts to connect distant regions and eliminate any imbalances, thus functioning as highways of power. Adopting such a tree structure for the system, bulk transfer of power over long distances using the more lossy low voltage lines is avoided, while also making the modeling of each voltage level independent of a more holistic necessity. Since this thesis concentrates on the transmission level, the operation and modeling of the low and medium-voltage networks will not be addressed. However, it is worth mentioning that a high penetration of RES into the power systems poses significant challenges to this hierarchy. Traditionally power has been generated by large units (hundreds of megawatts), connected directly to the extra high voltage grid, and then distributed to the consumers. Conversely, RES generators can be as small as only some kilowatts and hence are connected to lower voltage levels. Therefore, an alternative, so-called smart, operation of distribution grids that allows bi-directional flows among the voltage levels in a secure and optimal way is a topic under research development.

In principle, the transmission networks are divided into broad geographic areas that are operated with centralized control by utility providers known as transmission system operators (TSOs) or independent system operators (ISOs). TSOs are responsible for the synchronized and reliable operation of the power grids, as well as the compliance of all members (i.e., the producers and consumers) with certain specifications concerning the power quality, such as the voltage level, frequency, harmonics, power factor, etc.

2.1.2 Temporal hierarchy

Similarly to the spatial hierarchy, power systems are operated by also implementing a temporal hierarchy approach. The sophisticated temporally hierarchical structure of operating a transmission network stems from the lack of infrastructure for storing electrical energy in significant volumes and the primarily inflexible nature of power consumption. The hard constraint of energy conservation at all times and over the entire network requires significantly different approaches in comparison to other energy carriers, e.g. chemicals. Consequently, the analysis and modeling of transmission systems depends highly on the desired time scale of the corresponding research focus. Figure 2-1 displays the various functions of power systems with respect to the corresponding time-frame of their application. For instance, protection devices operate in the order up to a few seconds, whereas grid expansion techno-economic studies extend the order of several years.

The application of a hierarchical approach aims at de-coupling the different operational regimes with non-overlapping time frames, which is also reflected in the corresponding system modeling. For instance, a day-ahead market model would consider the transmission grid layout as given, while also assume a steady-state operation of the system, i.e., with no dynamic phenomena like switches or faults being considered. Such a de-coupling approach introduces some error and sub-optimal operation of the system; nevertheless, it renders the smaller, individual problems solvable.

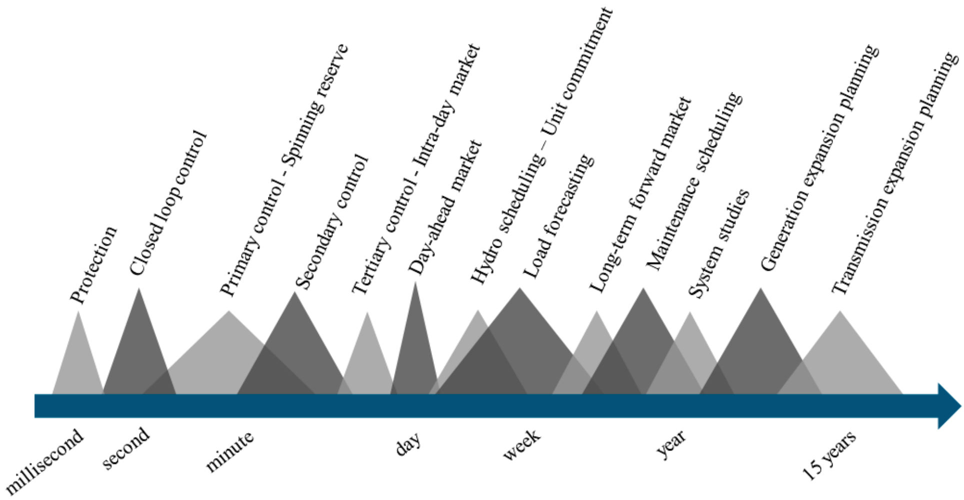

Figure 2-1 Various power system functions ordered by timescale. [2]

Covering all the levels in detail would be out of the scope of the thesis, however, since all of them are interconnected, a brief discussion of the two extremes (short-term and long-term areas) is deemed necessary. The very short-term or transient analysis spans the area between a few milliseconds up to some minutes and focuses on the stability of the system which can have significant implications both on the steady-state capability of the network to accommodate the desired power flows as well as the investment in new network elements.

Although power systems predominantly operate in steady-state conditions, smaller or larger disturbances are ever present. The system must always react and restore its frequency and voltage levels to within the permitted limits after a reasonable time in accordance with the corresponding regulations in order to prevent potentially harmful situations. Both frequency control and voltage control are regulated by multilateral levels of control schemes spanning different response times and geographical areas [3, 4]. The Union for the Co-ordination of the Transmission of Electricity (UCTE) has issued standards and guidelines within the synchronous area of the European Network of Transmission System Operators for Electricity (ENTSOE) in its Operation Handbook (OH) [5]. These standards regard the primary (or spinning), secondary and tertiary reserves. Primary control concerns the speed adjustment of generators via automatic controllers (governors) with a response time of a few seconds. On the other hand, tertiary control is responsible for distributing updated output references for the turbine governors after considering the scheduled generation, real-time demand and transmission flow limits. This control level can range beyond 10 minutes [3].

Similar provisions also exist for the voltage control, which is regulated via the reactive power management [5] and automatic voltage regulator (AVR) controllers. Reactive power flux can be controlled by synchronous machines, flexible AC transmission systems (FACTS), on-load tap-changer (OLTC) transformers or by shunt capacitor-based compensation.

Transient analysis is also used for the investigation of short-circuit faults, lighting strikes or stability studies of the synchronous machines (either static or dynamic). Due to the dynamic nature of the phenomena, non-symmetric operation, non-linearity of the grid elements, as well as the very short time scale, a detailed description of the system is required and so are, consequently, corresponding simulation schemes for solving the ordinary or partial differential equations. The high demand for computational resources from the corresponding numerical solvers, however, limits their scalability both in terms of network size and investigated time range.

On the opposite side, long-term planning concerns the design of investing or de-investing in generation and transmission capacities and typically span the area of several years. Transmission expansion planning (TEP) constitutes a wide area of research and, due to the very long life of the transmission network elements, a common approach is to address the problem simultaneously to the Generation Expansion Planning (GEP) problem. This joint approach becomes even more imperative when goals for energy mixes or CO_2 emissions are to be fulfilled. An example of a full description of the problem, originating from practice, is the cost-benefit analysis (CBA) method, developed and used by ENTSO-E [6], whereas a more simplified version based on linear optimization has been developed by Hagspiel et al. [7].

Lumbreras et al. [8] provides a thorough review of the TEP problem and its modeling strategies. Due to the multi-stage and long-term nature of the TEP problem, three different approaches exist for the decision dynamics, i.e. the static (only one future time snapshot), the sequential static and the full dynamic planning approaches. Regarding uncertainties, three techniques are the most prevalent, namely stochastic optimization, robust optimization and fuzzy decision analysis. Each TEP formulation depends on the specific research focus, nevertheless TEP problems typically use multi-criteria objectives.

2.2 Power flow modeling

The goal of a general power flow simulation is to efficiently calculate all system variables (voltages, currents, active power, etc.) for every part of the network at any time given known network parameters. The values of the control variables of the system, e.g., the power output of generators, are usually determined by a decision-making or market model, whereas the state variables merely obey the physical laws. The various grid components (e.g., generators, lines and loads) can be represented by a variety of models, whose validity depends primarily on the time-scale being investigated and the desired accuracy. Thereby, different assumptions and simulation schemes become more suitable for each case.

2.2.1 The static power flow equations

In contrast to the transient analysis of a power system, the term power flow modeling usually refers to steady-state operation of the network, where steady-state implies a quasi-static problem description, and therefore all variables can be simply represented by complex numbers (phasors) rather than time signals. Time dependency can be included by considering a sequence of quasi static states in discrete steps (minimum hourly or 15 minutes intervals), thus allowing the inclusion of some intra-day and higher dynamics.

Moreover, TSOs take particular care to balance the three phases by attempting to eliminate the inverse and zero symmetrical components. Thus, only the direct component may be considered and all three-phase circuits can be replaced by single line diagrams independently of their topology (e.g., star or delta). That would imply for example a single current phasor for a three-phase line.

Thereby, the entire power system can be represented by a graph with vertices (buses or busbars) and edges (transmission lines). Buses can be characterized by single voltage values (magnitudes and angles) and transmission lines by current flows and static electrical parameters. However, from a power system perspective, the most significant variables are the power rather than current flows, as these belong to the boundary conditions of the system, i.e., specific energy demand profiles that must be met. In this sense, fixed power flows can be directly applied to specific buses, where these flows can be either positive or negative, i.e. indicating either inflows or outflows. Moreover, such fixed flow conditions may concern the real and imaginary parts of the flow, i.e. the active and reactive power components, independently. This abstraction provides great flexibility to the analysis, since any part of the system can be virtually isolated from the rest by replacing equivalent inflows and outflows. Moreover, these flows are agnostic in terms of the source or technology behind them, e.g. it could be a single resistor, an electrical machine, a whole region or any kind of energy converter, consumer or generator, thus allowing the explicit coupling of various energy sectors by simply enforcing energy conservation on the interconnections.

Although the majority of the system's elements are passive, there is increased attention on integrating more active elements, e.g., FACTS, high voltage DC (HVDC) or phase shifting transformers into power systems in order to increase the controllability of power flows. However, these embedded automatic control systems insert an extra degree of freedom, which normally cannot be handled in a straightforward manner by a simple exact solver, but rather require some sort of optimization process [9].

2.2.1.1 Problem formulation

The general formulation of an electrical power flow problem can be described as a non-linear set of equations

$$f(x, u, p) = 0 \tag{2-1}$$

where ***f*** is a non-linear n-dimensional function expressing the energy conservation on every node, ***x*** is an n-dimensional vector containing *n* unknown states (e.g., voltage angles), ***u*** is a vector with the known (control) variables (e.g., active power of a load) and ***p*** is a vector with the parameters of the network components (e.g., line reactances and resistances). The dimensions of ***f*** and ***x*** must match in order for the results to have physically meaningful content; nevertheless, neither the existence nor uniqueness of the solution is guaranteed.

More specifically, the power flow equations for a node *k* can be written as follows:

$$P_k = U_k \sum_{m \in K} U_m (G_{km} \cos(\theta_{km}) + B_{km} \sin(\theta_{km})) \tag{2-2}$$

$$Q_k = U_k \sum_{m \in K} U_m (G_{km} \sin(\theta_{km}) - B_{km} \cos(\theta_{km})) \tag{2-3}$$

where K is the set of buses adjacent to k, including bus k, U is the magnitude of a bus's voltage, θ is the angle between two adjacent buses' voltages, $Y = G + jB$ are the elements of the nodal admittance matrix (see Appendix A) and P, Q are the net inflows/withdrawals from the system.

A necessary, yet not always sufficient, condition for the system (eq. (2-2), (2-3)) to be solvable is to have the same number of equations to unknowns. Therefore, the various buses hold different degrees of freedom, with the most common categories being the *PQ* buses with fixed values for active and reactive power injections usually representing the various loads of the system, the *PU* buses with controllable values for the active power and the voltage magnitude, which usually represent the buses connected to generators and one slack bus, which is a *Uθ* bus, i.e., with a fixed value for the voltage angle, hence acting as a reference point for the whole system.

2.2.2.2 Numerical approaches

The system of equations ((2-2), (2-3)) is in the form of eq. (2-1) and are non-linear with respect to both the voltage magnitudes and angles; therefore, a direct, analytical solution is rarely feasible. The most common approaches include either a linearization of the system or the application of an iterative method.

The iterative methods approach is applied to the non-linear system of ((2-2), (2-3)) and is commonly referred to as AC power flow analysis. The most popular and traditional methods are the Gauss-Seidel, Newton-Raphson and Fast or Pθ-QU decoupling method (P and Q indicate the active and reactive power, whereas θ and U the voltage angle and magnitude respectively). Nevertheless, non-iterative methods are also available, such as the Series Load Flow method [10] and the more rigorous Holomorphic Embedding method [11]. In particular, the latter method takes advantage of the mathematically powerful complex analysis tools and thus has the advantage, in contrast to the iterative methods, of always finding the right solution to the problem, as long as there is one.

2.2.2.3 Iterative methods

One of the first iterative methods that appeared is Gauss-Seidel method, which is an iterative, relaxation approach that is also applied to solving linear systems in general, where for power flow equations it relies on reconstructing eq.(2-1) in the form of

$$\boldsymbol{x} = \boldsymbol{h}(\boldsymbol{x}) \tag{2-4}$$

where $\boldsymbol{h}$ is a non-linear function of $\boldsymbol{x}$ itself. The idea is that after a sequential application of this function on the updated solution, $\boldsymbol{x}^{\nu+1} = \boldsymbol{h}(\boldsymbol{x}^{\nu})$, the process will converge to a stationary point, $\boldsymbol{x}^{*} = \boldsymbol{h}(\boldsymbol{x}^{*})$. The major drawback of this method is convergence, since this cannot always be guaranteed and even when it does, the rate is slower in comparison to other methods. Therefore, Gauss-Seidel is rarely preferred as a choice for real systems.

The Newton-Raphson method, on the other hand, is one of the most popular in the area of AC load flows as it normally shows quadratic convergence near the solution [12]. The concept of this method is the linearization of the function $\boldsymbol{f}$ in eq.(2-1) at the point $\boldsymbol{x}^{\nu}$, i.e.,

$$\boldsymbol{f}(\boldsymbol{x}^{\nu} + \Delta\,\boldsymbol{x}^{\nu}) \cong \boldsymbol{f}(\boldsymbol{x}^{\nu}) + \boldsymbol{J}(\boldsymbol{x}^{\nu}) \cdot \Delta\,\boldsymbol{x}^{\nu} \tag{2-5}$$

where $\boldsymbol{x}^{\nu+1} = \boldsymbol{x}^{\nu} + \Delta\,\boldsymbol{x}^{\nu}$ and $\Delta\,\boldsymbol{x}^{\nu}$ corresponds to the solution of the consequent linear system $\boldsymbol{f}(\boldsymbol{x}^{\nu}) + \boldsymbol{J}(\boldsymbol{x}^{\nu}) \cdot \Delta\,\boldsymbol{x}^{\nu} = \boldsymbol{0}$ until $\Delta\,\boldsymbol{x}^{\nu} \rightarrow \boldsymbol{0}$. The matrix $\boldsymbol{J}$ is the Jacobian matrix of $\boldsymbol{f}$ with respect to $\boldsymbol{x}$ and if the elements of $\boldsymbol{x}$ are ordered such that $\boldsymbol{x} = \binom{\boldsymbol{\theta}}{\boldsymbol{U}}$, it becomes

$$\boldsymbol{J} = \begin{pmatrix} \frac{\partial \boldsymbol{P}}{\partial \boldsymbol{\theta}} & \frac{\partial \boldsymbol{P}}{\partial \boldsymbol{U}} \\ \frac{\partial \boldsymbol{Q}}{\partial \boldsymbol{\theta}} & \frac{\partial \boldsymbol{Q}}{\partial \boldsymbol{U}} \end{pmatrix} \tag{2-6}$$

The Fast Decoupled method exploits this form of the Jacobian in order to decouple $\boldsymbol{\theta}$ and $\boldsymbol{U}$ equations and thus solve the linear system of each iteration more quickly. Both terms $\frac{\partial \boldsymbol{P}}{\partial \boldsymbol{U}}$ and $\frac{\partial \boldsymbol{Q}}{\partial \boldsymbol{\theta}}$ are approximately proportional to $\sin(\boldsymbol{\theta})$, which is usually small for steady-state operation, and therefore neglected. Despite this approximation, the method yields the correct solution, only with a lower rate than the Newton-Raphson approach. Nevertheless, the slow convergence is compensated by the quicker solution of the smaller linear systems in between, leading to better overall performance. The Fast Decoupled method may be considered as a mild version of the Dishonest Newton-Raphson or Shamanskii methods [13] that tries to deal with the complexities imposed by the Jacobian matrix.

A reasonable approach would be to apply the Newton-Raphson method to a so-called "cold start" problem, where the initial guess is far from the solution and exploiting its robustness, while performing the Fast Decoupled method for the slightly disturbed cases after reaching the Newton-Raphson solution ("hot start") in order to take advantage of its higher speed. Nevertheless, the important issue of the dependency of all iterative methods converging on the initial guess remains and can have a drastic effect on the value of the eventual solution, as well as the convergence rate. The Newton-Raphson method, for example, is known for producing complicated fractal patterns at the boundaries of the attraction basins, and there is no rigorous way to define how close a starting point may be to a solution.

2.2.2.4 Linearization approaches

Besides the performance level of the iterative methods, a further boost in the execution time of the simulations may be desired for very large systems or exhaustive optimization or contingency analysis routines that require multiple runs. A very popular way to accomplish such a challenge is to make further simplifying assumptions in order to linearize the whole problem, thereby sacrificing some accuracy for the sake of performance. The most popular model extends the Fast Decoupled method with the additional assumption of neglecting the reactive power flow, given that all voltage magnitudes are considered to be equal to 1 in reduced units.

Expressing all the assumptions quantitatively, $\sin(\theta) \cong \theta$, $U = 1\, p.u. (per\ unit)$ and $R = 0$ (*R* is the line's resistance which is assumed much smaller than the corresponding reactance and can thus be neglected), eq. (2-1) yields the following linear system $\boldsymbol{P} = \boldsymbol{B}\theta$ with $B_{km} = -{x_{km}}^{-1}$ and $B_{kk} = \sum_{m\in\Omega_k} {x_{km}}^{-1}$. The linear form is reminiscent of a simple ohmic circuit in which current sources are replaced by power injections and node voltages by node angles, hence the method is called the DC flow method. In fact, before the development of computers, simulating a full-sized power system would only have been possible via an ohmic circuit analog.

The validity of the DC flow approximation increases for higher voltages where the line resistance becomes smaller in comparison to the corresponding reactance value (the ratio is typically greater than 1:10 for levels higher than 275kV [14]), contributing to less than a 2% average error for high voltage grids [15]. Moreover, angle differences normally remain lower than 10^{o} for steady operations in transmission networks, which result in an error rate close to 1% [15]. The factor with the most significant impact seems to be the assumption regarding the neglect of reactive power flows, which is responsible for most of the DC flow method errors. In comparison to the AC flow, the error is usually around 5% after averaging over all lines; however, it can deviate significantly from that value when examining single lines only [15].

The DC approach exhibits various advantages, among which are [16]:

- Speed and robustness
- Minimal input data requirements regarding grid modeling
- Scaling and superposition features stemming from the linearity nature, suitable for economic analyses
- Accurate active power flows for the heavily loaded branches, responsible for constraining the system's operation

Room for improving the accuracy while preserving the highly important linearity aspect is small. Nevertheless, there exist various approaches to incorporate line losses within the linear scheme, and these can be divided into explicit and incremental methods [16]. The explicit methods can be further separated into various hot and cold start methods, depending on the availability of a reliable base point to apply the linearization. Furthermore, the incremental methods can be categorized in sparse matrix and sensitivity factor models. The increased complexity of applying these techniques is compensated for by obtaining results similar to AC power flows, at least for active power and contingency analysis studies [17]. The ability to predict reactive power flows, which also contribute to the line losses, is of high interest, and therefore researchers have also attempted to develop a corresponding linear model that incorporates these flows [18].

Besides the DC flow approach, the linear description of a power system also allows the development of linear sensitivity factors which can prove very useful for reliability calculations, market modeling and reducing network sizes. One of the most important and frequently used sensitivity indices consists of the power transfer distribution factor (PTDF) [19-22], which evaluates the impact of an increment in power transaction between two nodes of the system, onto a specific line's loading, described by eq. (2-8). PTDF values can be calculated for a reference node and then stored in matrix form, hence PTDFs for different node pairs can be calculated implicitly.

The PTDF method is one of the most popular for market-based simulations due to its linear nature, simple flow equations (see eq. (2-7), where F_l is the flow on line l and P_n is the power injection at node n) and its direct applicability to clusters of aggregated nodes which may represent entire market zones while maintaining information about the actual power flows. It is worth noting that if PTDF values are calculated based on DC flow simulations, the two methods are equivalent for the bus level.

$$F_l = \sum_n PTDF_{n,ref,l} P_n \ \forall l \in lines \tag{2-7}$$

The main drawback of this method arises from its sensitivity to the network topology and state of the system. In principle, PTDF values must be recalculated for each different topology. However, their sensitivity to the state of the problem is smaller and becomes insignificant for large enough systems, thus allowing computations with the same PTDF matrix [23-25]. However, Duthaler et al. [19] show that using PTDFs for describing highly reduced networks can lead to significant distortions of reality with high dependency on the hour and season of investigation, potentially leading to false conclusions.

In addition, a PTDF formulation results in a computationally inefficient description of the grid. Due to the passive nature of the electrical grid, all line loads will be affected by a difference in power injection at a single node. Therefore, PTDF matrices tend to form full matrices, creating memory, computational speed and accuracy issues.

$$PTDF_{i,j,l} = \frac{\Delta flow_l}{\Delta Power_{i,j}} \tag{2-8}$$

i,j: indices of areas/nodes that exchange power

l: line index

The PTDF matrix calculation follows directly from its definition and can be performed in three steps [26]. The first is to select a reference bus in order to reduce the admittance matrix ***B*** to non-singular, thus obtaining eq.(2-9), where $\boldsymbol{B'}$ does not include the row and column of the reference bus. The second step consists of calculating the matrix ***H*** that connects the line flows $\boldsymbol{P_l}$ with the reduced bus angles $\boldsymbol{\theta'}$. Assuming that line *k* connects the buses *i* and *j*, the corresponding element of the ***H*** matrix can be found via $H(k,i) = 1/x_{ij}$, $H(k,j) = -1/x_{ij}$ while the rest of the *k*th row is 0. The equation of the second step eq. (2-10) combined with eq. (2-9) results in the final PTDF matrix for the selected reference bus eq. (2-11).

$$P' = B'\theta' \Rightarrow \theta' = B'^{-1}P' \tag{2-9}$$

$$P_l = H\theta' \tag{2-10}$$

$$P_l = H \cdot B'^{-1} \cdot P' \Rightarrow PTDF = H \cdot B'^{-1} \tag{2-11}$$

As mentioned above, one of the main advantages of the PTDF sensitivities approach is the ability to develop linear descriptions of reduced equivalents of a detailed network while maintaining the fundamental electrical power flow properties. The mapping from a nodal to a zonal PTDF description is realized via the generation shift key (GSK) matrix (eq. (2-12)), which is, however, only valid for a single generation and load profile. Therefore, an optimal division of the zones is required in order to estimate insensitive GSK matrices [27] and be able to more accurately represent the real grid via a reduced model.

$$PTDF_{zonal} = GSK \cdot PTDF_{nodal} \tag{2-12}$$

Arguably, the second most significant sensitivity constitutes the line outage distribution factor (LODF) [28, 29], which indicates the effect of an outage in the grid on a specific line's loading, and is systematically used for security and contingency analysis calculations. Various other factors exist with corresponding functionalities, with the significant advantage for all of them stemming from the linear description of the network that results in the independence of those factors from the system's state of operation. In other words, all sensitivity factors depend merely on the parameters and topology of the system. Therefore, as long as the topology does not change, they can be simply calculated once and then used for all other calculations in the system. Besides the nodal based formulation of the sensitivity factors, Ronellenfitsch et al. [30] have recently demonstrated an equivalent dual formulation, i.e. based on network loops, which leads to better computational performance.

2.2.2 Electricity market modeling

The allocation of set points to the power output of flexible generators is known as generation dispatch and depends on the corresponding electricity market environment. While section 2.2.1 analyzes the laws that govern flows in power systems, equations (2-2) and (2-3) show the dominant driver of those flows, which consists of the boundary conditions of the systems, namely the active and reactive power sources and sinks of the system. Although managing reactive inflows is more related to the techno-economical and grid services area, defining the active inflows is less trivial from both the economic and energy sources perspective, hence also for modeling. Moreover, the primarily inflexible demand in conjunction with the lack of significant electricity storage in the contemporary power systems result in rather strict requirements to the flexible generators regarding energy conservation and stability of the system. For instance, only a deviation of 0.2 Hz from the nominal frequency under normal operation conditions is usually permitted [31], where the system frequency depends mainly on the energy balance of the system.

Generator outputs are constrained by the corresponding technologies, which however merely define a closed mathematical space in which all the valid combinations of generation outputs reside. A definite selection for each output and each time snapshot can only be described by some type of optimization formulation. Two main approaches traditionally exist for managing the allocation of the various power injections, merely differing in the ownership status, nevertheless both targeting the maximization of social welfare. In the first, more holistic, approach, one - usually public - institution owns all significant generation assets as well as transmission infrastructure, and attempts to cover demand for every time period with the objective of minimizing the total costs of the system. The second approach handles power as a commercial commodity that can be traded freely by all members in spot or futures/forwards markets. This free market-based operation of the power system has largely substituted the previous monopolistic, economy-of-scale-focused approach in most developed countries. The determination of the electricity price for a specific time interval is achieved using the so-called merit-order curve, a typical example of which is depicted in figure 2-2 for the German market. The intersection of the supply and demand curves defines the market clearing price, the power plants to be committed for generation, as well as the load that will be covered. Nuclear and coal thermal power units have high capital and low operational costs, therefore they are usually located first in the merit-order curve. The offers of all bidders are classified in ascending order and the volume of the total demand defines which unit will be committed to providing power for the specific time period. Since generation from RES is characterized by very low operational costs, it is normally located in the leftmost position of the merit order, therefore decreasing the final price. For instance, the inclusion of RES can be interpreted either as a translation of the merit-order curve to the right or a translation of the demand curve to the left.

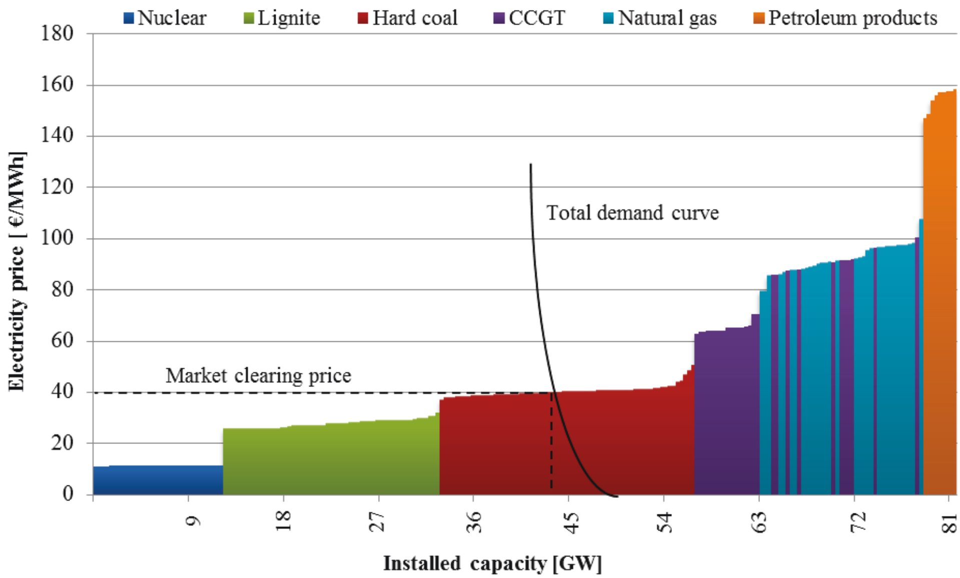

Figure 2-2 A typical merit-order curve including the various generation technologies and the demand curve, where CCGT refers to the closed-cycle gas turbine technology. [32]

Despite the various power transfers will eventually be limited by the network constraints, power in a single electricity market is traded freely assuming perfect grid conditions. This perfect grid assumption is more widely known as copper plate.

Ventosa et al. [33] provide a detailed overview of modeling electricity markets, including monopoly, oligopoly and perfect competition environments. Since the modeling of an oligopoly environment constitutes the most challenging to accomplish accurately, covering it would be beyond the scope of this thesis and therefore it will not be addressed in detail. The major studies are classified according to the level of network representation, time resolution and the inclusion of uncertainties. Moreover, all studies are further classified per market model, research focus, main feature, solution method as well as system size. The most usual focal points of research consist of market power analysis, hydro-thermal coordination, unit commitment and congestion management.

In the monopolistic market, the allocation of generator outputs is formulated as an optimization problem in which the objective is to minimize the total operational cost, which itself is a function of the output of each generator. The minimal size of such a problem, traditionally called economic dispatch (ED) problem, consists merely of constraints to total energy conservation and generator output limits. A linear description of the problem allows the application of various efficient methods, e.g., linear programming, lambda iteration or dynamic programming. With respect to the inclusion of power losses, these depend on individual power flows and therefore cannot be known beforehand. Nevertheless, they can be approximated via a loss-formula method that describes the losses as a linear or quadratic function of the generator outputs, thus retaining the nature of the objective function [12].

For the free market approach, two main forms of power trading exist, namely the bilateral or over-the-counter market and the pool- or spot-based market. During bilateral transactions, suppliers and consumers agree on the amount, price and time window of the power delivered with individual, usually long-term, contracts while also providing the corresponding TSO with either a fixed or market-based price for the network usage. In the spot market, electricity demand is traded on the day-ahead market, where a Power Exchange (PX), accepts bids from the suppliers using some auction mechanism. Such mechanisms may include English (or open ascending price auction where the highest bid is displayed), Dutch (or open descending price auction where the lowest price is displayed), First-Price Sealed Bid (FPSB or blind auction where bids are submitted simultaneously), Vickrey (similar to FPSB except that the winning bidder pays the second-higher bid), All Pay (all bidders pay regardless if they win), etc. [9]. The auction results in a unique price for the corresponding time-frame of the following day, which applies to all the participants of the specific bidding zone. Further information regarding energy trading in the European market can be found in the corresponding regulations [34, 35], as well as in the discussion paper of the German Federal Ministry for Economic Affairs and Energy [36]. From the modeling perspective, trading blocks are relatively hard to model, whereas a perfect spot market can be modeled sufficiently by using the monopolistic approach, i.e. maximization of social welfare.

The ED problem can be further extended to include temporal limitations which become important when dispatching hydro-plants or other electricity storage technologies as well as thermal power plants whose turning on-off constraints may span several hours. Hydro planning is often scheduled using dynamic programming [37], while steam plants dispatch can be optimized via mixed integer programming that usually concerns time periods of one week [38]. The latter problem is known as the unit commitment problem (UC), where the multi-period optimization needs to consider the maximum power ramping limitations, minimum output requirements as well as minimum on and off grid durations that are imposed by the boilers of thermal power plants and can cause negative electricity prices.

In the European context, market or bidding zones have evolved from the separate countries. Due to mainly political reasons, this configuration has primarily stayed the same except for a few cases where single countries are split into more zones (e.g. Sweden) or more than one countries form a single price zone (Germany-Austria-Luxemburg). Figure 2-3 shows the current bidding zone configuration in Europe, where each zone is denoted with a different color.

Figure 2-3 Configuration of the bidding zones in Europe. The only zone spanning more than one country consists of the Germany-Austria-Luxemburg zone. In each bidding zone a single price is applied uniformly after market clearing [39]. Own illustration.

2.2.3 Congestion management

A simple spot exchange market, based on the copper plate assumption, cannot include the energy transfer limitations imposed by the transmission grid and therefore, further congestion management (CM) practices are necessary to secure the network's undisturbed operation. The term congestion refers to one or more transmission lines having reached their transfer capacity limit. In high voltage grids, this capacity is defined by the maximum current allowed on the line and the corresponding thermal limits that relate to the maximum allowed expansion limits of the overhead lines, whereas low voltage grids are usually restricted by the maximum allowed voltage drop between a line's end points. Managing congestion is particularly challenging in power systems due to the passive nature of its elements. In contrast to other kinds of networks, e.g., telecommunications, traffic, or commodities, active control of the physical flows in a power system cannot be directly applied in most cases and non-intuitive phenomena may occur, e.g., removing a connection can lead to less congestion. Moreover, further system restrictions like bus voltage limits or maximum rotor angles must be taken into account.

In addition, one further factor determining the final dispatch is the fulfillment of the reliability condition. Critical unexpected contingencies may lead to cascading effects, thus putting the operation of the whole system at risk. A common choice for ensuring secured operation is the N-1 criterion, which demands stable operating conditions after any single element outage [5, 40], whereas for more complex combinations of N-2 and above, critical cases are usually selected from experience.

The term congestion management, however, can be sometimes confusing, since it may refer to different time-frames. The short-term CM, also known as re-dispatch, consists of the remedial actions that must be undertaken by the TSOs, primarily the re-allocation of generator outputs, in order to relieve congestion and secure the system's operation within time frames shorter than an hour. Although the maximization of social welfare remains the primary goal, the allocation of the higher final system cost (CM cost), as well as other market parameters allows the development of different CM schemes that primarily differ in terms of policies, efficiency and implied financial incentives. The free market approach to re-dispatching includes the intraday market, where reserves are auctioned in a similar manner to the day-ahead market and can be modeled via cost-based re-dispatch, e.g. Nüßler et al. [41], or power exchanges, e.g. Meyabadi et al. [42], whereas Hermans et al. [43] also discuss about the optimal power flow, optimal nodal prices and curative congestion management methods.

On the opposite side, congestion management over the long run refers to the necessary investments in system reinforcement and grid expansion so that the most frequent congestions are relieved.

The intermediate area between short-term re-dispatch and the long-term grid development planning is filled by mid-term congestion management. The main goals of mid-term CM are to provide the necessary market signals to prevent congestions occurring on the one hand and indicating desirable investments in new power plants and grid extensions, on the other. Kumar et al. [44] have grouped the various approaches into four main categories:

- Sensitivity factor based methods
- Auction-based congestion management
- Pricing based methods
- Re-dispatch and willingness to pay methods

Aside from the basic re-dispatch and power exchange methods [45], market coupling and market splitting constitute two of the most attractive methods for mid-term CM. Although originating from different starting points, both market splitting and coupling essentially lead to the same end goal, namely an electricity market with a so-called zonal pricing scheme. In such a market, the transmission grid is divided into different price zones, i.e., clusters of nodes that seldom encounter internal congestions, and the whole grid can then be reduced to a market-equivalent aggregate version [46]. Apart from various issues relating to market transparency, efficiency, liquidity and transmission rights [47], the administrative or TSO boundaries do not necessarily constitute a representative zonal clustering from the electrical and market perspective [48] and therefore many American electricity markets (e.g. PJM, ERCOT etc.) have switched to a nodal pricing scheme, in which every individual grid node is considered a separate price zone. The values of nodal prices can also be implicitly estimated via optimization problems, represented by the dual variables of the respective problem, and are usually known as locational marginal prices (LMP). LMPs indicate the increase in total operational cost for one megawatt (MW) increase of demand on the corresponding node. Within a copper plate assumption, all grid nodes will have the same LMP; however, when losses or flow constraints are included, the LMP of the various nodes may differ.

Conversely, and despite any arguments favoring nodal pricing [49], zonal pricing is implemented in the European region. A more elaborate description of the European case, together with its corresponding modeling, is stated in section 2.2.3.1 nevertheless, it is also worth mentioning some alternative methods for neighboring market interactions as well.

Generally, interconnected power systems demonstrate various advantages in terms of both stiffness enhancement and economic operation, and therefore it is of mutual benefit for two neighboring systems to co-operate with each other. However, primarily due to historical reasons, cross-border grid development is relatively weak in most cases, thus leading to frequent saturation of the corresponding lines usage. In that context, different CM methods have been applied for the capacity allocation of cross-border links, which traditionally has been realized with non-market based methods, including:

- Access limitation
- Priority list
- Pro-rata rationing

These methods are still used, for example in the southeastern European area, where political factors, including the recent Yugoslav wars, have hindered grid development and market integration [50].

Market-based methods, however, are continuously gaining ground, thus increasing the transparency and transaction volumes between the market zones. These methods consist of either explicit or implicit auctions of transmission capacity. A typical example of implicit auctioning is implemented in the European region in order to increase the available capacity utilization and transparency of the process. The method is formally named Price Coupling of Regions (PCR) and consists of an agreement among the involved electricity markets and the corresponding TSOs. The market participants do not explicitly bid for transmission capacity but rather behave as if there was no market coupling scheme. After receiving the various bids, the involved markets optimize the inter-market power trading using the EUPHEMIA algorithm [51] and later send the corresponding signals to the market participants and TSOs. Figure 2-4 shows the status of PCR membership in December 2018. Two market coupling methods exist, the Multi-Regional Coupling (MRC) project and the 4M market coupling (4MMC) which is intended to be merged with the former approach.

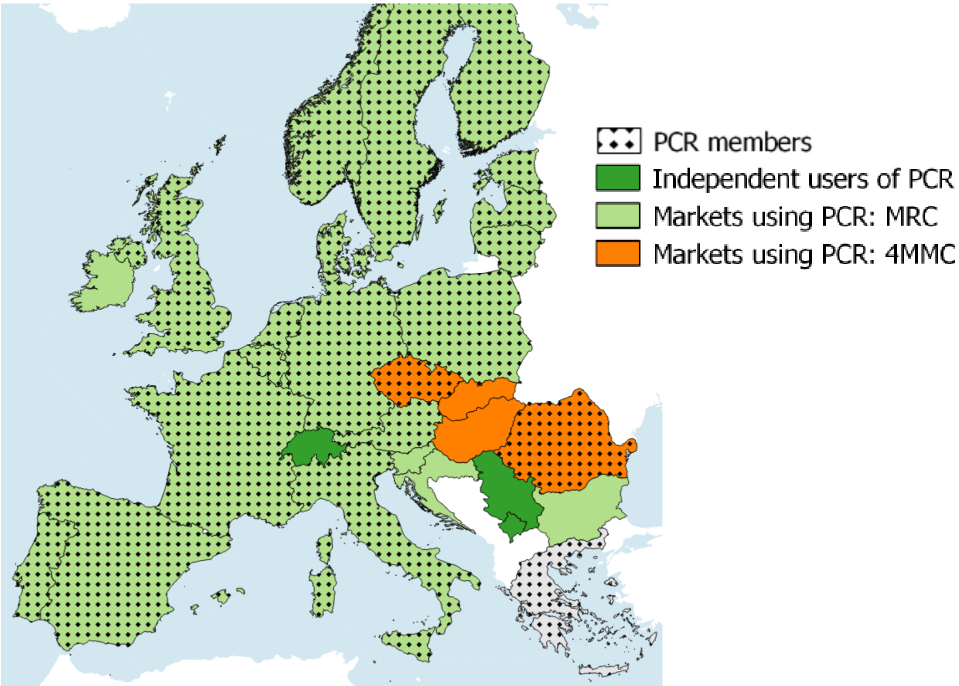

Figure 2-4 Price Coupling of Regions (PCR) membership by December 2018 [52]. Countries using the Multi-Regional Coupling (MRC) and 4M Market Coupling (4MMC) coupling methods are also depicted separately. Own illustration.

Christie et al. [53] extensively discuss three of the most popular CM concepts of that level and analyze them in terms of accuracy, efficiency and transparency. Accuracy demands minimal ex-post corrections by the TSOs, efficiency requires maximization of social welfare and minimization of the bidders' market power, while transparency is desirable from all participants for accessing both the methods and data that are used to define the outcome of the particular CM method. Each method may excel in a different area, however there is no optimal solution.

2.2.3.1 Transaction-based (network flow) modeling approach

Transaction-based modeling follows from the coupled energy markets and their desire to explicitly trade electric power, as well as allocate transfer capacities. Nevertheless, it does not necessarily have to be limited to that application. The participants of a coupled market buy and sell power as if they are in a single market zone. After the market clearing, the individual markets attempt to harmonize their prices with respect to the available transfer capacities (ATC) which represent the power transfer limitations between them. This harmonization process is conducted by exporting power from the low price to the high price areas, either until the prices converge and hence there is no motivation for further trading or until the corresponding power transfer limit is reached. Figures 2-5 and 2-6 show how the markets exchange power until their prices converge with and without capacity restrictions correspondingly. Similarly to the introduction of RES into the merit-order curve, trading can be interpreted as an increase in the demand for the export market and translation of the merit-order to the right. The final price difference ($\Delta Pr = Pr_{im,2} - Pr_{ex,2}$) that may occur due to capacity limitations is called congestion revenue.

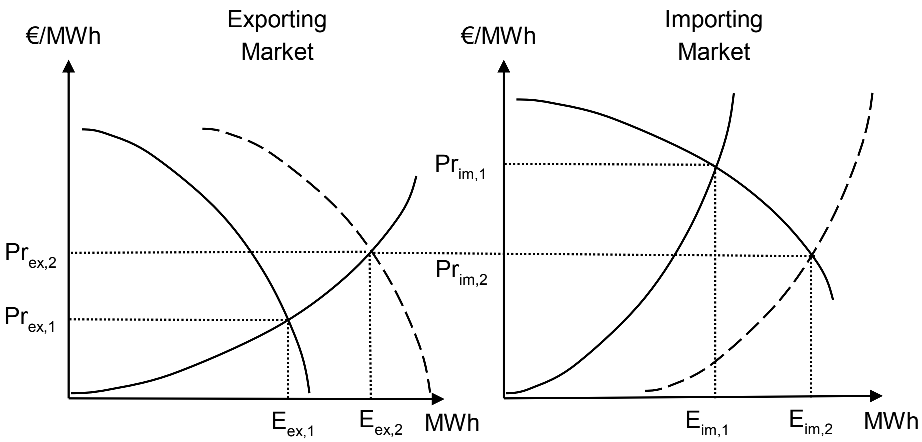

Figure 2-5 Power traded between coupled markets with no transfer limitations [54]. Prices are denoted with Pr, energy demand with E, importing market values with im and exporting market values with ex. The market states before coupling are indicated by the index 1 and after coupling by the index 2. Power exchange continues to take place until both prices converge ($Pr_{ex,2} = Pr_{im,2}$). Own illustration.

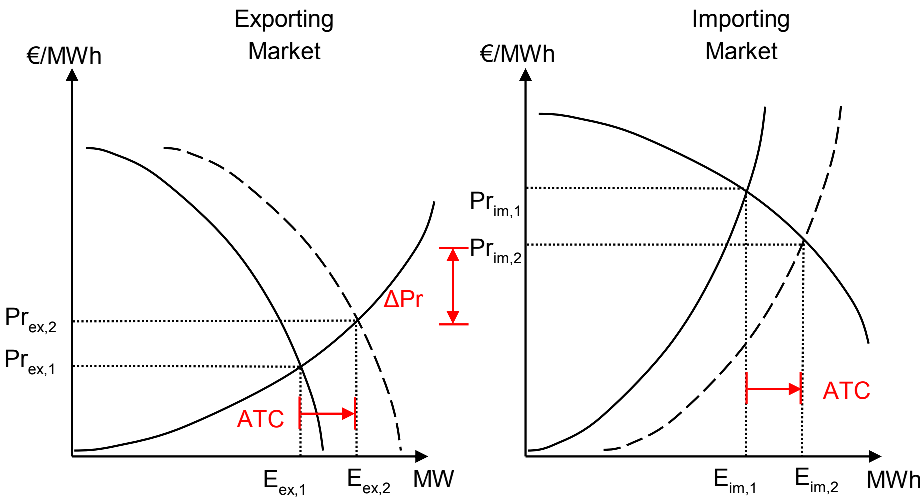

Figure 2-6 Power trade between coupled markets limited by a finite transfer capacity (ATC) that hinders complete price convergence [54]. Prices are denoted with Pr, energy demand with E, importing and exporting market values with im and ex respectively. The market states before coupling are indicated by the index 1 and after coupling by the index 2. The final price difference (ΔPr) multiplied by the ATC yields the congestion revenue. Own illustration.

The fundamental assumption of the transaction-based approach is to handle the interconnecting links (represented as a simple flowgate depicted in figure 2-7) as fully controllable elements that are only limited by a total transmission capacity which, however, stands in contrast to the passive nature of the power networks, since they do not normally allow such functionality. Therefore, although specific power trading quantities may have been agreed between two parties, the physical flows will always use the entire network to travel from a source to a withdrawal point, and not exclusively the cross-border lines of the corresponding interface. The power flows that cross third-party areas, also called loop flows or wheeling, are particularly present in highly meshed networks like those in the north-eastern part of the USA and central Europe. Loop flows use the transmission grid of third parties and therefore limit their capacities, hence researchers have tried to devise methods that would quantify their contribution and apply corresponding transmission usage tariff (TUT) schemes, e.g., postage stamps, dollars per MW mile or locational margin pricing (LMP) [55]. In addition, Schaefer et al. [56] have developed a method to trace flows over power networks and measure the contribution in line loadings. An example of the impact that loop flows may pose to a transmission is given by Van den Bergh et al. [57] in the context of Belgium.

Two main methods exist for calculating the capacities of the interconnecting links, net transfer capacity (NTC) and flow based market coupling (FMBC). The first method is more closely related to the market concept, whereas the latter one was developed as an improvement, by bringing the same concept closer to the physical world, thus allowing higher transaction volumes and better price convergence, especially for the high meshed areas. FMBC was firstly put into operation in May 2015 for the day-ahead market of Central Western European (CWE) area.

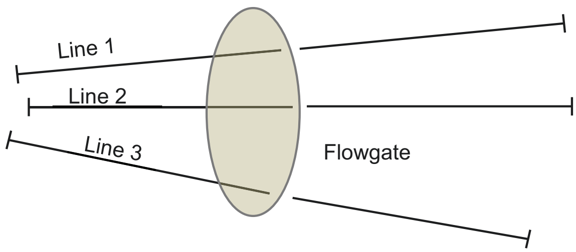

Figure 2-7 Example of a flowgate that includes three lines and can be used as a representative link between the connected areas.

With the NTC approach, the useful part of the capacity of a flowgate that is available for power transactions is calculated by the involved TSOs and is called net transfer capacity (NTC). NTC is part of the total transfer capacity (TTC) after subtracting the transmission reliability margin (TRM) [58, 59], which relates to the security of the system. A frequent concern regarding the NTC method is that TRM often ends up being too restrictive for highly meshed areas due to the way in which it is calculated [58]. Therefore, in order to better estimate this margin, the interconnected TSOs at the western border of Germany use a so-called C function [60, 61]. Regarding the computation of the TTC, the general approach consists of the continuation power flow (CPF) or repeated power flow (RPF) method [12]. Despite the complex calculations involved in the process, NTC is very popular for modeling transmission networks since their values are occasionally reported by ENTSO-E and already include security calculations.

The NTC values indicate the secure available capacities for power transfer; however, only a portion of them are available for power trading (the ATC), which constitute the remainder of the already allocated capacity (AAC). AAC refers to the transactions that have already been explicitly allocated outside the spot market mechanism. The summarizing equation that connects all the capacities is shown in eq. (2-13).

$$TTC - TRM = NTC = ATC + AAC \tag{2-13}$$

where TTC: Total Transfer Capacity

TRM: Transmission Reliability Margin

NTC: Net Transfer Capacity

ATC: Available Transfer Capacity

AAC: Already Allocated Capacity

Although the NTC approach has been relatively successfully applied to the markets of Scandinavia and California due to their elongated shape [53], its application in the highly meshed central European area has been subject to criticism, mainly due to its lower market coupling efficiency results. An alternative method that maintains the zonal approach but attempts to surpass the NTC concept limitations and bring the market closer to the physical world is the FBMC approach.

The major advantages of FBMC include the addressing of unscheduled and loop flows as well as the introduction of higher transparency, since TSOs work on a common grid, where the critical branches (CB) and outages (CO) are published. Nevertheless, there is still room for improvement in terms of both transparency and market efficiency. The model of the common grid that is used for the calculations is still only available to the TSOs and the identifiers of the CB/COs are intentionally incomprehensible for external users. For instance, a simple eleven digit number as branch identifier gives no indication for its position in the grid unless the grid model is known. Moreover, since an FBMC simulation may result in power flows from high price areas to lower ones, an alternative modification has been developed that is termed intuitive FBMC (IFBMC). IFBMC explicitly cuts off such non-intuitive from the market perspective phenomena, thus reducing the total social welfare, which was mostly achieved however by favoring bigger countries at the expense of the smaller ones [62].

Although FBMC maintains the zonal characteristic, individual critical branches are included in the calculation of the available capacity. Furthermore, critical branches/outages do not necessarily belong to a flowgate but may also be located inside the investigated zones. Similarly to the TTC/ATC concept, though applied for each critical line individually, a maximal flow is defined for each line from which a security or Flow Reliability Margin (FRM) is subtracted, as well as an F_{ref} value, which represents the already known allocations from the long-term contracts. The remaining part that is available for trading is the Remaining Available Margin (RAM) [63, 64]. The composition of both capacity allocation schemes is visually summarized in figure 2-8.

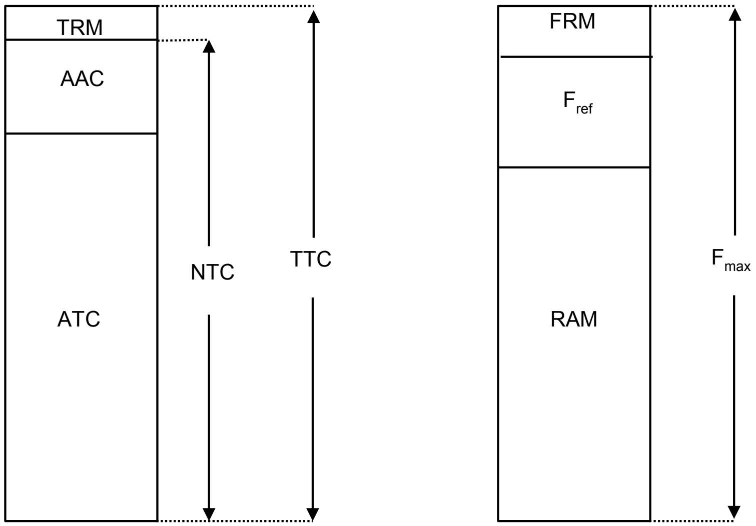

Figure 2-8 Capacity allocation according to the NTC and FBMC models depicted in the left and right pictures respectively [63, 65]. The allocation refers to the entire flowgate in the first case and to each critical branch for the latter.

Modeling the grid with the FBMC approach requires two parameters, namely the zonal PTDFs and RAMs of the branches, whose values will be used for the day-ahead market. However, since the values of the parameters depend on the outcome of the market itself, a prediction of the state of the system at the time of delivery is used for their computation [66].

In general, the FBMC approach allows better opportunities for price convergence, power trading and increasing total social welfare than the NTC approach. Experience from the first year of the FBMC application in the CWE area has shown that the frequency of full price convergence did increase with the new method, nevertheless the available capacities remain insufficient for full convergence during a whole year period [67].

2.2.4 The optimal power flow

The oldest and most established way to handle congestion is the optimal power flow (OPF) method. This was developed at a time when all parts of the electricity supply chain, i.e., generation, transmission and distribution, were operated by a single entity that owned all the necessary information corresponding to the system. Therefore, OPF is, by construction, a centralized scheme, which attracts criticism due to its low transparency.

In general, OPF can be formulated as an extension of the classical ED optimization by adding further constraints, including the power flow equations (either the full AC equations or DC approximations) and inequality constraints for the line capacity limits. A more complete list of the various components of a power system that can to be included in the OPF formulation is given by Frank et al. [68], while the original description of the problem was provided by Dommel et al. [69]. Objective functions may take various forms other than cost minimization, for example minimization of total losses, load shedding, CO_2 emissions or even combinations of objectives, thus resulting in multi-objective optimization problems.

Despite their age, the non-linear and non-convex nature of the full OPF problems, in conjunction with the dependency on both continuous and discrete variables (e.g., OLTCs), make them increasingly difficult to tackle, especially for realistic system sizes. The literature spans the early 1950s till recently, occasionally including review studies [67, 70, 71], with a great variety of approaches proposed by researchers. For each problem formulation, which reflects the interests of the corresponding researcher, a different method is most suitable. Frank et al. [72] suggest caution, however, when comparing performances amongst optimization algorithms, since all methods are regarded by their authors as the best. The relation between optimization problems and algorithm suitability can be described by the 'no free lunch' theorems for optimization [73], in which it becomes clear that a globally appropriate approach does not exist.

OPF, like most of the optimization algorithms, can be classified into two main categories according to the nature of their search strategy. The first category includes the deterministic methods that can be further divided into linear and non-linear programming methods, while the second category includes the non-deterministic methods that are based on heuristic or meta-heuristic algorithms.

A completely linear description of the optimization problem allows the application of powerful linear programming tools like the Simplex algorithm or the interior point method and therefore, despite its inaccuracies, the so-called direct current optimal power flow (DCOPF) method constitutes one of the most popular choices within the research community, as well as industry, mainly due to its computational benefits [74, 75]. More accurate extensions that try to maintain the benefits of linear programming include the use of piecewise-linear objective functions or some form of sequential linear programming [76, 77].

Although the DC flow approximation can be modified to incorporate active power losses, as shown in section 2.2.1, it still neglects the losses of the reactive current component as well as the influence of reactive power flow on the line capacities and busbar voltages. On the other hand, the full alternating current optimal power flow (ACOPF) approach covers these missing characteristics, nevertheless at a higher cost in speed, robustness and data requirements. The first iterative schemes that were developed for the ACOPF problem, but are still used in practice, were the Newton and quasi-Newton methods [78] and various gradient methods like the conjugate gradient and generalized reduced gradient [79]. One of the most popular classes for non-linear optimization in power systems, which can also be applied for linear problems, consists of the interior point methods [80, 81], whose some of their major advantages are fast convergence and efficiency in addressing inequality constraints [68]. Convergence issues may emerge for all iterative solvers when encountering non-convex problems, and therefore trust region versions have been developed [82] in order to tackle such problems at a relative price in the computational speed. Another class of methods consists of decomposition approaches, where the optimization problem is divided into smaller components that are solved faster [83-85]. Finally, OPF problem descriptions as semi-definite [86] and semi-infinite [87] problems have been proposed and solved accordingly.

Besides the deterministic approaches, many optimization approaches based on heuristic algorithms have been successfully tested on power systems. However, the convergence issues that arise for large systems, their high sensitivity to the parameters, as well as their inability to estimate the distance from the global optimum, prevent them from being broadly used. Frank et al. [72] discuss most of the existing approaches, including artificial intelligence methods, artificial neural networks, genetic algorithms (GA), evolutionary algorithms, ant colony optimization, bacterial foraging, simulated annealing, particle swarm optimization (PSO), chaos optimization, differential evolution and tabu search, as well as hybrid methods and fuzzy optimal power flow. Adding the hybrid imperialist competitive [88], gravitational search [89], black-hole-based [90] and biogeography-based [91] algorithms probably completes the previous list, thus presenting all possible choices for solving the optimal power flow problem as an optimization problem. Nevertheless, multi-agent approaches [92] have also recently started gaining attention due to their better scalability characteristics.

Security constraints can have a significant impact on the network usage, therefore corresponding OPF extensions have also been developed. Optimizing the system state, such that security constraints like the N-1 criterion are fulfilled, is not a trivial task from either a TSO or modeling perspective. The simplest approach for a modeler is, rather, to reduce all line capacities by a certain security margin, e.g., 20%. However, this can be too restrictive for some lines and lead to inaccurate results. The most rigorous approach is described by Alsac et al. [93] as an extension to the classical OPF problem, termed the security constraint OPF (SCOPF). Since then, there has been a lot of progress in the field, driven mainly by the highly demanding challenges that are posed by large and more realistic systems. Bhaskar et al. [70] and Capitanescu et al. [94] present comprehensive reviews of the existing approaches for tackling the SCOPF problem as well as corresponding future trends. For instance, Biskas et al. [85] provide a decentralized, linear approach for large, interconnected systems utilizing the LODF sensitivities and a multi-area approach, while Platbrood et al. [95] propose a method for solving the full non-linear and discrete case for large systems using parallel computing techniques. OPF method may also be used for more detailed cascading failure cases [96] either in DC or AC form. Besides OPF, however, various other methods have also been implemented based on network characteristic, load transfer, approximately DC power flow and hidden failure mechanism, DCOPF, as well as ACOPF and load shedding [96].

One further extension to the traditional OPF is the inclusion of uncertainties for the prediction of loads, as well as renewable generation profiles. The increasing penetration of RES and their heavy dependence on weather conditions, which cannot be forecast precisely, require the extension of the classical OPF formulation into a probabilistic OPF (POPF) form which can also handle random variables [97, 98]. The methods to solve a POPF problem can be classified into three categories, namely simulation, analytical and approximation methods [99, 100]. Simulation methods mostly refer to the computationally expensive Monte Carlo simulations, while analytical methods indicate a linearization scheme that will eventually introduce errors. Regarding approximation methods, e.g., the point estimation method, these stand in the middle ground, since they present accurate results with less computational effort than Monte Carlo simulations. However, the higher complexity renders their application impractical for large systems with many random variables. POPF constitutes one very promising area of research for energy modelers for investigating increasing RES-dependent systems.

2.3 Literature review

As described in the previous sections, the operation of power systems, i.e. the control of static power flows over transmission networks, depends on the determination of generation dispatch and the application of congestion management schemes with respect to the physical restrictions of the system. Each of these parts may be applied for different time frames and consider different static snapshots of the system. For very short time frames, however, primary control and more dynamic methods are applied in order to maintain the stability of the system.

The hierarchical approach of the system operation has direct implications on the modeling of power flows. The calculation of static power flows over transmission networks requires the determination of static generator outputs under the physical restrictions of the network, and can be obtained by decomposing the problem in three major modeling blocks (thus reflecting the corresponding operation of power systems). The first component consists of a market coupling model that describes the interaction between the various price zone areas, the second consists of a market model for the single price zones and the third component consists of the short-term congestion management within the individual zones. Figure 2-9 summarizes the main components and interactions that compose a complete power flow model. Inclusion of dynamics in such static approaches is usually included by considering discrete time series of consecutive static states.

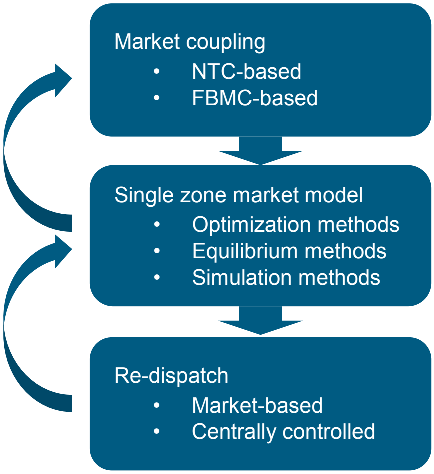

Figure 2-9 The fundamental model components that determine the power flows in a multi-zonal area. All components are inter-dependent and can be modeled either via an integrated or via a multi-level approach.

Since all modeling components depend on each other, the final outcome can be determined either via iterative or via integrated approaches. In an iterative approach, the different modeling levels are linked “softly”, i.e. the output of a top level is used as input for the following level, whose output in turn alters the output of the top level. The iteration can be terminated when the system converges sufficiently to a specific state. Typical iterative approaches include those of Schwippe et al. [101] and that formulated by the University of Duisburg-Essen [102], where an FBMC model for market coupling and an OPF model for re-dispatch are performed sequentially. On the other hand, integrated approaches optimize the operation of the system simultaneously, however usually by reducing the individual component accuracy. Typical integrated approaches constitute the DC and AC OPF or PTDF-based formulations that may consider either detailed or aggregated versions of the transmission network. The implied assumptions behind these methods include nodal pricing scheme for market interaction, no strategic bidding from the market players and re-dispatch based on total cost minimization excluding ramping effects. Despite their relatively simplistic assumptions, these methods are the most popular due to the favorable trade-off between computational performance and accuracy. Moreover, the generic nature of their formulation allows the inclusion of various technical constraints or behavioral extensions in complete systems.

In principle, iterative approaches require higher computational resources; nevertheless they allow more complicated modeling of the individual components. Regarding single market modeling, it can be implemented via optimization, equilibrium, simulation or hybrid methods, where simulation usually refers to agent-based modeling [103]. The high complexity of an accurate market model, however, limits its application to large systems both in terms of the number of variables/players, as well as with respect to time resolution. One of the most simple and scalable ways to describe an electricity market is by assuming perfect competition conditions and describing the entire system as an optimization problem, e.g., with an OPF or unit commitment formulation. Although electricity markets can rarely be considered to have such conditions, this centralized approach gains validity as an ideal case scenario, where all members behave in such a way that the total social welfare is maximized. Regarding modeling of market coupling, two main approaches exist, namely nodal or zonal pricing that can be implemented either via the NTC or the FBMC method. Finally, intra-zonal re-dispatch can be modeled either explicitly via a market-based approach (e.g., counter-trading), or by an integrated approach that simulates market clearing and re-dispatch simultaneously (e.g., OPF or PTDF-based optimization).

In this section, a list of studies related to power flow modeling is reviewed and classified according to different parameters, where only one representative study is presented in case a group of studies based on the same model exist. The most significant characteristic is the applied methodology; therefore a separate table is used for each different method, depicted in tables 2-1, 2-2, 2-3 and 2-4. In each table, the various studies are further classified according to grid resolution, geographical scope, main focus of research and year of publication. Furthermore, additional remarks are added when necessary. In general, the review focuses mostly on studies between 2011 and 2017 due to the high increase of the relative publications during those years.

The various methodologies are classified into four categories, namely the integrated approaches of DC OPF, AC OPF, PTDF-based and network flow. However, not all studies are restricted to one of those methods but may also use modified versions or implement iterative or multi-step approaches. In such cases, where the used method deviates from the standard formulation (e.g. for two-step approaches), the study is included in the category with the most similar congestion management scheme and the additional alterations are noted as remarks. The limited number of non-linear (AC) studies can be explained by the high data and computational requirements relatively to the improvement in accuracy. Therefore, it can be observed that this method is mostly used for technical and rarely for market assessments. Conversely, DC OPF constitutes the most popular power flow method for high spatial coverage, sufficient grid modeling accuracy and minimal data requirements with a relatively low computational demand.

Due to the increasing computational requirements with increasing network sizes, many researchers use smaller network equivalents for performing their studies. There is a growing interest in network reduction techniques that can be adopted from different scientific areas dealing with complex networks, however this topic will not be addressed in detail. In the following tables, a transmission grid is considered detailed when it is represented with the maximum possible geographical fidelity. On the contrary, aggregated grids refer to all models that reduce the original network to smaller, equivalent versions. An aggregated network can be the product of a clustering algorithm using zonal PTDFs, a simple representation via NTCs or even coarser models. Overall, detailed models are scarcer than their coarse counterparts due to the higher requirements for computational resources.

The review concentrates on studies referring to existing systems or future projections, hence geographical representation is sought for both detailed and aggregated networks. Therefore, despite the abundance of studies regarding electricity markets and congestion management, only few exist that focus on real-world systems with accurate geographical data. The review tables reveal a general interest towards the Central Western European (CWE) region, regardless of the research focus of the study. The driving force behind this interest probably originates from the increasing employment of wind farms in the North Sea, as well as the recent developments in the market coupling regulations of that region.

Regarding the research focus, it can be noted that most of the studies using power flow models concentrate on three main areas. The first of these focuses on the implications of different RES infeed scenarios into the grid and constitute the most dominant field of research incorporating power flow models. The power flow models that are applied for RES studies span all the methods that have been discussed so far, from AC OPF to network flow and from high-fidelity grids to very coarse clustering. Considering the highly undesirable characteristics of RES from the system point of view, i.e., their non-dispatchable nature and lack of generation controllability, detailed power flow simulations are seemingly required for an accurate evaluation of a high RES share impact on power systems. Nevertheless, RES integration has been extensively analyzed via aggregated grid representation, even by considering a copper plate assumption [104, 105]. A common pattern that can be observed in the reviewed RES-oriented studies is the connection to network and storage expansion planning, which constitutes the second area of applying power flow models. The volume of the corresponding literature indicates that the most preferred method for network expansion studies consists of the network flow method (not necessarily using NTC values), where no specific lines are proposed as extensions, but rather an increase in capacity of the neighboring power connections is suggested by the model. DCOPF is also used for network expansion studies; however, it can only be part of a more complicated or iterative scheme. The third major application of power flow models is related to the various CM approaches that have been proposed under the demand for liberalization of the electricity market and the directives for closer collaboration between the European market zones. Power flow models are used to assess the implications of market power, price convergence and social welfare from the various CM methods.

Unfortunately, the incorporation of power flow models into energy models does not remove the insufficiency of the latter in comparing the results of similar studies. The high complexity of the models, in conjunction with the lack of direct access to the corresponding implementations and data, reduces the validity of comparing the various studies. DeCarolis et al. [106] and Pfenninger [107] discuss this gap in transparency regarding scientific practice in the area of energy modeling; nevertheless, their conclusions also apply to models that incorporate power flow models. Thereby, a more quantitative evaluation or validation of the presented studies becomes almost impossible. Nevertheless, the literature review can show that the majority of the studies use either the network flow or the DC OPF methods as integrated approaches (or altered versions, depending on the focus of the study). This preference along with the justified theoretical background of the respective, underlying assumptions provides validity indicators for these two approaches.

Consequently, the most frequent assumptions regarding power flow modeling can be also derived from the literature review. Re-dispatch is rarely modeled explicitly, unless it is the actual focus of the study. The DC OPF method implemented on detailed grids includes re-dispatch implicitly, whereas aggregated methods like network flow neglect intra-zonal congestions entirely. Regarding market environment in power flow studies, it is usually modeled merely via a maximization of welfare objective. Moreover, linear description of the participants' behavior is also a common choice. Regarding congestion management, either a nodal pricing scheme is assumed (classical OPF), and thus no explicit modeling is required, or zonal pricing is selected, where only the interconnections are modeled using market-oriented capacities (NTC). Finally, security constraints are usually included either by simply reducing the line capacities in OPF methods or are inherently incorporated in NTC method and therefore no extra modeling effort is required.

Table 2-1 Power flow studies based on the DC OPF method, classified by geographical scope and research focus, where grid resolution refers to the level of the grid representation.

Grid resolution	**Geographical scope**	**Main research focus**	**Study**	**Year of Publication**	**Remarks**
Aggregated	Central West Europe and surroundings	RES, flexible demand	Koch et al. [108]	2015	Two step modeling for single market and market coupling
	Central West Europe	RES, Network planning	Blanco et al. [109]	2011	
	Europe	RES, Network planning	Fürsch et al. [110]	2013	
	Central West Europe	Impact of technical parameters on electricity markets	Gorner et al. [111]	2008	
	England	Evaluation of different pricing schemes and market power	Green et al. [112]	2007	
	UK and Scandinavia	Network expansion planning	Fuchs et al. [113]	2011	
	EU-28	Network expansion planning	Couckuyt et al. [114]	2015	Includes unit commitment modeling

Detailed	Northern Europe	Coordination of wind and hydro power plants	Farahmand et al. [115]	2015	Two step modeling for market and power flows
	Balkans	Network expansion planning	Kanevce et al. [116]	2013	
	Western continental Europe	Multi-purpose, RES	Leuthold et al. [117]	2012	Includes mixed-integer unit commitment formulation
	Continental Europe	Market trading	Hutcheon et al. [118]	2013	Capacities included only for the cross-border lines
	Synchronous European area plus Morocco	Validation of power flow modeling	Lie et al. [119]	2016	Market based modeling of hydro plants

Table 2-2 Power flow studies based on the AC OPF method, classified by geographical scope research focus. Detailed grid models have been primarily used for small geographical regions.

Grid resolution	Geographical scope	Main research focus	Study	Year of Publication	Remarks
Aggregated	District in Norway	RES, storage	Maffei et al. [120]	2014	Application on the distribution level
	Europe	RES, active control of power flows	Roehder et al. [121]	2013	
Detailed	Sardinia	RES	Celli et al. [122]	2013	Two step modeling for unit commitment and static AC flow simulations
	Denmark	RES	Lund et al. [123]	2000	Includes CHP modeling
	Northern Germany	Wind generation	Müller et al. [124]	2017	Based on open data, only static flows for worst case scenarios
	Central Europe	RES, network expansion planning	Eser et al. [125]	2014	
	Italy	Security constraint effect on market prices	Kim et al. [126]	2013	Includes security constraints

Table 2-3 Power flow studies based on the zonal PTDF method, classified by geographical scope and research focus.

Grid resolution	Geographical scope	Main research focus	Study	Year of Publication	Remarks
Aggregated	Central West Europe and surroundings	RES, multi-purpose	Bertsch et al. [127]	2015	
Aggregated	Germany	Simultaneous re-dispatch in multiple TSOs	Kunz et al. [128]	2013	Re-dispatch via counter-trading
Aggregated	Europe	RES	Barth et al. [129]	2009	Includes CHP and unit commitment modeling
Aggregated	Central West Europe	Market coupling	Oggioni et al. [130]	2013	

Table 2-4 Power flow studies based on the network flow method. The studies are classified by geographical scope and research focus, however grid representation is necessarily coarse. Network flow does not always coincide with using NTC values, since the various regions may also be smaller or larger than single countries.

Grid resolution	Geographical scope	Main research focus	Study	Year of Publication	Remarks
Aggregated	Europe	RES, Network expansion planning	Schaber et al. [131]	2012	Partitioning in 83 regions
Aggregated	Europe and Mediterranean sea countries	RES	Haller et al. [132]	2012	Partitioning in 20 regions
Aggregated	United Kingdom	RES	Pfenninger et al. [133]	2015	
Aggregated	Europe	RES	Van Hulle et al. [134]	2009	NTCs
Aggregated	Europe	RES, network expansion planning, storage	Steinke et al. [135]	2013	
Aggregated	Europe	RES, network expansion planning	Becker et al. [136]	2014	Each country represented as a single node
Aggregated	Europe plus Mediterranean countries	RES, storage, network expansion planning	Bussar et al. [137]	2016	
Aggregated	Europe plus Mediterranean countries	RES, storage, network expansion planning	Scholz [138]	2012	

2.4 Chapter summary and discussion

Power systems constitute vast systems which are operated hierarchically in both spatial and temporal dimensions, in order to cope with the high complexity and the inability to store significant amounts of energy. Hence, modeling of power systems follows the same principles of hierarchical decomposition. For time intervals higher than 15 minutes, the system state can be assumed to be quasi-static and the corresponding state equations to be time independent. For each such interval, the equations linking the power quantities to the electrical variables and parameters of the system are described as well as the various numerical methods to solve them. The non-linear nature of the equations, in conjunction with the typically large system sizes results into two main approaches that are usually followed by researchers along with the recent Holomorphic Embedding method, namely iterative methods or linearization approaches. The benefits and drawbacks of the linearization process are analyzed and evaluated.

On the higher temporal level, power systems are operated according to the respective market environment and congestion management scheme. A brief review of the electricity markets operation and modeling is introduced and the various methods of congestion management approaches are presented, with a focus on inter-zonal congestions and the situation in Europe. Besides the market approaches, the classic optimal power flow (OPF) method is presented as an operational as well as a popular modeling tool for power systems. The various numerical approaches for its solution are reviewed and its frequent extensions including inter-temporal, security-constraint and probabilistic OPF are discussed.

Finally, a literature review is conducted regarding the methodologies used for modeling power flows across transmission grids from the research community. It is found that the majority of the studies prefer an integrated, linear optimization approach (either DC OPF or network flow) over a multi-level or iterative one. Considering the lack of quantitative verification attempts in the power system modeling community, these methods gain validity due to their dominant presence in the corresponding literature and their solid theoretical justification.

The information presented in this chapter provides useful insight regarding the selection of the methodologies that would be suitable for the purposes of this thesis. Since this thesis focuses on the investigation of the transmission level of the European grid, the linearized DC flow methodology is considered adequate for modeling the power flows across the system. Moreover the DC OPF approach is selected as the primary tool of combining both generation dispatch and congestion management into an integrated optimization problem. Such a centralized approach becomes more suitable from a modeling perspective, while the underlying assumptions of perfect competition and transparency of the market as well as optimal utilization of the grid infrastructure constitute the targets for system operators as well. Hence, although the allocation of generation and transmission capacity does not explicitly follow the existing processes, it corresponds to an ideal operation of the system in terms of social welfare. Moreover, this approach is found to constitute the principal methodology of modeling the European power system with high spatial resolution in the existing literature.

3 Methodology

The integration of intermittent sources into power systems has emerged as one of the greatest challenges of electric power engineering both from the economic and technical perspectives. The different ways to evaluate the impact of intermittency can be classified into three categories. The first category concerns the grid operation, including frequency and voltage stability or the balancing market [7-9], where the analysis typically focuses on perturbed static systems [10] or probabilistic methods [11]. The second category involves models with usually declined technical modelling detail like dispatch [12, 13] or adequacy forecast models [14]. By this, the time resolution gets coarser and the studied period is increased to one or more years. Hence, the analysis can focus on market implications and security of supply issues. The third category includes investment models, which concentrate on the long-term evolution of the system [15, 16], thereby they usually involve clustering methods in time and space in order to reduce the problem size while retaining critical characteristics of the system [139]. Their goal is to provide development pathways under techno-economical and often political constraints.

The current thesis focuses on the implications of introducing demand response into a system with a high share of VRES and the corresponding contribution into the VRES integration. Such a system requires an analysis on the pan-European level due to the correlations of weather-dependent power generation, especially wind energy, that span on the continental level as well as the increased convergence of the European market zones as mandated by the EU. Nevertheless, a sufficient detail at the spatial and temporal representation of the system is also of critical importance to capture the high variations of wind and solar generation. Due to computational limitations, a dispatch model is used in order to capture the majority of the afore-mentioned dynamics. Unlike integrated methods, a multi-level approach is applied, such that both spatial and temporal resolutions can be sufficiently represented.

The approaches presented in this chapter are described primarily in terms of formulation and implementation where the applicability and justification of the underlying assumptions are analyzed in more detail in chapter 4, where the verification of the selected approaches is conducted. A fundamental assumption regarding market conditions, which applies to all the described model formulations, consists of considering all products to be traded in a wholesale market framework under perfect competition and transparency conditions, i.e. exercising market power is impossible and all participants are merely price takers.

3.1 Generation dispatch modeling

As described in section 2.1, a power system can be operated via three separate market mechanisms, whose products span different time-scales. Despite the difference in temporal scope, all these products are limited to energy trading. Although capacity market mechanisms have also started to be introduced into the European electricity markets [140], these can be interpreted as alternatives to the classical energy-only markets that allow scarcity pricing (i.e. without bidding caps), where such caps are imposed primarily due to political reasons, such that abuse of market power is inhibited. Nevertheless, allowing scarcity pricing is supported as a market scheme by the economic theory to suffice for a secure system operation. Hence, no capacity mechanisms are considered in this thesis and all markets are considered to be energy-only.

The different market levels consist of the long-term, day-ahead and intra-day markets. Due to computational and data limitations, only hourly dynamics are considered therefore intra-day products can be ignored. On the other hand, hedging via futures or other risk related derivatives are ignored as well, since they fall outside of the scope of this thesis. If block and other complex orders are also excluded, all energy is assumed to be traded continuously in hourly products, i.e. only the day-ahead market is considered. This fundamental assumption together with the inclusion of transmission grid constraints (which would be partly resolved by an intra-day market) forms the basis for the selected dispatch problem formulation. Despite the involved simplifications, the selected approach is verified against historical market data, as described in chapter 4.

Under the afore-mentioned assumptions, a single electricity market can be modeled via a social welfare maximization problem, as described by eq. (3-1), (3-2) where g expresses the energy balance constraints. Assuming a price-inelastic demand, which is the typical case for electricity markets with the exception of big industrial consumers, translates the problem to the classical economic dispatch formulation (see eq. (3-3) – (3-5)), where the demand becomes a mere parameter, rather than an optimization variable. Moreover, generation capacity restrictions are introduced in this formulation as well to better reflect actual generation technologies. The original welfare maximization problem is essentially transformed to an equivalent minimization problem of operational costs. Although the supply function of each producer generally depends on the underlying generation technology (e.g. quadratic function for steam turbines), only linear functions are considered for the purposes of this thesis, due to the high computational performance of linear programming algorithms. Thereby, the sum in the objective function of eq. (3-3) is transformed according to eq. (3-6), where $c_{i,t}$ denote the marginal costs of generation for each producer. The adoption of marginal costs as the bidding prices originates from the perfect competition assumption, where each generator's optimal bidding strategy consists of its marginal cost of operation. Moreover, the linear formulation of 1-1 allows the interpretation of the shadow price[1] of the demand from eq. (3-4) as the clearing price of the market.

Problem 1

$$\max_{\{p_{i,t}{}^{L}\},\{p_{i,t}{}^{S}\}} f\left(\{p_{i,t}{}^{L}\},\{p_{i,t}{}^{S}\}\right) = \sum_{t}\left[\sum_{i} U_{i,t}\left(p_{i,t}{}^{L}\right) - \sum_{i} C_{i,t}\left(p_{i,t}{}^{S}\right)\right] \tag{3-1}$$

s.t.

$$g\left(\{p_{i,t}{}^{L}\},\{p_{i,t}{}^{S}\}\right) = \sum_{i} p_{i,t}{}^{L} - \sum_{i} p_{i,t}{}^{S} = 0 \;\forall t \tag{3-2}$$

where $p_{i,t}{}^{L}$ is the consumption of consumer i at time t in MWh

$p_{i,t}{}^{S}$ is the generation of generator i at time t in MWh

$U_{i,t}$ is the utility function of consumer i at time t in €

$C_{i,t}$ is the supply function of generator i at time t in €

[1] In linear programming shadow prices coincide with the Lagrange multipliers of the corresponding affine constraints and can be interpreted as the change in the objective function by marginally relaxing the respective constraint by one unit. For instance, if a constraint is not binding, the corresponding shadow price becomes 0.

Problem 2

$$\min_{\{g_{i,t}\}} f(\{g_{i,t}\}) = \sum_t \sum_i C_{i,t}(g_{i,t}) \tag{3-3}$$

s.t.

$$\sum_i g_{i,t} - \sum_i d_{i,t} = 0 \; \forall t \tag{3-4}$$

$$\underline{P}_{i,t} \leq g_{i,t} \leq \overline{P}_{i,t} \tag{3-5}$$

where $g_{i,t}$ is the generation of generator i at time t in MWh

$C_{i,t}$ is the supply function of generator i at time t in €

$d_{i,t}$ is the consumption of consumer i at time t in MWh

$\underline{P}_{i,t}$ is the minimum allowed generation of generator i at time t in MW (typically 0)

$\overline{P}_{i,t}$ is the maximum generation capacity of generator i at time t in MW

$$f = \sum_t \sum_i C_{i,t}(g_{i,t}) \rightarrow f = \sum_t \sum_i c_{i,t} \cdot g_{i,t} \tag{3-6}$$

where $c_{i,t}$ is the marginal cost of operation for generator i at time t in €/MWh

Although the linear formulation of 1-1 would suffice to describe the electricity market operation of a single zone with a linear formulation, technology-specific components may be either implicitly overestimated or not addressed adequately. The existing generation technologies can be classified in three principal categories with regard to their modeling, namely thermal, hydro and VRES technologies. Since all generation technologies are essentially transforming energy from a primary source form (e.g. natural gas) into electricity, the fuel provision along with the technology-specific transformation constraints varies among the afore-mentioned categories.

Thermal units may include either steam turbine, combustion or closed-cycle technologies, where the fuel may have either fossil (e.g. coal) or renewable (e.g. biogas) origins. In all cases nevertheless, fuel provision is considered to be unlimited, since its supply is considered directly controllable and the fuel can be stored relatively easily in significant amounts. Therefore, eq. (3-5) can be merely replaced by

$$\underline{P}_{i,t} \leq g_{i,t} \leq \overline{P}_i \tag{3-7}$$

where $\overline{P}_i$ is the nominal capacity of generator i in MW.

Although such a description would suffice for combustion engines, additional generation constraints would be required for the less flexible steam turbine technologies that would require a unit-commitment (UC) formulation. Such constraints may include power ramping limitations, minimum load (i.e. power output) restrictions or additional start-up and shut-down costs (cumulatively referred to as cycling costs). The most accurate way to model UC-related constraints would be by introducing additional binary variables for each generator and time snapshot that would indicate their status, either on or off. However, such a formulation would pose significant restrictions to the scale of the investigated system due to computational limitations stemming from the introduction of integer variables. Alternative approximations to such a mixed-integer linear programming (MILP) approach that can retain the desired linear characteristics have been developed for power plant aggregates. Such methods include the "two-variable" [141] and "effective generation" [142] approaches. Both of these methods have been compared to the more accurate MILP formulation for a system with high levels of wind generation by Göransson [142], where the loss of accuracy in estimating the total cycling costs against the increase in computational performance is analyzed.

For the purposes of this thesis, the "effective generation" approach is selected due to its favoring relation between cycling costs inclusion and computational performance. The central idea behind this approach consists of replacing the actual generation variable $g_{i,t}$ with an effective generation variable ${g_{i,t}}^{eff}$ in the objective function. The new variable can incorporate additional costs related to technology-specific cycling costs and minimum load but only affects the actual generation indirectly. The additional constraints for the new variable are shown in eq. (3-8) and (3-9), while typical parameter values for the corresponding constraints are shown in table 3-1.

$$ {g_{i,t}}^{eff} \geq g_{i,t} \tag{3-8} $$

$$ {g_{i,t}}^{eff} \geq N \cdot g_{i,t-k} \qquad \forall k \leq K \tag{3-9} $$

where N is the minimum load of the units in the corresponding aggregate

K is the start-up time of the units in the corresponding aggregate

Table 3-1 Modeling parameters for the "effective generation" approximation of the UC formulation as described by eq. (3-8) and (3-9) [143].

Technology	Fuel	N	K
Steam turbine	Nuclear	80%	24
	Coal	40%	6
Closed-cycle	Natural Gas	50%	6

Regarding hydro power plants, these can be dispatched similarly to thermal plants, however the fuel provision cannot be considered unlimited due to limited storage capacity as well as uncontrollable fuel supply (water). For this reason, hydro plants are modeled as storage units, where additional variables for the charging and discharging rates as well as the state-of-charge along with their respective capacity limits are further required as shown in eq. (3-10) – (3-13) which refer to hourly time steps.

$$0 \leq sud_{i,t} \leq \bar{S}_{i,t} \tag{3-10}$$

$$0 \leq suc_{i,t} \leq \bar{S}_{i,t} \tag{3-11}$$

$$0 \leq soc_{i,t} \leq \overline{SOC}_{i,t} \tag{3-12}$$

$$soc_{i,t} = soc_{i,t-1} + \eta_{i,t}{}^{store} \cdot suc_{i,t} - sud_{i,t} + inflow_{i,t} - spillage_{i,t} \tag{3-13}$$

where $sud_{i,t}$ is the discharging rate of storage unit i at time t in MW

$\bar{S}_{i,t}$ is the maximum charging/discharging capacity of storage unit i at time t in MW

$suc_{i,t}$ the charging rate of storage unit i at time t in MW

$soc_{i,t}$ the state of charge of storage unit i at time t in MWh

$\overline{SOC}_{i,t}$ is the maximum storage capacity of storage unit i at time t in MWh

η^{store} is the charging efficiency

$inflow_{i,t}$ is the primary energy inflow rate for storage unit i at time t in MW

$spillage_{i,t}$ is an optimization variable accounting for the inflow spillage of storage unit i at time t in MW

for $t = 0$ the term soc_{t-1} can be either set to a fixed initial state of charge or set to be equal to the value of the last time step soc_T, thus implying cyclic operation

Similarly to thermal units, hydro plants operation may bear operational costs as well. These should also be reflected in the objective function (see eq. (3-14)), while the energy conservation constraint from eq. (3-4) should be extended as well (see eq. (3-15)).

$$f = \sum_t \left[\sum_i c_{i,t} \cdot g_{i,t}{}^{eff} + \sum_i c_{i,t} \cdot sud_{i,t} \right] \tag{3-14}$$

$$\sum_i g_{i,t} + \sum_i sud_{i,t} - \sum_i suc_{i,t} - \sum_i d_{i,t} = 0 \; \forall t \tag{3-15}$$

The last type of generation technology consists of generators with zero or very limited fuel storage capabilities, e.g. PV or wind turbines. In such cases, eq. (3-5) and (3-6) can still be applied, however the term $\overline{P}_{i,t}$ does not refer to an installed generation capacity but rather to an available generation potential that follows the inflow of the primary energy source. For instance, the respective constraints for a wind turbine could be written as $\overline{P}_{i,t} = \bar{P}_i \cdot cf_{i,t}$, where $\overline{P}_i$ is the installed capacity of turbine i and $cf_{i,t}$ the corresponding time-varying capacity factor that depends on the local weather conditions.

3.1.1 Combined heat and power generation

Although most of the power plants operate to provide power to the electricity system, some thermal power plants exploit part of the fuel energy to provide thermal energy to customers. This additional source of revenue is not reflected in the afore-mentioned dispatch formulations, however it may lead to significantly misestimating the output of such combined heat and power (CHP) plants.

CHP operation can be modeled in different detail, depending on the research focus. In principle, several additional model components need to be added such as a spatially and temporally resolved heat demand served by CHP plants, corresponding network and storage infrastructure, additional operational constraints of CHP plants (e.g., extraction or back pressure method [144]) and ideally a heat market, which in most European countries including Germany has not been formed. Moreover, plant operators typically show distinct behaviors depending on the primary product and source of profit. For instance, relatively big coal power plants can be considered as “power-driven” plants where heat can be considered as byproduct whereas relatively small gas plants may be considered “heat-driven” with electricity being the byproduct. However, there is hardly a consistent criterion that can define whether a CHP plant can be classified to one of these categories. For these reasons, CHP operation is not modeled in the same way over the literature. In the context of power system modeling however, it typically falls into the following three categories:

- No special CHP modeling [137, 145-149], where the limitations of the model are merely acknowledged
- Exogenous feed-in or must-run constraints [41, 117, 150, 151]
- Sophisticated models or co-optimization of heat and power generation [110, 123, 152-155], potentially including heat storage as well

Considering that the driving reason for modeling CHP operation lies merely at the impact of CHP generation in the power market, the exogenous feed-in approach becomes the most prominent candidate for including the respective special conditions without importing unnecessary complexity into the model. Two ways are selected to incorporate CHP-related constraints into a linear model. The first method assumes a strict must-run condition for each CHP plant based on an assigned heat demand profile (which additionally need the inclusion of costly demand reserves to ensure feasible optimization solutions) and a constant ratio between the power and heat outputs, independent of the operational point (Stromkennzahl). The second method imposes a time-varying reduction on the available power capacity of steam turbine and combined-cycle power plants. This reduction is caused by the heat output requirements covered by steam extraction that can no longer be used to generate electricity. This reduction is typically expressed by a coefficient (Stromverlustkennziffer) defined by eq. (3-16) [156], where P_0 is the nominal power capacity (in condensation operation) and P and Q the power and heat outputs correspondingly. Although this coefficient depends on both the operational point as well as the corresponding technology [156], a constant average value of 0.185 [156] is assumed.

$$S(t) = \frac{P_0 - P(t)}{Q(t)} \tag{3-16}$$

For the implementation of the first method, a top-down approach is selected to assign must-run generation profiles to all CHP plants. A methodology to generate overall heat demand profiles can provide only marginal benefits to the specific problem, since only the heat demand covered by CHP plants is required while also the underlying district-heat networks are generally difficult to obtain. Therefore, the selected approach is directly based on national statistics that concern only CHP operation. The methodology consists of a temporal and a spatial dimension, where the spatial refers to distributing national energy statistics to each plant whereas the temporal to assigning time-varying heat demand patterns.

Regarding the temporal dimension, a normalized profile is assigned to each power plant based on the ambient temperature at that location. The methodology follows the rationale of NEP [154], where it is assumed that 9% of the total heat demand is related to water heating and is constant over the year, while the rest of the demand fluctuates based on an effective temperature, defined by eq. (3-17), as long as this temperature does not exceed a threshold of 16 ^{0}C, beyond which space heating requirements drop to zero. The effective temperature, in addition to the ambient temperature also takes into consideration the corresponding temperature of the previous day, which reflects the heat stored inside the buildings. Hourly ambient temperature profiles are considered using the Eurocordex regional climate model (RCM) with driving model "MPI-M-MPI-ESM-LR" and experiment "rcp26" , which are provided for every point of a 0.11^{o} (~12.5 km) grid over Europe and 3 hours resolution [157]. In order to assign profiles to each power plant, their positions are translated to the Eurocordex rotated pole system [158, 159] and profiles are calculated for each point using bilinear interpolation.

$$T_{eff}(t) = 0.7 \cdot T_{ambient}(t) + 0.3 \cdot T_{previous\ day\ average} \tag{3-17}$$

The spatial dimension consists of scaling the generated normalized profiles such that they meet the national statistics under the technical and methodology's constraints. Regarding national statistics, information is available from [160], where the annual power generation from CHP plants is reported per energy carrier. Scaling the calculated effective temperature ($T_{eff,t}$) profiles taking into account the NEP approach translates into finding coefficients α and β for each generator in eq. (3-18) while satisfying equations (3-19), (3-20) and (3-21).

$$P_{min,g}(t) = \begin{cases} \alpha_g \cdot \left(T_{eff,g}(t) - T_{thres}\right) + \beta_g, & T_{eff,g}(t) \leq T_{thres} \\ \beta_g, & T_{eff,g}(t) > T_{thres} \end{cases} \tag{3-18}$$

$$\sum_g \int_t P_{min,g}(t)\, dt = P_{total,C} \qquad \forall g \in C \tag{3-19}$$

$$\sum_g \beta_g \cdot \Delta t = c \cdot P_{total,C} \qquad \forall g \in C \tag{3-20}$$

$$P_{min,g}(t) \leq P_{nom,g} \qquad \forall t \tag{3-21}$$

where g refers to each power plant belonging to the energy carrier C (e.g. natural gas), T_{thres} is 16 ^{0}C, c is 0.09 and Δt is 8760 hours for the year 2015.

Considering the non-linearity stemming from the capacity limits in eq. (3-21) as well as the lack of information in how total generation for a fuel type is distributed among the individual generators, the system can be solved by decoupling equations (3-19) and (3-20) for each generator by assigning a constant distribution factor using the power plant capacities as weights. Hence, they can be written in the form of (3-22), (3-23) and (3-24).

$$\int_t P_{min,g}(t)\ dt = P_{total,g} \qquad \forall g \in C \tag{3-22}$$

$$\beta_g \cdot \Delta t = c \cdot P_{total,g} \qquad \forall g \in C \tag{3-23}$$

$$P_{total,g} = \frac{P_{nom,g}}{\sum_g P_{nom,g}} \cdot P_{total,C} \qquad \forall g \in C \tag{3-24}$$

Finding the coefficients α and β in eq. (3-18) can be then accomplished iteratively due to the non-linearity of capacity limits. The process is shown in figure 3-1, where β is increased by at least 0.001 to avoid slow convergence near the convergence point.

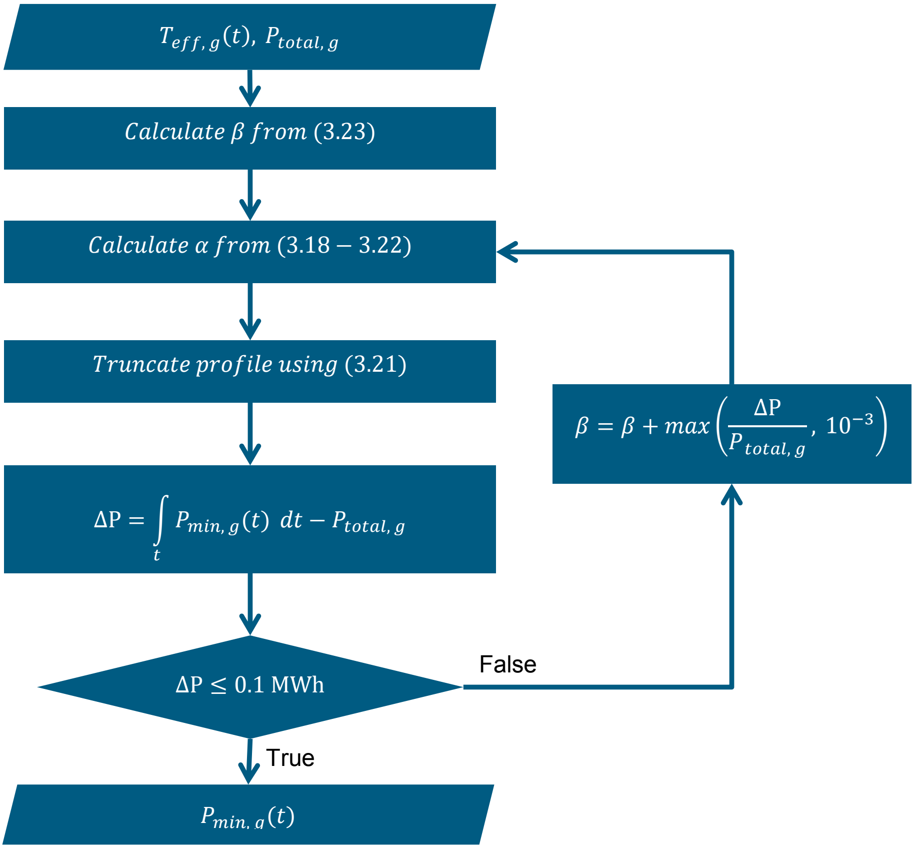

Figure 3-1 Diagram for generating the must-run profiles for CHP generation from the corresponding effective ambient temperatures.

The resulting profiles can also be used to calculate the reduced capacity for steam turbine or combined-cycle CHP plants from eq. (3-16). Figure 3-2 shows the must-run constraints as well as the capacity reduction for a 406 MW, hard coal, steam turbine, CHP plant in Altbach, Germany for the year 2010. It can be observed that the must-run constraints are rather low

(< 20%) and would be insignificant in a unit-commitment formulation but regarding the capacity reduction, it can be seen that this may drop up to 10%.

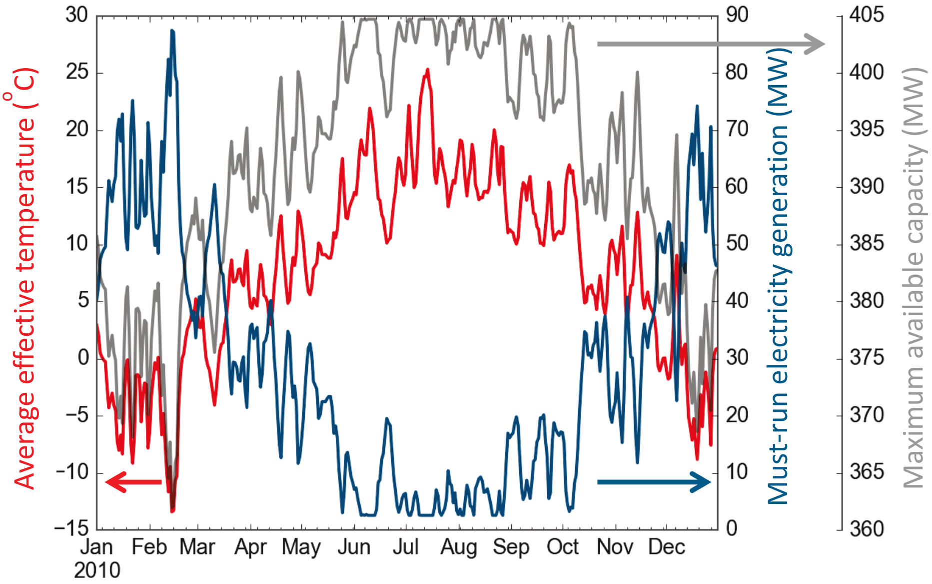

Figure 3-2 Minimum must-run constraints and capacity reduction for a hard coal, steam turbine, CHP generator in Altbach (BNetzA ID – BNA0019) with 406 MW capacity for the year 2010.

3.2 Modeling of transmission grid constraints

The economic dispatch problem described in section 3.1 assumes no restrictions in power transfer between generators and consumers within the single market pool. Nevertheless, such limitations can be also included by merely extending the corresponding formulation, which can be accomplished by introducing an additional nodal index to all equations as well as additional constraints reflecting the power flow transfer laws. As described in chapter 2, the most frequently selected methodologies to model transmission grid constraints consist of the DCOPF, ACOPF, PTDF and “network flow” methodologies. Considering that ACOPF requires a non-linear description and PTDF constitutes an equivalent formulation to DCOPF, only the DCOPF and “network flow” approaches are considered in this thesis.

The “network flow” constitutes the typical approach to model the transfer of goods or other elements in economics and computer science. The fundamental principle behind this approach assumes that a quantity can be transferred between two nodes through a link or channel and that the corresponding flow rate can be directly controlled by the link alone and only limited by a maximum flow rate capacity. Thereby, the “network flow” method can be implemented by merely introducing independent flow variables $f_{i,t}$, along with the corresponding constraints as shown in eq. (3-25).

$$\underline{F}_{i,t} \leq f_{i,t} \leq \overline{F}_{i,t} \tag{3-25}$$

where $\underline{F}_{i,t}$ is the minimum allowed flow of link i at time t for the defined direction in MW

$f_{i,t}$ is the flow rate of link i at time t in MW

$\overline{F}_{i,t}$ is the maximum allowed flow of link i at time t for the defined direction in MW

In addition, the energy balance constraint needs to be updated for a multi-nodal system in order to accommodate the corresponding power exchanges. The modified constraint is shown in eq. (3-26), where energy conservation is enforced to all nodes.

$$\sum_i g_{i,n,t} + \sum_i sud_{i,n,t} - \sum_i suc_{i,n,t} - \sum_l K_{nl} f_{l,t} - \sum_i d_{i,t} = 0 \ \forall n, t \tag{3-26}$$

where K_{nl} is the incidence matrix for the network graph that takes the value 1 if the link departs from node n and -1 if the link arrives at it

l refers to all links adjacent to node n

The dual variable associated with eq. (3-26) can still be interpreted as the clearing price of the system. Nevertheless, a spatial dimension has been added as well, meaning that all nodes have their individual nodal prices (or zonal if the nodes represent market zones) that may differ from each other. With regard to power systems, the "network flow" approach appears useful for modeling market coupling, where the interconnections hold a more economic interpretation as described in section 2.2.3.

Regarding the DCOPF method, this can be formulated in a similar manner, where the main difference originates from the interdependence of the individual power flows over AC transmission lines as described in section 2.2.1. Therefore, although the constraints described by (3-25) and (3-26) remain unaltered, the flow variable f cannot be considered independent but rather related to an additional independent variable θ that stands for the nodal voltage angles. The relationship is expressed by the DC approximation shown in eq. (3-27), while an additional constraint for the angle of the slack node is required similarly to the static DC flow.

$$f_{l,t} = \frac{\theta_{n0,t} - \theta_{n1,t}}{x_l} \tag{3-27}$$

where x_l is the per unit reactance of line l

The two types of power flow modeling, i.e. "network flow" and DCOPF, can also be combined within a single framework. For instance, a transmission grid with mixed AC and HVDC lines can be represented by using the appropriate methodology for each line based on its type, since power flows over HVDC lines can be controlled directly and independently of the surrounding network, and therefore modeled using the "network flow" approach. Another potential application consists of a "hybrid" model where specific zones are represented in detail by their transmission grids, while others are represented as single nodes assuming copper plate conditions within the zones. The flow constraints between such differently modeled zones may not be sufficiently represented by the individual cross-border line capacities alone due to security constraints. Therefore, the application of cumulative constraints using values calculated by a CM scheme (see section 2.2.3), as shown in eq. (3-28), may result in more representative interconnection capacities.

$$\underline{NTC}_{L,t} \leq \sum_{l \in L} f_{l,t} \leq \overline{NTC}_{L,t} \tag{3-28}$$

where L is the set of cross-border lines for an interconnection

NTC is the total secure capacity of the interconnection

3.3 Software implementation

Models that are implemented based on the afore-mentioned formulations may be applied to large networks and systems comprising of thousands of generators and lines, thus forming problems with several millions of variables and respective constraints. Therefore, solving such systems within a reasonable time require efficient optimization and data handling software. For the purposes of this thesis, gurobi [161] is used as the respective optimization software and pyomo [162] as the algebraic modeling language software to generate the desired models. Moreover, the energy modeling framework PyPSA [163] is used as the tool to handle the power system data and set up the corresponding optimization problems via pyomo. PyPSA is an open source energy modeling framework written in the python programming language based on the pandas, networkx, numpy and scipy libraries. Regarding power system optimization, it can be used for both linear dispatch and investment modeling, including the network flow and DCOPF formulations as well as the storage-related constraints. Its open source nature allows the modification and extension of the framework, e.g. adding the afore-mentioned linear UC formulation or the formulations described in the rest of this chapter. Finally, the Message Passing Interface (MPI) 3 library port for python called mpi4py [164] is used to split problems with temporally decoupled states into multiple sub-problems that can be solved simultaneously in different processors.

3.4 The multi-level approach

One of the most significant advantages of linear optimization problems consists of the existence of computationally powerful approaches to solve them. Nevertheless, considering that a detailed pan-European problem would imply several hundreds of millions of variables, the described methodology may lead to practically unsolvable problems with the current technological level of computational resources.

For this reason, a novel multi-level approach is developed such that both the temporal and spatial resolution detail is maintained in high levels, while the total problem is solved in reasonable time. The central idea consists of splitting the original problem into smaller parts with different spatial resolution and temporal coupling and solving them sequentially. By these means, the spatial and temporal dynamics, although not considered simultaneously, their interaction can be still captured to a considerable degree.

The first level consists of the “country” or “market” level, where the European power system is represented by market zones that coincide with the existing country boundaries. The problem formulation follows the description below, where the linear UC methodology is used for the generation dispatch, hydro plants are modeled as storage units with yearly horizon and the grid via the “network flow” approach. The goal of this level is to calculate the scheduled generation of power plants including hydro as well as thermal plant constraints, within a market coupling framework. Grid restrictions are still represented between countries, although with a more economic interpretation. Nevertheless, due to historical developments, the grid tends to be weaker on the interconnections rather than within countries, hence the selected regionalization is considered sufficient. In addition to the generation scheduling, market prices for each zone can also be computed and used by the following model levels.

Problem – “country” level

$$\min \sum_{t} \sum_{n} \left(\sum_{i} c_{i,n,t} \cdot g_{i,n,t}{}^{eff} + \sum_{i} c_{i,n,t} \cdot sud_{i,n,t} \right) \tag{3-29}$$

s.t.
eq, (3-7)-(3-9) – linear UC constraints
eq. (3-10)-(3-13), storage unit constraints
eq. (3-25), (3-26) – “network flow” grid constraints

where
$$\underline{P}_{i,n,t} = \begin{cases} 0.45 \cdot P_i^{nom} & if\ i\ is\ Nuclear \\ 0 & else \end{cases} \tag{3-30}$$

The constraints in (3-30) express the explicit enforcement of must-run conditions for nuclear power plants at 45% of their nominal capacity at all times.

The second, “grid”, modeling level considers the hydro scheduling information from the “country” level and incorporates it in a LOPF formulation that can take the complete transmission grid into account. The power injection from hydro plants into the system is incorporated as dispatchable generation with individual capacity limitations as well as cumulative constraints that respect the grouped (national) scheduling. In case of negative generation (i.e. charging/pumping) the power withdrawal rate from the system is added to the existing demand. Introducing hydro plants with this method essentially allows the decoupling of the various time steps of the overall problem. The individual hourly sub-problems can therefore be computed independently, since the minimum yearly solution equals the sum of the minimum hourly solutions. The most significant output of this level consists of the resulting nodal prices that can be used to identify the major bottlenecks of the system.

Problem – “grid” level

$$\min \sum_{n} \left(\sum_{i} c_{i,n} \cdot g_{i,n} + \sum_{i} c_{i,n} \cdot g_{i,n}{}^{su} \right) \quad \forall t \in \{0,1,2,\dots,8759\ (or\ 8783)\} \tag{3-31}$$

s.t.

eq, (3-7), (3-30) – generation capacities

eq. (3-25)-(3-27) – DC flow

$$\sum_{i \in G,t} g_{i,t}{}^{su} \leq \max\left(0, g_{G,t}{}^{su}\right) \tag{3-32}$$

$$d_{i,t} \leftarrow d_{i,t} - \min\left(0, g_{i,t}{}^{PHS,scheduled}\right),$$ PHS pumping is added to demand

where $g_{i,t}{}^{su}$ and $g_{G,t}{}^{su}$ are the scheduled generation for storage unit i and group of storage units G respectively at time t in MW

G refers to a group of storage units

Although the results of the “grid” level constitute a reasonable first approximation of the system operation, the contribution of hydro plants in relieving congestion is not effectively taken into account. To this end, the problem is reduced in space such that multiple time steps can be solved simultaneously. Hydro plants can then be considered as storage units, where collective constraints on the state-of-charge variables as shown in eq. (3-34) can be added to respect the long-term hydro scheduling as well as long-term energy balance. Moreover, the generation dispatch is also respecting the corresponding scheduling from the “country” level model, thus the formulation takes the form of a redispatch problem as shown in eq. (3-35)-(3-38). This formulation allows the final generation of a unit to deviate from the original scheduling only in the case of grid congestion, since ramping a generator either up or down is associated with additional costs to the system. Finally, demand flexibility can also be introduced at this level, since multiple time steps can be coupled in a single optimization. Nevertheless, a more elaborate description of the corresponding demand response approaches is presented in section 3.5.

Problem – "clusters" level (for daily horizon)

$$\min \sum_{t}^{t+T} \sum_{n} \left(\sum_{i} c_{i,n,t} \cdot g_{i,n,t}{}^{up} + \sum_{i} zp_{i,n,t} \cdot g_{i,n,t}{}^{down} + \sum_{i} c_{i,n,t} \cdot sud_{i,n,t} \right) \ \forall t \in \{0, 24, 48, \dots, 8736\ (or\ 8760)\} \tag{3-33}$$

s.t.

(3-7) – generation capacities

eq. (3-10)-(3-13), storage unit constraints

(3-25), (3-27) – DC flow

$$(1 - tol) \cdot soc_{G,tt} \leq \sum_{i \in G,tt} soc_{i,tt} \leq (1 + tol) \cdot soc_{G,tt} \quad \forall tt \in \{0, 24, 48, \dots, 8760\ (or\ 8784)\} \tag{3-34}$$

$$\sum_{i} g_{i,n,t} + \sum_{i} g_{i,n,t}{}^{up} - \sum_{i} g_{i,n,t}{}^{down} + \sum_{i} sud_{i,n,t} - \sum_{i} suc_{i,n,t} - \sum_{l} K_{nl} f_{l,t} - \sum_{i} d_{i,t} = 0 \tag{3-35}$$

$$0 \leq g_{i,n,t}{}^{up} \leq \overline{P}_{\mathrm{i,n,t}} - g_{i,n,t} \tag{3-36}$$

$$0 \leq g_{i,n,t}{}^{down} \leq g_{i,n,t} - \underline{P}_{i,n,t} \tag{3-37}$$

$$\sum_{i \in G,t} g_{i,t} = gs_{G,t} \tag{3-38}$$

constraints related to flexible demand (discussed in section 3.5)

where $zp_{i,n,t}$ is the zonal price corresponding to generator i in node n at time t in €/MWh

$g_{i,t}{}^{up}$ and $g_{i,t}{}^{down}$ refer to the upwards and downwards redispatch of generator i at time t in MW

T is the storage operation horizon (here 24 hours)

tol is a tolerance for numerical errors, e.g. 0.01

$gs_{i,t}$ and $gs_{G,t}$ is the scheduled generation of generator i and group of generators G respectively at time t in MW

The reduction in space can be performed such that the major grid bottlenecks of the system are preserved. To this end, the average nodal prices from the "grid" level are used as weighting factors to cluster the grid nodes by applying a spatial k-means algorithm [165]. Nevertheless, although such a clustering methodology can estimate the topology of an equivalent, reduced grid, the estimation of the equivalent lines' electrical parameters remains non-trivial. For this thesis, a simplified approach is selected, where the equivalent transfer capacity is taken as the 65% of the sum of the cross-border line capacities due to security considerations [166]. Regarding the estimation of an equivalent reactance, this is accomplished by assuming equivalent virtual 380kV lines connecting the regions' centroids. In this way, the cross-border lines are essentially extended such that the distance between regions is also reflected in the reactance calculation as shown in eq. (3-39), where the denominator indicates the number of equivalent typical 380kV lines. A detour factor of 1.25 is further applied to the "beeline" distance calculation since grid lines typically follow geographical characteristics that result in higher actual distances than the shortest path [167].

$$x_{line\_eq} = \frac{length_{line\_eq}\,[km] \cdot \hat{x}_{380kV}\left[{}^{Ohm}/_{km}\right]}{capacity_{line\_eq}[MW] \Big/ capacity_{380kV}[MW]} \tag{3-39}$$

The resulting information from the application of the "cluster" level can be introduced to a fourth, "redispatch", modeling level where a detailed version of the transmission grid is used. The corresponding formulation resembles the "grid" level, however instead of merely dispatching generators, a redispatch problem is solved similarly to the "clusters" level. Regarding the demand, collective constraints are introduced as shown in eq. (3-41). The results of this level are considered to represent the final, calculated state of the power system. Hence various information about the system may be extracted like VRES curtailments, line loadings and generators output.

Problem – "redispatch" level

$$\min \sum_n \left(\sum_i c_{i,n,t} \cdot g_{i,n,t}{}^{up} + \sum_i zp_{i,n,t} \cdot g_{i,n,t}{}^{down} \right) \ \forall t \in \{0,1,2,\dots,8759\ (or\ 8783)\} \tag{3-40}$$

(3-7), (3-35)-(3-38) – generation redispatch constraints

s.t. $g_{i,t} = gs_{i,t} \quad \forall i \notin G$ – redispatch condition for explicit generators

(3-32) – Storage units as generators/demand

$$\sum_{i \in G,t} d_{i,t} = d_{G,t} \tag{3-41}$$

where $d_{i,t}$ is an optimization variable constrained by $d_{G,t}$

A comprehensive diagram of the described multi-level model is summarized in figure 3-3, where the linking among the various levels is depicted as well. Furthermore, the conceptual modeling of the different system components for each level is further described in table 3-2. It can be seen that although the different modeling levels may share common approaches, each level constitutes a distinct formulation of the same system, depending on the respective focal point.

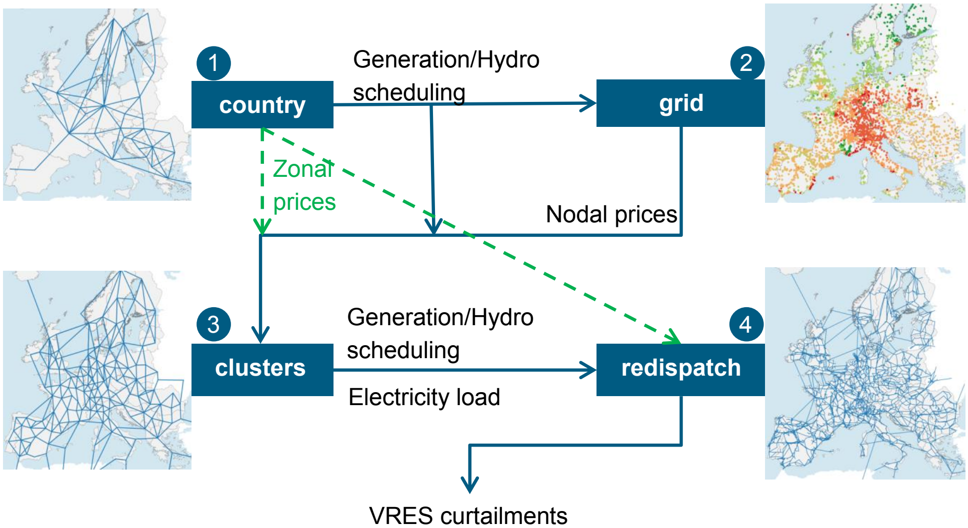

Figure 3-3 Soft linking diagram between the four levels of the multi-level modeling approach.

Table 3-2 The different ways to model the power system components for the four levels of the multi-level modeling approach. The output of each level may be used by a subsequent levels as shown in figure 3-3.

level	thermal genera-tion	hydro genera-tion	VRES genera-tion	demand	grid	optimi-zation horizon	output
country	linear UC	storages	linear	fixed	network flow – countries	1 year	scheduled generation, zonal prices
grid	linear	genera-tors	linear	fixed	DC – full grid	1 hour	nodal prices
clusters	redis-patch per group	storages	redis-patch per group	flexible	DC – reduced grid	1 day	scheduled generation, demand
redis-patch	redis-patch	genera-tors	redis-patch per group	fixed per group	DC – full grid	1 hour	VRES cur-tailments

3.5 Flexible demand

Although the current electricity demand at the transmission level may be considered relatively predictable and price inelastic, future consumers may show a more flexible behavior. Developing a supply system that relies heavily on inflexible sources (like the current wind and PV technologies) may lead to energy imbalance issues which in turn can pose significant dangers to the secure operation of the system. Traditional sources of system flexibility include the transmission grid (i.e. energy trading), energy storage (e.g. batteries) and demand side management (DSM), where the grid equilibrates spatial variability and energy storage temporal variability respectively. DSM aims at addressing temporal variability as well; however, since it does necessarily rely on energy storage, it can be more energy efficient.

DSM technologies may vary significantly depending on the individual application and can span from the residential sector up to large industrial consumers. Despite the variety in implementing DSM behavior [168, 169], its effects can be typically classified into two categories from the system perspective, namely load curtailment and load shifting. Load curtailment correspond to the willingness of a consumer to reduce their demand at a specific time interval given a respective signal from the system, e.g. if the electricity price exceeds a given threshold. On the other hand, load shifting refers to the responsiveness of the consumer by deferring part of their demand either forward or backward in time, typically spanning a few minutes or hours. In this study only the second category of demand flexibility is considered, hence it is assumed that consumers are not willing to curtail their demand unless it is necessary due to adequacy issues. Such behavior is implemented by assigning a high cost, 1000 €/MWh [170], to the loss-of-load instances, hence load shifting will prioritize the reduction of such instances.

In contrast to load curtailment, load shifting does not alter the total consumption but rather shifts part of the demand to different times, when the supply may be more abundant and thus cheaper. Since this thesis attempts to assess the flexibility of demand merely as a tool for higher integration of VRES, only a generic, technology-agnostic approach for modeling DSM is pursued. Such approaches can be classified into two categories. The decoupled approach relies on price signals that are assumed to be unaffected by the shifting itself (due to its assumed small scale). Advantages of this include the decoupling of time steps, which may lead to better performance and thus allow higher spatial detail, however drawbacks may include high sensitivity to the involved parameters [145] and potential DSM shifting synchronization that could lead to sub-optimal system operation [171]. Moreover, total energy consumption before and after shifting may not be explicitly preserved. On the other hand, in the coupled approach, the generation and demand are optimized simultaneously, thus their interaction is considered as well. Coupling demand response together with generation allows the optimization of DSM utilization from the system perspective and is therefore selected to constitute the investigated methodology for this thesis.

Various methodologies have been implemented in the literature to introduce demand response into power system optimization models. Such methodologies include formulations with hourly power limitations and overall energy balance constraints but without specific shifting duration limits [172, 173], modeling via virtual storages [174, 175] or formulations where shifting duration limitations are considered [143, 176].

For the purposes of this thesis two approaches are implemented and compared by applying them to a selected system. The first approach follows the virtual storage rationale, where for each flexible consumer a virtual storage unit is introduced as in eq. (3-10)-(3-13), however it is set such that discharging is not possible. The shifting duration and load recovery constraints are introduced by setting fixed constraints on the state-of-charge level of the virtual storage buffers at the beginning and end of time periods that are set explicitly. The starting state-of-charge level is set to zero, whereas the final level is set equal to the total amount of deferrable load for that period (see eq. (3-42)). Moreover, additional ramping constraints on the charging rate between the time windows are imposed as well (see eq. (3-43)), to avoid undesirable demand ramping. The explicit selection of time windows may lead to a sub-optimal utilization of the available demand flexibility, nevertheless this shortcoming is compensated by the computational benefits of decoupled time periods that can allow its application to systems with high spatial resolution.

$$\begin{cases} soc_{i,t} = 0 \\ soc_{i,t+T} = D_t \end{cases} \quad \forall t \in \{0, T, 2T, \dots\} \tag{3-42}$$

$$suc_{i,t+T} - r \leq suc_{i,t+T+1} \leq suc_{i,t+T} + r \quad \forall t \in \{0, T, 2T, \dots\} \tag{3-43}$$

where D_t is the total deferrable demand between the shifting period $[t, t+T]$ in MWh

r is the ramping constraint in MW

The second approach that is implemented regarding modeling demand response follows the methodology introduced by Zerrahn et al. [176] and applied by the DIETER model [177]. This approach can be described by the equations (3-44)-(3-47), where the central idea consists of introducing upwards and downwards shifting variables with their corresponding power capacities and allow them to be used only within a fixed time window surrounding each time step. Although this approach constitutes a more accurate description of the DSM behavior, the corresponding computational requirements become higher, mainly due to the second time index tt, which can limit both the size of the of the investigated system as well as shifting window range.

$$DSM_t{}^{up} = \sum_{tt=t-L}^{t+L} DSM_{t,tt}{}^{do} \quad \forall t \tag{3-44}$$

$$DSM_t{}^{up} \leq \overline{DSM}^{up} \quad \forall t \tag{3-45}$$

$$\sum_{t=tt-L}^{tt+L} DSM_{t,tt}{}^{do} \leq \overline{DSM}^{do} \ \forall tt \tag{3-46}$$

$$DSM_{tt}{}^{up} + \sum_{t=tt-L}^{tt+L} DSM_{t,tt}{}^{do} \leq max\left\{\overline{DSM}^{up}, \overline{DSM}^{do}\right\} \quad \forall tt \tag{3-47}$$

where $DSM_t{}^{up}, DSM_{t,tt}{}^{do}$ are the DSM variables for upwards and downwards shifting respectively

$\overline{DSM}^{up}, \overline{DSM}^{do}$ are the maximum DSM power capacities for upwards and downwards shifting respectively

L is the maximum shifting duration

3.6 Chapter summary

In this chapter the modeling methodology that is used in the context of this thesis has been described in detail. Considering the requirements of the posed research questions, a novel multi-level dispatch model based on linear programming is developed. Such requirements include the consideration of extensive geographical and temporal scope, both considered with fine resolution. Solving the complete problem is limited by the existing computational resources, hence the multi-level approach constitutes an alternative approach to acquire a sub-optimal solution that can capture the majority of the system dynamics by decoupling the spatial and temporal dimensions.

The core part of a dispatch model lies in the underlying electricity market assumptions and power flow modeling. Complexities arising from the generation scheduling of thermal and hydro plants are tackled using a perfect competition assumption for the electricity market and a linear approximation of the unit commitment problem. Dispatch horizon depends on the corresponding model level; nevertheless the overall model assumes perfect foresight for one year. Power flows over the transmission network are modeled via the DC flow approximation, where constraints are imposed by the physical limits of the individual lines and system security considerations. The main limitations of the model are associated with the involved linearization assumptions and market operation that may overestimate the system's flexibility and efficiency.

Finally, flexible demand modeling from the power system perspective is reviewed and different formulations are described for load shifting. Two approaches that couple generation and load shifting are implemented. The DIETER approach introduces additional load shifting variables, which however lead to a significant increase of the final problem size, especially for high shifting windows. On the contrary, the virtual storage approach scales better computationally for bigger problems and shifting windows. However, the available demand flexibility is only sub-optimally utilized due to the use of fixed shifting intervals.

4 Verification and Model Development

After analyzing the literature in chapter 2, it can be concluded that the most frequent approaches to model power systems rely on simplified, linear methods for both the electricity market operation and grid constraints. Both of these assumptions are based on sufficient theoretical justification. The linearization of grid modeling has been discussed in sections 2.2.1 and 2.2.3, while the linearization of the market modeling stems from the assumption of perfect market competition conditions. Such conditions result in the optimal bidding strategy for each participant to consist of bidding with their marginal cost of operation. Such behavior however constitutes the target for a market design that aims at maximizing the social welfare. Nevertheless, the combination of these assumptions and the behavior of such a model have only rarely been tested against actual data of power system operation, or at least rarely are such model verification attempts reported in scientific articles. The term “verification” is not universally accepted for this type of modeling, since such concepts apply mostly to models that simulate physical systems like fluid flows or chemical reactions. Other used terms include “validation” or “plausibility check”, however verification will be used throughout this section, whose scope will also be defined for better clarity.

The verification of a model for such complex systems can become a tedious task, mainly due to the lack of available data. The availability of data refers to the lack of open and reliable data sources for the system variables and parameters that are required for both reproducing historical system conditions, as well as serving as reference data for verification. The latter issue is discussed more extensively by Dehmel [178] and Hirth et al. [179] for the case of ENTSO-E data where several inconsistencies can be observed. In addition, the verification of a simplifying model against highly complex systems should not be aspiring to match actual data for single elements or time snapshots, but rather is expected to merely capture the behavior of the system in average as shown by Svendsen et al. [145]. The concept of overfitting, known from statistics, applies to modeling in general as well according to Grittith et al. [180], meaning that a model should not be calibrated too much to fit historical data, because of the danger of behaving more poorly for different system states. An additional source of uncertainty that is difficult to include originates from the nature of economic models in general, where although an optimization approach (e.g. welfare maximization) should be able to sufficiently predict a well-designed market behavior, exogenous or unknown parameters can lead to significant deviations as shown by Trutnevyte [181] for the case of the United Kingdom.

One of the most prominent attempts to validate a pan-European dispatch and power flow model has been conducted by Lie et al. [119] for the year 2014. The applied model is based on a linear OPF approach however with line capacity limitations applied only for the cross-border lines. The authors focus on power generation and cross-border flows as verification quantities by comparing model results with data reported by ENTSO-E, however without analyzing their quality as a reference source. Regarding generation, they compare the total energy mix per country, broken down merely to four fuel types, i.e. thermal, nuclear, VRES and hydro, while hourly comparison stays on a more qualitative assessment. Regarding cross-border flows, the evaluation follows again the same mixture of quantitative and qualitative assessment. In this case, the verification focuses on the average flows and seasonal trends. Moreover, some notable modeling difficulties like the high costs of thermal generation in Greece as well as German loop flows over Czechia are noted. Finally, it is pointed out how sensitive models for such highly interconnected and complex systems can become to the various assumptions and minor introduced errors.

Another notable validation attempt has been conducted by Eser et al. [182] for the year 2013 in the area of central Europe. The applied methodology is based on an AC OPF including cycling (unit commitment) constraints for thermal plants at unit level while pumped hydro storage plants are operated with a weekly horizon assuming no natural inflow. The verification evaluation focuses only on generation but with higher detail than Lie et al. [119]. Despite the high complexity of the model and detailed data, discrepancies in total generation can still be observed between lignite and natural gas generation, where natural gas generation tends to be significantly underestimated. These discrepancies are attributed by the authors to the insufficiency of a mere cost optimization assumption that cannot capture the market behavior of plant operators, since significant amount of electricity is traded via over-the-counter (OTC) bilateral contracts outside the wholesale market. Nevertheless, the model shows significant agreement with measured data on an hourly basis for specific hard coal units excluding weekends.

The selection of assumptions and resolution level for a model depends highly on its scope; thereby the verification of such a model should also follow the same rationale and requirements. Besides a qualitative assessment however, the results for any model gain additional validity through a verification process in a quantitative manner in order to better estimate potential shortcomings as well as spot the most significant sensitivities.

Considering the high sensitivity on data and the fact that higher modeling complexity does not automatically guarantee better accuracy, it is deemed necessary to verify the modeling approaches used for this thesis and calibrate the corresponding data and parameters. Due to the scale of the investigated area, the selected approaches must remain linear, such that computational performance issues can be limited. Therefore, the modeling methodology itself should be evaluated first and independently of the respective data, which can be calibrated afterwards. Since the focus of the study is to answer questions regarding the pan-European system as a whole, the verification process should also focus on assessing the average behavior of the system and not on individual lines or units. Moreover, the primary verification indicator should be the total energy mix, while the line loading and flows would also constitute strong indicators of verified behavior.

Since both methodology and data assumptions need to be verified, the process is split into two steps so that the contribution of each part can be assessed independently. Therefore, in the first section of this chapter the linear OPF approach is evaluated for a system where the involved data are of high quality. Consequently, in the second section the data assumptions are further assessed for the pan-European case.

4.1 Linear OPF – the case of Germany

Considering the requirement for low complexity approaches stemming from the scale of the investigated area as well as the data availability, the linear OPF approach aspires to be one of the most suitable candidates that compromise power system modeling accuracy and computational performance. Moreover, this selection is strongly supported by its well-established scientific background and presence in literature, as shown in chapter 2. Since the evaluation of the modeling methodology should be decoupled from the involved data, the selected test case must incorporate highly reliable power system data. Although a relatively lowly interconnected system, e.g. Ireland, would be the ideal candidate due to low interference with other systems, the availability of power system data is considered of higher priority for a correct modeling of the system's parameters and boundary conditions. Despite its size, data availability about the German power system is one of the highest in Europe, where detailed databases are available and updated regularly. Moreover, Germany constitutes one of the regions with the highest data quality and coverage in the Open Street Map (OSM) community regarding the transmission grid.

In this section the modeling of the German power system is described as well as the minimal set of improvements that can lead to a sufficient level of the model's verification. The selected year is 2015 and the evaluation focuses on the linear OPF approach as the core methodology.

4.1.1 Transmission grid

The minimum set of information to model a power system from the operational point of view can be divided into five different blocks, namely the transmission grid, the conventional power plants, the hydro generation, the VRES generation, the electricity demand and the system interconnections to neighboring systems. For a better understanding of the contribution of grid constraints, a copper plate case, i.e. assuming that power transfer is not limited over the whole country, is also examined and compared to the linear OPF methodology.

The transmission grid model is based on the Open Street Map (OSM) raw data [183] that are extracted, filtered and synthesized in a topological network using spatial and graph algorithms, as implemented by the SciGRID project [184].

The OSM data constitute of elements that can be one of the following three types:

- Nodes – they constitute the fundamental mapping object in OSM and they are defined by their coordinates (longitude and latitude)
- Ways – they are ordered groups of nodes between 2 and 2000 in size that can represent either a closed line area (e.g. a substation, building or park) or an open line object (e.g. a transmission line, street or railway)
- Relations – they constitute the most complex elements of the OSM data set. They include nodes, ways or even other relations. Objects contained in a relation are engaged to a common spatial or logical association (e.g. power lines, towers of the power line and adjacent substations)

Each object in OSM carries specific meta-data under the 'tags' field which contain further information about the element and may indicate associations it belongs to. Each tag consists of two attributes, a key and a value. For instance, transmission lines, substations, power plants, towers etc. have the tag key 'power' in common where the corresponding tag value for a transmission line would be 'line'. Further tags may include information about voltage, frequency, length, TSO etc.

One of the strongest aspects of SciGRID is that it takes advantage of the advanced information provided by relations in order to build the network graph. In this way, individual lines can be distinguished more easily even when they intersect or overlap with other lines or substations. However, the quality of the resulting network still relies on the quality of the original

OSM data, which originate from the input of volunteers and although any addition or alteration of data is reviewed, reliability issues may remain. Moreover, there can be elements with missing or outdated information and elements that have not been mapped yet. In addition, the OSM mappers are not necessarily familiar with power systems and may be more interested in the geographical only rather than the electrical aspects of such systems. A direct implication can be the difficulty to map and add electrical parameters for underground lines and other important power system components like transformers, switches, shunt elements or generators. Such inaccuracies can provide false or ambiguous information about actual electrical connections within substations or even in simple T-junctions as shown in figure 4-1, where the actual network topology differs from the implied spatial topology. Due to the lack of information about transformers, lines of different voltage levels are assumed to be coupled ideally, thus neglecting any additional reactance contributions or capacity constraints to the network.

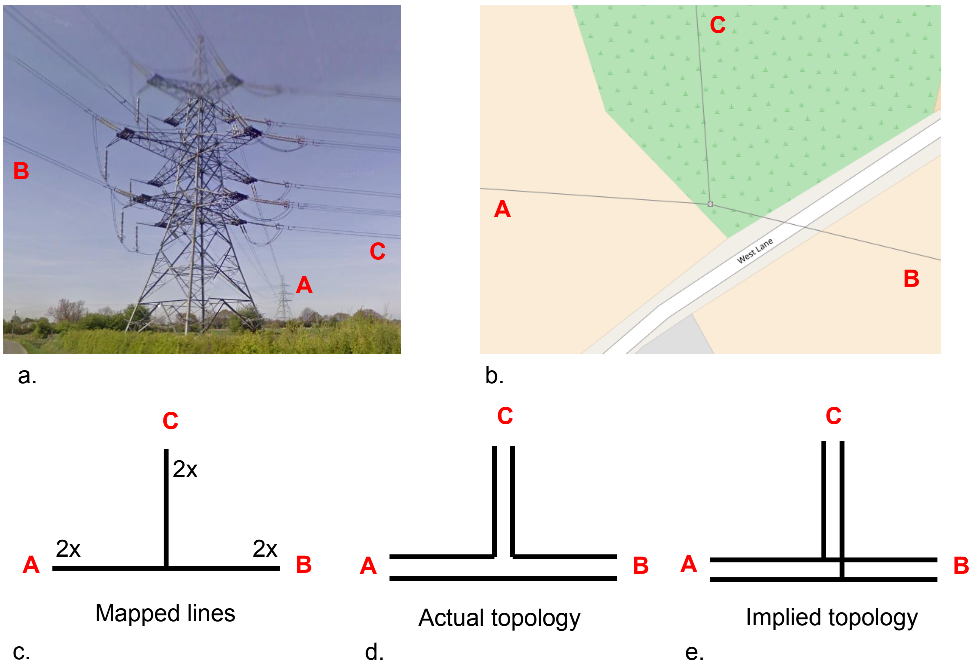

Figure 4-1 A T-junction tower at the point with latitude 53.6366337° and longitude -1.0692832° in the UK, where the coordinates refer to the World Geodetic System (WGS84) coordinate system. In picture (a.) [185], the actual topology of the junction is shown, also depicted in the sketch (d.). The same junction is mapped by OSM as in picture (b.) that can also be translated to sketch (c.). The available information implies a topology shown in sketch (e.) that differs from the actual topology.

The generated network from the SciGRID extraction, although highly detailed, is still requiring further modifications to increase its accuracy. Such a modification is the connection of nearby substations (< 850m), since relations information for such short lines appears to be missing in OSM [186]. Another example consists of the inclusion of the “Baltic Cable” and

“Kontek” HVDC interconnectors to Sweden and Denmark respectively. The final network is depicted in figure 4-2 via point to point connections.

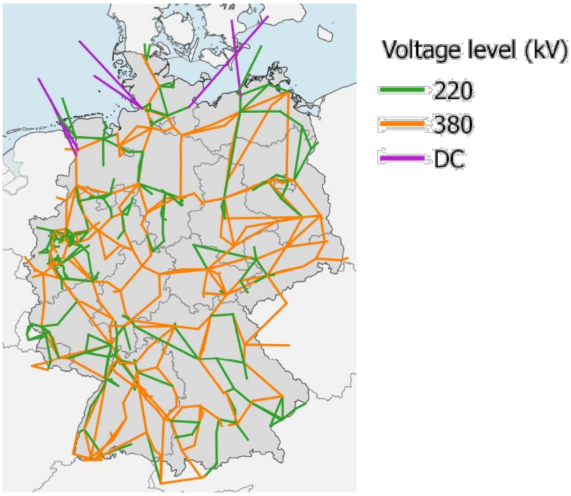

Figure 4-2 The German transmission grid used for the verification process. It is based on SciGRID [184] with additional modifications. Own illustration.

Although the final network disregards the actual pathways of the grid lines, the resulting dataset contains accurate information regarding line lengths and node coordinates as well as further information that can be used to estimate their electrical parameters. As described in section 2.2, the minimum set of parameters to represent a transmission grid for the DCOPF methodology, besides the topology, consists of the reactances and power transfer capacity limits (capacities) for the AC lines and power transfer capacity limits for the DC lines. While the capacities of DC lines can be easily inserted from the corresponding project websites, the electrical parameters for the AC lines are not directly available from the raw data. Instead, these parameters can only be estimated based on the available information, namely the voltage level, the number of cables and the number of wires, where cables and wires follow the OSM terminology and correspond to the number of circuits and conductors respectively, i.e. three cables correspond to one circuit and two wires to a 2-conductor bundle.

The electrical parameters for transmission lines depend only on the tower and conductor geometries as well as the electromagnetic properties of the conductors. Regarding the line reactances, these depend on the line length but remain relatively constant over the whole length and depend only on the tower and conductor geometries and the electromagnetic properties of the conductor’s material, which in the majority of the cases consists of an aluminum-conductor steel-reinforced (ACSR) configuration. Regarding line capacities, these are typically limited by the maximum current-carrying capacity (ampacity) for short transmission lines (as assumed by the DC approximation). The ampacity of a line depends on various factors but is not related to the line length. The most important factor for high voltage lines consists of the heat generated due to the conductor resistance (Joule’s effect - $P = RI^2$) that can increase the line’s temperature and hence its length, whose increase is limited by the maximum allowed sag. Therefore, the ampacity of a line depends not only on the distance between two towers, the corresponding topography and conductor geometry and material properties but also on the weather conditions (e.g., wind, irradiation, ambient temperature) and potential ice loading. In addition, the ampacity of a line depends on the duration of the applied current, since the shorter the duration, the higher the current a line can sustain. Moreover, a line's current depends on the apparent power and not only on the real part. Therefore it is of high economic significance to keep the transferred reactive power low. Considering the dynamic nature of ampacity and the emerging overhead line monitoring technologies that can allow more dynamic rating would exceed the scope of this thesis and therefore, a mere static capacity rating approach is applied. A detailed derivation of reactance and ampacity formulas are described in Grigsby et al. [187], however due to the lack of information about the actual tower geometries, such formulas provide only low merit for the electrical parameters estimation using OSM data. Thereby, literature values are selected that correspond to typical tower/conductor configurations for Germany [188]. The corresponding values are shown in table 4-1 and depend only on the rated operating voltage. Nevertheless, since these values correspond to a typical number of cables and wires, better estimations can be derived by scaling a line's parameters according to the OSM information regarding the actual number of cables and wires. The applied formulas for the reactances and capacities are shown in equations (4-1) and (4-2), where the reactances are scaled based on the parallel circuits law (i.e., inverse of the reciprocals' sum) and the capacities are scaled proportionally to the number of parallel conductors.

Table 4-1 Electrical parameters for typical transmission lines in Germany [188].

Line type	C_r (ohm/km)	C_x (ohm/km)	C_c (nF/km)	C_I (kA)
220 kV 2-bundle	0.080	0.32	0.0115	1.3
380 kV 4-bundle	0.025	0.25	0.0137	2.6

$$x\left[{}^{Ohm}/_{km}\right] = \frac{C_x}{\frac{\#wires}{\#wires_{typical}} \cdot \frac{\#cables}{3}} \tag{4-1}$$

$$I_{th,max}[kA] = C_I \cdot \frac{\#wires}{\#wires_{typical}} \cdot \frac{\#cables}{3} \tag{4-2}$$

$$S_{max}[MVA] = \sqrt{3} \cdot V_{nom}[kV] \cdot I_{th.max}[kA] \tag{4-3}$$

Despite its significance, validation of grid data is not a trivial task, primarily due to the absence of a reliable reference source. Although ENTSO-E provides a static snapshot of the European network, the intended distortion of geographical information renders it impossible to compare it with other network models. One of the most significant attempts to validate grid data from OSM has been attempted by Hörsch et al. [189] with the introduction of the PyPSA-Eur model, where the generated networks from the osmTGmod project [190] (based on OSM as well), the ELMOD-DE model [147] and the GridKit [191] extraction of the ENTSO-E interactive map [192] are compared for the area of Germany. One of the main difficulties in comparing such models is that the nodes and lines do not necessarily coincide and therefore the authors introduce a clustering methodology based on k-means and networks are then evaluated on the resulting clusters. It is shown that with regard to interconnection line volumes, PyPSA-Eur and osmTGmod show the best correlation, while ELMOD-DE shows weaker connections.

During the verification process, the quality of the used data remains a potential source of inaccuracies. Such shortcomings concern the grid data as well, where it can be observed via comparing with the VDE map [193] that some lines, although existing in the OSM dataset, do not have a relations field and therefore are excluded through the SciGRID abstraction process. The final grid that is used for the verification process is shown on the right-hand side of figure 4-2.

4.1.2 Conventional power plants

Modeling the power plants fleet constitutes one of the most critical elements of modeling a power system. Especially when evaluating the OPF as an adequate modeling methodology, the assumption of perfect market competition is being contested and therefore selecting the correct parameters can highly affect the verification of the methodology itself. Due to their different operational conditions, power plants can be divided into three categories, each one having their separate modeling approach. These include conventional, VRES and hydro power plants. Because of the different operational flexibility levels, VRES and hydro plants are modeled differently from the conventional plants. These sources are taken into account by considering fixed, historical generation profiles that participate in the electricity market (and objective function) with zero cost, thus being part of the residual. Introducing this type of generation with inequality instead of equality constraints allows the model to freely curtail any generation that cannot be transferred due to inaccuracies in the spatial distribution of the resources. Such inaccuracies can be later evaluated by measuring the final curtailments, which are expected to be close to zero. By representing all renewable generation merely as boundary conditions of the system, the linear OPF is essentially tested for the behavior of conventional (or dispatchable) power plants only, whose fuel provision is assumed unlimited. In an energy-only market, electricity prices and generator dispatch are governed by the asset owners' bids. Hence, the verification should test the assumption of perfect competition under network constraints which translates to bids close to the marginal operational costs for each power plant regardless of the market level (from short-term to long-term products).

Calculating the operational costs of power plants can be complex, especially if ramping or start-up costs are included, and in principle depend on the individual generation technology. A time-decoupled approach that is suggested by the simple OPF methodology can be represented by equation (4-4), where the operational cost for each generator unit is composed of three terms, namely fuel costs, emission allowance costs and variable operational and maintenance (O&M) costs. All terms can be modeled as time-dependent variables; nevertheless they remain constant over each time snapshot. The only exception consists of the efficiency which in general depends on the power output itself, thus introducing non-linearity in the objective function. A typical approximation for steam turbines is to assume a quadratic cost function which can be solved using quadratic programming methods that can also show high performance. However, this approach constitutes an approximation as well, since many power generators operate with more than one steam turbines (in different pressure levels), whose modeling may lead to non-convex problems. Due to data shortcomings and to retain a linear programming formulation, all efficiencies are assumed to be constant and independent of the operational point. Moreover, fuel costs and emission costs (related to the Emission Trading System – ETS) are considered constant over the year, since similar assumptions can only be applied for future scenarios as well.

$$\begin{aligned} &Marginal\ cost\ \left[\frac{€}{MWh_e}\right] \\ &\quad = \frac{fuel\ cost\ \left[\frac{€}{MWh_{th}}\right]}{efficiency} + \frac{specific\ emissions\left[\frac{tCO_2}{MWh_{th}}\right]}{efficiency} \cdot ETS\ price\ \left[\frac{€}{tCO_2}\right] \\ &\quad + variable\ O\&M\ \left[\frac{€}{MWh_e}\right] \end{aligned} \tag{4-4}$$

With the exception of nuclear power plants, for which various data sources including that of the International Atomic Energy Agency (IAEA) exist, reliable and detailed information about the rest of the power plants in Europe are not always available for all countries. One of the most well maintained databases that also includes geographical information, crucial for power flow simulations, is published by the Federal Network Agency (Bundesnetzagentur – BNetzA) [194] of Germany and provides information for all power plants bigger than 10 MW. Nevertheless, this list also bears some drawbacks. For instance, the geographical information is not provided in exact coordinates, there is no efficiency information and occasionally individual units are included instead of power plants.

The Open Power System Data (OPSD) project [195] constitutes one of the first open source projects with the primary purpose of creating a reliable database dedicated for energy system modeling. Despite its name and open source code to develop the platform, not all provided data hold clear licenses which by default means that they are not open. For the case of Germany, OPSD takes the BNetzA list and merges it with the power plant list from the Federal Environmental Office (Umweltbundesamt – UBA) [196] of Germany by applying various data cleaning and standardizing methods. In addition to the available information, OPSD includes the geolocations of power plants as well as efficiency values for selected power plants via an individual research. For the missing efficiencies, an estimation based on their commission year is also provided. Moreover, all power plants are classified based on their energy carrier and technology, which helps distinguishing the generators in terms of marginal cost of operation.

Despite the high quality level of the OPSD data, these cannot be directly used for the verification process. In addition to the original efficiency estimations, data from Robinius [32] are used to correct efficiencies by matching the BNetzA data. Furthermore, generators with missing coordinates are detected and their locations are identified by their zip code and set as the geographical centroid of the corresponding areas [197]. The final marginal cost of each generator is calculated from eq. (4-4), where the individual parameters per fuel type are shown in table 4-2 and the ETS price is assumed to be 7 €/tCO_2 [198] for 2015.

Table 4-2 Conventional power plant statistics and parameters for the German power system of 2015 for power plants >10 MW, aggregated by fuel. Underlying technologies may include steam turbines, combustion engines, open-cycle and closed-cycle turbines.

Energy carrier	#gen-erators	Capacity (GW)	Fuel cost (€/MWh) [32]	Specific emissions (tCO_2/MWh) [199]	Variable O&M (€/MWh) [200]	Average efficiency	Average marginal cost (€/MWh)
Nuclear	8	11.08	1.63	-	5.84	0.35	10.51
Natural gas	275	26.38	33.73	0.201	2.26	0.42	87.46
Hard coal	98	29.48	10.29	0.337	3.59	0.41	34.62
Lignite	64	21.98	4.53	0.384	3.68	0.39	22.3
Bio-mass and bi-ogas	63	1.2	-	-	3.09	0.38	5.72
Oil	53	4.07	49.86	0.264	27.97	0.42	151.13
Waste	82	1.67	-	-	3.09	0.33	6.11
Other (e.g. sewage gas)	35	2.53	40	0.298	-	0.33	125.43

The resulting database is compared to other public sources in terms of total installed capacities. Figure 4-3 shows the total installed capacity per fuel type, where the used database shows sufficient agreement with the official sources. In addition, figure 4-4 shows that the spatial distribution of the installed capacities additionally matches sufficiently with the reported values from the Network Development Plan (Netzentwicklungsplan – NEP) 2030 [198].

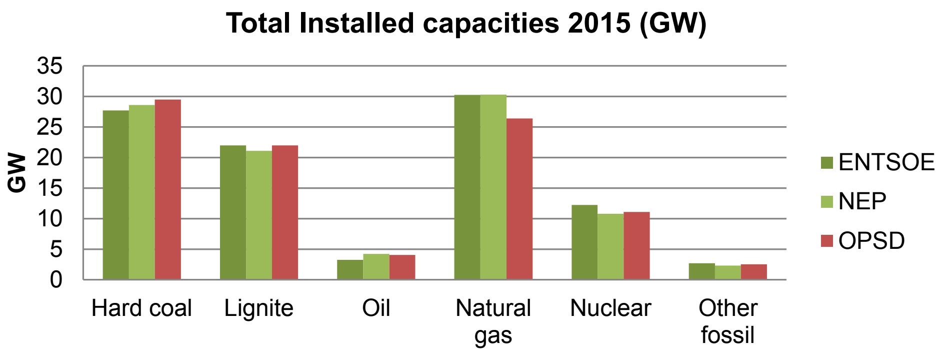

Figure 4-3 Total installed capacity per fuel type in Germany for 2015 according to ENTSO-E [201], the NEP 2030 [198] and the OPSD database that is used for the verification.

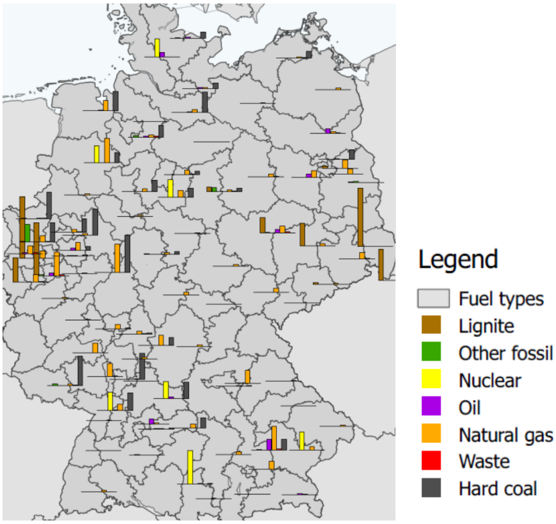

Figure 4-4 Geographical distribution of conventional power plants per fuel type into administrative regions. Own illustration.

As shown in the beginning of the chapter, one of the main findings of verification attempts via cost optimization models is the underestimation of the generation from natural gas power plants. Table 4-2 shows that due to the higher fuel price, natural gas is generally more expensive than coal and therefore succeeds it in the merit order. Hence, a simple cost optimization model will always favor coal, unless other constraints are present. Nevertheless, in contrast to the claim by Eser et al. [182] that this behavior can be attributed to the difference between wholesale market and bilateral agreements, it is proposed that this difference occurs mainly from the different market conditions applied to co-generation of heat and power (CHP) plants, where natural gas is prominent. After all, OTC futures do not differ significantly from the wholesale market prices and it is also hard to explain why natural gas should be preferred in such cases. On the other hand, CHP plants operate under different market conditions, similarly to the renewable energy sources act (Erneuerbare Energien Gesetz - EEG) [202], where separate compensations and tariffs are applied, in order to support their use as a mean to advance a more efficient and environmentally friendly energy system [203]. To this end, the modeling workflow described in section 3.1.1 is used to incorporate the consideration of the special conditions of CHP plants operation.

For an electricity market model based on copper plate assumption, the so far described methodology would suffice for a complete inclusion of power plants. However, for a model that incorporates grid constraints, all generators have to be additionally assigned to network nodes. Considering the lack of information with regard to the exact network topology and the connecting points of generation, the assignment of power plants to the network is based on the principle of nearest substation. Given a point in the World Geodetic System (WGS 84) spatial reference projection system, finding its nearest neighbor from a set of points can be accomplished using the ball tree algorithm [204, 205] with the Haversine distance as metric. The Haversine distance corresponds to the arc length between two points on a spherical surface (may also be referred as beeline) and is given by equations (4-5) – (4-7). Although the earth is not a perfect sphere, this approximation is sufficient for the purposes of this thesis.

$$a = sin^2\left({}^{\Delta\varphi}/_2\right) + cos\varphi_1 \cdot cos\varphi_2 \cdot sin^2\left({}^{\Delta\lambda}/_2\right) \tag{4-5}$$

$$c = 2 \cdot atan2\left(\sqrt{a}, \sqrt{1-a}\right) \tag{4-6}$$

$$d = R \cdot c \tag{4-7}$$

where the final distance d has the same units with the radius R (6371 km for Earth) and $\varphi,\ \lambda$ are the latitude and longitude in radians correspondingly.

4.1.3 Residual load

The residual load is usually defined as the demand that has to be covered by dispatchable generators and therefore consists of the electrical load subtracted by the wind and PV infeed. However, in the context of the OPF verification as a market model, the residual load includes all generation and demand of the system except for conventional power plants, i.e. the residual load consists of the demand, the VRES infeed as well as historical profiles of hydro plants dispatch, imports and exports, as shown in eq. (4-8). For all of the sources of residual load, the main challenge lies in adequately emulating the system conditions taking into account the absence of highly resolved data. For the purposes of this verification, a top-down approach is followed for all quantities, where the main challenge is translated to disaggregating profiles and assigning them to network nodes.

$$Residual\ load = Load - VRES\ infeed - Hydro\ generation + Exports - Imports \tag{4-8}$$

One of the most significant quantities determining the residual load consists of the electricity demand. In most cases, information about electricity in high temporal resolution is only available by national and international agencies like ENTSO-E (typically, aggregated hourly profiles per country are reported) or by TSOs (typically, aggregated 15-minute or hourly profiles for their control areas). Aggregating profiles over large areas has the tendency to smoothen out statistically independent variations and gains validity by assuming the existence of a sufficiently strong grid. Assigning the same profile to all nodes inside an area ignores any local discrepancies but on the other hand, it renders the profiles deterministic, while the main intraday dynamics are still represented.

Unlike most countries, the German transmission system is operated by more than one operator, each of which publishes the hourly demand within their corresponding control areas. These areas are shown in figure 4-5, where it can be seen that the partition does not follow any spatial property of the electricity demand since each area includes various rural, urban and industrial regions. Robinius et al. [206] considered these and additional information to assign load profiles for each of the 11,254 municipalities in Germany by using the gross domestic product (GDP) as indicator, while additionally corrected the weights using the information of total consumption reported by the German federal states. The load profiles for the year closest to 2015, i.e. 2013, are considered for the verification process by assuming that the corresponding profiles did not change significantly. Nevertheless, all profiles are rotated such that the weekdays of 2013 correspond to the ones from 2015 (e.g. Monday to Monday), thus retaining one significant factor that determine load profiles. Since the network below 220 kV is not considered, the municipality profiles are aggregated to county level [207] before assigning them to the network nodes. The final spatial distribution of the demand is shown in figure 4-6, where it can be observed that the load density is concentrated in the big urban and industrial regions.

Figure 4-5 The four TSO control areas in Germany. Own illustration.

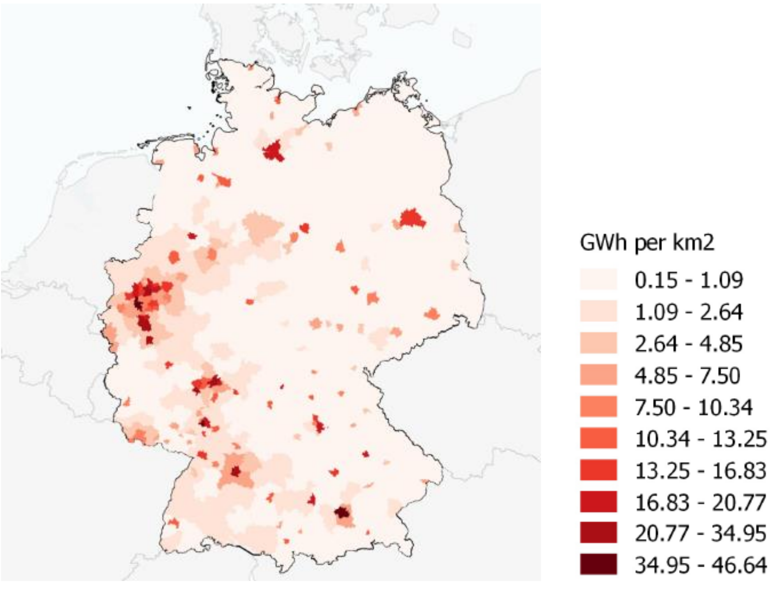

Figure 4-6 Spatial distribution of electricity load for 2013 [206]. Own illustration.

Considering the lack of information about the low and medium voltage networks, projecting profiles from counties to network nodes can be accomplished via two methods. In both cases, all T-junction type of nodes are excluded from the process, since it is impossible for a lower voltage network, generator or consumer to be connected there directly, therefore only substations are considered.

The first approach distributes a region profile to all substations inside the respective region uniformly. For regions without any substations, the corresponding profiles are added to the existing load of the substation, nearest to the region's geometrical centroid. This approach is useful because of its simplicity; however, its validity drops for smaller regions and starts depending heavily on the regionalization. For instance, administrative and network regions do not necessarily coincide (e.g. substations can be located outside a city's limits).

The second approach follows the principle of nearest neighbor, which implies a network topology similar to a minimum spanning tree topology for the lower voltage. Although this is not necessarily true, it constitutes a common assumption in energy system modeling when the actual network topology is unknown [124]. Partitioning an area, such that all points of a region have the same nearest neighbor out of a given set of points constitutes an old geometric problem that can be solved via the so-called Voronoi diagram (or tessellation). Using the network substations and a rectangular envelope enclosing the investigated area, the corresponding Voronoi diagram can be generated. Profiles from a different partition (e.g. the German counties) can be then mapped to the Voronoi regions by measuring the geometric overlay. An example for such a procedure is shown in figure 4-7, where the regional (administrative) profiles are overlaid over the Voronoi regions generated by the HV substations.

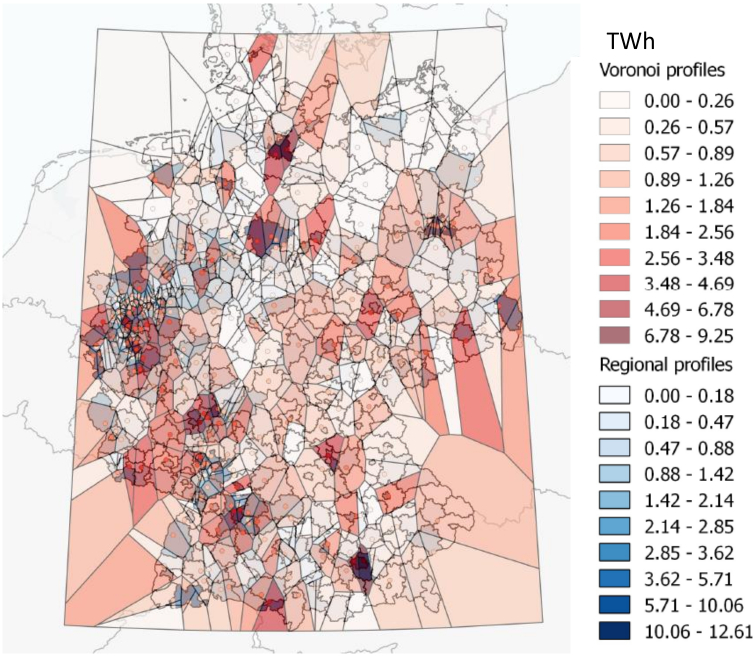

Figure 4-7 Overlay between the regional (administrative) distribution of positive residual load for 2015 and the Voronoi diagram of the high voltage grid. The assignment is completed by measuring the area overlay.

Following this methodology, all other sources of residual load can be imported into the network as well, given that the corresponding profiles are available for a specific regionalization. Similarly to the demand approach, infeed time series for wind and PV are obtained from the reported values of the four TSOs and processed by the OPSD platform [195]. Regarding wind, Tennet reports offshore generation separately from onshore, whereas 50-Hertz provides only one aggregated time series that can be split according to the installed capacities. The further spatial distribution of onshore profiles follows the distribution of the installed capacity as well. Information about the spatial distribution of capacities can be found using the available geographical data of each registered project that has been reported until 2015 on the EnergyMap platform [208]. Among other information, data regarding the nominal capacity, type and zip code for each project are available. Despite missing data issues, the total capacities are in good agreement with total reported values. Hence, matching the zip codes at the 3rd level (i.e. the first three of the total five digits) to the four control areas, the corresponding TSO profiles can be scaled down to smaller regions and then imported to the network. The same approach is followed for biomass as well, since the power plants included in the BNetzA list constitute merely about one seventh of the total installed capacity. Therefore, the remaining biomass generation is imported as fixed profiles, distributed using the national profile available from ENTSO-E [201]. Regarding hydro generation, a similar approach is followed, where the profiles are taken again from ENTSO-E, however the capacities are taken from the results of the powerplantmatching (PPM) tool [209] and aggregated to the zip code 3 regions. When the generation for pumped hydro storage (PHS) plants becomes negative (i.e. the units consume energy for pumping), the respective quantities are added to the existing demand.

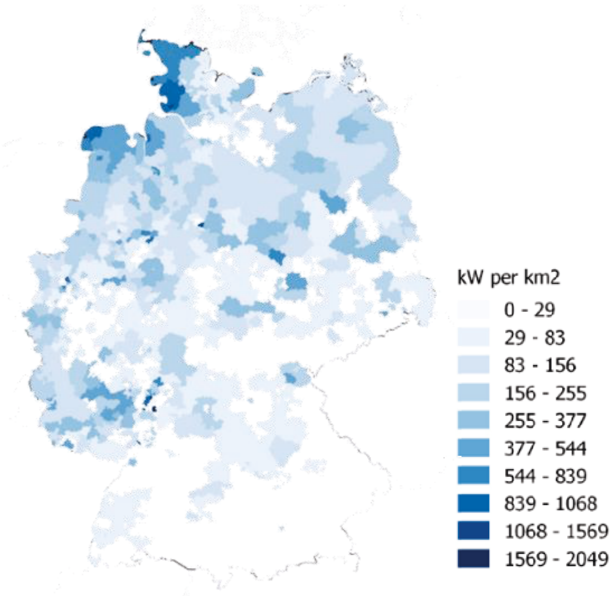

Figure 4-8 Spatial distribution of installed wind capacity for the year 2015. Own illustration.

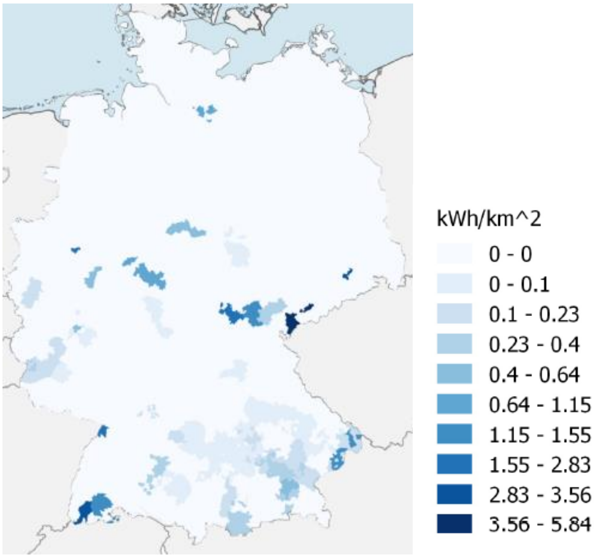

Figure 4-9 Spatial distribution of hydro power generation for the year 2015. The distribution follows the corresponding installed capacity. Own illustration.

The last contributor to the residual load consists of the power exchanges with the neighboring countries. In highly interconnected systems with high shares of VRES, power exchanges and the behavior of neighboring systems may have considerable influence on an individual power system operation, as it is shown in Appendix C for the German power system. Nevertheless, since this verification focuses on a single market under historical conditions, the interactions with any neighboring systems are considered as fixed profiles, based on reported exchange data. From the nature of these quantities, exports can essentially be regarded as sinks or demand and imports as sources or generation respectively. Total cross-border flows are reported by the ENTSO-E transparency platform on an hourly basis [201]. However, they only refer to aggregated flows with the flows on individual cross-border lines remaining unknown. There can be at least three ways to connect the neighboring countries to the main network, all of which attempt to tackle the lack of information about flows on individual lines. The first approach would be to simply distribute the profile of a neighboring country to the corresponding cross-border nodes uniformly. This approach disregards the local conditions and differentiation between stronger and weaker lines as well as the internal grid of the neighboring country which would allow different flow portions on the various cross-border lines at different time snapshots. The other two approaches follow the same principle and only differ on their implementation. The idea lies in inserting a virtual node for each of the neighboring countries and connecting them to the cross-border nodes in a way that loop flows through this node are avoided. One way to accomplish this is to represent the connections as AC lines with very high reactances in comparison to the German grid values, while the alternative way would be to represent the connections as controllable virtual links that allow only unidirectional flow but then two virtual nodes per country would be required, one for exports and one for imports respectively. In both cases, the introduced connections should hold adequate capacities to accommodate all flows, which may still be limited by the actual cross-border line parameters. For the purposes of this verification the AC line approach is selected and depicted in figure 4-10, which is also extended to the offshore generation, since the assignment of profiles to offshore nodes faces similar issues.

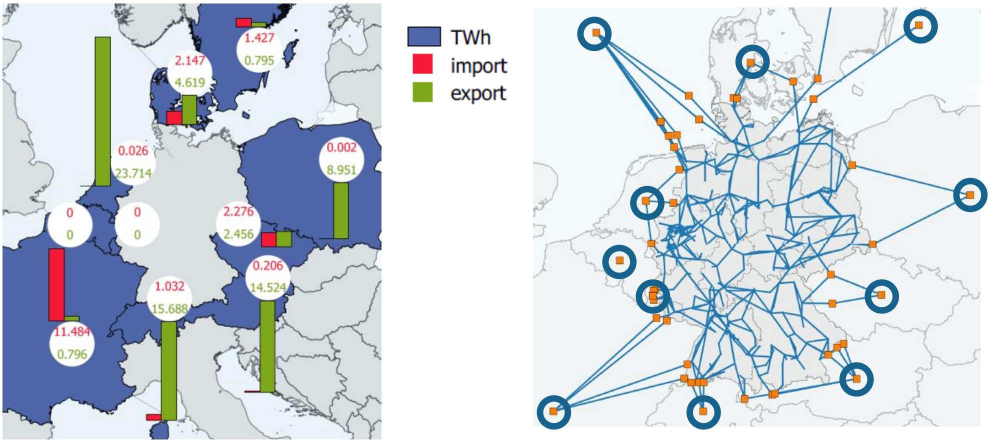

Figure 4-10 Total imports and exports to the neighboring countries for the year 2015 are depicted in the left picture. Exchanges with Belgium are 0 since there is no direct connection, while exchange data with Luxembourg are not reported. On the right picture the “virtual node” method is depicted as a method to model the imports and exports when given as fixed profiles.

The final picture of the power system boundary conditions is depicted in figure 4-11. Although with the described formulation, CHP must-run conditions cannot be curtailed like VRES sources, they behave as fixed generation and can therefore be considered parts of the residual load.

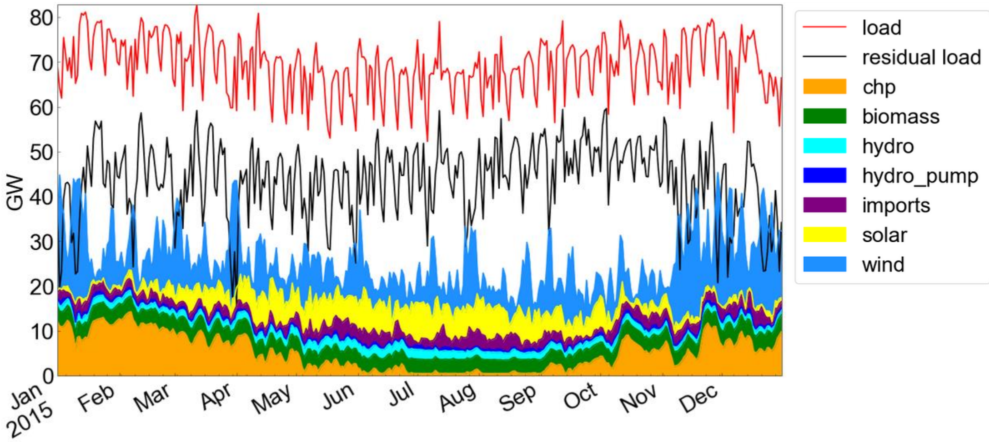

Figure 4-11 Daily averaged, accumulated residual load for Germany 2015, depicted with its constituents.

4.1.4 Verification results

The described methodology is applied to reproduce the German power system conditions for each hour in 2015 following the requirements of a LOPF formulation, which is sought to be verified as an adequate approach for the purposes of this thesis. Besides the normal LOPF problem that includes grid restrictions, an equivalent problem with copper-plate conditions is also assessed and compared to the original problem. As mentioned in the beginning of the chapter, the main verification indicator consists of the total energy mix and not the generation patterns for individual power plants. Another expected behavior, since historical conditions are assumed, is the absence of any generation or load curtailments. Finally, a strong verification indicator would be to compare the line loadings or power flows, where similarly to the generation only average behavior is to be expected and not exact replication for individual lines or time snapshots.

Figure 4-12 shows the total generation per fuel type for 2015 and different modeling settings and formulations. As verification reference, the reported values from the BNetzA monitoring report [210] are considered and marked with the green color. It can be observed that in all cases the agreement in renewables generation is high and that the only discrepancy concerns the waste power plants, for which no special consideration has been taken since it only constitutes a small part of the installed thermal capacity (1.7%). On the one hand, this increases the validity of the used data, but on the other hand it also constitutes an indicator that the selected allocation methodology of profiles suffices for the purposes of this thesis.

Regarding the conventional power plant mix, it can be observed that the various modeling settings may bear a significant impact on it. For the copper plate case, in spite of the application of CHP constraints, the model still shows significant discrepancies from the reported values. In particular, the lignite generation remains too high, and while the natural gas improves significantly, the 22.5 TWh that correspond to the must-run conditions are generated only. On the other hand, applying the LOPF methodology results into natural gas generation even without CHP constraints; however, in this case, hard coal generation is being overestimated. Applying all the settings that are listed in table 4-3 brings all four major fuel types (i.e. nuclear, lignite, hard coal and natural gas) within a 10% discrepancy margin and the total weighted average mix discrepancy to 3.6%. Moreover, considering that the total energy not served (ENS) is only 4.13 TWh (i.e. 0.7% of the total demand), it can be concluded that in terms of energy mix the LOPF methodology can give adequately satisfactory results for the purposes of this thesis.

By examining the verification results from figure 4-12, the impact of the various settings can be identified. Regarding the “CHP 1” setting, its most significant contribution affects the natural gas generation and to a lesser extent lignite, where the gas value approaches the range of the reference value. The main drawback however is the increase in load curtailment requirements. The “CHP 2” setting mostly affects the hard coal generation, bringing it closer to the reference value, but beyond that it only poses minor effects. The last three settings concern the improvement of the grid and the different ways to assign profiles to the network. Their contribution to the energy mix is only minor besides a small increase in cheap nuclear and lignite generation. However, they lead to significantly lower load curtailments as well as more accurate line loadings, as can be seen in figures 4-13 and 4-14.

Table 4-3 Explanation of model settings for the figure 4-12 which are applied through the verification process

Model setting	Explanation
CHP 1	Minimum CHP must-run constraints.
CHP 2	Capacity reduction of steam turbines due to CHP operation.
Neighbors	Model exchanges with neighboring countries via virtual nodes
Grid correction	Improve transmission grid
Voronoi	Allocate residual load profiles to nodes using Voronoi tessellation.

Table 4-4 Explanation of the different LOPF versions used for verifying the German power system for 2015.

LOPF version	Explanation
LOPF 1 (initial)	DC optimal power flow
LOPF 2	LOPF 1 + CHP 1
LOPF 3	LOPF 2 + Neighbors (see figure 4-10)
LOPF 4	LOPF 3 + Grid correction (see figure 4-2)
LOPF 5	LOPF 4 + Voronoi (see figure 4-7)
LOPF 6 (final)	LOPF 5 + CHP 2

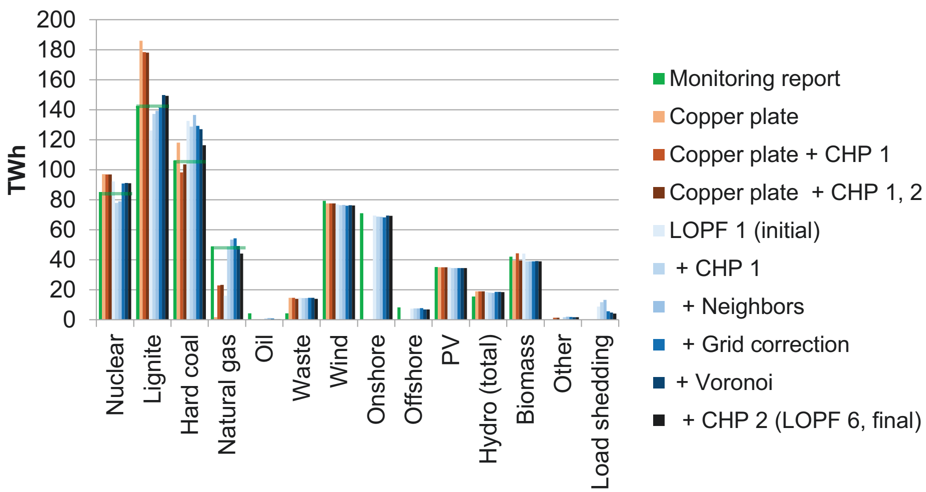

Figure 4-12 Energy mix for different modeling methodologies compared to the BNetzA monitoring report. Red shades correspond to copper plate approach, whereas blue shades to LOPF with the full transmission grid. For the copper plate case, CHP 1 and CHP 2 setting are shown as well. For the LOPF case, each improved version corresponds to an additional setting from table 4-3 being considered. The final version incorporates CHP modeling via must-run constraints and capacity reduction, modeling of neighboring countries via virtual nodes, an improved transmission grid and allocation of the residual load profiles using Voronoi tessellation.

Figure 4-13 shows the load curtailments distribution before and after applying the settings in table 4-3. It can be observed that most of the curtailments occur near the borders and can be reduced significantly after applying the corresponding corrections. Similarly, figure 4-14 indicates the critical lines in terms of utilization by measuring their overloading frequency over the yearly operation. The results can be compared with the figure from BNetzA monitoring report [210]. It can be seen that most of the cross-border lines are relieved after the application of the corrections; however significant congestion is still observed in the areas with high density of network nodes, something that does not appear in the reference case. This condition can be partly explained by the increased inaccuracies imposed by the approximated spatial distribution of demand and its allocation to substations and partly by the fact that lower voltage grid levels (e.g. 110 kV) can accommodate significant part of power flows for such short distances but in this case they are not represented. Nevertheless, apart from these dense areas, the most critical lines along with their severity can be identified and the results adequately match to the reference data.

Overall, it can be concluded that the final model, i.e. the LOPF 6 version that includes all modeling improvements of table 4-3, can adequately represent the year 2015 for the scope of this thesis and therefore can be considered verified. Regarding the verification of the OPF methodology as a suitable approach for modeling a power system, it can be denoted that except for the CHP modeling part, the rest of the model development merely contributes to an accurate representation of the German system conditions and does not directly affect the assessment of the method itself. On the other hand, the additional constraints to model CHP generation constitute a deviation from the original formulation. Nevertheless, this can be deemed necessary since their operation also depends on conditions outside the electricity market itself. Interpreting the additional constraints as part of the system's boundary conditions, it becomes possible to assess the OPF methodology alone as a tool to model the electricity market, including the long-term, day-ahead as well as intra-day components simultaneously. The agreement in the final energy mix constitutes adequate indication that the OPF methodology suffices to represent the market behavior for the purposes of this thesis.

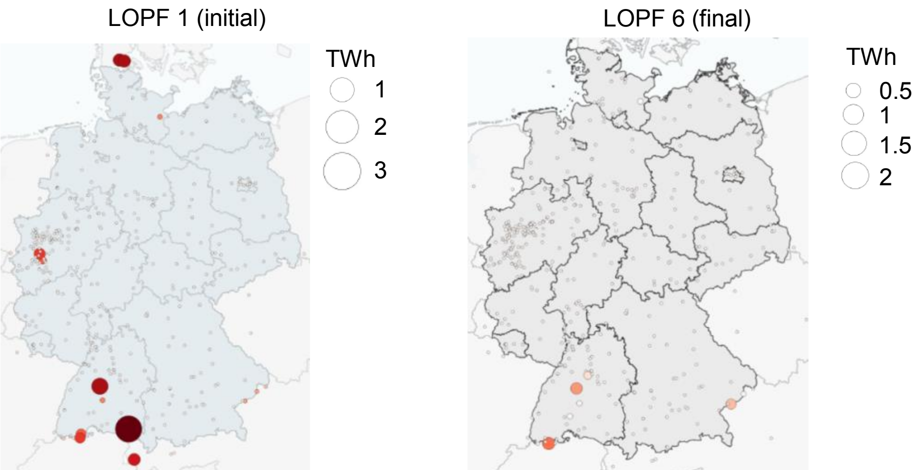

Figure 4-13 Load curtailments distribution for the initial and final models. Curtailments are reduced significantly, especially for the nodes close to the borders.

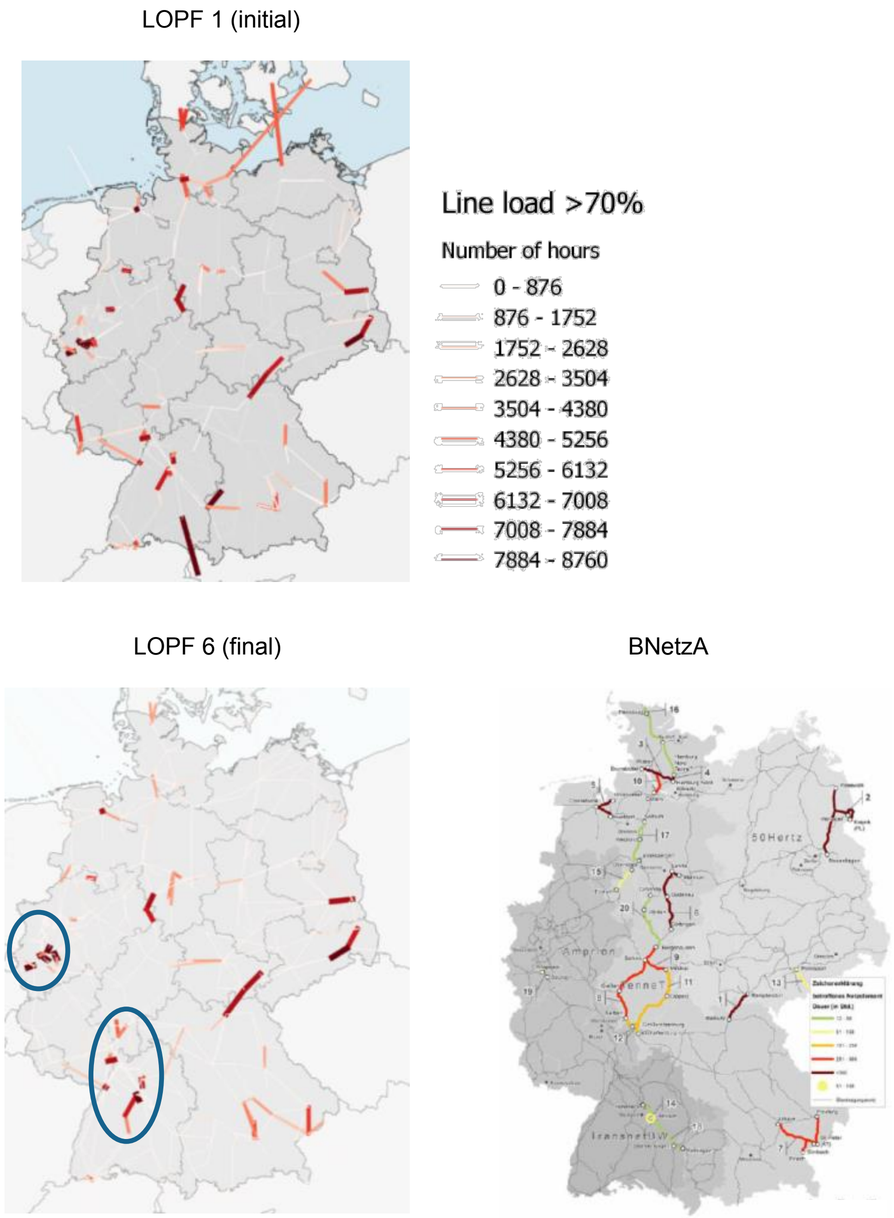

Figure 4-14 Critical transmission lines for the initial and final models as well as according to BNetzA [210]. Cross border congestion is reduced significantly after applying modeling improvements however congestion in areas with high node density remains considerable.

4.2 Pan-European model verification

Although the OPF methodology can be sufficient for modeling a single electricity market, its application to the European context needs to be additionally verified, considering the complexities arising from modeling market coupling, hydro scheduling, the challenges imposed by lower data quality and quantity as well as calibrating costs for the different countries. In this section, it is attempted to verify the European power system for the year 2015 by primarily assessing the total energy mix while also using the cross border flows and curtailments as additional indicators. By referring to the European power system, only the ENTSO-E countries are considered excluding Turkey, Cyprus and Iceland. Similarly to section 4.1, the OPF methodology constitutes the foundation of the European verification, since its performance has already been verified for the German system.

4.2.1 Transmission grid

Similarly to the German case, transmission grid data for Europe are hard to obtain, especially when geographical information is desired. Although such data can be available by ENTSO-E [211], the lack of geographical data renders them unsuitable for the purposes of this thesis, since the allocation of generation and demand assets becomes impossible. Besides this dataset, ENTSO-E also provides maps with an approximate representation of the European transmission grid either in static or interactive form [212, 213], however the corresponding data are protected by user rights and moreover their information needs to be extracted, in order to become useful. The approximate representation means that for security reasons, the substation locations are slightly distorted from reality, while the lines are depicted merely as beelines instead of following the correct paths.

Considering the lack of official sources, only open data sources remain as alternative for modeling the transmission grid. Bialek et al. [118, 214] provide grid data from the ENTSO-E static map which have been georeferenced by Jensen et al. [215] to the WGS84 system. However, some drawbacks of the data include the limited geographical scope that covers only the synchronous, continental area (former UCTE), the lack of thermal capacities for non cross-border lines and the relatively outdated data. Regarding OSM data, they are available for the European continent as well, however, unlike Germany, the data quality and quantity is lower, while the “relations” information is usually missing. Considering that SciGRID only uses this information to generate the corresponding network, alternative approaches need to be considered to process OSM data, such as the osmTGmod [190] and GridKit [216] models. The former can combine objects with and without relations while the latter disregards this information.

For the purposes of this thesis, GridKit is refactored to follow the SciGRID structure and used as the primary tool to extract the OSM data and generate the European network. In this work, GridKit is refactored to follow the SciGRID structure and extended to include more nodes as well as remove wrongly mapped objects. The resulting network is not directly suitable for performing power flow analysis since electrical parameters have to be assigned similarly to section 4.1.1. However the approach cannot be applied directly, since the number of cables and wires is not always available in the European dataset. Therefore, the extracted grid is compared with a reference network [189] via geospatial methods and it is found that merely assuming default values for each voltage level, i.e. 2-bundle conductors for 220 kV and 4-bundle conductors for 380 kV, is deemed sufficient. Moreover, HVDC lines are identified and marked as such. Resolving the missing data allows the calculation of the line electrical parameters based on the factors in table 4-1, where the values corresponding to typical German tower geometries are assumed for Europe as well. For the parts of the grid that do not fall into one of the 220 or 380 kV categories like the transmission grid in the Baltics (330 kV), linearly interpolated values are used.

The final network is compared to the ENTSO-E map data [191] in terms of cross-border capacities and by applying Louvain clustering [217] with the thermal capacities as gains. Louvain is an iterative method for community detection in large networks using a modularity metric ranging from -1 to 1, where the clustering iterations stop when no more modularity gain can be achieved. Thereby, the number of the final clusters is determined by the algorithm. Figure 4-15 shows the total cross-border thermal capacities for the European countries and the reduced networks after applying Louvain clustering. Regarding the cross-border capacities, it can be observed that they are generally lower than ENTSO-E (only higher for the central European regions), with the discrepancies being higher for the peripheral borders which may constitute an indicator of insufficient OSM data. Regarding the Louvain clustering, the reduced networks differ significantly, hence little information can be extracted from this comparison. Nevertheless, this behavior can be attributed to the significant difference in the number of nodes of the initial networks as it can be seen in table 4-5.

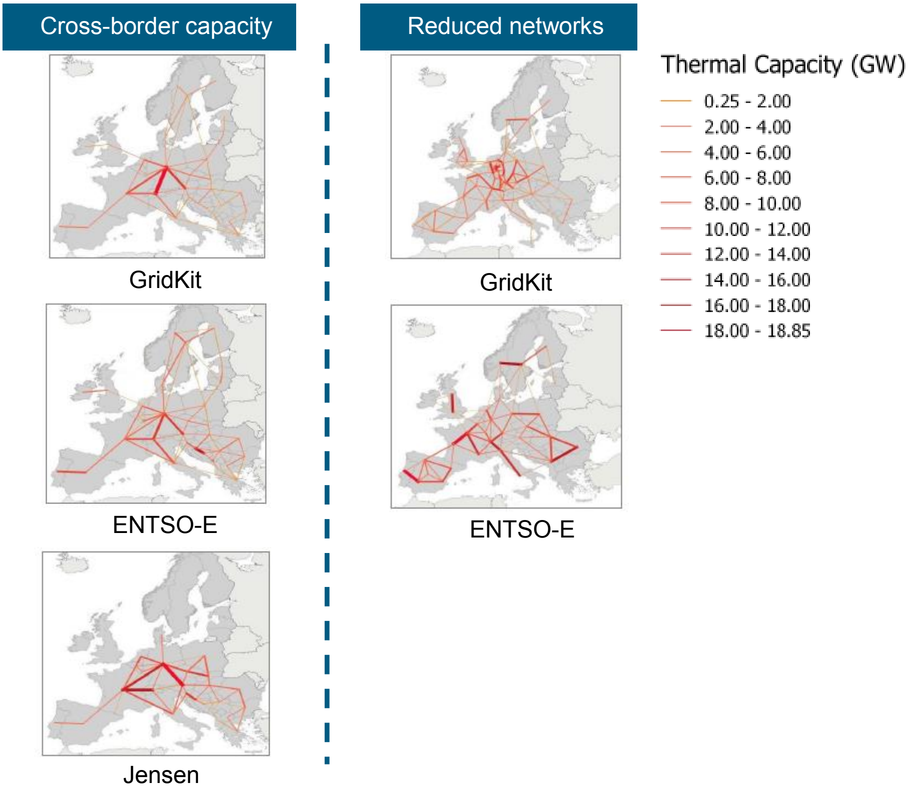

Figure 4-15 Comparison of the GridKit network that is used in this thesis with the corresponding datasets of ENTSO-E [191] and Jensen et al. [215] in terms of total cross-border capacity and by applying Louvain clustering.

Table 4-5 Number of nodes and lines for the GridKit and ENTSO-E grid before and after applying Louvain clustering.

	GridKit	**ENTSO-E**
initial #nodes	8059	4403
reduced #nodes	65	32
initial #lines	11363	5984
reduced #lines	132	69

Due to various shortcomings, further enhancements of the GridKit dataset are deemed necessary. Such enhancements include:

- Manually adding missing lines [212, 218] (mainly in the Baltics and Balkans areas)
- merging parallel lines
- connecting unconnected nodes with less than 1.5 km distance
- removing isolated networks with less than 20 nodes (excluding islands)
- adding HVDC lines from public sources [219-221]
- adding missing lines in Norway [222]
- removing redundant “beads”, i.e. T-junction nodes that connect only two lines
- clustering connected nodes with less than 5 km distance

Clustering the network nodes according to the connection distance is implemented in order to reduce the high number of nodes and lines and hence the corresponding problem sizes. Various threshold distances are examined with regard to computational time (one day simulations projected to a whole year) as well as the value of the objective function for the first day of 2015 are used as indicators to define a suitable threshold.

Figure 4-16 shows the variation of computational time and total system costs for different threshold distances. The decrease in computational time becomes significant already for small thresholds; however the total system costs starts deviating as well, mainly due to distortions in assigning the generation assets and demand profiles. The distance of 5 km is selected as a compromise between performance and accuracy. As shown in figure 4-17, the final number of lines drops to 5178 from 13,359 and the number of nodes to 4036 from the initial 8308, thus reaching a similar grid size to that of ENTSO-E (see table 4-5). The final grid is shown in figure 4-18, where the lines are classified by nominal voltage level as given by the OSM data.

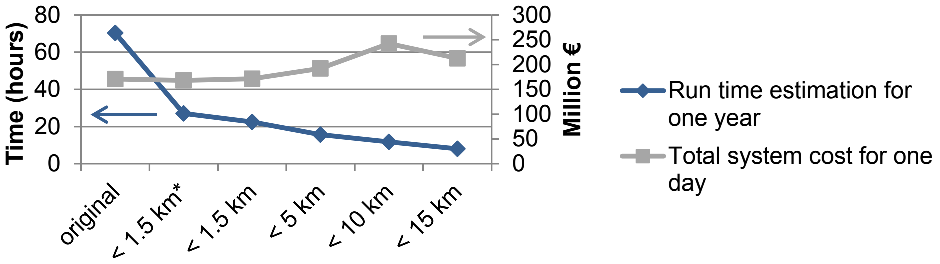

Figure 4-16 Yearly computational run time estimation and total system cost of the first day of 2015 for different distance thresholds used to reduce the network size. Simulations are performed for one day only, hence the yearly run time is estimated based on these results. The star (*) indicates that the unconnected nodes with less than 1.5 km distance remain unconnected. The computational time does not include any parallelization of the problem.

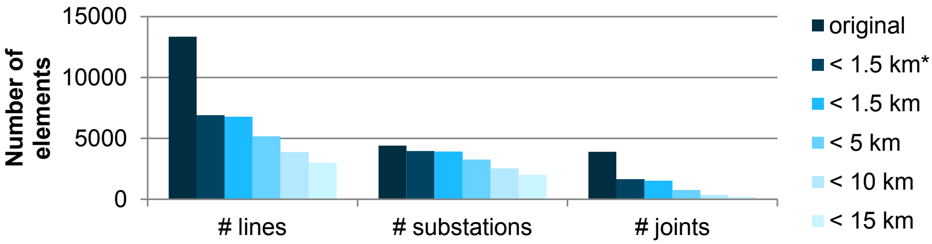

Figure 4-17 Reduction of line and node elements for increasing clustering distance threshold. Joints refer to T-junction nodes.

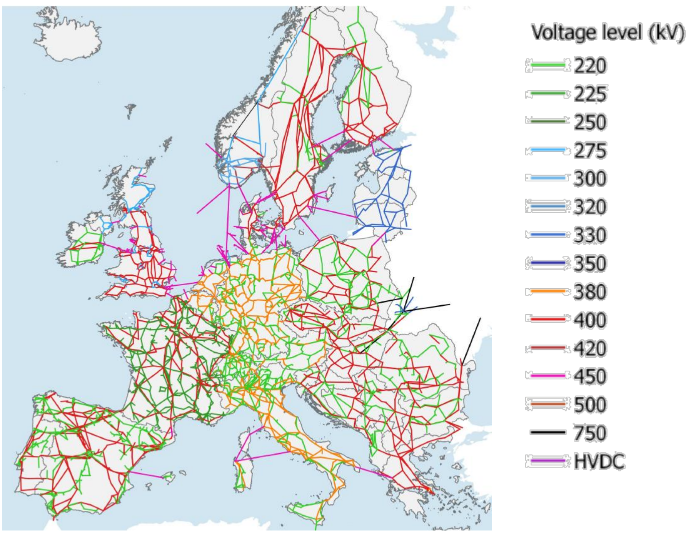

Figure 4-18 The transmission grid of the ENTSO-E area that is used in this thesis based on Gridkit and OSM data. The voltage levels follow the information from the OSM entries. Own illustration.

4.2.2 Conventional power plants

Similarly to grid, power plant information for all of Europe is hard to obtain, since the operators are not willing to publish their data due to trade secret and market competition reasons. However, the growing need for energy system modeling due to the desire for transiting towards RES has motivated projects to collect and provide data acquired from public sources and individual contributions similarly to the OSM scheme. Despite such efforts, most of the existing open databases do not reach the total installed capacity values reported by ENTSO-E for all countries, especially for RES plants. Thereby, many researchers have to rely on commercial data like the S&P Platts database [223].

Besides the crowd-sourcing based databases, additional projects have also emerged that aspire to collect and combine data from various open sources including these databases. Such projects include the Open Power System Data (OPSD) platform [195], the World Resources Institute (WRI) database [224] and the powerplantmatching (PPM) tool [209]. The latter tool is used and extended for the purposes of the thesis, since it can incorporate further data sources than the ones provided by the authors. Some key modeling aspects are discussed in this section.

The powerplantmatching tool (as of July 2017) constitutes a tool that uses the open source deduplication engine Duke [225], which in turn is based on the Lucene search engine, and its purpose is to identify similar record entries for power plants data from various sources [189]. Duke computes conditional probabilities between the data entries using different attributes, e.g. coordinates and names (where scores are assigned using character similarity metrics), and determines whether different entries may refer to the same entity (in this case power plant). Hence, powerplantmatching can compare several power plant databases and merge them in one database with unique power plants. The original tool of July 2017 combines the OPSD [195], WRI [224], Global Energy Observatory (GEO) [226], Carbon Monitoring for Action (CARMA) [227] and ENTSO-E [201] databases to generate a pan-European power plant dataset. The further inclusion of Jensen et al. [215], Meller et al. [228] and European Energy Agency (EEA) [229] databases along with alterations of the tool (e.g. countries extension, consideration of commissioning year from GEO power plant units, extraction of technology or CHP information potentially hidden in the plant name) increase the information content significantly as can be seen in figure 4-19.

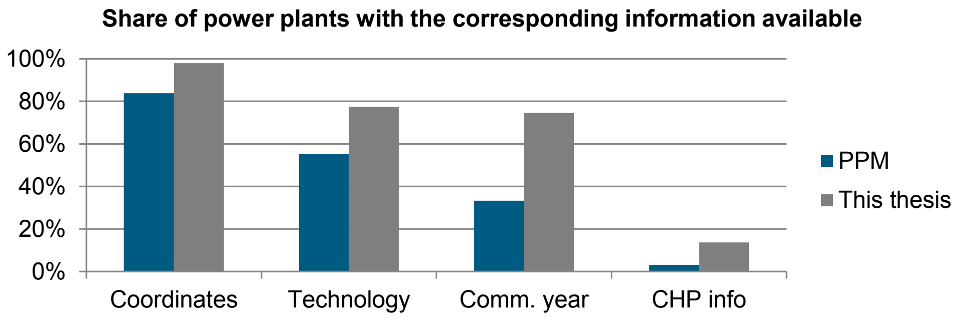

Figure 4-19 Share of power plants where the corresponding information is available. PPM refers to the published powerplantmatching results as of July 2017 [209].

A significant drawback of verifying the resulting dataset, as well as any pan-European model for 2015 consists of the lack of reliable source for reference data about power plants. Various inconsistencies appear even for aggregated values or among reports from the same source. Nevertheless, the comparison to reference sources allows the post-processing of the resulting dataset, including the identification of decommissioned plants as well the correction of fuel types and coordinates. The final dataset is depicted in figure 4-20, where the power plants are classified by fuel type.

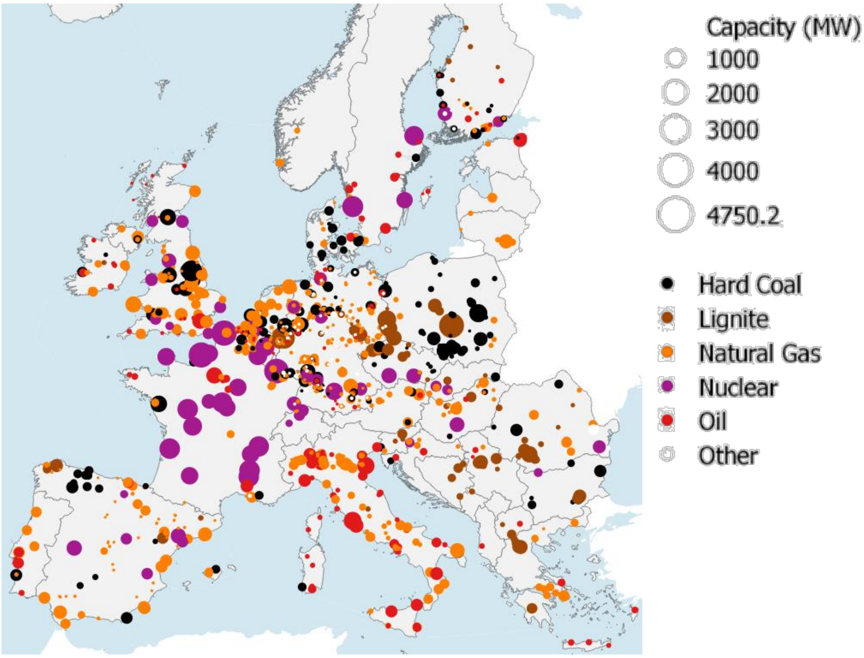

Figure 4-20 Conventional power plants of Europe considered in this thesis, classified by fuel type. Own illustration.

Obtaining information about efficiencies for individual European power plants constitutes a rather tedious task that goes beyond the scope of this thesis. Although a common practice is to assume average values for all power plants of the same fuel type and technology, this approach can lead to two limitations. On the one hand, using the same efficiencies leads to the same marginal costs of operation and therefore a multiplicity of solutions with the same total cost. Although the energy mix would not be affected, power flows over the grid may show significant deviations. On the other hand, the merit order could also be significantly distorted when different fuel types have similar marginal costs. In such cases the merit order, and consequently the energy mix as well, can become very sensitive to external parameters like fuel cost. Figure 4-21 illustrates such behaviors, where it can be observed that for 70% higher coal prices than 2015’s values, natural gas CCGT technology becomes more competitive than the least efficient hard coal plants. However, this behavior cannot be captured by assuming merely constant efficiencies.

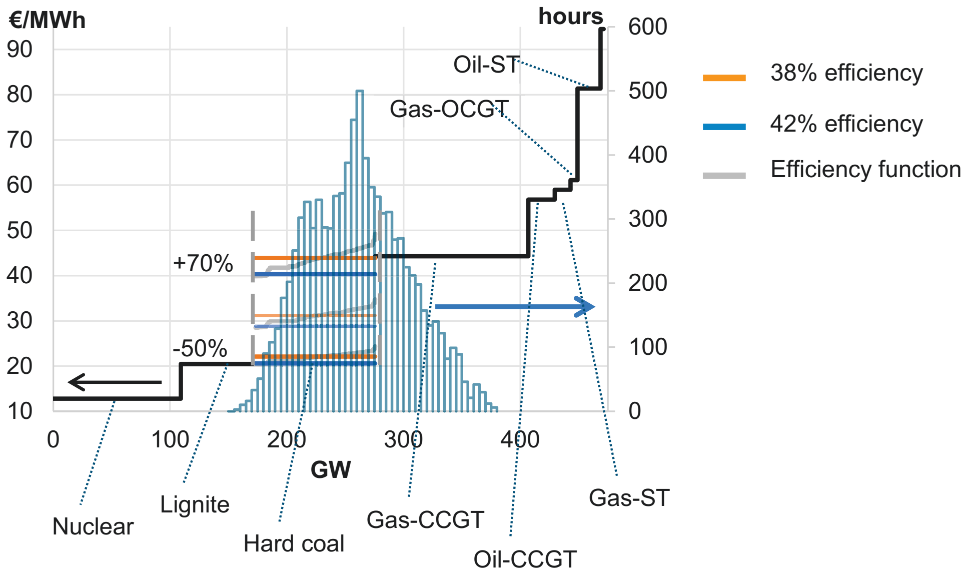

Figure 4-21 The pan-European merit order curve (depicted by the black line) combined with the corresponding positive residual load histogram for 2015. The hard coal marginal costs are represented by constant efficiencies as well as by a variable efficiency function and are depicted for the reference hard coal fuel prices as well as for -50% and +70% cases respectively. OCGT refers to open-cycle gas turbines, CCGT to closed-cycle gas turbines and ST to steam turbines.

A common approach to assign different efficiencies to power plants is to assume a correlation between efficiency and commissioning or retrofit year. This assumption is based on the rationale that technology advancements lead to higher efficiencies over time and the approach has been implemented by OPSD as well as by Schröter et al. [230] and Hintermann et al. [231]. The main drawback of this methodology is the requirements for commissioning and retrofitting information which, especially for the latter, is not available in the obtained European dataset. Moreover, all the aforementioned applications rely on values of German power plants, which may not necessarily be representative of all European plants. For this reason, the powerplantmatching tool is used to identify power plants that exist in both EEA and ENTSO-E databases, where annual fuel consumption and electricity generation information are available respectively. Using the calculated efficiencies from the matched power plants, linear regression is performed to generate linear functions between efficiency and commissioning year. The results for hard coal power plants can be seen in figure 4-22, where the resulting function shows a slower progress rate than the approaches in the literature.

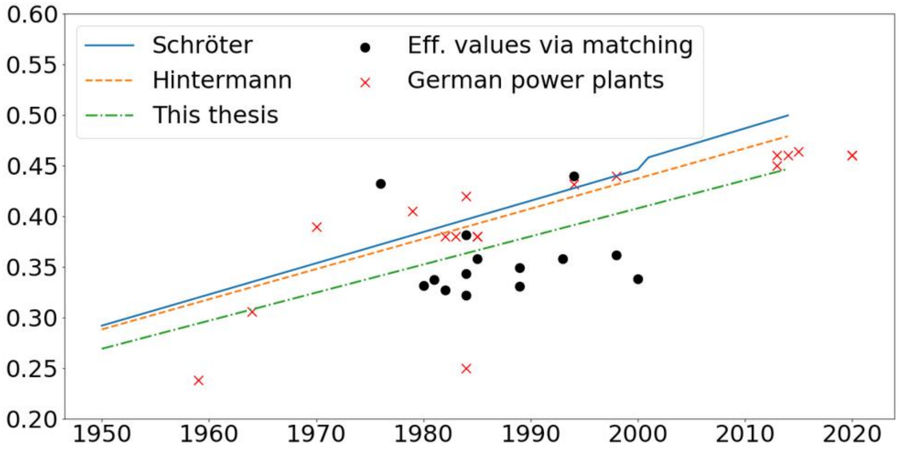

Figure 4-22 Efficiency of hard coal power plants as a function of commissioning year. “Eff. values via matching” values correspond to calculated efficiencies of European power plants via the matching of fuel consumption and electricity generation, whereas “German power plants” values correspond to known efficiencies for German power plants. The resulting regression function is compared to the approaches of Schröter et al. [230] and Hintermann et al. [231] that are based on German values only.

Besides efficiencies, calculating the marginal costs of power plants with eq. (4-4) additionally requires information about fuel prices, specific emissions and variable O&M costs which may differ for different countries. For instance, natural gas prices are not uniform over Europe and calculating lignite prices depends on each individual case since lignite is not a traded good. Moreover, heating values of coal may vary, thus leading to different specific emissions. In order to resolve such disparities, country-specific values are considered whenever possible and all parameters are calibrated to 2015 since literature values may diverge significantly from each other. A summary of the used values is shown in table 4-6 along with corresponding literature sources. For the ETS price, the value of 7.61 $€/_{tCO_2}$ is selected, which corresponds to the average value for 2015 [232] and is slightly more accurate than the German verification case.

Table 4-6 Average conventional power plant parameters over the investigated European region, classified by fuel type and technology. Literature values (e.g. fuel cost) are averaged when individual country values vary.

Energy carrier	Tech-nolo-gy	Gen-era-tors	Ca-pacity [GW]	Fuel cost [€/MWh]	Specific emissions [tCO_2/MWh]	Variable O&M [€/MWh]	Average efficien-cy	Average marginal cost [€/MWh]
Nuclear	Steam turbine	61	108.98	3.48 [233]	0	2.32 [233]	0.33	12.74
Lignite	Steam turbine	103	61.67	4.86 [234]	0.41 [235]	4 [236]	0.37	22.89
Hard coal	Steam turbine	211	102.51	6.9 [237]	0.34 [199]	6.21 [238]	0.38	31.1
Natural gas	CCGT	370	132.85	21.5 [237]	0.2 [199]	3.4 [238]	0.5	49.81
	OCGT	49	7.04				0.4	60.84
	Com-bustion engine	7	1.43				0.4	71.14
	Steam turbine	148	14.96				0.4	59.73
Oil	CCGT	51	23.11	28.66 [237]	0.27 [199]	1 [235]	0.54	58.6
	OCGT	40	3.38			10.368 [238]	0.37	92
	Com-bustion engine	18	2.48				0.37	97.89
	Steam turbine	55	19.91				0.4	79.36
Other fossil fuels	-	92	3.99	-	-	-	-	67
Bioen-ergy	-	58	1.28	-	-	-	-	11.3

Similarly to section 4.1.2, minimum must-run and capacity constraints related to heat generation are imposed to CHP plants as well. Although the methodology remains the same, data availability becomes the main obstacle for applying it to the European scale. On the one hand, despite the applied powerplantmatching improvements, a lack of data regarding which power plants are of CHP type is observed for some countries in comparison to the total national capacities [239]. The distribution of the total capacities to individual fuel types follows the distribution of the corresponding total generation. In the case of missing CHP capacity, existing power plants are gradually transformed to CHP plants until the national targets are reached. For this purpose, hard coal and lignite plants are gradually transformed starting from the largest plants, whereas for natural gas the smallest plants have priority, assuming that for this fuel type the business cases where heat generation is the primary driver becomes more probable for smaller power plants. Regarding the heat-related electricity generation from CHP plants, annual values for 2015 [240] are considered.

A further consideration regarding power plants modeling that needs to be addressed for the European level consists of the availability of power plants. Assuming 100% capacity availability may overestimate the generation from the cheaper power plants, where availability refers to either unplanned or planned outages, e.g. for maintenance. Although detailed data about historical outages for each individual plants would replicate the system conditions for 2015 in the most accurate way, such data are hard to obtain, while also such an approach would provide little merit to the application of the model for future scenarios. Alternative approaches would be to model outages either in a probabilistic way, following historical distributions of outage durations per fuel type or apply a maintenance optimization formulation, where each plant is shut down in periods of low profit margins (e.g. summer time for northern countries). Both approaches however introduce undesired properties into the model, either by introducing non-deterministic behavior or increased complexity with low gain in accuracy respectively. Therefore, a simpler method is applied, where all power plants are considered available at all times but with lower capacities than their nominal ones. This reduction in capacities is applied using historical availability factors per fuel type as shown in table 4-7.

Table 4-7 Technical availability factors for conventional power plants.

Energy carrier	Technology	Availability factor [238]
Nuclear	Steam turbine	0.87
Lignite	Steam turbine	0.87
Hard coal	Steam turbine	0.85
Natural gas	CCGT	0.82
	OCGT	0.81
	Combustion engine	0.83
	Steam turbine	0.87
Oil	CCGT	0.82
	OCGT	0.86
	Combustion engine	0.85
	Steam turbine	0.86
Other fossil fuels	-	0.84

The final conventional power plants dataset is used in a simplified European market model and verified for 2015 using the total energy mix, cross-border flows and zonal prices as indicators. In this model, each country is represented by a single node, thus following a similar zonal configuration to 2015 market zones. Interconnections are modeled via a transport model using constant but not necessarily symmetrical NTC values over the year. Time-varying NTC values, as reported by ENTSO-E [201], would be able to formulate a more accurate representation of the grid but these values are typically much lower than the indicative ones for 2011 [241] and 2020 [242], as well as than the physical flows reported by ENTSO-E for 2015 [201]. This can be clearly depicted in figure 4-23 for the Germany to Poland interconnection and can be explained by the fact that the time-varying data refer to the NTCs available for day-ahead trading only but not the technically available transfer capacities.

The residual load is implemented similarly to section 4.1, i.e. wind, solar, hydro generation and demand are considered as fixed profiles for each node [195, 201, 243], where load curtailments cost 1000 $€/_{MWh}$. Moreover, due to the small-scale nature of bioenergy applications, a discrepancy between the total capacity from the derived database and the corresponding national capacities is often encountered. Thereby, any missing bioenergy capacity is added to each country using a 0.6 availability factor, which is derived from reported hourly generation [201]. Regarding interactions with the neighboring countries (e.g. Turkey, Ukraine), these are taken into account by introducing them as virtual nodes with fixed import and export profiles according to historical data.

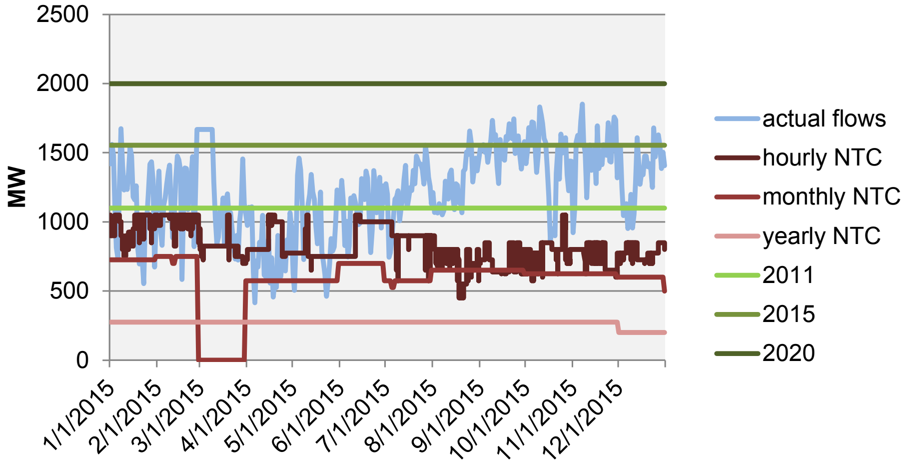

Figure 4-23 NTC values for the Germany to Poland direction compared to the physical flows reported by ENTSO-E [201] displayed as daily averages. The indicative values for 2011 [241] and 2020 [242] are significantly higher than the reported NTC values in higher temporal resolution.

4.2.3 Hydro power modeling

In contrast to conventional power plants, hydro power plants, although dispatchable, cannot be modeled in a similar way due to fuel provision and storage limitations that can normally be ignored for the case of conventional plants. For hydro plants, on the other hand, fuel (i.e. water) is not readily available over the year, since it depends on the weather and climate conditions, while on the other hand its storage is additionally limited. Modeling hydro generation as part of the residual load like in section 4.1 is helpful for verification purposes. However, applying the same approach for future scenarios would limit one of the most significant sources of flexibility for the system, especially when considering systems with high shares of VRES. In this section, the approach to model hydro plants as dispatchable plants with variable energy flow is described, where the methodology can be independent of the underlying grid modeling.

Although all hydro plants generate energy using the same principle (i.e. by transforming the potential energy of the water into electricity), in terms of modeling, they can be classified in three main categories, namely run-of-river (ROR), reservoir and pumped hydro storage

(PHS) plants. ROR plants are designed to exploit the natural flow of a river or stream and typically have very small storage availability (poundage) and head. Therefore, they are typically operated like an intermittent source, although with significantly lower fluctuation than wind and solar plants. Reservoir plants are built at the base of a dam that can restrict and control the flow of water, thus provide much higher flexibility, although water flow cannot be restricted completely due to environmental and agricultural reasons. Nevertheless, water can be stored in significant amounts and for long periods to provide seasonal flexibility to the power system. PHS plants resemble reservoir plants but with the additional option to operate in motor mode, where electricity is consumed to pump the water from a low to a high gravitational potential location. For this reason, they typically require two reservoirs in different altitudes; however they do not necessarily depend on natural water inflow to be operated. Currently, PHS plants constitute the most significant option for storing electrical energy and their significance will probably increase for increasing VRES penetration.

The operation of the different plant types necessarily dictate the way they are modeled. ROR plants are modeled similarly to wind and PV, i.e. as generators with variable capacity factors depending on the river inflow and with zero variable costs. On the other hand, reservoir and PHS plants are modeled as storage units (see chapter 3) with fixed charge and discharge capacities, fixed storage capacity and variable energy inflow related to the corresponding water inflow. PHS plants require in addition a pumping efficiency (round-trip efficiency is typically 70-80% [244]), while reservoirs essentially have zero charging capacity. Data regarding location, capacity and type follow the procedure of conventional plants, i.e. using the powerplantmatching tool, where in addition only a single type for each hydro plant is assigned when multiple are registered and installed capacities are scaled, when these deviate significantly from the total national values. French plant types are further corrected to match the capacities reported by the French TSO, RTE [245]. Regarding energy storage capacities, the data from Geth et al. [246] are used for identified PHS plants and further used to generate linear capacity/storage functions, similarly to Gimeno-Gutiérrez and Lacal-Arántegui [247]. Two functions are generated by applying linear regression on the available data, one for plants with capacity less than 450 MW and one for plants with a higher capacity. Corresponding data for reservoir plants are not available, therefore national storage capacities [248] are distributed by installed capacity to the corresponding plants. The extracted hydro plants dataset is shown in figure 4-24, where it can be seen that the majority of the installed capacity is located in the most mountainous regions.

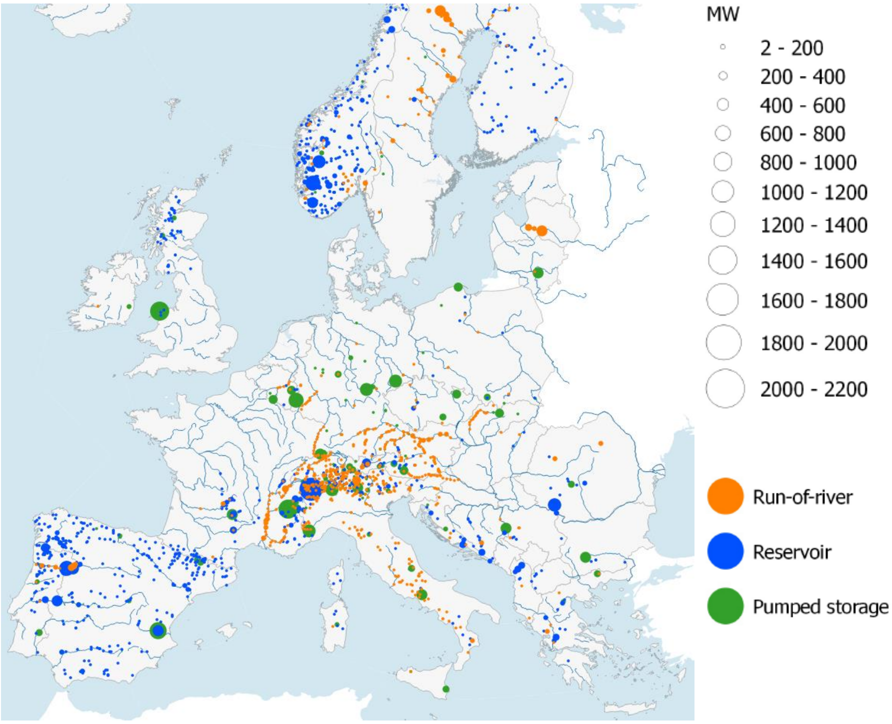

Figure 4-24 European hydro power plants for 2015 classified by installed capacity and type. Own illustration.

Regardless of the hydro plant type, a variable energy inflow based on the corresponding river discharge pattern is modeled. Since the information regarding which PHS plants use natural inflow is missing, all plants are assumed to have natural inflow as well. The developed methodology is necessarily dictated by the availability of data as well as the scope of the thesis. Equation (4-9) shows the fundamental way to calculate the available power output of a turbine given plant characteristics and water inflow. Since height information is typically not available, a common approach is to consider elevation data and approximate the desired value by the maximum gradient. The quantity that would be the hardest to estimate however consists of the water inflow. A bottom-up approach would be to define the drainage area for each plant, consider precipitation data within that region and estimate the water flow at the point of interest. The main drawbacks of such an approach would be the significant amount of data and effort required to model all potential water storage forms (e.g. underground, lakes, ice/snow), water use and evaporation until the water reaches the point of interest as well as the portion of such a water flow that can be used for electricity generation.

$$P = \rho \cdot h \cdot Q \cdot g \cdot \eta \tag{4-9}$$

where: P is the turbine power output (W)

ρ is water density (~1000 kg/m^3)

h is the elevation height (m)

Q is the flow rate (m^3/s)

g is the gravitational acceleration (~ 9.81 m/s^2)

η is the turbine efficiency

Alternatively, a top-down approach is implemented, which is based both on historical generation values as well as river discharge rates. The methodology follows the top-down rationale of calculating the minimum must-run constraints for CHP plants and consists of scaling individual profiles such that the total area of these profiles equals an energy quantity that matches historical values. In this case, the profiles correspond to the water inflow pattern, while the total value corresponds to the reported generation for the corresponding year.

Regarding the runoff profiles, two methodologies are developed and described in detail by Pfister [249]. The first one considers the total runoff regional climate model (RCM) data from Eurocordex [250] provided in a two-dimensional grid and daily resolution. Hence, the profile at a desired point can be computed by applying bilinear interpolation. The second approach considers measurement data of river flows from the Global Runoff Data Center (GRDC) [251]. The GRDC stations span various locations over Europe and provide data for various time periods with daily resolution. Due to the inconsistency of data availability (see Appendix D), all stations with data within the period 1956-2005 are considered in order to increase the number of used stations. Since the interest lies primarily in the seasonal variation of the inflow that does not change significantly over the years (e.g. dry summers in the south or snow melting periods in late spring), the profiles for each station are merged into one representative year, thus sacrificing yearly variation for the sake of better spatial representation. The allocation of profiles to desired points follows a more involved method that is described in Appendix D and is based on matching hydro plants and stations that belong to the same catchment area. The second approach is used in this thesis, where the profiles are downscaled to hourly resolution as demanded by the power system model formulation by assuming constant flows during the day.

The generated profiles are normalized and scaled such that the total energy inflow equals the total generation per plant type and country for that year. Determining the total generation per type and country is not entirely straightforward due to the lack of data. The exact process is described in Pfister [249], where data from Eurostat [252], ENTSO-E [253] and the Swiss Federal Office of Energy [254] are used. In addition to that, French production values are corrected using data from the French TSO [255]. Some typical inflow profiles are shown in figure 4-25, where it can be seen that the seasonal variation fits well with the literature and that the Eurocordex approach shows higher fluctuations.

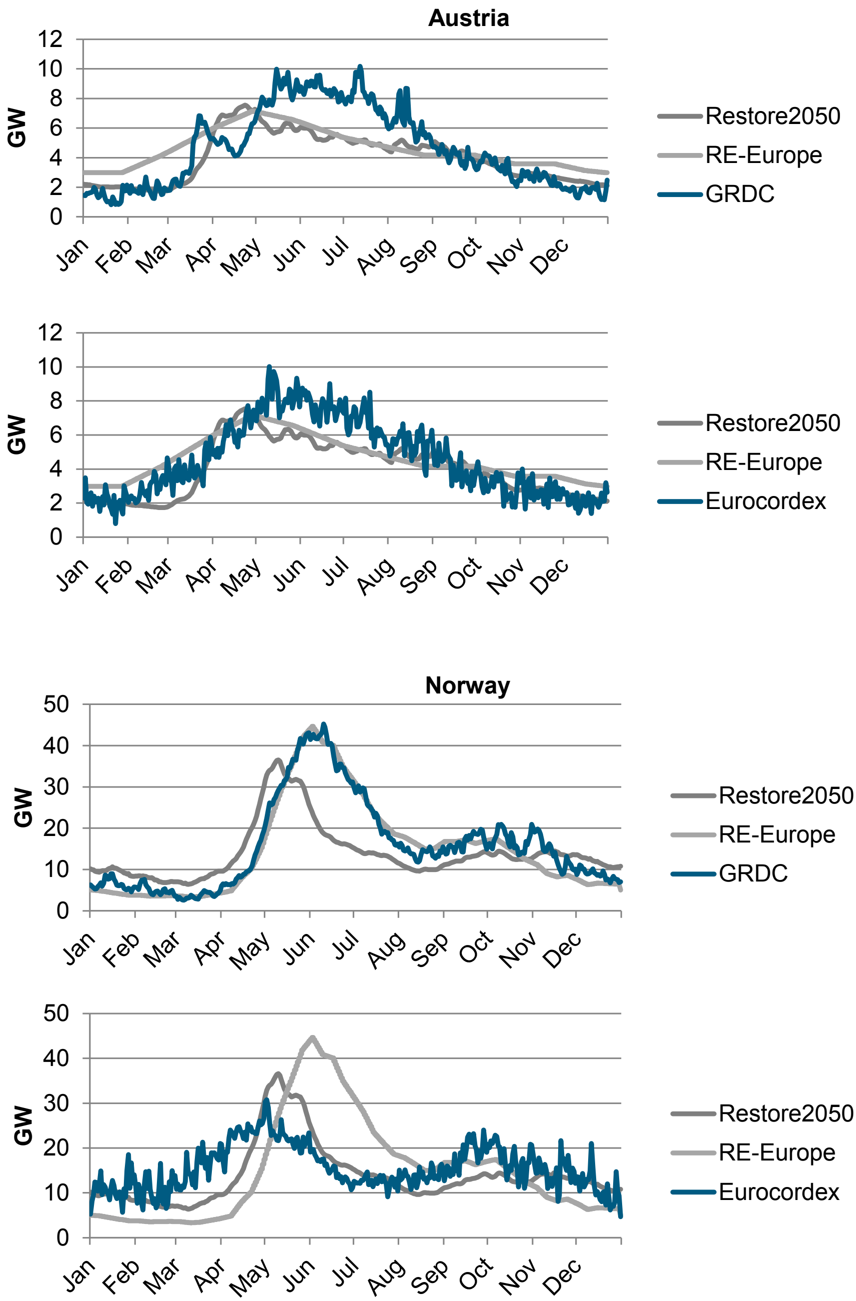

Figure 4-25 Comparison of hydro energy inflow profiles for the countries of Austria and Norway. Both GRDC and Eurocordex approaches are shown in comparison to the RE-Europe [215] and Restore2050 [256, 257] projects.

The large number of hydro plants may pose computational restrictions; therefore, a clustering strategy is applied to reduce their number. Due to their uniform storage-to-power capacity ratios as well as to their significantly higher number, the reduction methodology is applied only to reservoir plants. The clustering is applied for each country separately, where the 6^{th} Pfafstetter level catchments [258] (see Appendix D) are used to group the power plants. Grouping by catchment areas follows the rationale that hydro plants with similar inflow patterns are grouped, such that the spatial dynamics are retained. The clustering process results into 153, out of the originally 635, equivalent reservoir plants.

4.2.4 VRES infeed

The most significant VRES technologies for 2015 consist of wind (onshore and offshore) and PV. Due to the high spatial variability of these generation technologies, a mere application of reported national or TSO profiles would be insufficient for the verification purposes of the European power system. Despite the lack of official sources for higher spatial resolution, corresponding results of scientific studies that are validated on the national level for Europe are used.

Wind generation is separated into offshore and onshore technologies, where offshore wind refers only to the North Sea region. Hourly capacity factors separated by country are considered for offshore wind by Aparicio et al. [259] and applied to all corresponding offshore parks. Information about parks [260], namely capacities (MW) and locations, are considered, which are further connected to the nearest node of the respective country. Hourly onshore wind capacity factors are also provided by Aparicio et al. [259] at country and NUTS2 levels. NUTS (Nomenclature des Unités Territoriales Statistiques in French, meaning Classification of Territorial Units for Statistics) correspond to the European administrative regions used by Eurostat to report its various statistics [261]. The NUTS number indicates the different spatial resolutions where 3 is the maximum. For instance, 0 corresponds to countries. These profiles are combined with the respective information of installed capacities reported by ENTSOE [259] in order to create wind generation profiles for each region.

The solar generation profiles are calculated in a similar manner, i.e. using historically validated capacity factors multiplied by installed capacities. In a following study, Aparicio et al. [262] provide PV capacity factors and installed capacities at the end of 2015 for the NUTS2 regions as well. Nevertheless, due to the rapid growth of PV installations, these capacities do not correspond to an average value for 2015. Therefore, in order to avoid an overestimation of their production, the final generation profiles are compared at country level with the reported generation from ENTSOE [201] and scaled down respectively (on average 83.3%). Despite its detail, the dataset does not provide PV generation data for Denmark, Luxemburg, the Baltic and all western Balkan countries. Hence, these countries are considered as separate regions and the model of Pfenninger et al. [263] is used instead. The final generation distributions are shown in figure 4-26 for the onshore wind and PV technologies.

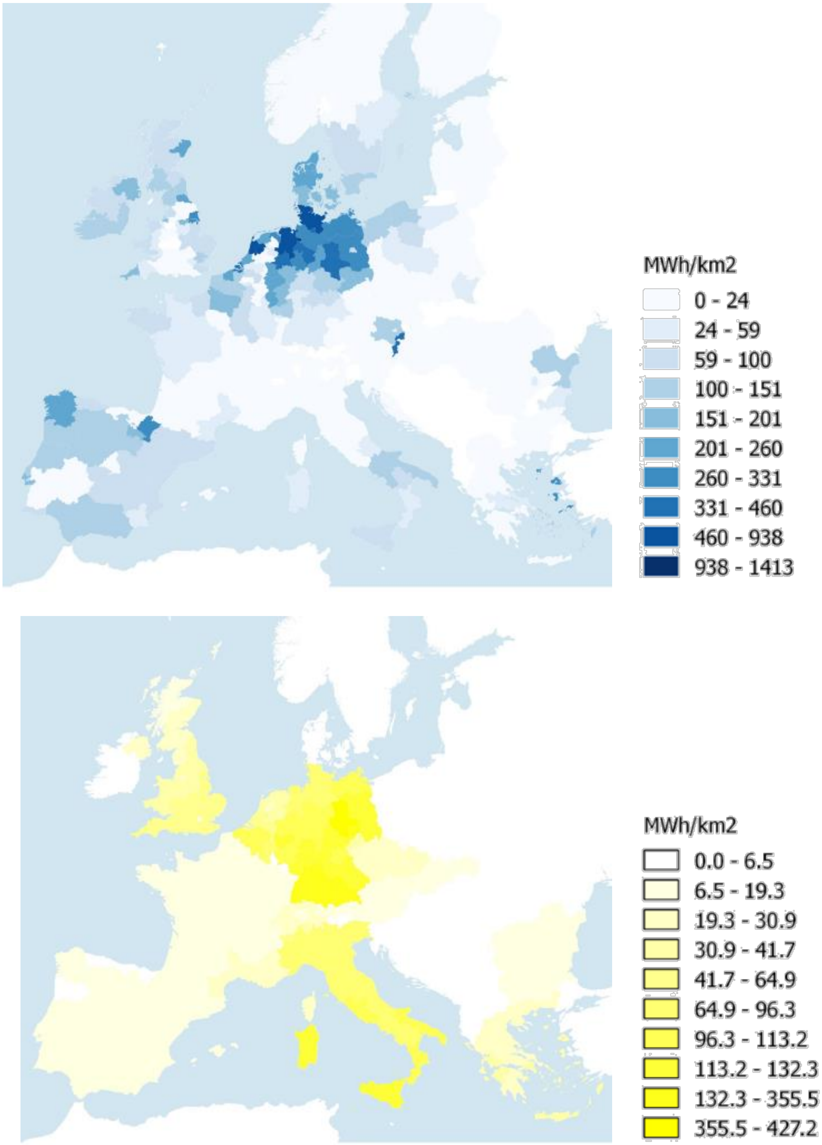

Figure 4-26 Onshore wind (top) and PV (bottom) generation density for 2015. Own illustration.

4.2.5 Electricity demand

Electricity load is one of the most crucial elements of the power system operation since it constitutes the primary driver for the development of the whole system itself. Typical consumers constitute lighting, heating, information, communication and electric motor applications which are usually modeled separately for households, transportation, industry and trade and commerce sectors (e.g. Singh et al. [264]). Since demand side management (DSM) technologies are still not implemented to a considerable extent besides large industrial consumers, electricity demand is usually modeled exogenously of the power system development. A bottom-up approach would consist of generating spatially and temporally resolved load profiles for each consumer (e.g. Elsland et al. [265], Kotzur [266]). However such a detailed analysis is out of scope for this thesis, hence a more top-down approach is preferred.

A top-down methodology consists of disaggregating a cumulative, usually deterministic, profile (e.g. at national or TSO level) to individual regions or nodes using spatial indicators. Such indicators could be either static like population and gross domestic product (GDP) or variable like ambient temperature. The majority of studies applying such a top-down approach use the population as the only indicator for spatially distributing electricity demand [111, 119, 124, 215, 267-270]. Thereby, besides the different scaling, profiles for all nodes are identical. Similar approaches have also considered either GDP as the only spatial indicator [206] or a fixed combination of population and GDP share [128, 189, 271] to additionally account for industrial demand. Despite the reasonable arguments behind such approaches, there is not always adequate quantifiable evidence to support them or estimate approximation error margins.

In this section, several spatial parameters are examined as possible indicators for distributing aggregated load profiles. These parameters include population in NUTS3 resolution [272-275], GDP in NUTS2 resolution [276-280], Gross Value Added (GVA) in NUTS3 resolution [281], temperature and irradiance in a 0.5^0 latitude x 0.625^0 longitude grid [282] or combinations of such parameters like population density or GDP per capita. The approach relies on applying multivariate regression analysis, where time-varying weights related to the corresponding indicators are trained using historical, regional profiles. The selected profiles consist of the 12 RTE (the French TSO) regions for 2015 [283]. Since respective data at NUTS3 level are not available, the set of RTE regional profiles provides one of the best available training datasets for the purposes of this analysis. Alternative dataset would include for instance the 6 Italian bidding zones [284] or the 4 German TSO control areas [195], which not only provide less training data, but also the corresponding regions do not allow a reasonable use of the selected indicators, since dense urban centers are aggregated together with large rural areas. Furthermore, the French regions span both of the two main climate zones of Europe (oceanic and Mediterranean) which may affect consumption behavior.

Before applying the multivariate regression analysis however, it is worth to investigate how the usual approaches behave for regional, historical values. For this purpose, three methodologies are tested, namely distribution by population, distribution by GDP and a hybrid version where the portion of the households consumption [285] is distributed by population and the rest by GVA. Figure 4-27 shows two plots where the three methodologies are applied. On the top figure, the time-varying datasets for France, Italy and Germany for 2015 are selected and evaluated by the average R^2 score (coefficient of determination) of each region's time series as defined by eq. (4-10), where the distributed national profiles are assessed as predictors of the corresponding historical ones. It can be observed that no methodology shows a consistently better prediction behavior. Moreover, it can be seen that there is a great variation of the score among the regions, especially for the cases of France and Italy, where the total consumption distribution shows higher deviations. On the bottom figure the same datasets are compared in terms of absolute deviation from the total annual consumption, since no timely resolved information is available. In addition, the annual data for Germany in 2013 as well for Spain in 2015, both in NUTS1 resolution (see Appendix E) are also examined. Similar conclusions can be deduced by this figure as well, where no methodology performs clearly better than the others in a consistent way, while also regional scores can deviate significantly. The most common approach, i.e. distribution by population, performs the best for France, where both the R^2 score and total deviation show higher match to the historical values. Furthermore, the number of regions as well as the regionalization itself may affect the performance of each indicator significantly, which can be seen on the second picture of figure 4-27 for the German case.

The R^2 score used for measuring the fitness between two time series is given by

$$R^2(y,\, \hat{y}) = 1 - \frac{\sum_{i=0}^{n-1}(y_i - \hat{y}_i)^2}{\sum_{i=0}^{n-1}(y_i - \bar{y})^2} \tag{4-10}$$

where $\bar{y} = \frac{1}{n}\sum_{i=0}^{n-1} y_i$ and the $\hat{y}_i$ and y_i correspond to the predicted and true values respectively.

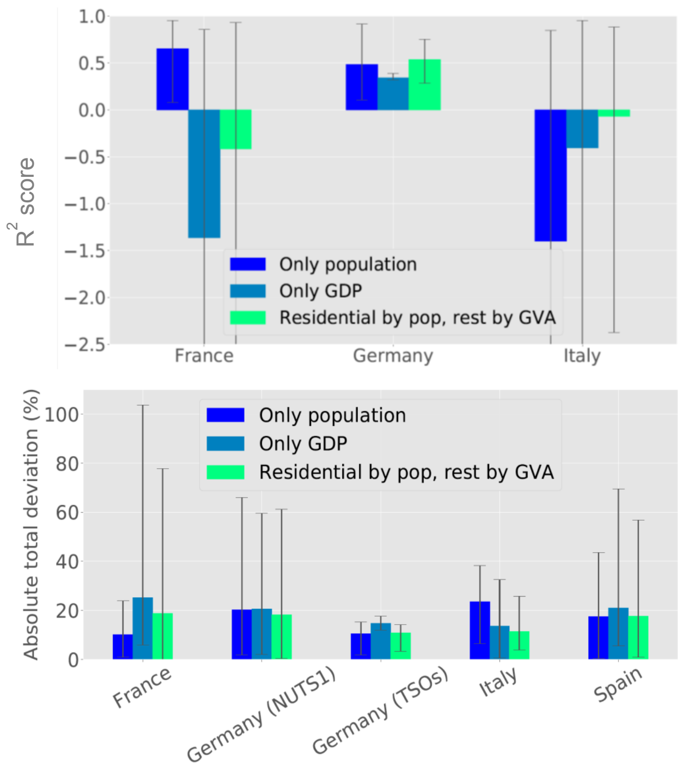

Figure 4-27 Application of the most common literature methodologies using historical data. On the top figure, time series data are evaluated by the average R^2 score (dimensionless). On the bottom figure, only cumulative, yearly data are used and the average total deviation is shown. The error bars indicate the range of all regions.

Since using a single indicator to spatially distribute electricity demand may be limiting, researchers have also applied combination of indicators to better capture both households and industrial demand. Hewes et al. [271] consider linear factors of 30% for population and 70% for GDP, whereas Hörsch et al. [189] use a 40%-60% split for population and GDP respectively. Such an approach may lead to better estimations than using single indicators only, however the limitations that the different temporal variability of the disaggregated profiles are still ignored, as well as further indicators that may affect the spatial distribution or even non-linear correlations. For instance, the GDP of a region may not correspond to its consumption, e.g. financial centers may show very high GDP to consumption ratios, or an energy-intensive industry may not contribute significantly to a region's GDP [206].

The idea of using multiple spatial indicators is expanded in this section by investigating several novel indicators as well as non-linear regression functions. The applied methodology can be described by eq. (4-11) and (4-12), where given an aggregated (national) demand profile D_t, normalized spatial indicators $w_{r,t}$ that may be time-dependent, regression functions f^i for each indicator and true (training) demand profiles $d_{r,t}$ for each region, we seek the time-varying parameters b_t and $c^i{}_t$ that minimize the distance between the predicted $\hat{d}_{r,t}$ and true demand profiles. The training data that are used correspond to hourly profiles for the 12 RTE regions and year 2015. Due to the considerable size of the described problem, it is split into smaller independent regression problems by decoupling the time steps, i.e. by solving 8760 non-linear, multivariate regression problems, each using 12 training points. These problems are implemented using the curve_fit function of the scipy package [286]. If non-linear regression functions are used, the final solution may additionally depend on the initial guess. Nevertheless, the results presented in this section have shown sufficient robustness for a variety of initial states.

$$\min\left\{\sum_{r,t}\left\|\hat{d}_{r,t}-d_{r,t}\right\|^2\right\} \tag{4-11}$$

$$\frac{\hat{d}_{r,t}}{D_t}=b_t+\sum_i f^i\left(c^i{}_t,w^i{}_{r,t}\right) \tag{4-12}$$

where:
- r stands for regions
- t stands for time snapshots
- i denotes the indicator (e.g. population, GDP etc.)
- $\hat{d}$ is the predicted demand value in MW
- d is the true demand value in MW
- D is the national demand value in MW
- b is the intercept
- c are the trained parameters
- w are the normalized indicator weights
- f are the regression functions

The simplest and most common regression function consists of the simple linear function, thus translating the problem to a multivariate, linear regression problem. The power of this approach stems from its simplicity as well as robustness to extreme values and overfitting. Figure 4-28 shows the average coefficients after applying linear regression using the indicators shown in table 4-8 and their combinations. It can be seen that the only significant indicators are the population and irradiance, since all other coefficients are almost 0. GDP appears to have a negative correlation; however negative factors are intentionally avoided by bounding the optimized coefficients to values equal or higher than zero only. Negative coefficients may lead to negative demand when extrapolated to data outside the training set, which would be obviously incorrect.

Table 4-8 Coefficients of multivariate linear regression together with the respective indicators.

coefficient	indicator	comments
c1	Population	Assuming constant consumption per person, a linear correlation is expected.
c2	GDP	Higher economic activity may imply higher energy usage. Could be problematic for financial centers.
c3	Population density	Higher density implies urban population, therefore more industry or higher consumption at night.
c4	GDP per capita	Richer regions may consume more energy.
c5	Ambient temperature (averaged over a region)	Correlated to heating and cooling demand, i.e. electric heaters, heat pumps or air-conditioning
c6	Irradiance (averaged over a region)	Lower irradiance may require higher consumption for lighting.

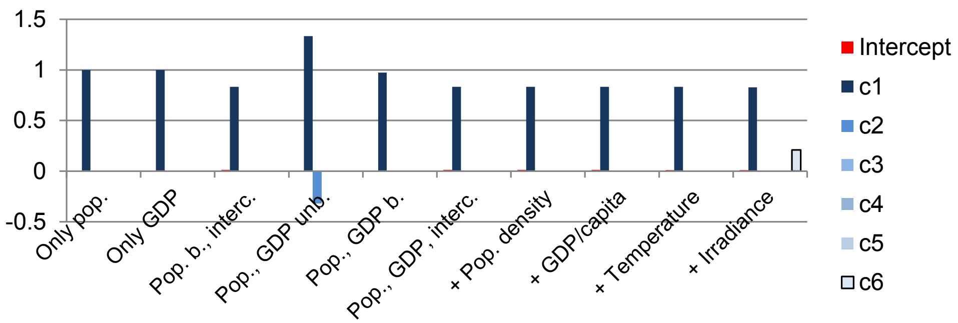

Figure 4-28 Average coefficients for regression problems with different combination of indicators. The c coefficients correspond to the various indicators as explained in table 4-8, b. refers to bounded (non-negative) coefficients and unb. to unbounded coefficients. Problem names starting with + (e.g. + Irradiance) refer to the previous problem formulation with the additional corresponding parameter included.

Although it becomes clear that population constitutes the parameter showing the highest statistical significance with electricity demand, it is worth investigating whether this correlation can be better expressed in a non-linear fashion or whether different indicators can show such behavior. Figure 4-29 shows the overall consumption ratio over the population ratio for each RTE region. It can be observed that although most points follow a linear trend, the rightmost dot that corresponds to the region of Paris (Île-de-France) does not obey this rule. Including this point would require a function that can be close to linear for small values but develop a saturation behavior for larger values. The $tanh$ and $arctan$ functions are commonly used in such cases, since their curvature can be directly controlled by their parameters. Nevertheless polynomial functions are examined as well. As it can be seen in figure 4-29, the polynomial functions with unbounded coefficients show the best match for the given data. However, they behave undesirably outside the training data range, especially for the area closer to zero, where most of the NUTS3 region values lie as shown by the corresponding histogram. On the other hand, polynomial functions with only non-negative coefficients coincide for the 2nd and 3rd degrees and are very close to a simple linear regression line. Regarding the $tanh$ and $arctan$ functions, these show similar behavior with each other nevertheless differ from the linear case. Therefore it is worth investigating whether they can provide a more suitable representation than the linear regression. Nevertheless, it can be noticed in figure 4-29 that using the French data may significantly underestimate coarser regionizations like Germany and Italy. On the other hand, such data may not reflect the behavior of finer regionizations, as it can be observed by the histogram of the NUTS3 regions, and therefore should not be used as reliable training datasets.

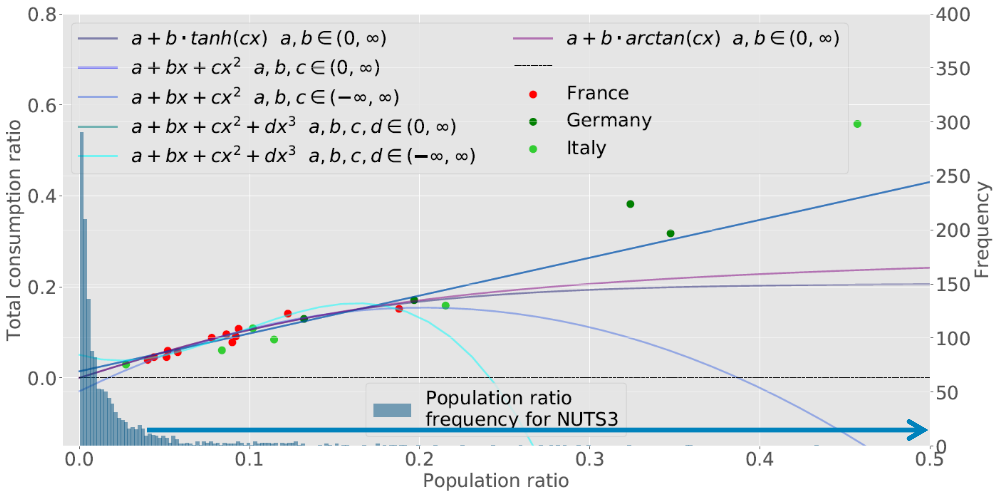

Figure 4-29 Overall electricity consumption ratio over the population ratio for each region of France, Germany and Italy and the corresponding regression functions for France. The histogram corresponds to the population ratio distribution of all Europe for NUTS3 regionalization.

The obtained regression functions are applied to the total French profile, thus generating regional profiles that can compared against the reference data. Figure 4-30 shows the weighted average R^2 score for various combinations of indicators and regression functions. It can be observed that only the unbounded cases show significant improvement, which however cannot be accepted due to robustness issues. From the bounded cases, only the last combination of {$\tanh(population)$, $\tanh(GDP)$ and linear irradiance} shows slightly better performance. However, such marginal improvement cannot justify the use of such a complicated approach. Thereby, the population is selected to be the mere indicator for the spatial distribution of electricity demand.

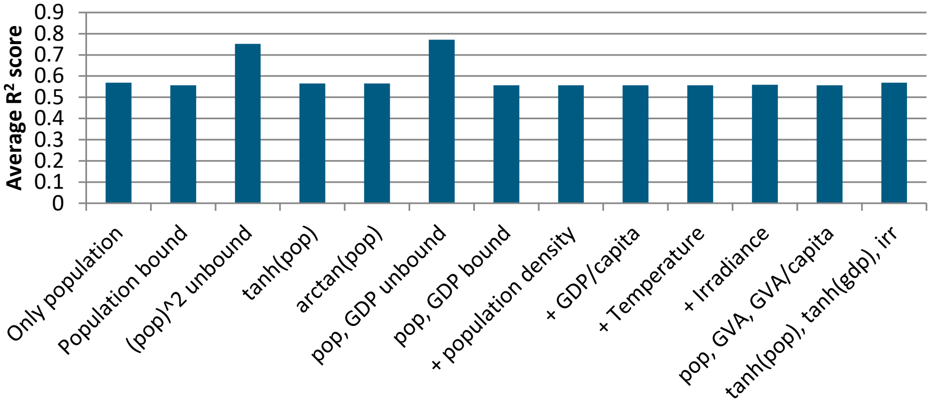

Figure 4-30 Weighted average of the R^2 score for each regional profile as predicted by applying different regression function combinations. The names starting with + (e.g. + Irradiance) refer to the previous problem formulation with the additional corresponding parameter included.

Assigning the regional demand profiles to the HV substations using the Voronoi methodology as described in section 4.1.3 may lead to inaccuracies due to the different ways the NUTS3 regionalization follows urban center boundaries for different countries. An illustrating example is shown in figure 4-31 for the area of Stockholm, where the corresponding NUTS3 region covers a large area that exceeds the city limits. Following the described methodology would inaccurately assign most of the demand to substations away from the city due to larger area coverage. For this reason, finer spatial information about population distribution is required, as shown in the last two figures. Instead of the existing methodology, population weights on a 0.25^0 x 0.25^0 grid are calculated using population density data for each country [287] and are aggregated to the Voronoi cells generated by the HV substations. The national demand profiles can be then distributed based on these weights.

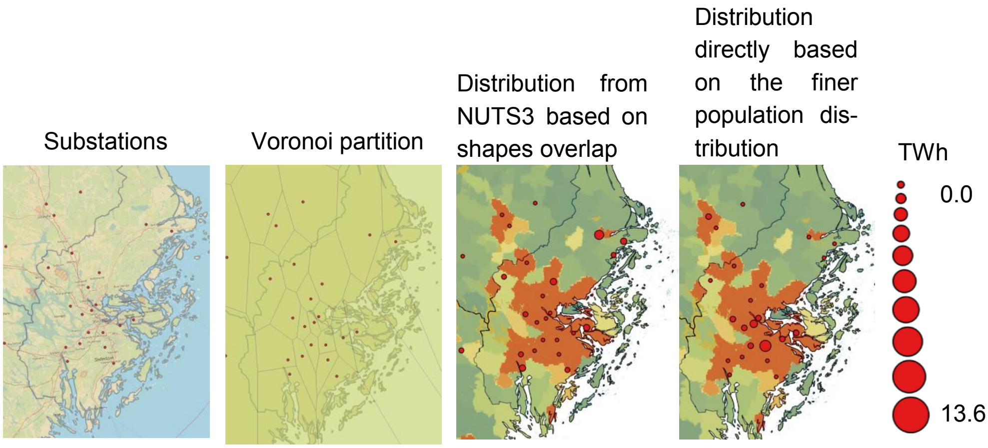

Figure 4-31 The NUTS3 region for the Stockholm area along with the high voltage substations and the corresponding Voronoi regions. With the area overlapping method, most of the demand is applied to the least dense nodes which are located away from the population and demand center. Considering finer population distribution information gives more realistic distribution of demand to the nodes.

4.2.6 Verification results

Similarly to the verification process in section 4.1, the pan-European model is verified using the total energy mix as the main indicator, while also considering the cross-border flows and load and RES curtailments as secondary indicators as well. One significant difference from the German verification case is that there are many countries for which the total energy mix should be predicted. For this reason, an “energy mix” verification indicator is calculated for each country by eq. (4-13), where the differences in annual generation for all fuels, including imports and exports, are averaged using the total country generations as weights, thus prioritizing agreement for the dominant sources. These indicators can be averaged for all countries using eq. (4-14), where the total generations are used as weights as well, thus each country participates based on its share over the total European generation.

$$ind_c = 100 * \frac{\sum_n \left| G_{model,\,n,c} - G_{ref,\,n,c} \right|}{\sum_m G_{ref,\,m,c}} \tag{4-13}$$

$$ind\_total = \frac{\sum_c ind_c \cdot \sum_m G_{ref,\,m,c}}{\sum_c \sum_m G_{ref,\,m,c}} \tag{4-14}$$

where G is the annual generation, $n \in \{dispatchable\ fuel\ types\}$, $m \in \{all\ fuel\ types\}$, and $c \in \{countries\}$

Different models are selected for the verification process implementing different ways to model the transmission grid as well as the hydro generation, as shown in figure 4-32 and described in table 4-9. The first model (“NTCs”) constitutes the simplest case, which is also typically selected for investment models. It represents each country as a single node, a partition close to the current bidding zone configuration, and uses a transportation model formulation with yearly NTC values for interconnection capacities as described in section 4.2.2. The second model ("hybrid") constitutes a mixture of the NTCs model and the verified LOPF model of Germany of section 4.1. The two parts are merged into a single optimization problem, where collective constraints are applied to the German cross-border lines using the NTC values. By this way, loop flows are allowed but hold a more economic sense. The third model ("grid – NTC constraints") introduces the full European transmission grid as described in section 4.2.1 with fixed hydro generation where collective constraints are also applied on the cross-border lines using NTC values to account for the constraints related to secure grid operation. A more simplifying, yet popular, approach consists of limiting all transmission line capacities by a security factor of around 70% [288] (i.e. 30% reduction) to ensure safe operation without the danger of cascading failures (e.g. N-1 criterion) and is selected as the fourth model ("grid – security factor"). The final model ("two-level") uses both "NTCs" and "grid – security factor" models sequentially, where the "NTCs" models hydro generation as described in section 4.2.3 and exports the scheduled generation to the "grid – security factor" model. For all models with full grid representation, hourly imports and exports from the neighboring countries outside the ENTSO-E region are also included similarly to section 4.1.3.

The selection and comparison of these models aspires to provide useful insights regarding the selection and merit of the final model as opposed to the different alternatives. The "NTCs" model, typically selected for investment models, constitutes the simplest pan-European version after a complete copper plate assumption and its simplicity and performance may compensate for potential inaccuracies. The "hybrid" model constitutes an extension of the German model introduced in section 4.1 and can be used when the "island" assumption for Germany is too limiting. The "grid" models are essentially identical and only differ in the way they handle security constraints. They may also be considered as the extension of the German verification process to the pan-European level, i.e. the system is represented with historical boundary conditions that include imports/exports and hydro generation. Although exchanges with third countries are less significant for the pan-European case, hydro generation can play a significant role in the power system operation, especially for higher VRES shares. Therefore, hydro plants dispatch modeling needs to be verified for 2015 as well. This is accomplished using the "two-level" model, where hydro generation also becomes an optimized variable.

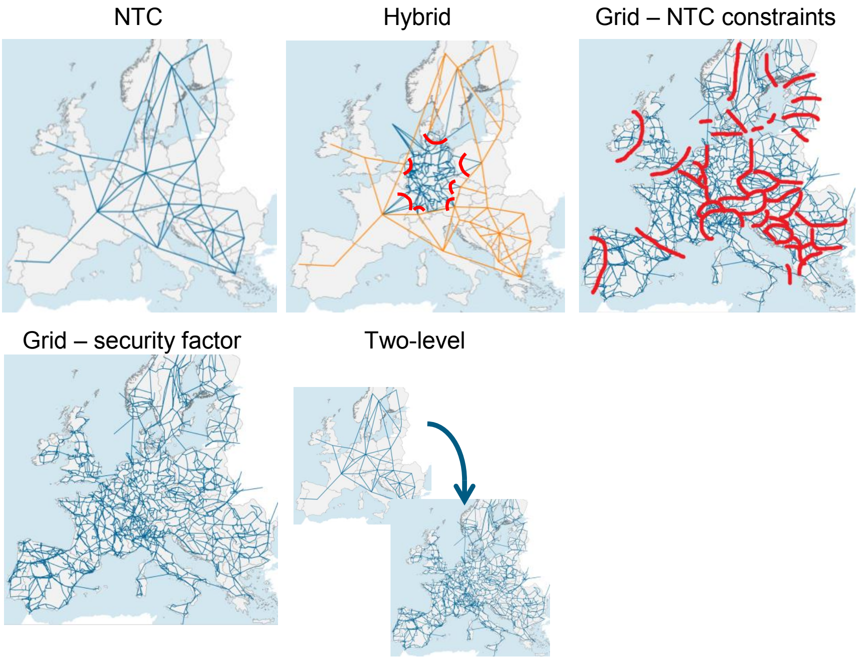

Figure 4-32 Visual representation of the five models to be verified as described in table 4-9.

Table 4-9 Description of different pan-European models in terms of grid representation and hydro generation.

name	Grid representation	Hydro generation
NTCs	• Each country is a node • Transportation model using yearly NTC values as capacities	• Fixed historical profiles from ENTSOE
Hybrid	• Germany with transmission grid as in section 4.1.1 • Other European countries as in the NTCs model • Collective constraints on cross-border German lines using NTC values	• Fixed historical profiles for Germany as in section 4.1.3 • Fixed historical profiles for the rest European countries as in NTCs model
Grid – NTC con-straints	• Pan-European transmission grid as described in section 4.2.1 • Collective constraints on cross-border lines using NTC values	• Fixed historical profiles from ENTSOE
Grid – security factor	• Pan-European transmission grid as described in section 4.2.1 • Uniform reduction of AC line ca-pacities by 30%	• Same as above
Two-level	• Same as above	• Hydro genera-tion/consumption profiles calculated using the NTCs model with hydro plants op-eration as storage units

Pan-European power flow simulations are performed with all models and their results are compared using the “German mix” indicator from eq. (4-13), the “European mix – total” indicator from eq. (4-13) as well but for the total European mix, the “European mix – by country” indicator from eq. (4-14) as well as a cross-border (CB) flows indicator. Load and RES curtailments remain, as expected, low for all cases (e.g. only 1% load and 2.5% VRES curtailments for the “two-level” model), therefore these values are not used for comparison purposes. The German mix is used as a verification indicator separately from the European mix for various reasons, including:

- The reliability of both model and reference data is one of the highest for Germany
- The versatility of generation technologies is one of the highest among European countries
- The total generation is high, therefore the model can predict such aggregated values more accurately
- It is located in one of the most densely meshed areas, hence the verification becomes more challenging and gains additional merit
- It is located away from the borders, thus more robust in modeling exchanges outside Europe

Unlike generation mix, a corresponding indicator for cross-border flows cannot be based on averaging total values, since flows can also be negative. For instance, a net average flow between two regions could fall close to zero and thus lead to misleadingly high relative discrepancies. Alternatively, considering that the reported physical flows can be provided in hourly resolution, a different approach is possible. Since the focus remains on average behaviors, a time series comparison using goodness-of-fit metrics like R^2 or root mean square error (RMSE) would be out of the scope for these verification purposes. Instead, the selected metric consists of comparing the probability density function (PDF) distributions for each border and measuring the corresponding area overlap. Figure 4-33 shows the PDFs of the reference flows as well as the corresponding results from the “NTCs” and “grid – security factor” models for the Austria-to-Germany border. It can be observed that even when the average flows may be close, the respective PDFs may differ significantly. The “spike” behavior shown in figure 4-33 for the “NTCs” model is typical of this modeling approach for other borders as well, where interconnections tend to be used to their maximum for most of the time. On the other hand, using the full grid typically gives more diverse distributions. Another distinction to the mix indicator stems from the difficulty to define weights on borders, since there is no clear methodology to distinguish them by significance. Thereby, the total European indicator for the flows consists of simply averaging all individual border indicators.

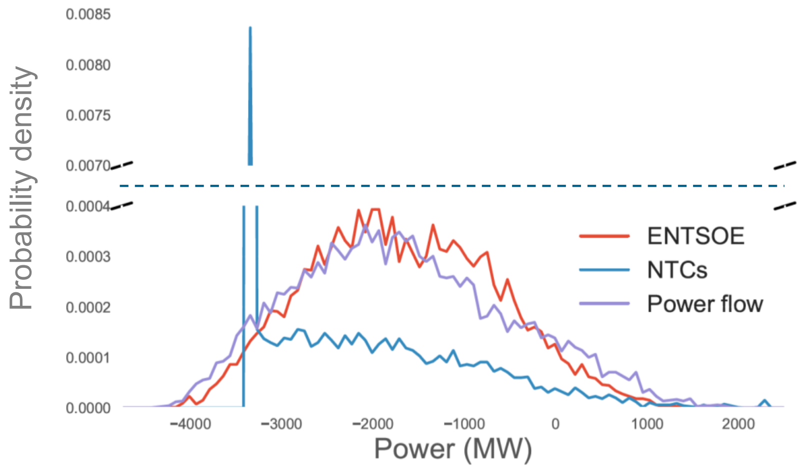

Figure 4-33 Probability density functions of the cross-border flows between Austria and Germany with direction to Germany. “ENTSOE” refers to the reported physical flows and “power flow” to the “grid – security factor” model.

All four indicators are shown for the various models in figure 4-34. It can be observed that despite the model differences, the indicators that mostly vary are the “German mix” and “European mix – total” which follow the same trend with the former being consistently lower. The “European mix – by country” remains in the same range for all models but at a higher level. This shows the importance of modeling the power plant fleet and parameters, which cannot be easily compensated by improving the model formulation. For example, Greek lignite is more expensive than the model assumes, while the Italian classification of generation capacity into fuel types also involves inaccuracies. Such shortcomings have a direct impact on the flows as well, whose indicator remains relatively high, although it improves for the models that use the full transmission grid. Regarding the modeling of security constraints, it can be seen that the “security factor” approach yields a lower value for the “German” indicator while only slightly worse results for the “European mix – by country” indicator than the “NTC constraints” approach. Considering its simplicity as well, this method is selected to be used in chapter 6 where the future European scenarios are investigated. Besides the verification of the conventional generation, the “two-level” approach shows adequately satisfactory results as well. Hence, it is considered that the hydro plants operation is verified too, thus promoting the “two-level” model as the main tool for assessing future scenarios with a quantifiable range of accuracy and limitations.

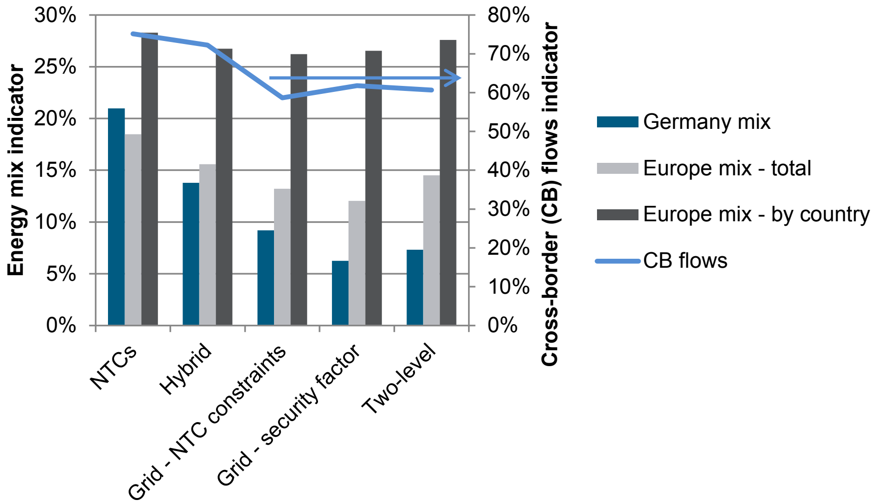

Figure 4-34 Verification results using the “German” and “European - total” indicators defined by eq. (4-13) and “European – by country” indicator defined by (4-14) as well as the cross-border (CB) flows indicator for different pan-European models for 2015 as described in table 4-9. Bars, i.e. mix indicators, refer to the left axis, whereas CB flows to the right axis.

Further insightful figures and analysis regarding the 2015 pan-European verification are shown in Appendix F. More detailed results about the energy mix are discussed for the main four models (“grid – NTC constraints” is excluded), while the net flows and grid bottlenecks are also analyzed for the “two-level” model.

4.3 Chapter summary and discussion

In this chapter, the verification of a pan-European dispatch model has been discussed. It was shown that such a task can become rather extensive, originating mostly from the lack of available data. Therefore, verification attempts are only rarely encountered in the literature, while also such attempts may result in significant deviations even for averaged values. Besides the lack of available data for modeling and their low quality, corresponding shortcomings are faced with regard to reference data as well, which should represent the reality and form the basis for verification. Such data become typically available from TSOs which however do not necessarily constitute exact measurements of the desired quantities and may also not be checked for errors.

In the first section the German power system is verified for 2015. In contrast to other verification attempts, it is shown that an adequate modeling of CHP generation can significantly improve the estimation of the output from thermal power plants. Weaknesses that could be improved in future works constitute better modeling of the grid data and the allocation of the residual load to the substations. Despite the limitations, it was shown that with the described linear OPF methodology, the desired system quantities can be adequately reproduced. It was also shown that the total electricity generation per fuel type could be predicted within a 10% margin.

In the second section several pan-European models sharing common modeling components were described and verified for 2015. Similar conclusions to the German case apply to the European case as well, where however cross-border flows and hydro dispatch modeling are also verified. The lack of modeling and reference data pose significant challenges to the verification process since the system conditions have to be reproduced accurately for a modeling approach to be verified.

The modeling of all power system components are described in detail as well as evaluated independently. The transmission grid is modeled based on geographical data from OSM. The conventional power plants are modeled using various public sources and the powerplantmatching tool, including manual corrections. The power plant parameters are calibrated for each country, fuel type and technology while also a novel method to estimate the efficiencies is developed. The hydro power plants data are obtained similarly to the conventional plants, while in addition the variable energy inflow related to water runoff is modeled based on river discharge data. Wind and PV generation profiles are taken from a validated model in high spatial resolution. Finally, the spatial disaggregation of electricity demand was investigated via a novel methodology based on multivariate, non-linear regression analysis.

The verification process resulted in a discrepancy lower than 10% and 15% for the German and European energy mix respectively. It was also shown that the most significant modeling components consist of the power plant capacities and cost parameters as well as the modeling of CHP plants generation, the availability of power plants, the security constraints for grid operation and the allocation of the electricity demand to substations. The final “two-level” model shows sufficiently accurate results for both conventional and hydro power plants generation as well as cross-border flows for the purposes of this thesis.

The overall verification process provides validity to the developed model with respect to both the selected approach and data.

- The verification of the selected approach, which is based on linear OPF and was tested on the German power system, supports the electricity market and grid operation assumptions used in this thesis. Therefore, the application of this approach is justified for examining different scenarios as well.
- Moreover, the verification process over the whole ENTSO-E area allows the adoption of the selected methodology for pan-European investigation as well.
- Finally, the verified model and dataset can form a strong background for:
    - benchmark calculations
    - comparison of different operational models
    - analyzing the existing European power system
    - developing highly resolved future scenarios

  For the purposes of this thesis, the obtained dataset will constitute the basis for describing all of the investigated future scenarios.

5 Scenarios

Power system analysis using dispatch models requires the complete definition of the system boundary conditions, such as the power plant fleet, the transmission grid infrastructure and the electricity demand. Although such conditions can be modeled with a relative confidence for historical states, predicting the power system of the future is far from trivial and such a task falls outside the scope of this thesis. Alternatively, system evolution is examined under a variety of different but plausible assumptions that result in different scenarios respectively. The focus of this work does not involve the analysis of these scenarios as accurate system forecasts but rather lies in the investigation and understanding of the system operation and behavior as well as in obtaining an estimation of the desired system quantities.

Designing such scenario frameworks and developing a respective investment model would fall outside of the scope of this thesis as well, therefore corresponding work from external official sources is considered, including the ENTSO-E and the European Commission. However, investment models along with the respective scenario assumptions typically use simplified and spatially reduced versions of the system. Thereby, further assumptions may be required for a more detailed power system description based on each scenario's guidelines. To this end, the pan-European model developed in section 4.2 and verified for the year 2015 serves as the foundation for developing any corresponding scenarios for the future power system.

Although the model developed in section 4.2 has been verified for the historical system state of 2015, future versions may require further modifications that better reflect the expected technological advancements. Such advancements include the gradual replacement of fossil CHP units by heat pump and power-to-gas technologies that can assist decarbonizing the heating sector [289]. Thereby, the CHP constraints related to heat generation are not considered in future systems, which might lead to an overestimation of VRES integration. Moreover, the electricity demand is expected to play a vital role into the overall system operation, since future consumers (e.g. battery electric vehicles – BEV) and the evolution of DSM technologies will allow a more responsive and flexible electricity load. Hence, the additional modeling levels described in section 3.3 along with the modeling of load shifting presented in section 3.5 are included as well for the future systems.

Dispatch models require static representations of the power system, which can only be modified exogenously. To this end, corresponding system descriptions are developed for the years 2030, 2040 and 2050, where it is assumed that the system is not altered during the course of these years but only among them. The selection of these years follows the available scenario data and is considered adequate to represent the system evolution.

5.1 The Ten Year Network Development Plan (TYNDP)

Planning power systems has been traditionally performed on national level with limited coordination among the European states. However, the mandate of the European Union to liberalize the gas and electricity markets, as described by the Third Energy Package, resulted into forming pan-European organizations like the European Network of Transmission System Operators for Electricity (ENTSO-E) and Gas (ENTSO-G) or the Agency for the Cooperation of Energy Regulators (ACER) in 2009. ENTSO-E's objectives include the promotion of closer collaboration across Europe and the support in implementing EU's energy and climate policies such as the integration of RES and the completion of the internal energy market. To that end, ENTSO-E is involved in several activities, some of which include reporting seasonal outlooks regarding security of supply issues twice a year, the conduct of mid-term adequacy forecast annually and the development of the ten year network development plan (TYNDP) for the European transmission grid biannually. The TYNDP constitutes the only pan-European development plan and is conducted using a cost-benefit analysis (CBA) approach developed by ENTSO-E as well as consultation with stakeholders. The considered projects additionally form the basis for the selection of the projects of common interest (PCI) from the European Commission. PCI constitutes a list of crucial infrastructure projects, first published in 2013, that can have a significant impact on improving the pan-European market integration and efficiency, as well as enhancing the security of supply and contributing to achieving the EU’s energy and climate targets.

The TYNDP 2016 serves as the primary source for investigating the power system of 2030, where its scenarios are developed following two distinct dimensions that can significantly influence the system evolution. Based on these two dimensions, four visions (i.e., scenarios) are developed, as shown in figure 5-1. The first dimension consists of whether the coordination among the member states will be fostered to more integrated designs, whereas the second dimension evaluates the degree of progress towards the energy and climate goals set by the European Commission in the Energy Roadmap 2050 [235].

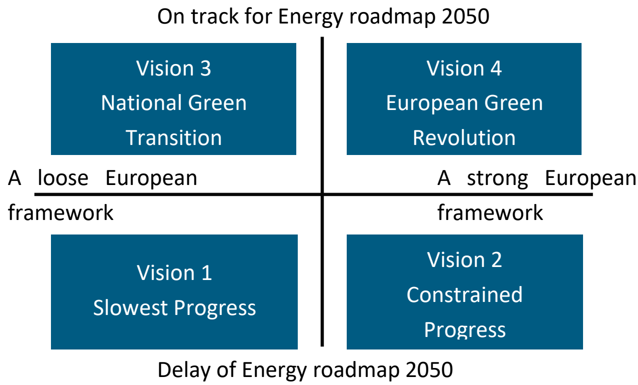

Figure 5-1 The scenario development of TYNDP based on two distinct dimensions, the strength of a European framework and staying on track with the Energy roadmap 2050 targets [242].

The data of the TYNDP are provided in aggregated form for each country member while also including a list of all candidate projects regarding the grid expansion. Besides the individual projects however, future NTC targets are listed for the inter-country connections as well, which can be used for the “country” modeling level. Regarding the individual projects, these can be classified into three categories, namely DC lines, new AC lines and upgraded AC lines where the upgrade refers to replacing an existing line by one with either higher operating voltage (typically from 220kV to 380kV) or composed of high-temperature low-sag (HTLS) designs (e.g. aluminum conductors composite core – ACCC) that offer higher power transfer capacity. The identification of the lines to be upgraded as well as the geographical information of the additional projects (that are not always defined as distinct lines) is completed using the information from the TYNDP projects list and map [218], the PCI map [290] as well as individual project websites when available. The final set of all candidate projects until 2030 are shown in figure 5-2, where the AC and DC lines are depicted separately. Since the TYNDP does not necessarily include all the projects suggested by the individual national development plans but only the ones with pan-European significance, all the suggested project candidates are assumed to be completed by 2030, despite this may not necessarily reflect the reality.

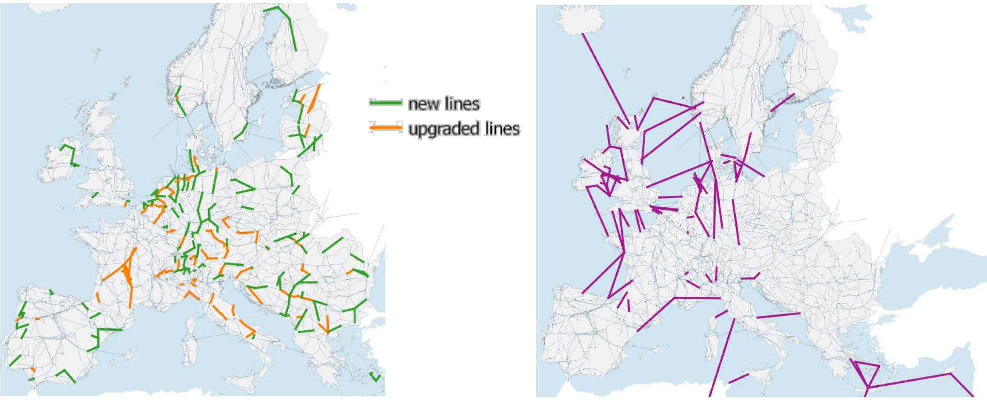

Figure 5-2 All candidate projects until 2030 as described by the TYNDP 2016. On the left picture the AC lines are depicted whereas on the right picture the new HVDC projects are shown [218]. Own illustration.

Although the TYNDP does not intend to be interpreted as a forecast for the European system development, its four scenarios can be considered to form the state space of the system's evolution. Therefore, these scenarios are selected to be investigated for the purposes of this thesis as representative for the 2030 European power system. The phase out strategy of the conventional power plants as well as the VRES generation is discussed in section 5.3, since they are applied for all future scenarios, including 2040 and 2050. Regarding the electricity demand of 2030, the TYNDP provides projections for the national time series for all the corresponding visions. Thereby, this information can be applied to the respective models by merely adjusting the time series to the individual time zones and distributing them to the grid nodes using the current population distribution as indicator.

5.2 The e-highway project

Developing long-term scenarios beyond 2030 rarely involves models with high spatial resolution, mostly because of the significant degree of the underlying uncertainties. Nevertheless, due to the rigorous and challenging political targets set for 2050, many studies have attempted to design corresponding scenarios and predict the system's evolution. One of the most elaborate corresponding studies, funded by the European Commission and focusing on the transmission grid development, consists of the e-highway project [291]. In this project a consortium of 28 partners including ENTSO-E, TSOs, universities, research institutes, NGOs, companies and energy associations has developed a set of pan-European scenarios for 2040 and 2050 as well as the corresponding grid extension requirements via 9 working packages starting from the TYNDP results. Considering the novelties and impact of this study as well as the focus on the transmission grid and the connection to the TYNDP, the scenarios developed by the e-highway project are considered to set a reasonable frame of the long-term European power system evolution. Similarly to the TYNDP visions, these scenarios merely constitute boundaries of where the actual system might end up. Thereby, analyzing the system of 2050 should not be restricted to one scenario only.

The e-highway project defines 5 different scenarios, described in appendix G, that can represent sufficiently distinguishable pathways, all satisfying the European climate targets. In contrast to the TYNDP, the study does not consider the full transmission grid, although it assumes that all the corresponding projects will be completed by 2030. Alternatively, it reduces the network representation to 100 clusters for the ENTSO-E area plus 16 regions for the neighboring countries and North Sea regions. The considered regions was the result of a developed clustering algorithm as well as consultation with stakeholders. Hence, the suggested grid reinforcements only apply for this aggregated grid version, thus concrete individual line installations or upgrades cannot be directly deduced. Moreover, the resulting power plant capacities are also provided in aggregated form at country level for 2040 and at clusters level for 2050. Therefore, the translation of these target capacities to individual plants as well as calculating the generation profiles from VRES resembles the TYNDP process and thus described in section 5.3.

5.2.1 Electrical load

Contrary to the TYNDP, electricity load profiles are not explicitly reported by the study. However, the applied methodology is described and thus can be reproduced. According to that methodology, the electricity demand for each scenario can be calculated using a top-down approach where the total load is split into several components as depicted in figure 5-3. The total consumption of each component and country is calculated based on assumptions following each scenario's rationale, using indicators like energy efficiency policy, population and economy growth. The resulting values can be found in the D2.1 report [292], where the approach for generating the spatio-temporal profiles is also described.

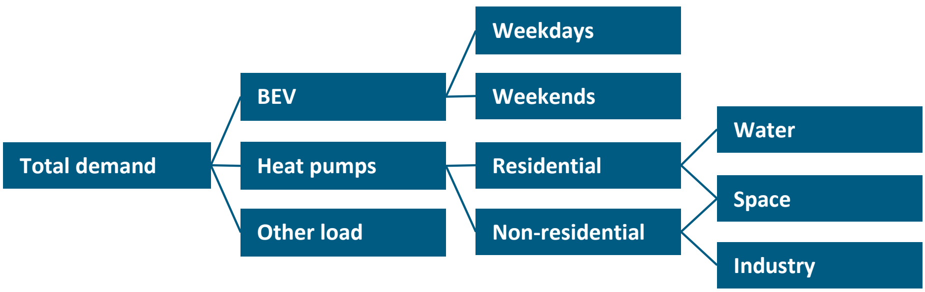

Figure 5-3 The components of generating load profiles according to the e-highway top-down methodology. The total consumption values follow each scenario rationale regarding indicators like energy efficiency, population growth and economy, whereas the profiles are fixed based on corresponding assumptions and historical values.

The top-down approach of determining the profile of each component in figure 5-3 consists of scaling a respective normalized profile by the total consumption of this component. The profiles related to the charging of electric vehicles (EV) can be divided into three categories based on the responsiveness of the vehicle to grid signals, namely non-active, semi-active and active. The daily normalized charging profiles for the non-active and semi-active categories are shown in figure 5-4, while the profiles of the active category are assumed to coincide with the semi-active but are later determined by applying a flexible demand modeling approach as described in section 3.5. Regarding the electricity load related to heating, two contributors are considered, the residential and the non-residential heat-related demand. In both cases, a significant electrification of the heat demand is assumed via heat pumps and boilers depending on the corresponding scenario. The residential heat demand consists of two components, the water heating and the space heating demand as depicted in figure 5-5. According to the e-highway methodology, the demand related to space heating is applied only for the months were the average temperature is below a given threshold. However, since this approach may lead to high load gradients between the transitional months, instead of whole months, ambient temperature time series in 6 hour intervals [282] and averaged over the corresponding regions are considered. Regarding the industrial heating demand, this is considered to be constant over the whole year. Finally, the profiles related to the rest of the electricity demand are taken from historical data at country level [195, 201, 215, 243, 293, 294] as reported by ENTSO-E. Due to various cases of incomplete or inconsistent data, only the years 2011-2015 are considered, where it was possible to apply corrections to the profiles of all countries. The spatial distribution of the aggregated profiles to the grid nodes follows the methodology described in section 4.2.5.

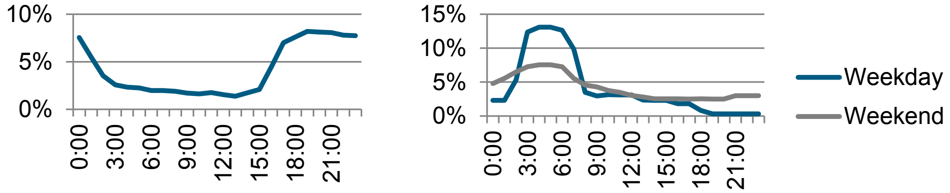

Figure 5-4 Daily normalized load profiles due to electric vehicles charging. The left picture corresponds to non-active vehicles and the right picture to semi-active vehicles which exhibit different behaviors between weekdays and weekends.

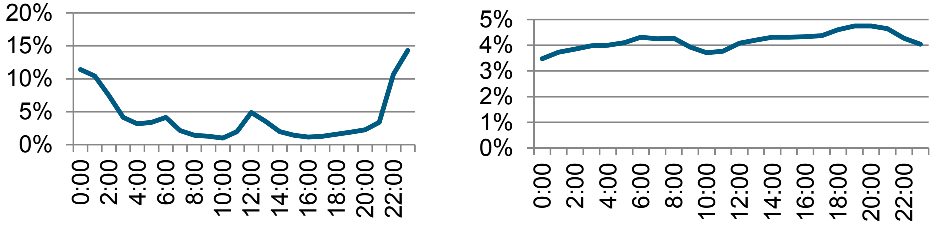

Figure 5-5 Daily normalized load profiles due to water and space heating correspondingly.

5.3 Spatial distribution of generation capacity

For all of the investigated scenarios, the generation capacity is described merely in aggregated form, i.e. either at country or at e-highway cluster level. However, a model with high spatial resolution would require the assignment of such capacities to the grid nodes. To this end, power plants are distinguished into two categories, namely conventional and RES power plants. For each category a separate strategy applied. Moreover, regardless of the scenario's suggestions, no expansion of the current hydro plant capacities is assumed.

Regarding the spatial distribution of conventional power plants, this is assumed to rely on the existing fleet, which can either be expanded or phased out. The primary reasons for limiting the future spatial distribution to the existing configuration consist of the future spatial distribution of the demand as well as economic considerations. Despite any demographic changes, it is assumed that the population distribution will not change significantly. Therefore, the future load distribution is assumed to follow the current population distribution pattern. Since the existing capacity distribution along with the transmission grid infrastructure has been developed such that the existing load distribution is covered, it becomes evident that the existing capacity distribution constitutes a reasonable indicator for the future distribution as well. Furthermore, economic reasons suggest that existing infrastructure should be capitalized upon, including fuel provision, cooling systems as well as connecting substations.

The alteration of the existing power plant capacity can be either positive or negative depending on their fuel type. For instance, coal power plants may need to be reduced whereas gas plants are to be expanded. The evolution of the power plant stock needs to take into account several considerations, including:

- the non-linearity of the individual plant capacities, since they consist of units of finite size
- economic reasons, since the less efficient plants have higher operational costs
- adequacy issues, where a less efficient plant may be preferred over a more efficient one due to its location and the corresponding concerns regarding regional security of supply

Considering all these issues, a strategy of replacing, expanding or phasing out conventional power plants is developed as depicted in figure 5-6. At first, the target capacities per region and fuel are compared to the existing ones for 2015 in order to identify which categories need to be phased out and which ones need to be expanded. For both cases, power plants bigger than 300 MW are split into several corresponding units of that size as maximum. If after replacing all units, additional capacity remains to be allocated, it is either added proportionally to the existing capacity. In case no power plant of the same type already exists, a new plant is introduced at the region's centroid. On the other hand, if additional capacity remains to be phased out, this is accomplished by withdrawing the units by descending age (since it is correlated to efficiency). However, due to adequacy concerns, when scenario targets are provided at country level, the remaining phase out capacities are first distributed proportionally to the e-highway clusters before dropping the units by their commissioning year. Since no retrofitting strategy has been considered for the verified case of 2015, it is neglected for the future development as well.

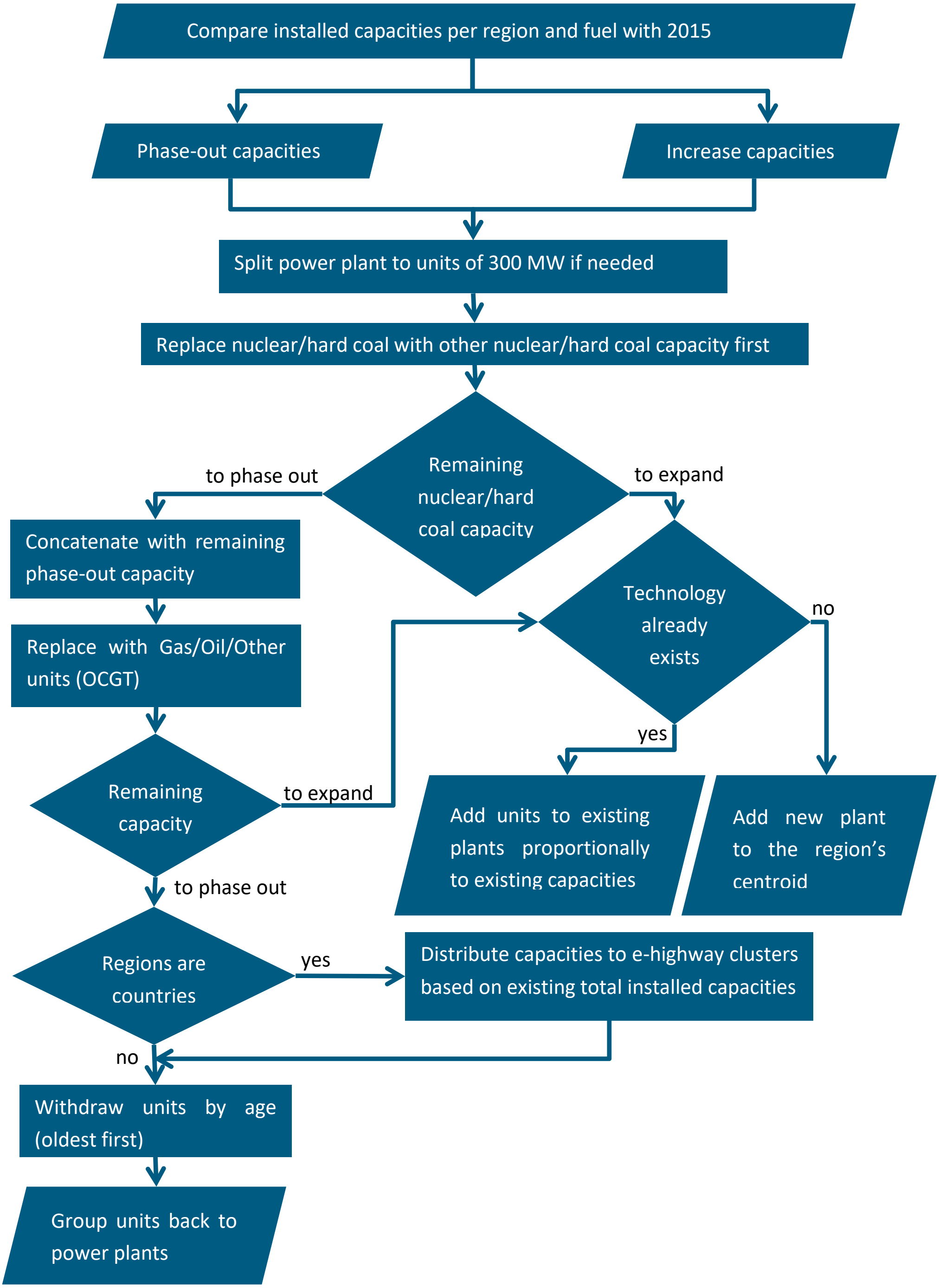

Figure 5-6 Diagram of the strategy for replacing the current conventional plants to meet regional targets set by future scenarios. Lignite power plants can only replace other lignite plants.

Regarding the RES power plants, only four technologies are considered for all future scenarios, namely wind turbines (onshore and offshore), PV (rooftop and open-field), concentrated solar power (CSP) and bioenergy. The spatial distribution of the corresponding generation capacity follows similar principles for all technologies and generally depends on the rationale of the investigated scenario.

Regarding power generation from wind, offshore production follows the methodology from section 4.2.4, while onshore production is calculated via an alternative approach that is applicable to all of Europe. This approach consists of selecting available turbine locations until regional capacities are reached and then generating power injection profiles for each location [295] based on weather data and assuming the installation of a typical V136-3450 Vestas turbine [296]. The determination of the turbine locations is accomplished by selecting a subset of all eligible turbine locations over Europe, which have been pre-identified by Ryberg et al. [297]. The selection of the locations within each e-highway cluster follows the highest average wind speed criterion, while the determination of the total cluster capacity when scenario data are provided at country level follows the e-highway methodology. This methodology suggests the use of two weighting factors as determinants for the corresponding spatial distribution, whose values depend on each scenario and its underlying rationale. The first indicator consists of the average capacity factor, thus prioritizing economic efficiency, while the second indicator consists of the corresponding regional demand, thus prioritizing regional self-sufficiency. For instance, the “Large Scale RES” scenario uses a weight relation of 1/10 between the two indicators, whereas the “Small & Local” scenario uses a 5/1 relation instead.

Solar power generation is incorporated via considering the PV and CSP technologies. Calculating the PV generation profiles follows the methodology of section 4.2.4, where distributing national capacities to the e-highway cluster level is accomplished similarly to the wind distribution. Further distributing from the cluster to the NUTS2 level is performed proportionally to the average capacity factors. Regarding the generation from CSP, the corresponding e-highway methodology is followed to account for the variability of this technology, which is normally much lower than PV generation during the day due to the easier intermediate energy storage. Hence, CSP generation merely follows square daily profiles between 06:00 and 21:00. The height of these profiles is determined such that the daily generated energy equals the generation of a PV farm with the same capacity but double capacity factor.

5.4 Chapter summary and discussion

In this chapter, the European power system of 2030, 2040 and 2050 are described. Since a highly resolved dispatch model is selected for the system analysis, all the exogenous variables including the transmission grid, generation capacity and electricity demand have to be defined a priori. For this purpose, the scenarios developed by studies whose results constitute the primary sources for developing the European transmission grid of the future are selected. Nevertheless, due to the high spatial resolution requirements of the dispatch model, further assumptions must be deployed for translating the corresponding scenarios to the desired resolution.

Considering the multitude of the involved shaping factors along with the various uncertainties, an accurate prediction of the European power system constitutes a highly challenging task. Even by assuming a simplified pathway of merely cost minimization, various system configurations can satisfy the climate goals with only small cost differences. As also stated by the corresponding studies, none of the scenarios is considered more likely than the others, whereas all of them should be considered as a frame inside which the actual system might fall. Therefore, for each investigated year more than one scenarios needs to be examined, while the corresponding results should be interpreted under the same prism as well.

In addition to the scenario assumptions, further assumptions were required for the spatial distribution of the power system quantities. The most significant of these assumptions regard the grid and generation assets, whereas distributing the demand by population has already been discussed in section 4.2.5. With respect to the grid development, all of the projects from the TYNDP 2016 are assumed to be completed by 2030, although this might not be entirely accurate since further projects may be developed or replace existing proposals. Beyond 2030, forecasting individual projects becomes increasingly challenging, hence no further development is assumed. Nevertheless, this study focuses on the investigation of demand response alone as an option for integrating VRES generation, therefore grid development is excluded from the options of increasing system flexibility. Regarding generation, although the developed methodology of phasing out and replacing conventional power plants relies on reasonable assumptions, the actual fleet evolution may deviate from the predicted values. Furthermore, the spatial distribution of the VRES generators may follow the assumed determining factors to a different degree or involve further factors that are neglected by the implemented approach. Finally, hydro plants are assumed to stay constant, hence any further capacity extension that could contribute to further RES integration is ignored.

Although the afore-mentioned assumptions may result in discrepancies between a highly resolved system and its reduced equivalent, such discrepancies can be only partly attributed to these assumptions. A significant source of discrepancy regards the spatial aggregation itself and the inherent statistical property of VRES generation to show less correlation over larger areas and thus less fluctuating profiles when aggregated.

The implemented scenarios from this chapter can determine the power system conditions of the future, which can then be further analyzed by the dispatch model described in chapter 6.

6 Results and discussion

In this chapter the developed and verified pan-European power system model is applied for the future scenarios described in chapter 5. The analysis of the corresponding results focuses on the integration of VRES and the impact of applying demand flexibility onto relieving congestion as well as mitigating generation and demand curtailments. The influence of various parameters including demand flexibility, applied weather year and different scenario frameworks is examined.

6.1 Demand flexibility

In section 3.5 two methodologies of introducing load shifting into power system optimization models were presented. The DIETER approach constitutes a more accurate representation of demand shifting however it significantly increases the complexity and the corresponding computational requirements for large networks and long shifting periods. On the other hand, the virtual storage (VS) approach scales better with regard to the network size and shifting period but it leads to sub-optimal utilization of the available flexibility since demand shifting is allowed only within predefined time windows. In this section, these two approaches are applied to a selected future scenario and compared in terms of computational performance and accuracy with respect to the scope of this thesis.

Regarding the VS approach, two different implementations are further examined with respect to the nature of the ramping constraints between the shifting periods. For the first, “coupled”, implementation, all time steps are optimized simultaneously, whereas for the “decoupled” implementation each shifting period constitutes a separate optimization problem. In the “decoupled” approach, consecutive shifting periods are merely linked softly by limiting the flexible consumption of the first time step based on the corresponding value of the last time step from the previous period. Since this method is more prone to generate infeasible problems, the ramping constraints are allowed to be relaxed up to 2% in case of problems with no feasible solution, i.e. double than the maximum load gradients experienced by the aggregated European profile. Furthermore, for both the coupled and decoupled implementations, cyclic ramping constraints are applied for yearly operation.

Figure 6-1 shows the total VRES curtailments for all three modeling approaches along with the corresponding execution time for solving each model on the same machine[2]. The investigated system for the comparison should consist of a system with high VRES shares and therefore the “Large-scale RES” scenario of the e-Highway project for 2050 is selected (see Appendix G) while the flexible demand is assumed to constitute 5% of the original demand and that it can be shifted over 12-hour periods. Regarding the reported execution time, this refers to the time required to generate and solve the model using both pyomo and gurobi but excludes the time for any data processing or I/O operations required to develop each model. These execution times however merely constitute indicative values, since no rigorous testing conditions were applied, e.g. each case was executed only once and potentially in parallel with other applications as well. Moreover, no specific software or hardware enhancements were applied for the individual cases, while the same gurobi parameters [298] were applied

[2] 2x Intel® Xeon® Gold 6154 CPU 3.00 GHz (18 cores per CPU), 512 GB RAM, OS Windows 10 Pro

to all cases[3]. Regarding the decoupled VS approach, its execution time refers to a parallel execution on 16 processors.

It can be observed that although the execution time varies significantly among the different models, the VRES curtailments show a lesser variation. Besides the differences in the modeling of demand shifting, this lesser variation can be also attributed to the limited resources for load shifting as well as its limited impact on reducing VRES curtailments. Nevertheless, since this thesis focuses on the integration of VRES, all approaches are selected to be evaluated with that regard. With respect to the computational performance, it can be noticed that the DIETER approach shows the worst scaling among the investigated approaches with respect to the number of clusters, where 150 nodes already becomes a prohibitively high number. On the other hand, the decoupled VS approach shows considerably higher computational performance, but also the lowest reduction of curtailments due to the higher temporal restrictions in demand shifting. Nevertheless, the performance benefits are considered to outweigh the underestimation of the demand flexibility effects, hence the decoupled VS approach is selected for the rest of this thesis unless stated otherwise.

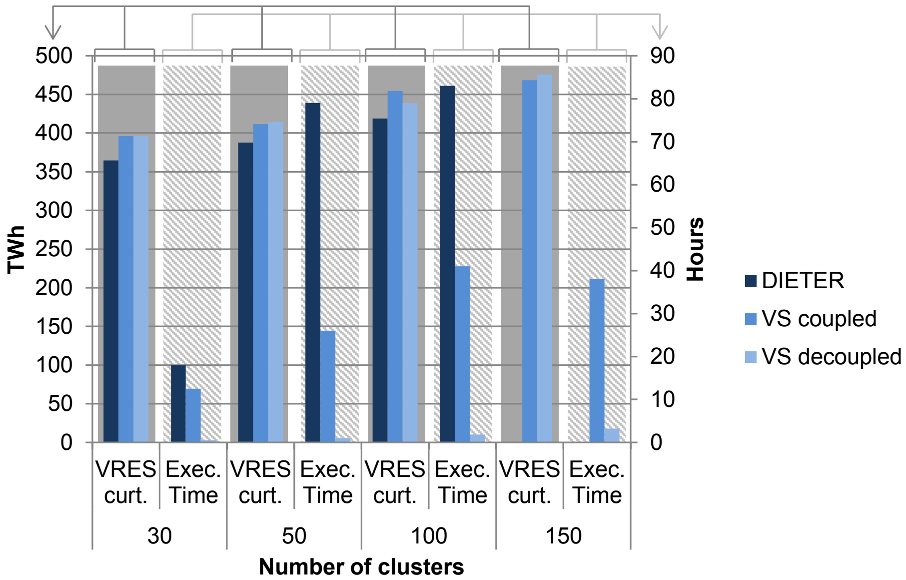

Figure 6-1 Total amount of VRES curtailments and execution time for different number of clusters and demand flexibility modeling.

6.2 Europe

In this section the developed pan-European model is applied to analyze the implemented scenarios of the European power system for 2030, 2040 and 2050, where the integration of VRES and the impact of demand flexibility constitute the primary focal points of the investigation. As mentioned in chapter 5, due to a variety of uncertainties, it is impossible to accurate-

[3]method: 2, crossover: 0, barHomogeneous: 1, FeasibilityTol: 1e-5, BarConvTol: 1e-8, ScaleFlag: 2

ly predict the system evolution, therefore a collection of scenarios is required to better describe the situation of the future. In that sense, the scenarios and consequently the corresponding results of this chapter as well are not intended to serve as predictions of the future but rather to set the framework and illustrate indicative values and behaviors of a future European system based on RES. However, since the focus of this thesis concentrates on the investigation of systems relying primarily on VRES, the consideration of CCS technology as a valid alternative for the decarbonization of the European power sector falls out of the scope of this thesis. Thereby, the e-highway scenarios “Big & market” and “Fossil & nuclear” are excluded from the following analysis.

6.2.1 Reference case

Although a variety of scenarios is necessary to describe a future power system, measuring the impact of various modeling parameters requires the selection of a reference case. Considering the long-term focus of the thesis, as well as the interest in systems with high RES shares, the scenario “Large-scale RES” for the year 2050 is selected. Moreover, the rationale behind this scenario regarding more centralized solutions and high electricity demand renders the integration of VRES a more challenging task in comparison to a more decentralized scenario. Regarding the weather year, the same year is selected for all RES generation and demand such that any underlying correlations can be captured. The selected year is 2011, as recommended by Gerhardt et al. [299] to be a representative year for Europe with regard to energy system modeling. As for demand flexibility, the available flexibility is set to 10%, a value that may be considered conservative for 2050, however it will be shown that a further increase in load flexibility does not improve system flexibility significantly. Finally, although the modeling formulation of load shifting is essentially technology-agnostic, the maximum shifting duration is selected to be 24 hours (i.e. daily shifting), since most industrial and residential applications would not be willing to exceed this limit.

Detailed information regarding the spatial distribution of generation for the selected “Large-scale RES” scenario is depicted together with the other scenarios in Appendix G, nevertheless key aspects are also discussed in this section as well. In this scenario, large-scale RES solutions are selected, e.g. high shares of offshore wind installed in the North Sea and solar generation in Northern Africa. The national capacity mix for each European country is shown in figure 6-2, where it can be observed that wind generation is generally preferred over PV. For instance, the total VRES capacities for Germany are 98.6 GW onshore wind, 20 GW offshore wind and 54 GW PV. The scenario further assumes significant GDP growth as well as electrification of the heating and transport sectors. However, since the attitude of the public is considered passive, only little improvements in energy efficiency are assumed which result in high electricity demand, the highest among all scenarios. The spatial distribution of the demand over the countries is depicted in figure 6-3, where the highest consumer is Germany with 815 TWh.

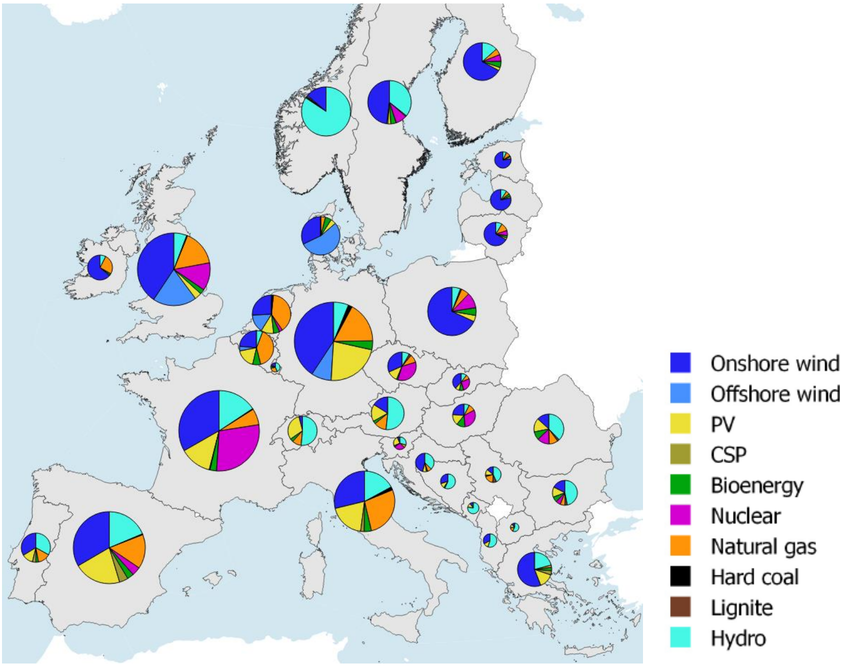

Figure 6-2 Installed generation capacities per country according to the “Large-scale RES” scenario. Own illustration. The country with the largest total capacity is France with 253 GW.

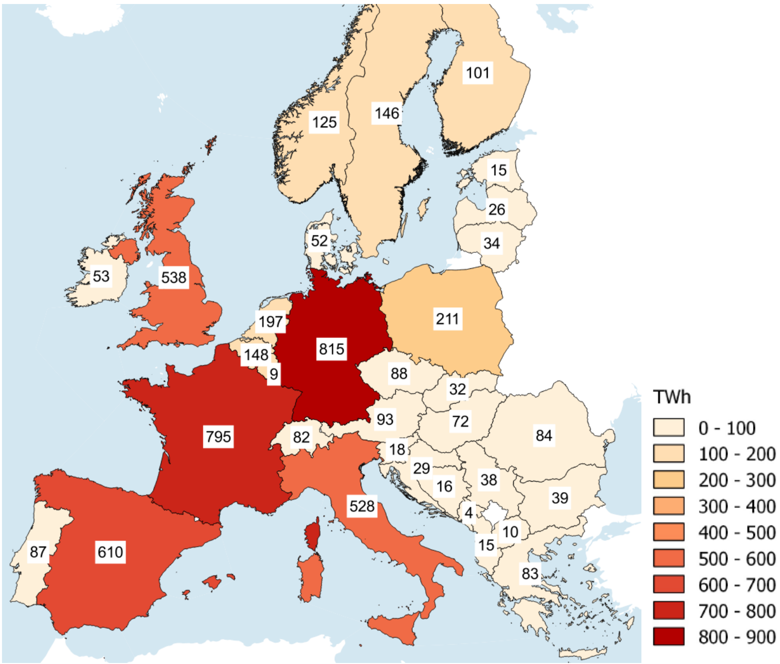

Figure 6-3 Total electricity demand per country according to the “Large-scale RES” scenario in TWh. Own illustration.

6.2.1.1 The “country” level

The first of the four modeling levels consists of the “country” level, whose spatial partitioning resembles the current configuration of the zonal electricity market. Figures 6-4 and 6-5 show the principal results of this level, namely the zonal prices and generation dispatch scheduling. It can be observed that, despite the high RES share, average prices are typically higher than today’s values due to the absence of the relatively cheap coal generation as well as the limited storage options, which result in a considerable dependency on the expensive natural gas generation. The highest prices are observed in central Europe, which are designed as net importers due to their higher demand in comparison to their RES potential. On the contrary, the combination of wind, hydro and nuclear generation in northern Europe results in significantly lower average prices, especially for the Scandinavian countries where hydro potential is abundant. Overall regarding price convergence, it can be noticed that distinct geographical areas appear to form clusters of almost uniform prices on average, while significant price differentials can be identified between these clusters indicating requirements for grid reinforcement. The most prominent of such differentials can be observed between northern and central Europe, where the corresponding grid limitations may be deemed responsible for limiting the diffusion of cheap wind and hydro generation into the central European countries.

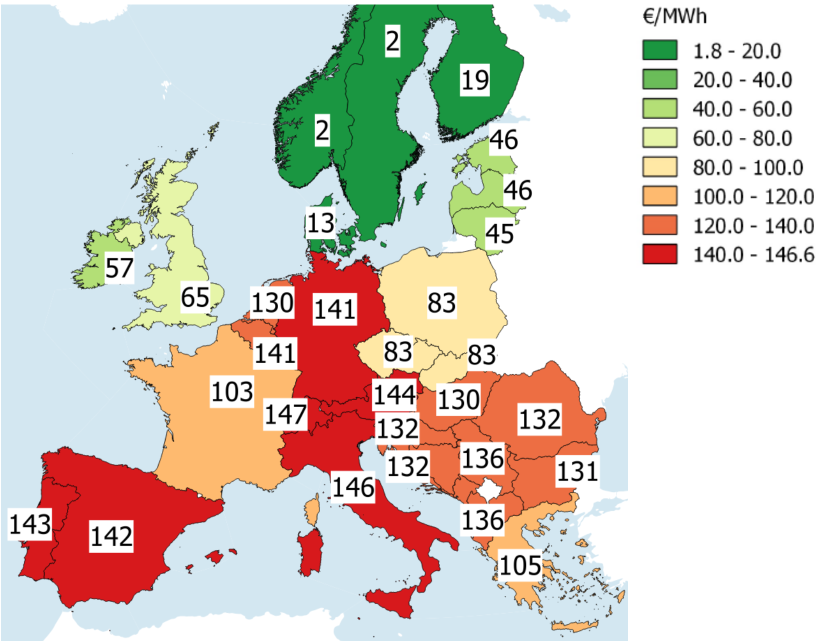

Figure 6-4 Average zonal prices for the “country” modeling level of the reference case, i.e. “Large-scale RES” scenario for 2050.

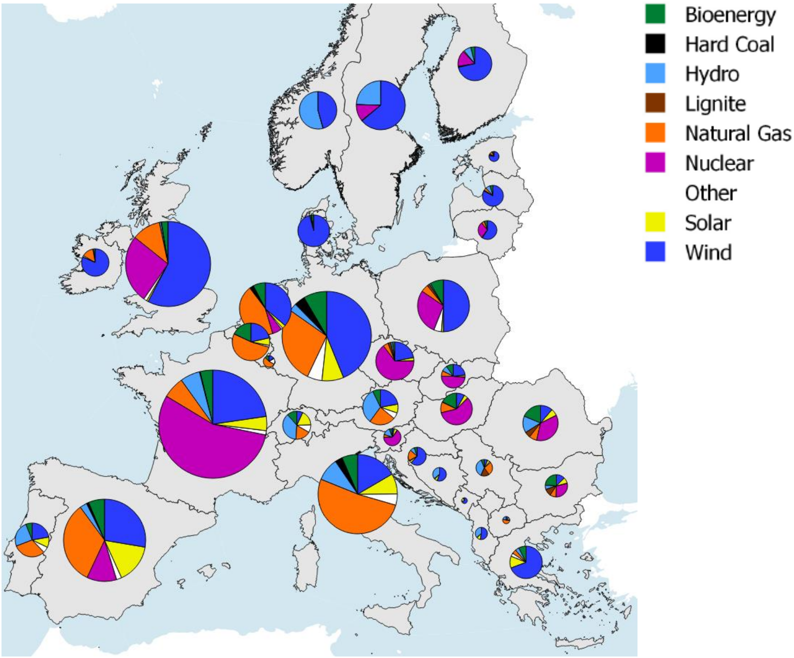

Figure 6-5 Energy mix for the “country” modeling level of the reference case, i.e. “Large-scale RES” scenario for 2050. The highest total generation occurs for France with 915.3 TWh.

6.2.1.2 The “grid” level

Applying the obtained scheduling of hydro generation to the “grid” level yields a similar picture for the European system, as it is shown in figure 6-6. The average nodal prices follow a similar trend to their zonal counterparts, where grid bottlenecks can be identified with a higher spatial accuracy including intra-zonal congestion, for instance in southern France and in northern Germany. Moreover, it can be observed that these bottlenecks are also spatially correlated to VRES generation curtailments, which are shown in the second picture of figure 6-6. Although the exact source of these curtailments cannot be uniquely identified, since no corresponding priority strategy has been applied, the locations of the curtailments imply a strong relation with wind energy around the North and Baltic seas as well as solar energy in northern Africa, which is not depicted in the picture. Therefore, achieving higher integration of VRES into the system would require the ability to transfer this curtailed wind energy to the load centers in central Europe.

Nodal prices

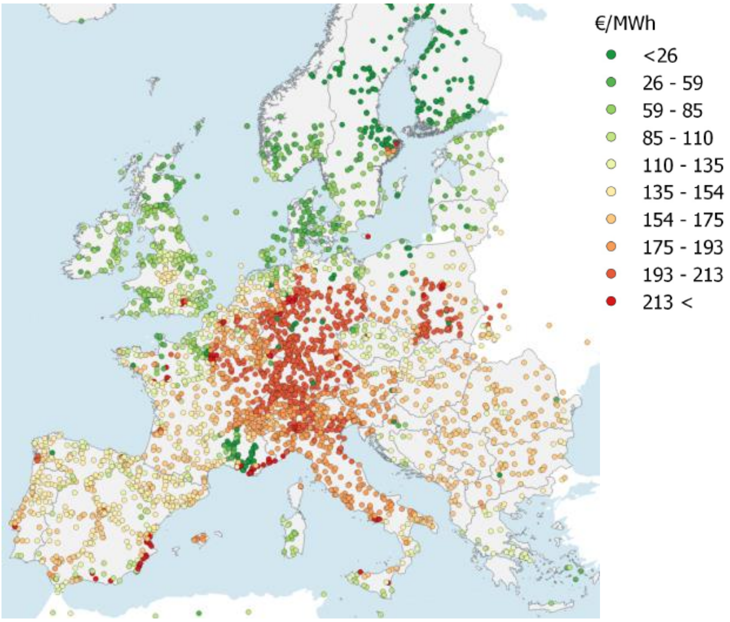

VRES curtailments

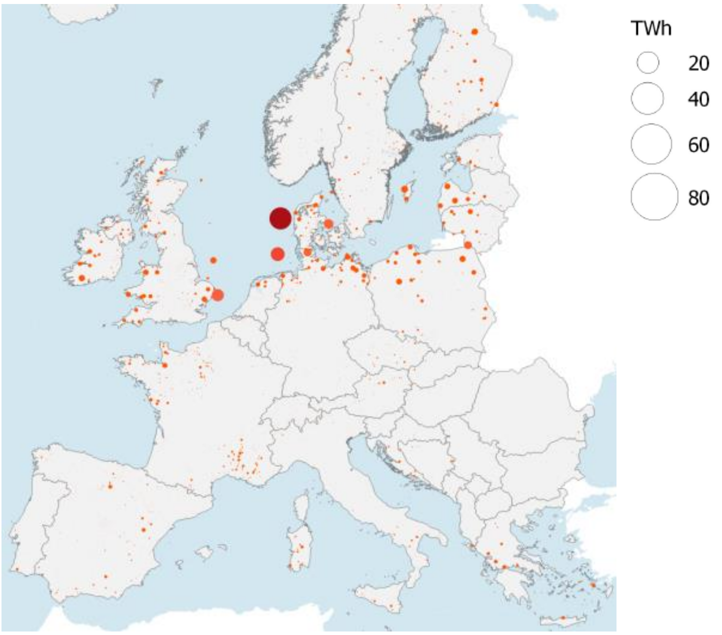

Figure 6-6 Average nodal prices (top picture) and VRES curtailments (bottom picture) for the "grid" modeling level excluding load curtailment costs.

By grouping the VRES curtailments, depicted in figure 6-6, into national profiles, it can be observed that the countries with the highest wind shares also show the highest amount of curtailments. In figure 6-7 it is shown that Great Britain, Denmark and Germany constitute the countries with most curtailments reaching 101, 98 and 88 TWh respectively, where the German value agrees with corresponding literature for 2050 [300]. Conversely, southern European countries that include more flexible generation alternatives and fewer requirements for transmitting bulk amounts of power over long distances exhibit lower curtailments. Furthermore, the duration curves of the national curtailment profiles of the top eight countries are shown in figure 6-8. It can be observed that the Denmark, France, Sweden and Ireland curves show less gradient than the others which are steeper, hence potential investments in energy storage, energy conversion or expansion of interconnections may become economically viable by exploiting the frequently occurring curtailed energy in these countries.

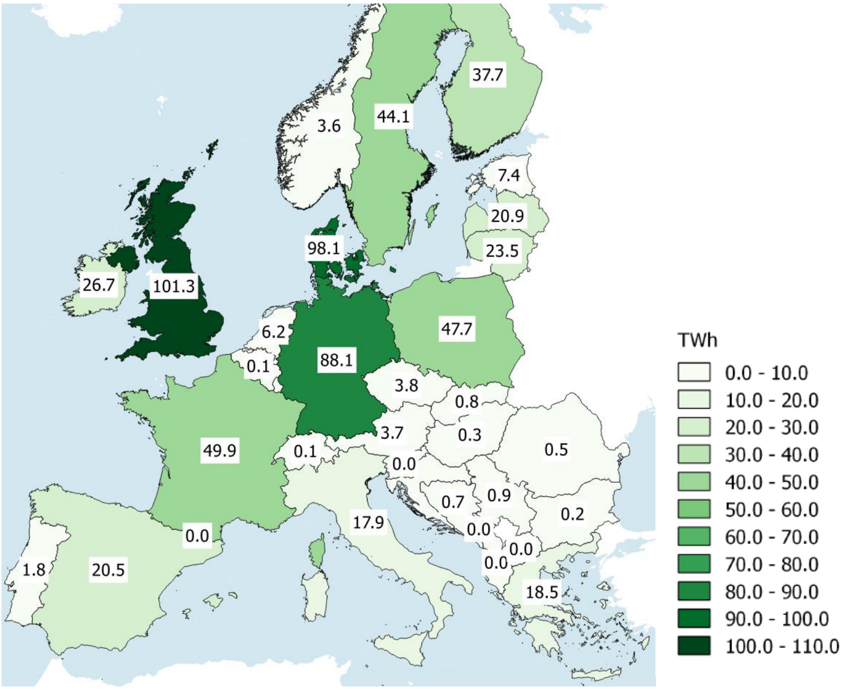

Figure 6-7 Total VRES curtailments per country in TWh.

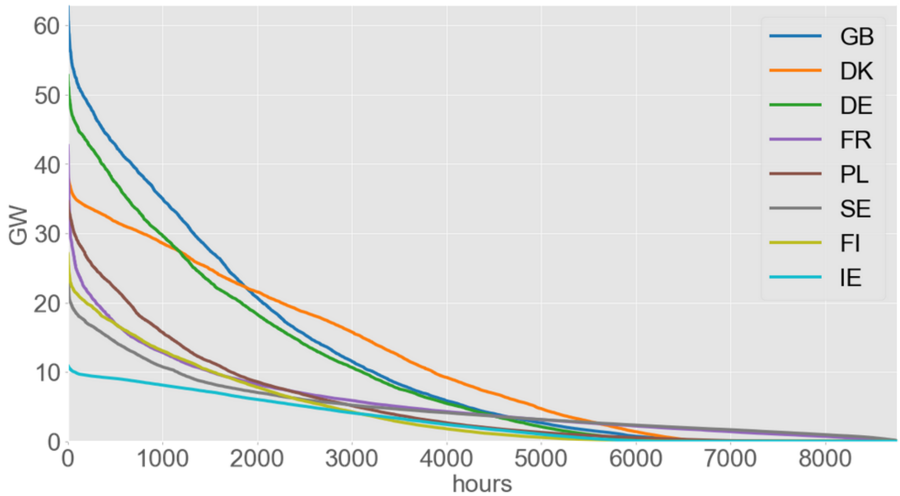

Figure 6-8 Duration curves of total VRES curtailments for 8 countries with the highest total curtailments. The country names appear in their ISO 2-digit code.

This centralized generation nature of the selected scenario can be further illustrated in figures 6-9 and 6-10, where the “grid” level results are clustered into regions whose total net positions are depicted along with the total net power flows between them. The rationale of the investigated “Large scale RES” scenario can be clearly depicted, where significant amounts of centralized generation (i.e. wind turbine placement following the locations with the highest capacity factors) need to be transferred to the demand centers. This behavior becomes clearer in the western European part, where, in contrast to the eastern part, regions appear less balanced, with specific regions exhibiting either strong net consumer behavior like southern Great Britain, southern Germany or the Paris and Madrid regions or strong net generating behavior like the North Sea, northeastern France and northern Africa. Such imbalances result in significant net power flows from the generating regions towards the consumer centers, which are observed again primarily in the western European part. For instance, it can be observed that there appears a significant net flow from the North Sea region and eastern France towards southwestern Germany, high net flows towards southern Great Britain from the other regions of the country with high wind generation as well as strong exports from northern Africa towards Europe.

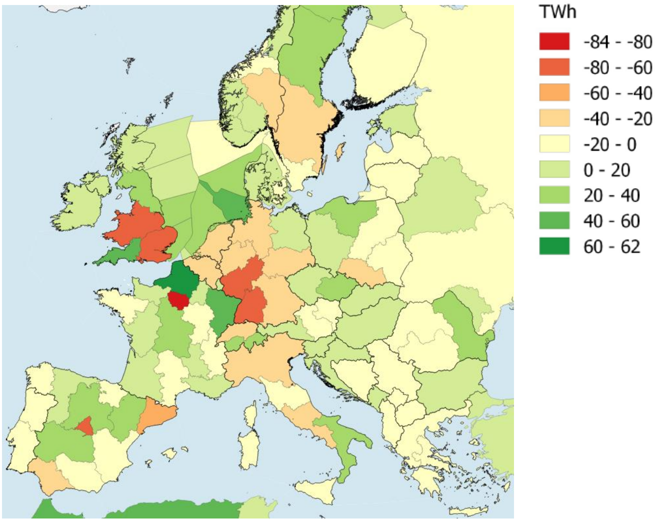

Figure 6-9 Total net positions of European regions for the 2050 “Large scale RES” scenario. The selected regionization of Europe follows the grid clusters of the e-Highway project, defined by Anderski et al. [166].

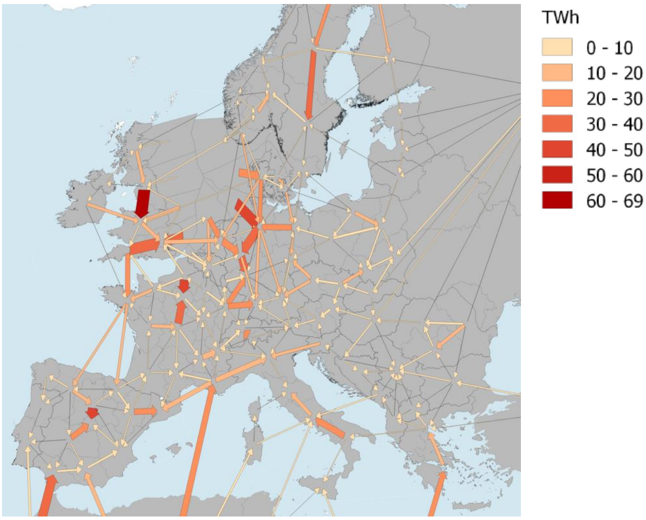

Figure 6-10 Net flows of European regions for the 2050 “Large scale RES” scenario and 2011 weather year. The selected regionization of Europe follows the grid clusters of the e-Highway project, defined by Anderski et al. [166].

Representing the power system in high spatial resolution allows additional options for its analysis that may not be possible with electricity market models that ignore grid constraints. Nevertheless, such analyses may go beyond the scope of this thesis. For instance, in Appendix H the market value factor of wind generation is discussed including the spatial dimension.

6.2.1.3 Analysis for Germany and comparison to literature

A closer look into Germany can provide additional insight regarding the investigated scenario and the corresponding results. Moreover, a comparison with literature values for 2050 can show the plausibility of the respective values. Figure 6-11 shows the total generation and installed capacities per fuel type in 2050 for Germany based on this thesis in comparison to the corresponding values of 2015 and different studies describing the German power system of 2050. It can be observed that although the total electricity demand is assumed to be one of the highest, the generation capacity is typically lower than the respective suggestions of the other studies. Hence, it can be noticed that the system depends heavily on imports, whereas in other cases these may become negligible. Unlike most of the literature values, the e-highway scenario does not distinguish between country-specific targets and therefore does not encourage generation investments in Germany which is designed as a net importer.

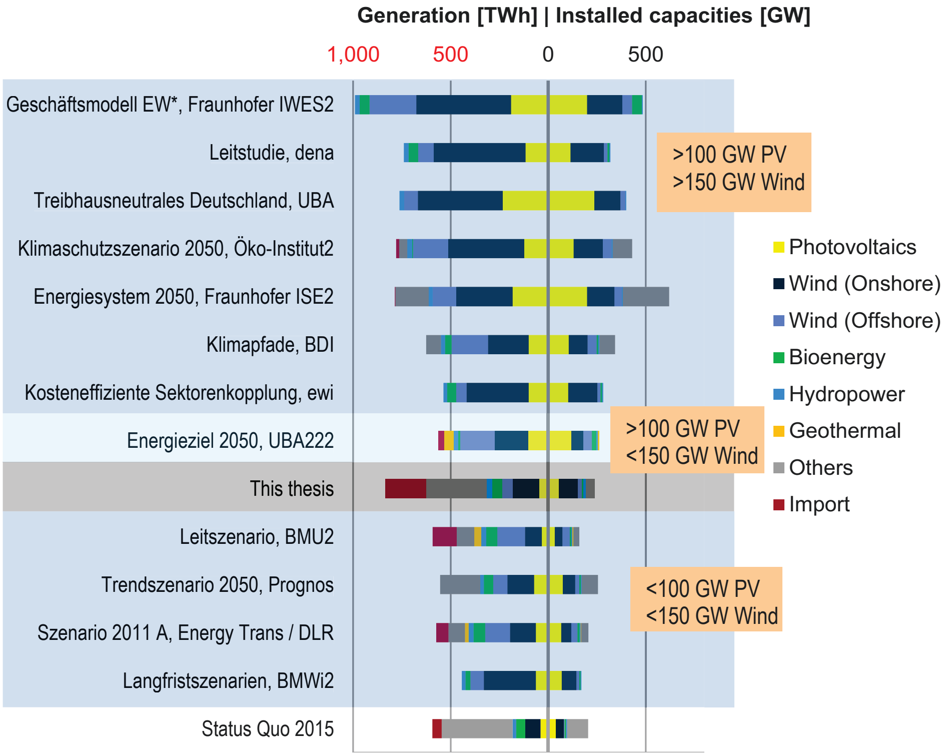

Figure 6-11 Generation and installed capacity mix for Germany in 2050 according to this thesis and the following studies: Leitszenario (BMU) [301], Energieziel 2050 (UBA) [302], Szenario 2011 A (Energy Trans/DLR) [303], Trendszenario 2050 (Prognos) [304], Geschäftsmodell EW* (Fraunhofer IWES) [305], Klimaschutzszenario 2050 (Öko-Institut) [306], Energiesystem 2050 (Fraunhofer ISE) [307], Klimapfade (BDI) [308], Kosteneffiziente Sektorenkopplung (ewi) [309], Langfristszenarien (BMWi) [310], Treibhausneutrales Deutschland (UBA) [311] and Leitstudie (dena) [312]. The capacity mix for this thesis corresponds to the “Large-scale RES” scenario of the e-highway study [291]. The status of 2015 is also included as reference.

Regarding VRES integration, it can be observed that despite the relatively low corresponding capacities, a considerable amount of curtailments is found (88 TWh in total) which agrees with respective literature values for 2050, as it is shown by Thema et al. [300], where 13 respective studies are reviewed. These curtailments can be primarily attributed to wind generation (98.1% of the total curtailments) and the noticeable grid congestion between northern and southern Germany which is clearly depicted in figure 6-6. This congestion originates from the centralized generation rationale of the “Large-scale RES” scenario that prioritizes the exploitation of wind locations with high average capacity factors, which are located in the north and close to each other (hence with high correlation). However, this turbine placement results in a situation that, if not accompanied with the necessary grid expansion, may lead to a decrease in the actual capacity factors of the generators after dispatch due to curtailments. This behavior is illustrated in figure 6-12, where it can be seen that the average capacity factor for both onshore and offshore wind generation stays significantly lower than the literature values, 15.6% and 29.8% respectively. These literature values, nevertheless, correspond to studies where spatial imbalances are typically not taken into account in detail, since a much coarser representation of the transmission grid is considered.

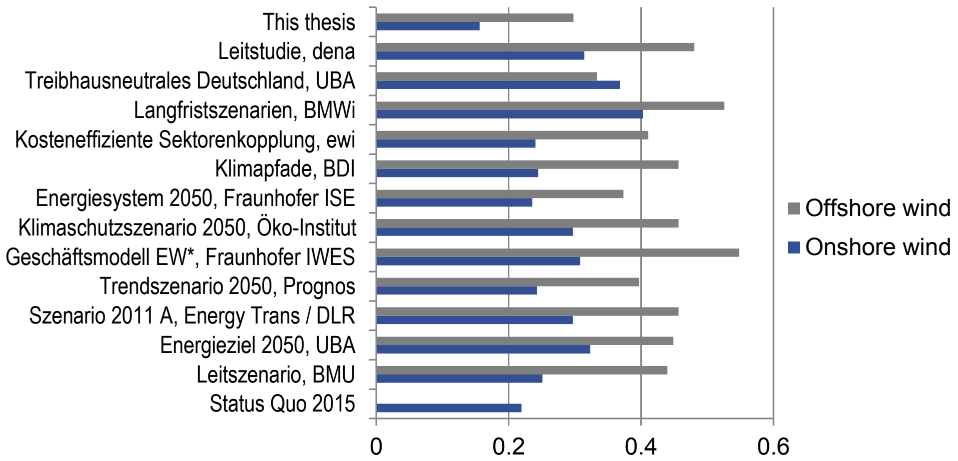

Figure 6-12 Average capacity factors of onshore and offshore wind generation in Germany for 2050 according to this thesis and the following studies: Leitszenario (BMU) [301], Energieziel 2050 (UBA) [302], Szenario 2011 A (Energy Trans/DLR) [303], Trendszenario 2050 (Prognos) [304], Geschäftsmodell EW* (Fraunhofer IWES) [305], Klimaschutzszenario 2050 (Öko-Institut) [306], Energiesystem 2050 (Fraunhofer ISE) [307], Klimapfade (BDI) [308], Kosteneffiziente Sektorenkopplung (ewi) [309], Langfristszenarien (BMWi) [310], Treibhausneutrales Deutschland (UBA) [311] and Leitstudie (dena) [312]. The capacity mix for this thesis corresponds to the “Large-scale RES” scenario of the e-highway study [291]. The status of 2015 is also included as reference.

Information on the spatial distribution of VRES curtailments is not typically included in the literature either because the corresponding research focus is different or because the spatial dimension is not considered in significant detail. Figure 6-13 shows the distribution of curtailments based on this thesis as well as the respective values from Robinius et al. [313] and

Jentsch et al. [314] for the German power system with a high share of VRES. It can be observed that although the system conditions may differ considerably and that a direct comparison of the respective values would not be meaningful, the spatial distribution of the curtailments for all three cases shows noticeable similarities. In particular, it becomes clear that the majority of the sources of curtailed energy are located in northern Germany, near the coastline where the wind generation potential is higher. Therefore, although the centralized generation principle of the "Large-scale RES" scenario may lead to considerable spatial imbalances on the German power system, the resulting distribution of VRES curtailments agrees with what can be found in the literature as well.

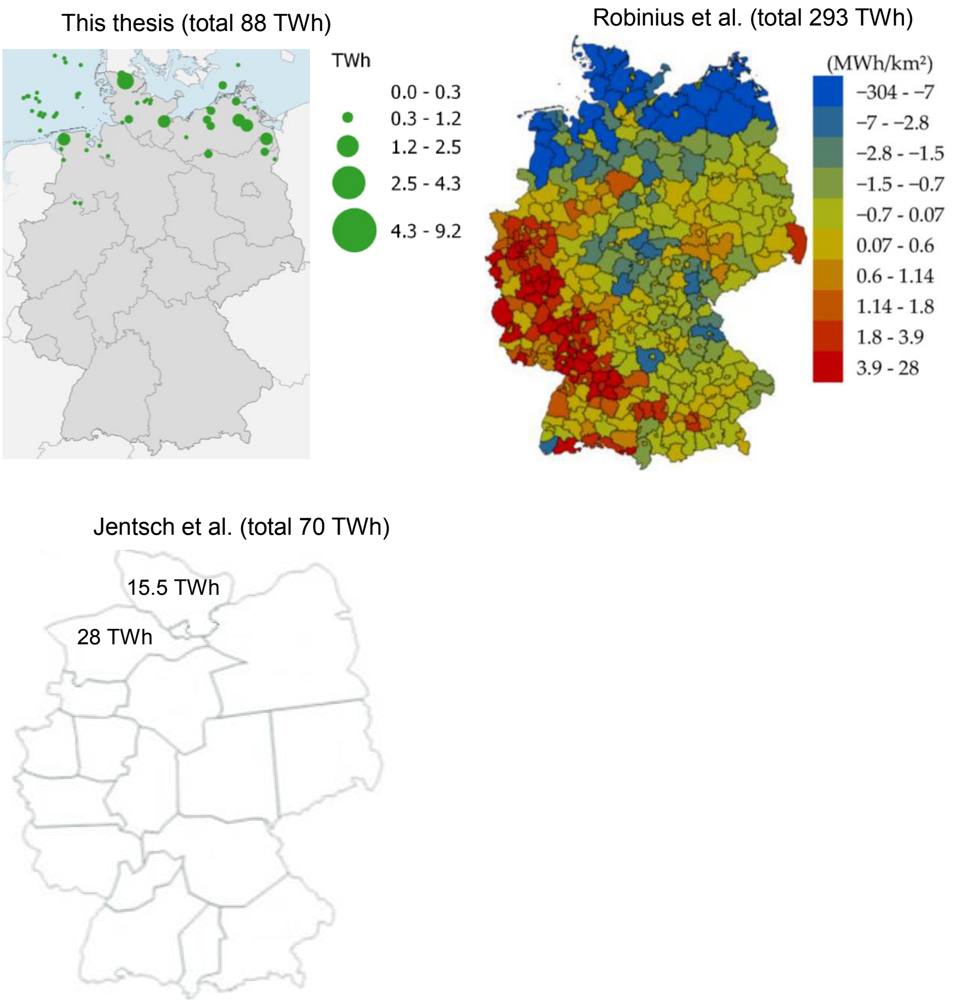

Figure 6-13 Spatial distribution of VRES curtailments according to this thesis (top left) where the offshore curtailments are distributed to the offshore buses uniformly, Robinius et al. [313] (top right) where the negative and positive values correspond to VRES curtailments and generation from conventional sources respectively and finally Jentsch et al. [314] (bottom) where the values for all regions besides the depicted ones are less than 5 TWh.

6.2.1.4 The “clusters” level

The average nodal prices obtained by the “grid” modeling level are used as weighting factors to reduce the original transmission grid to 150 representative clusters that reflect the system congestion conditions. The number of clusters is selected based on the information of figure 6-14, where it can be seen that using 200 clusters substantially increases the execution time without significantly altering the total surplus value. As expected, the total amount of VRES curtailments gradually increases for increasing number of clusters, since the representation of the grid is improved. However, the corresponding execution time increases as well due to the problem growth in size and complexity. Thereby, the number of clusters is selected to be 150 for the rest of this thesis as a compromise between grid representation and computational performance. This compromise does not need to be optimized since, regardless of the number of clusters, the corresponding results are applied to the “redispatch” level where the highly resolved transmission grid is considered.

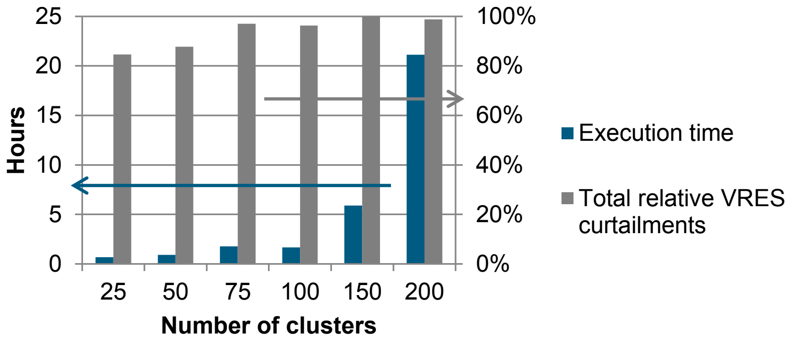

Figure 6-14 Total execution time and total relative VRES curtailments for different number of clusters. The curtailment percentages refer to the maximum appearing value.

This reduced version of the grid is applied in the third, “clusters”, modeling level where demand flexibility is further introduced. The reference case regarding load shifting is selected to consist of 10% flexibility and maximum shifting of 24 hours. Figure 6-15 shows the average daily European demand for the reference case, where the aggregated profile has been averaged across all days for each hour of the day. It can be seen that the conventional electricity demand follows a typical curve with two distinct peaks, in the morning and evening, and considerably lower consumption during night hours. On the contrary, the EV and heat pump load profiles show higher activity during night hours than daytime. Nevertheless, the morning and evening peaks remain discernible in the total average profile as well (depicted by the black line). However the noon valley increases in relative depth while the night drop is delayed from around 19:00 up to 00:00.

Applying load shifting results in the realized load depicted by the red line in figure 6-15. It can be observed that the two peaks do not reduce significantly while the main shifting occurs between night and day hours. This can also be seen in figure 6-16, where the net total upwards shifting reaches maximum around noon and downwards shifting becomes highest around midnight. Unlike load shifting in conventional power systems, that are benefitted from a more constant generation, in systems with high VRES shares, demand shifting tends to follow the VRES generation patterns that can vary significantly. This can be noticed in figure 6-15, where the night valley drops even further after applying flexibility in favor of day consumption instead of leading to an overall smoother profile. This can be explained by the high, regular fluctuations of solar generation within the course of a day depicted by the yellow stripped area. On the contrary, the remaining VRES generation, shown by the blue stripped area, does not show such a strong preference with respect to the hour of a day. While slower patterns may be observed in other VRES, limiting the maximum load shifting to 24 hours renders it impossible to be exploited by this approach. Therefore, it can be concluded that solar generation constitutes one of the main drivers for the observed load shifting behavior.

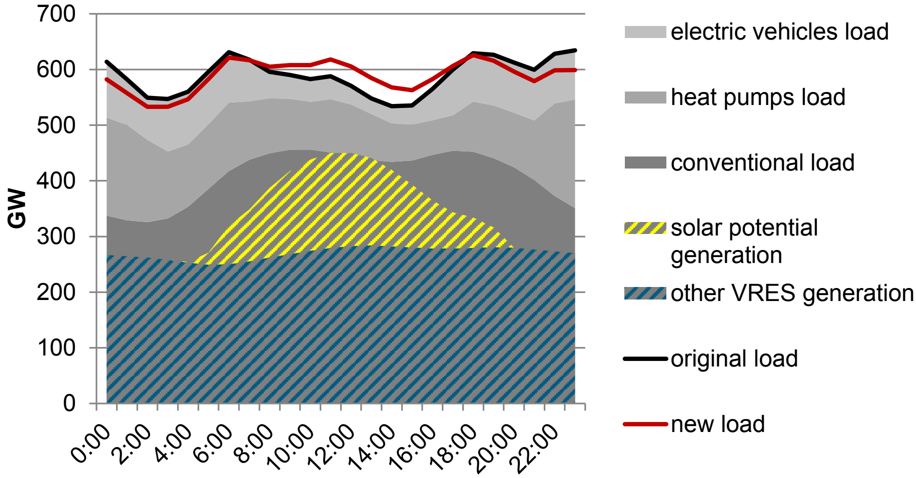

Figure 6-15 Total load and VRES generation profiles for Europe, averaged for each hour of all 365 days. The gray colors indicate the different components of the electricity demand with the black line showing the total demand before applying flexibility. The red line indicates the realized load after applying flexibility. The yellow area shows the generation potential from solar, whereas the blue are the generation from the other VRES sources.

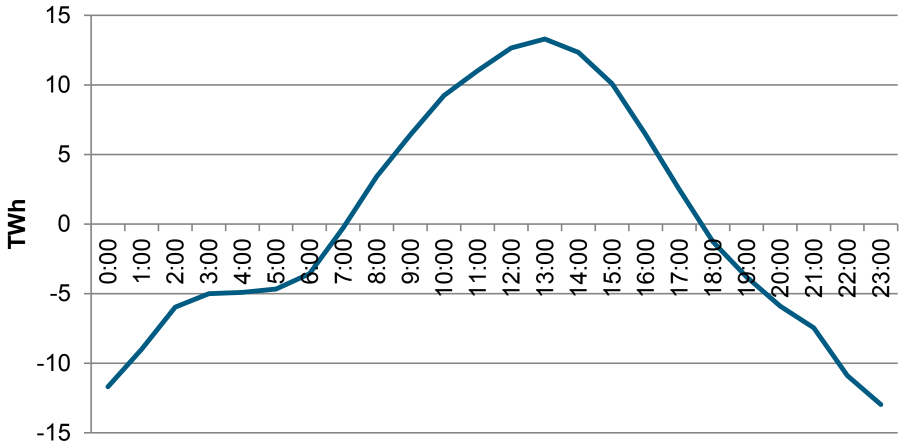

Figure 6-16 Total net load shifting after the application of demand flexibility, corresponding to each hour of the day for all Europe. Upwards shifting is indicated as positive, whereas downwards shifting as negative.

Regarding the spatial dimension of the load shifting effects, two metrics are considered, the utilization of flexibility and the reduction of curtailments. The flexibility utilization is derived by comparing the original and adapted load profiles and measuring half of the area of the respective difference, i.e. corresponding either to the total upwards or downwards shifting. These utilization values can be expressed relatively to the corresponding original demand where only a minor variability can be observed over the different nodes. Nevertheless, the average utilization steadily increases for higher available flexibility as shown in figure 6-17. The average utilization for the reference case amounts to 2.41% with a merely 0.21% standard deviation among the nodes. The relatively low values do not necessarily indicate that all system cost reduction potential is exploited, since with higher available flexibility a higher utilization can be achieved. Thereby, the constraints in maximum power shifting as well as the uniform application of demand flexibility over all time steps are deemed to constitute the limiting factors for obtaining higher load shifting utilization.

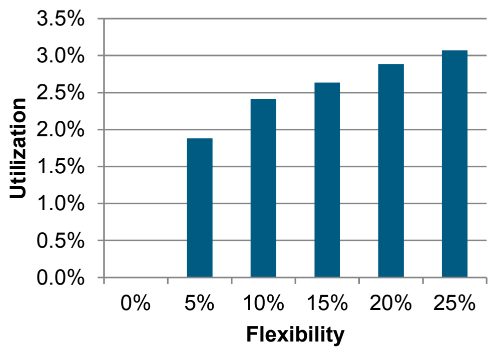

Figure 6-17 Average utilization of flexible demand as a function of the available flexibility.

Figures 6-18 and 6-19 show the spatial distribution of the load and VRES curtailments before applying demand flexibility as well as the corresponding reduction after its application. Unlike the almost uniform distribution of flexibility utilization, the respective distribution of the effects on curtailments reduction shows a significantly higher variation. This discrepancy can be attributed to the underlying assumption that load shifting is not accompanied with costs but only bound by energy and time constraints, hence it can be utilized for both alleviating congestion and reducing operational system costs even if the cost benefit may merely be marginal. Moreover, flexible load behavior is optimized simultaneously on all nodes, hence all the resources adjust correspondingly to reach the total system cost reduction. Thereby, although demand flexibility is activated on all available nodes, the resulting benefits in curtailments reduction may vary. A more realistic evaluation of the impact of the flexibility usage for the individual nodes could be obtained by applying penalties in shifting utilization such as additional costs or energy losses associated to shifting.

Similarly to the “grid” level results, the majority of the load curtailments are concentrated in central Europe, whereas most of the VRES curtailments are located near the regions of North and Baltic seas where wind generation is primarily located. However, these major curtailment centers experience only a mild relative reduction after the application of demand flexibility. On the other hand, areas with lower total curtailments may achieve higher reductions. The corresponding reduction is depicted by the color, where the positive values indicate a reduction of curtailments, i.e. less than the initial amount. The area experiencing most of the relative reductions, regarding both load and VRES generation, corresponds to the Iberian Peninsula. This can be attributed to solar generation that is more prevalent in this region as well as in the neighboring regions of North Africa. Constraining the shifting duration to 24 hours essentially limits the integration of wind energy which is also limited by power transfer restrictions.

Load curtailments reduction

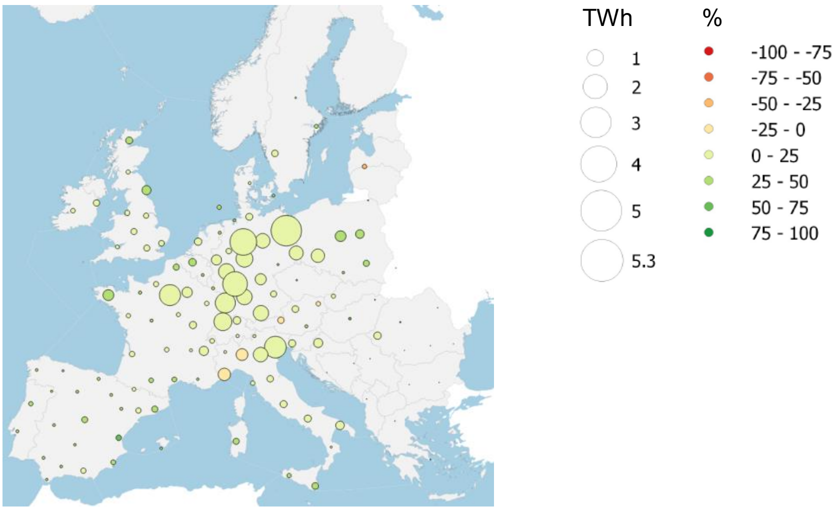

Figure 6-18 Spatial distribution of the reduction in load curtailments due to demand flexibility. The circle size indicates the amount of initial curtailments, whereas the color indicates the relative reduction. A negative reduction implies an increase in curtailments.

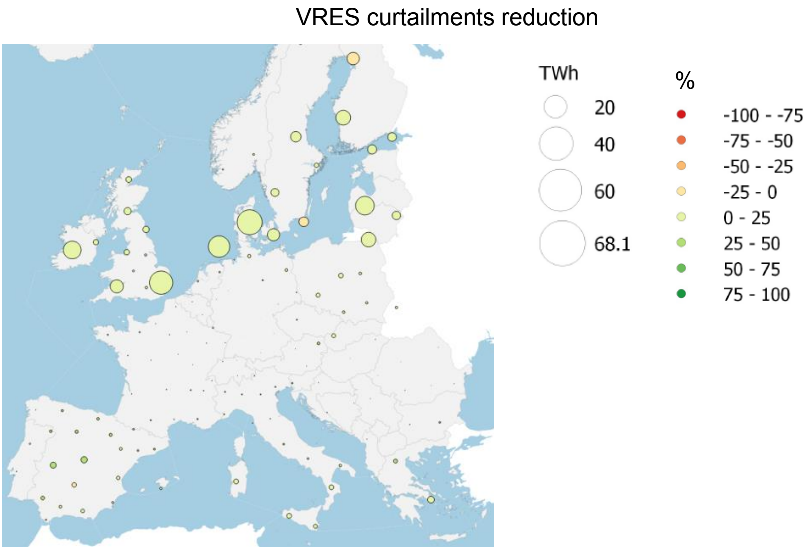

Figure 6-19 Spatial distribution of the reduction in VRES generation curtailments due to demand flexibility. The circle size indicates the amount of initial curtailments, whereas the color indicates the relative reduction. A negative reduction implies an increase in curtailments.

6.2.1.5 The "redispatch" level

Applying the information regarding load shifting from the "clusters" level back to a model with high spatial resolution, i.e. via the "redispatch" level, allows a more detailed analysis of the VRES curtailments and integration. Figures 6-20 shows the total curtailments for each transmission node where it can be noted that it resembles the corresponding picture from figure 6-6 but with more diverse spatial distribution and with lower total volumes overall. It can be observed that the location with the highest amount of curtailments is located in western Denmark, whose internal grid prevents a significant part of the corresponding wind generation potential from reaching neighboring countries. Thereby, a further investigation for grid or storage reinforcement measurements in that area that could contribute to a higher integration of wind generation is recommended. Although such measurements may reduce VRES curtailments, it is not always deemed economically efficient to eliminate them entirely. Since such curtailments are therefore practically unavoidable, further exploitation options may be considered as well, such as power-to-gas or power-to-heat technologies which can provide energy to different sectors besides electricity. Selecting the most suitable locations for such installation necessarily depend on the total amount of available curtailment energy, nevertheless properties of the corresponding time series may also constitute decisive factors as well. Since a more elaborate investigation would require the inclusion of specific costs for the individual technologies which exceeds the scope of this thesis, the following analysis attempts to provide a more technology agnostic insight to that matter.

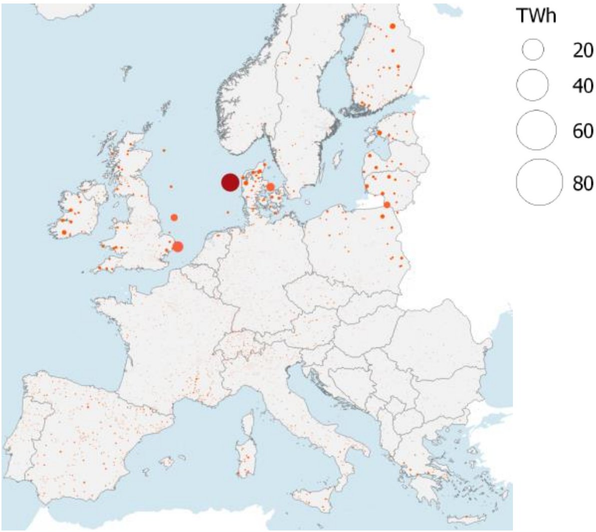

Figure 6-20 Spatial distribution of the total VRES curtailments aggregated to transmission grid nodes for the 2050 “Large scale RES” scenario and 2011 weather year, after applying all modeling levels with 10% demand flexibility, deferrable by 24 hours.

Figure 6-21 shows the normalized duration curves of the VRES curtailments for four selected transmission nodes. The selection process follows the filtering of all nodes with total curtailments lower than 1% of the largest observed value as well as nodes outside the European borders. The depicted four nodes are selected out of the reduced node list based on the available normalized energy that can be transformed by placing an ideal converter with a power capacity corresponding to the 50th and 75th percentiles of the respective curtailments time series. This energy is depicted by the shaded areas underneath the truncated duration curves of the first picture and can be expressed as duration curves as well, shown in the second picture. The node “3903”, located in southwestern Ireland, exhibits the highest normalized energy corresponding to the 75th percentile power, while the offshore node “GBR_midnorthNS”, located in the east of Great Britain has the lowest value. Respectively, the node “3251”, located in western Denmark, shows the highest normalized energy for the 50th percentile power, while the offshore node “GBR_southNS” the lowest energy for the same percentile power. It can observed that the nodes with the steepest duration curves correspond to offshore nodes, where no demand is directly present while also fewer connections that could contribute to the distribution of any excess power to neighboring nodes are available.

The absolute values of the energy corresponding to the 50th and 75th percentiles are depicted for all the filtered transmission nodes in figure 6-22, where it can be observed that the 50th percentile energy becomes significant only for the nodes in western Ireland and western Denmark. Hence, all other curtailment duration curves exhibit a steeper trend, i.e. the majority of the curtailment energy content is concentrated in only few occurrences over the year. While this does not necessarily constitute a suboptimal system development, nodes with more frequent curtailments may be indicative of requirements for grid expansion or energy storage that could assist the integration of the corresponding VRES generation.

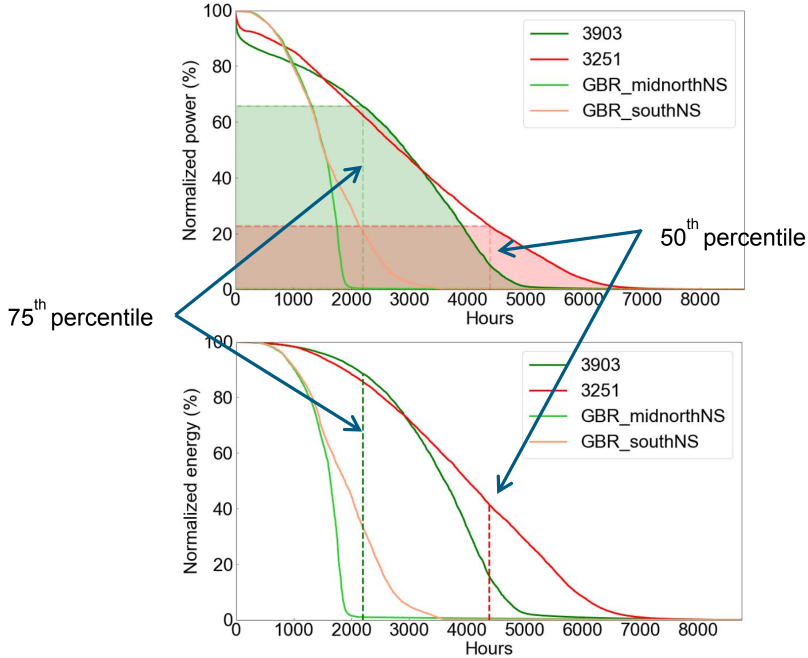

Figure 6-21 Normalized duration curves of curtailed power for selected transmission nodes with high overall curtailments after the application of demand flexibility. The 3903 and 3251 nodes correspond to the highest relative power that corresponds to the 75th and 50th percentiles respectively. The top picture shows the duration curve of curtailed power, whereas the bottom picture depicts the total energy converted by an ideal converter with capacity equal to this power. The 3903 node is located in southern Ireland and the node 3251 in western Denmark.

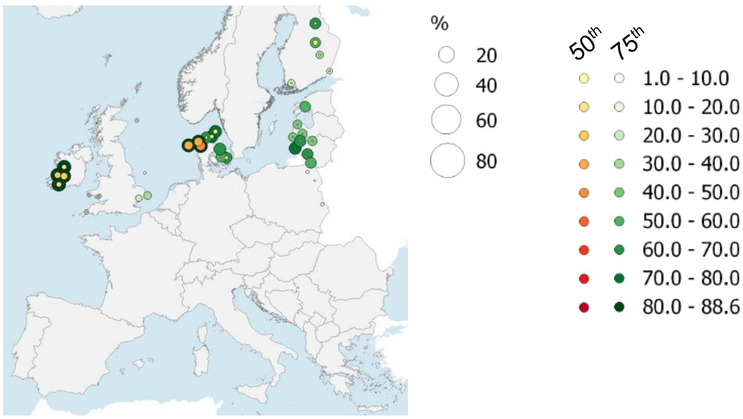

Figure 6-22 Normalized energy available for an ideal energy converter of limited power capacity. The red and green scales refer to the power that corresponds to the 50th and 75th percentiles of the respective curtailment time series. Only the nodes with high total curtailments are depicted.

The merit of an ideal converter installation can be measured by comparing the available normalized energy that can be harvested as function of the corresponding normalized curtailment power for each node, which is shown in figure 6-23. It can be observed that the nodes with flatter, more concave duration curves can extract more energy with the same normalized installed capacity For instance, installing a normalized capacity of 20% results in a total energy of less than 30% for the “GBR_midnorthNS” node, while the same relative capacity may obtain up to 40% of the respective curtailment energy for the “3251” node. Overall, the best candidate locations for utilizing curtailments energy in terms of both volume and time series quality correspond to western Ireland and western Denmark.

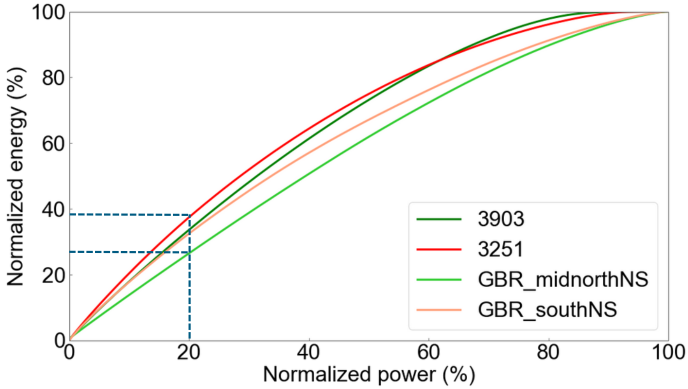

Figure 6-23 Normalized converted energy of an ideal converter as a function of its normalized power rating for locations with high total curtailments. 20% of curtailed power corresponds to different relative values of available curtailment energy available for conversion.

6.2.1.6 Comparison of modeling levels and spatial load shifting

The results of all four modeling levels are summarized in figure 6-24 in terms of total curtailments and emissions, depicted by the blue colored bars. Although all levels essentially represent the same power system, a direct comparison is not entirely possible, since different components may have been modeled differently or with different horizons. Nevertheless, since a problem capturing both maximum spatial resolution and yearly horizon operation simultaneously becomes computationally challenging, such a comparison can still provide a valuable insight on the effects of different spatial resolutions. Regarding VRES curtailments, it can be observed that considering only countries (i.e. 33 nodes) as spatial partitioning can underestimate the total amount by a factor of 2.3 (328.5 TWh against 767.3 TWh respectively), while even considering 150 clusters (452.4 TWh) does not manage to reach the level of the corresponding estimations from the models with high spatial resolution (i.e. the “grid” and “redispatch” levels with 3818 nodes and 767.3 and 729.5 TWh respectively). The impact of the transmission grid becomes more apparent when considering the whole European system as copper plate, where it is found that the total curtailments constitute merely 13.8 TWh. Furthermore, it can be seen that the application of demand flexibility does not result in significant reduction of curtailments in comparison to the fixed demand results of the “grid” level, which amounts to merely 37.8 TWh (4.9%). Unlike VRES curtailments, the application of demand flexibility results in higher relative reduction of load curtailments (27.9%), nevertheless these still remain considerable (239.7 TWh). It can also be seen that for load curtailments as well, the modeling levels with the highest spatial resolution show substantially higher curtailments than those with a coarser resolution. In contrast to curtailments however, total emissions do not change significantly for all the modeling levels. This may be anticipated due to the redispatch formulation of the “clusters” and “redispatch” levels that does not encourage the ramping down of conventional generation. Nevertheless, the total emissions for the “grid” level are similar as well, thereby it can be deduced that these are affected primarily by the residual load profile characteristics rather than the power flow constraints posed by the transmission grid.

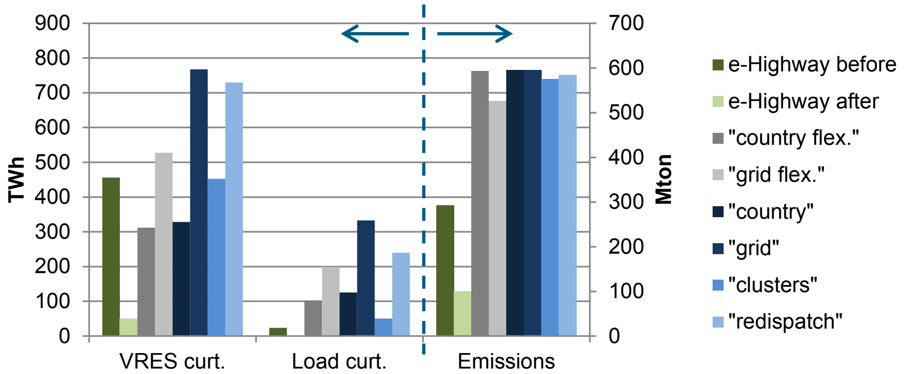

Figure 6-24 Total VRES and load curtailments as well as CO_2 emissions for different modeling approaches and levels. The green color corresponds to the values reported by the e-Highway 2050 project before and after grid expansion. The grey color corresponds to applying demand flexibility during the generation dispatch, while the blue color corresponds to the application of the four modeling levels as described in section 3.3.

As described in section 3.3, the development of the multi-level model incorporates demand flexibility modeling within a re-dispatch formulation, such that the information regarding the thermal flexibility constraints are taken into account. The drawback of such formulation consists of the system preference to ramp down generation from zones with low prices, i.e. with already higher RES shares, instead of zones with more conventional generation in their mix. This paradoxical phenomenon resembles the “merit order” effect of generation dispatch where RES tend to cannibalize their own market revenues. Moreover, shifting demand cannot essentially contribute in replacing conventional generation with RES since the system costs would remain unchanged. On the other hand, the use of a more accurate grid representation from the “clusters” level in comparison to the “country” level may provide a better evaluation of the ability of load shifting to alleviate grid congestion.

For these reasons, it also becomes noteworthy to investigate the application of demand flexibility directly at the dispatch, i.e. “country”, level and its effects on curtailments and emissions reduction. In this case, the “clusters” and “redispatch” modeling levels essentially lose their significance; nevertheless applying the dispatch results on the “grid” level as well may provide further insight into the impact of the transmission grid. Since the “country” level ignores any intra-zonal power flow restrictions, the spatial distribution of the national realized load profiles to the transmission nodes becomes a challenging task. Although following the distribution of the original demand may result in the conservation of this initial distribution, a more relaxed approach is selected to also incorporate any grid congestions into account. Instead of assigning a fixed profile to each node, a new variable is introduced for each node with the additional cumulative equality constraint requiring the sum of the new variables to equal the flexible demand part of the realized load profile for each time step, which has been calculated by the “country” level. The benefit of this approach consists of the optimal spatial allocation of the flexible demand utilization. However, it is based on the relatively generous assumption that demand can essentially be shifted in space, or traded among consumers. Despite its optimistic perspective, this approach can provide additional valuable insight into the effects of demand flexibility into the integration of VRES. The corresponding results regarding curtailments and emissions are shown by the grey colored bars in figure 6-24. It can be observed that both curtailments are only slightly reduced for the respective “country” level (5.1%), hence temporal shifting alone cannot effectively eliminate load curtailments, while the emissions remain to a similar degree. On the other hand, the corresponding “grid” level results show considerable reduction in both curtailments as well as emissions (31.3% and 11.6% respectively), which shows the significant theoretical advantage of spatial shifting over temporal shifting. The difference between the initial flexible load distribution, i.e. by population, and the corresponding distribution after allowing shifting in space for each country is shown in figure 6-25. Such shifting could correspond, for instance, to the relocation of energy intensive industries that are not bound by geographical constraints. It can be observed that demand is generally shifted from the highly populated areas towards the locations with lower nodal prices, thus related to higher VRES generation potential. For instance, demand is shifted from southern to northern Germany and from northern to southern Italy. Besides illustrating the underlying grid congestion, figure 6-25 additionally shows favorable locations for installing energy intensive applications that are not heavily bounded by other spatial constraints.

Finally, the green colored bars in figure 6-24 show the corresponding results reported by the e-Highway study [315] itself for the analyzed “Large-scale” 2050 scenario. The dark green values correspond to the 2030 grid, while the light green corresponds to the values after grid expansion. Notable differences to this thesis include the use of several weather years, the expansion of hydro plant capacities and the use of only 100 nodes to represent the whole system. It can be seen that the total curtailments before expansion are similar to the results of the “clusters” level which is based on the grid of 2030 as well. Therefore, the generated results as well as the conclusion regarding the impact of spatial resolution gain additional validity, since the number of nodes for both approaches is similar as well. The respective results after grid expansion show a substantial decrease in curtailments, however these probably still significantly underestimate the values that would be derived by including a more detailed representation of the transmission grid. Regarding the total emissions, a considerable discrepancy can be observed between the current work and e-Highway results even for the case before grid expansion (584 and 292 Mton CO_2 respectively). Although all the results of the current work also include the emissions from bioenergy (which amount to 95 Mton CO_2, hence the net balance of the biomass cycle is ignored), the discrepancy remains significant (67.5% higher). This discrepancy can be attributed to the difference in hydro plant capacities and potentially to a different handling of the conventional plant flexibility.

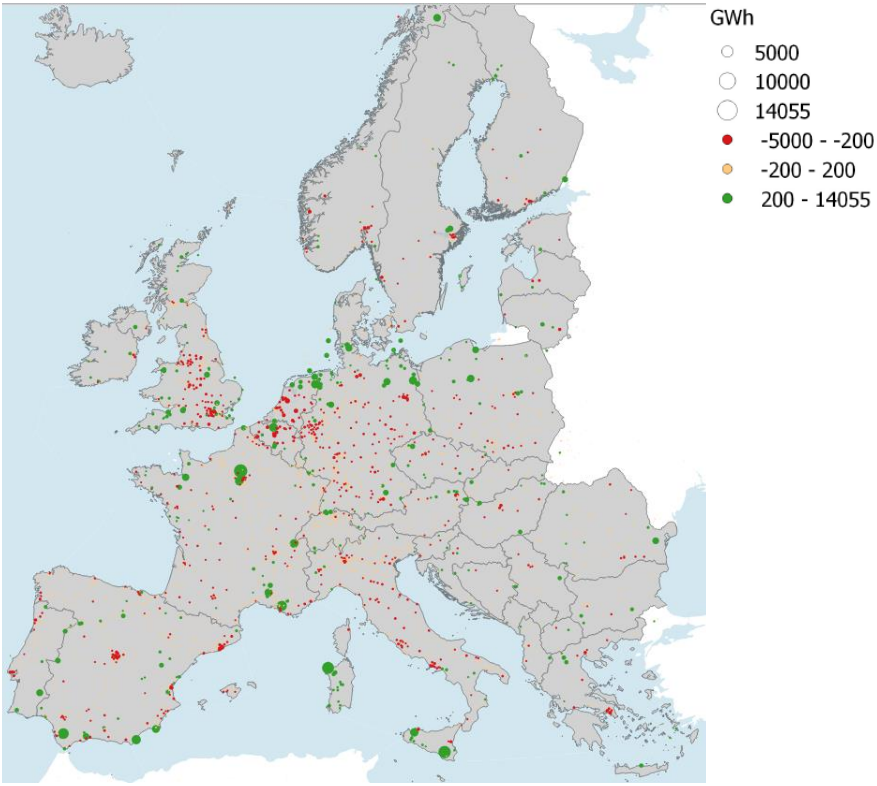

Figure 6-25 Load difference between the initial flexible load distribution and when shifting in space is allowed for each country. Demand is shifted from the locations with negative values towards the locations with positive values.

6.2.2 Impact of demand flexibility parameters

The investigation of the reference case in section 6.2.1 provided useful information regarding the state of the system for 2050 including the impact of applying demand flexibility as well as a spatio-temporal analysis of the VRES curtailments. However, further investigation of the flexible demand parameters is deemed essential to better comprehend its impact on reducing both VRES and load curtailments. The following results correspond to the “Large-scale RES” scenario of e-Highway for 2050 with weather year 2011 and the “clusters” modeling level with 150 clusters.

Figure 6-26 shows the total curtailments for different levels of available demand flexibility and a maximum allowed time shift set to 24 hours. While reducing load curtailments is accompanied with direct reductions in system’s operation cost, a respective reduction in VRES curtailments is only implicitly encouraged. The respective mechanism derives from their zero marginal costs, which grants them priority in replacing other more expensive sources of generation during congestion relief and hence the corresponding curtailments are decreased. For zero flexibility, i.e. fixed load, the total VRES curtailments amount to 490 TWh, whereas the load curtailments to 58 TWh. Allowing 5% of the initial demand to be shifted leads to an immediate drop by 6% and 12% in VRES and load curtailments correspondingly. However, a further increase in the available flexibility does not lead to a significant further reduction, which finally reaches a merely 8% and 16% reduction for VRES and load curtailments respectively. This low sensitivity indicates that increasing the available demand flexibility can merely overcome power shifting constraints, however further benefits are limited by the maximum allowed shifting duration. Furthermore, as shown in section 6.2.1, the application of 10% demand flexibility, deferrable by 24 hours, at the "country" level results in similar reduction rates of the total VRES and load curtailments, amounting to 5% and 18% respectively. Therefore, the redispatch formulation of the "clusters" level does not constitute a limiting factor for a higher impact of demand flexibility on VRES integration.

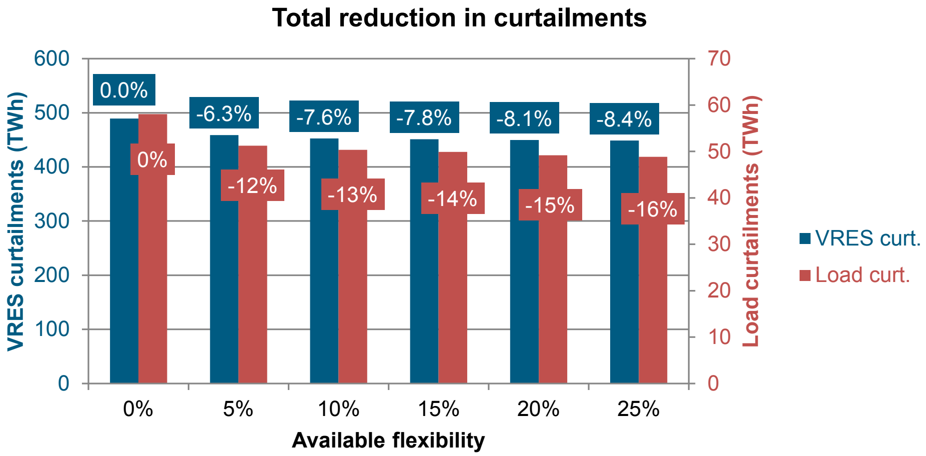

Figure 6-26 Total reduction in load and VRES curtailments due to demand flexibility for different amounts of available flexibility. The maximum shifting period is 24 hours.

Averaging the total realized load profiles over each hour of the day can provide further insight on the impact of the available demand flexibility, as shown in figure 6-27. It can be seen that 5% available flexibility can already alter the original profile significantly, while further increase in flexibility only leads to minor differences in the average profile that appears to converge to a specific pattern. Similarly to figure 6-15, the shifting direction can be observed to also shift demand from the night hours towards the midday where solar is more accessible. Increase in available flexibility appears to mostly influence the constraints related to shifting power, thus gradually allowing the reduction of the morning and midnight peaks as well as the increase of the midday valley.

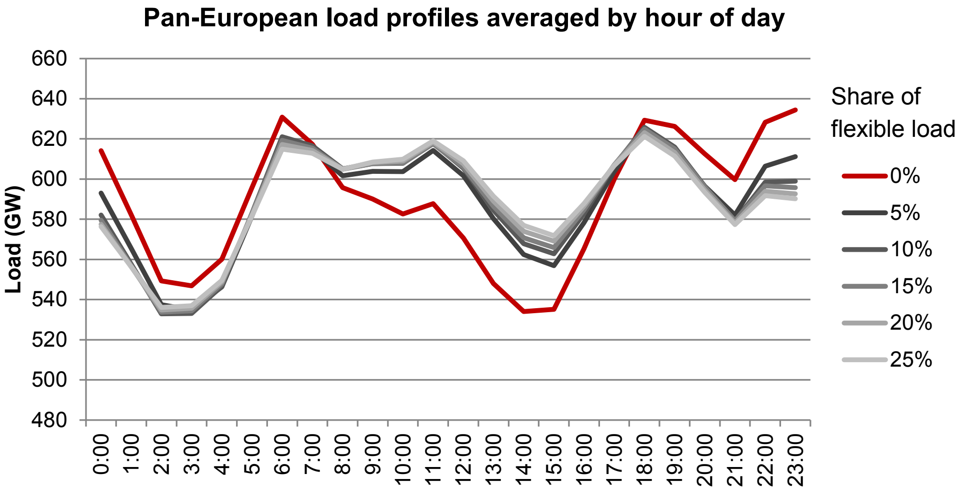

Figure 6-27 Total pan-European load profiles, averaged by the hour of day, for different values of available flexibility.

Besides demand flexibility availability, the impact of the second modeling parameter, i.e. the maximum shifting duration, is investigated as well. Figure 6-28 shows the total curtailments for different shifting durations spanning 3 hours up to a whole year, where the available flexibility is maintained constant at 10%. It can be observed that allowing shifting for less than a 6-hour period can only provide marginal reduction or even increase in curtailments, while allowing longer shifting periods becomes more beneficial. During such short shifting periods, VRES generation may not show adequate variation to contribute to the system's cost reduction, which is primarily driven by the reduction of load curtailments. Moreover, it can also be observed that the 12-hour shifting can yield a higher reduction in curtailments than the 24-hour shifting due to the discontinuous implementation of modeling the load shifting. However, the most significant reduction in load curtailments can be achieved for shifting periods greater than one week, where reductions up to 92% can be reached for the yearly flexibility. On the other hand, VRES curtailments reduction only reaches a maximum of 27%, since VRES generation exhibits higher fluctuations in absolute values while also the replacement of conventional generation is essentially only encouraged in the case of grid congestion. Overall, it can be concluded that higher available flexibility in terms of available time shifting provides considerable benefits in reducing both VRES and load curtailments. However, since these results refer only to the operation of the system, no estimations of the implementation costs for such a behavior can be safely deduced. In both private and industrial consumers, short-time load shifting can be realized via demand response, smart metering and communication among the power system actors, where a consumer may choose to shift their demand by merely storing the desired product, e.g. laundry. However, since such a behavior can become economically undesirable for longer shifting periods, seasonal flexibility could be implemented primarily via energy storage and an energy carrier with high energy density and low self-discharge rate.

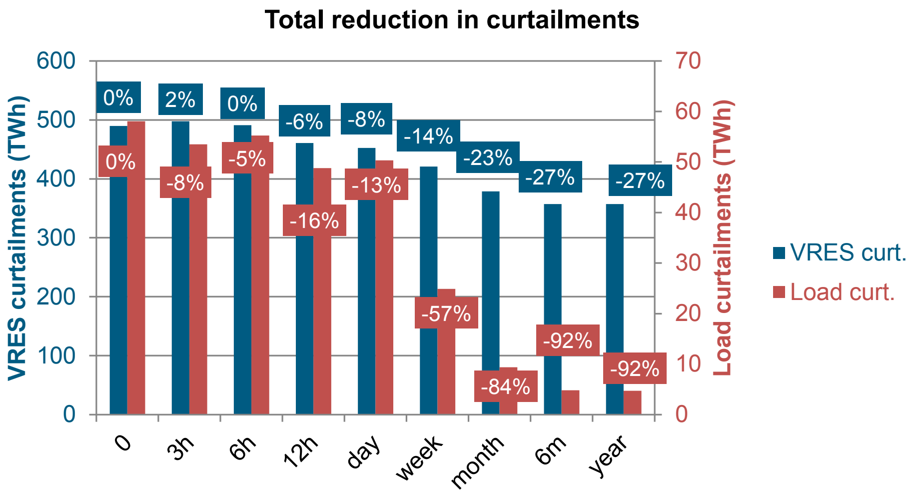

Figure 6-28 Total reduction in load and VRES curtailments due to demand flexibility for different periods of maximum shifting. The available flexibility is 10% of the initial demand.

Similarly to the investigation of the available flexibility variation, averaging the total realized load can provide further insight in the influence of the maximum shifting duration. Figures 6-29, 6-30 and 6-31 show such averaged profiles over different temporal scales. In figure 6-29 the load profiles are averaged over the hour of each day and it can be observed that shifting for 3 or 6 hours does not substantially alter the original average profile. However, already for shifting periods beyond 12 hours, the average daily profile appears to also converge to a specific pattern.

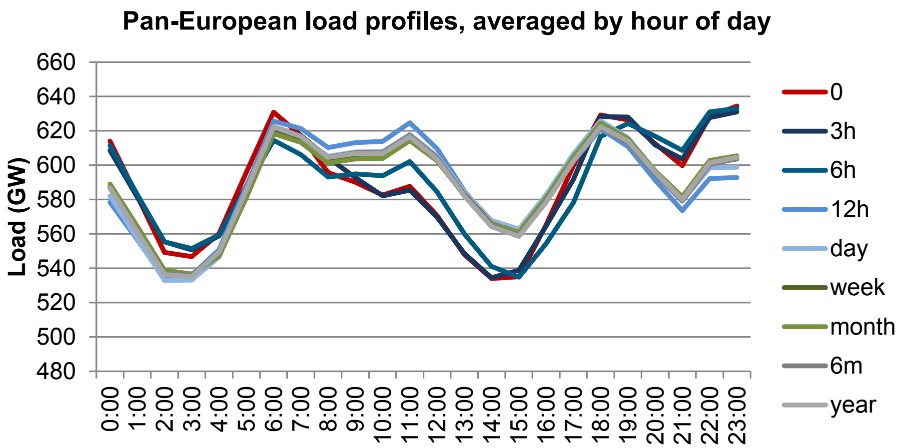

Figure 6-29 Total load profiles, averaged by the hour of day, for different values of maximum allowed load shifting.

Figure 6-28 shows a further reduction in curtailments for shifting durations beyond 24 hours, which can be obtained by inter-day load shifting. Figure 6-30 depicts the total realized load of Europe, averaged for each day of the week. As expected, shifting durations lower than 24 hours cannot alter the initial weekly profile, while longer shifting durations appear to shift demand from working days towards the weekend, where the load is lower. Finally, the realized load profiles for all shifting durations are also averaged over each month of the year in order to identify any seasonal shifting variations. Figure 6-31 shows that only shifting periods of 6 and 12 months can show such an impact, where the resulting profiles for both cases demonstrate similar behaviors. It can be observed that demand is shifted from the cold months of January and February, exhibiting the highest consumption of the year, towards spring and autumn, where more hydro potential is also available.

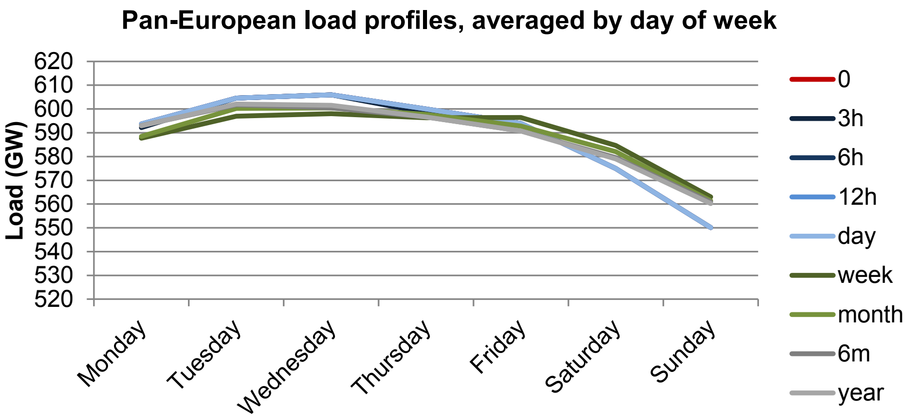

Figure 6-30 Total load profiles, averaged by the day of week, for different values of maximum allowed load shifting.

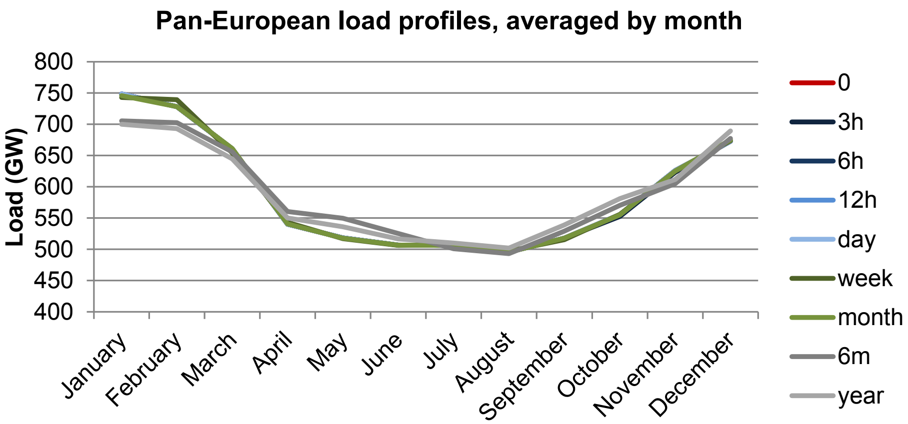

Figure 6-31 Total monthly averaged load profiles for different values of maximum allowed load shifting.

6.2.3 Sensitivity analysis

The application of the multi-level model on the reference scenario with 10% available demand flexibility, deferrable by 24 hours resulted in a total amount of 730 TWh of VRES curtailments, 240 TWh of load curtailments and 584 Mton of CO_2 emissions. These values however merely correspond to the "Large-scale RES" scenario and therefore cannot constitute a representative estimation for the year 2050. Moreover, they also correspond to the weather year of 2011 which might as well constitute a misrepresentation of the system, since renewable generation and electricity demand depend highly on the weather conditions including wind, solar radiation, precipitation and ambient temperature. Finally, VRES curtailments can also be evaluated for the years preceding 2050, thus obtaining a more detailed trajectory of the European system's evolution.

6.2.3.2 Weather years

Regarding weather years, the years 2005 to 2015 are selected, since they correspond to the latest climate conditions. In figure 6-32, the total curtailments and emissions for all weather years with respect to the reference scenario, i.e. 2011, are shown as well as the respective average values. It can be observed that, although the values vary strongly from year to year, almost all weather years exhibit lower amount of both curtailments and emissions with comparison to 2011 and thus, the average value is closer to the minimum observation. Considering the average VRES curtailments over all of the investigated weather years, it can be observed that a reduction of 7.7% from the reference case of 2011 is obtained, a value that is comparable to the impact of applying load shifting and hence not negligible.

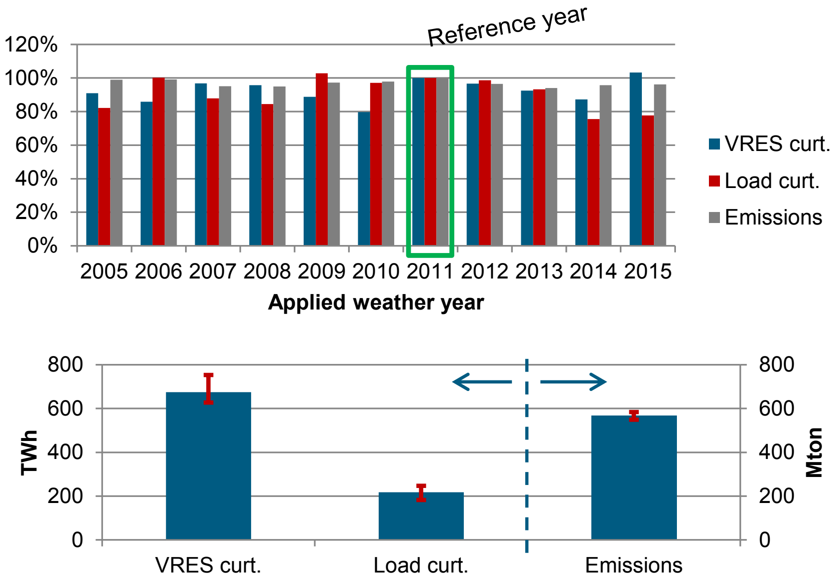

Figure 6-32 Impact of the weather year on curtailments and emissions. The top picture shows all values for all years, normalized based on the values of weather year 2011. The bottom picture shows the average values for all years with the corresponding extrema values shown via error bars.

The application of different weather years may result in discrepancies in the amount and spatial distribution of curtailments that cannot be easily interpreted in a straightforward manner. For instance, it can be noticed from figure 6-32 that there is no evident correlation between VRES curtailments, load curtailments and emissions, while also consecutive weather years may result in significant variations for the same system. Since the installed generation capacities as well as total demand remain unchanged, weather conditions with regular yearly patterns on average, like ambient temperature and solar irradiation, are expected to have only little influence on the total curtailments for the different weather years. On the other hand, the more irregular wind patterns are expected to constitute the primary driver for the observed strong variation of curtailments among the different weather years. This behavior can be illustrated in figure 6-33, where the total available, actually generated and curtailed energy from wind and solar are shown in relative terms with respect to the values of 2011. It can be observed that the solar generation values, although not identical, deviate only slightly from the reference case. On the other hand, wind generation values exhibit higher fluctuations over the wind years, where the curtailed energy variations become more prominent in relative terms due to the lower respective absolute values. This sensitivity to weather years therefore may require the consideration of multiple years for mid- and long-term studies on systems with high shares of wind generation.

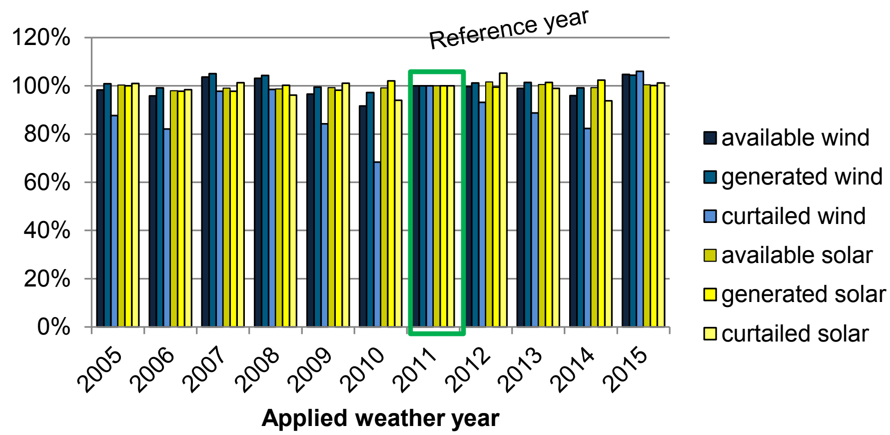

Figure 6-33 Total available, generated and curtailed wind and solar energy for different weather years in comparison to 2011.

By considering all weather years instead of only one, a more reliable picture for the most prevalent locations of grid congestion in 2050 can be obtained. In figure 6-34 the average frequency of line overloading incidents over the weather years 2005-2015 is depicted. Overloading is selected to correspond to flows over 70% of the line capacity, after its correction by the security factor. Hence, overloading can be merely interpreted as loading near the security limit of a line rather than an actual overloading, since exceeding this limit is explicitly prohibited by the respective optimization constraints. It can be observed that, although multiple years are considered, the most frequently congested lines are concentrated in specific areas that typically coincide with the highest nodal price differentials depicted in figure 6-6. Therefore, it can be deduced that grid congestion is not significantly affected by the selected weather year. The location of these areas can be indicative of the sources that cause the corresponding congestions which can be classified in three main categories, namely related to wind, solar and hydro generation. Frequent congestions due to wind generation can be identified between the coast of North and Baltic seas and the inland Europe, e.g. France, Germany and Poland, as well as at the interconnections between countries with high wind generation like the British Isles and Denmark and central European countries. Congestion due to solar generation can be observed at the landing points of the interconnections with North Africa in France, Italy and Greece. Potential approaches to reduce this congestion may include the selection of a different landing substation or the consideration of multiple ones such that the cheap solar energy from the south can be more easily diffused into the European grid. An additional significant bottleneck related to solar generation can be also noted in the Southern Italy. Regarding the congestion related to hydro generation, it can be observed that the considerable corresponding potential of the Scandinavian countries allows a higher integration of wind generation in these areas on the one hand, however, the limited interconnection capacity to the neighboring countries restricts this cheap source of energy from diffusing towards the demand centers of central Europe, thus leading to frequent overloading incidents of the interconnectors. A further significant bottleneck related to hydro generation can also be identified in southern France. Figure 6-6, 6-25 and 6-34 show a consistent picture of critical locations with regard to grid congestion and can provide a strong indication on the requirements for grid reinforcement, beyond the expansions suggested by the TYNDP for 2030.

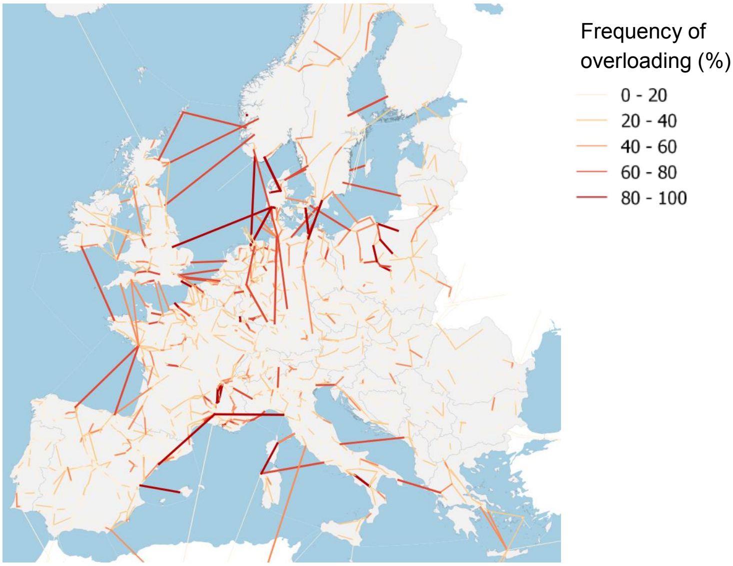

Figure 6-34 Average line overloading frequency over the weather years 2005-2015 for the “Large scale RES” scenario for 2050. Overloading incidents are considered when power flows exceed the 70% threshold of the corresponding line’s capacity, after its correction due to operational security considerations. The frequency of 100% corresponds to 8760 hours for 2050.

6.2.3.2 Scenarios

Besides the impact of the weather years, one of the most significant sensitivities with regard to future VRES curtailments consists of the selected scenario framework, since it may drastically alter the boundary conditions of the system and therefore its operation as well. Since the scenarios including CCS technology have been ruled out of consideration, only the “Large-scale RES” – X5, “100% RES” – X7 and “Small and local” – X16 scenarios are investigated, where the corresponding generation and demand conditions are depicted in Appendix G. The examination of the scenario sensitivity can also be expanded for the years 2030 and 2040 which may also demonstrate considerable uncertainties. Moreover, such an investigation can further provide a clearer illustration of the evolution of the VRES curtailments until 2050. Figure 6-35 depicts the total VRES and load curtailments as well as the total CO_2 emissions for the investigated scenarios of the years 2030, 2040 and 2050. In addition, the total emissions related to power generation are also shown for the years 1990 and 2015 as well as the emission levels corresponding to 50%, 80% and 95% reduction of the 1990 value [316].

Regarding the influence of the various scenarios, it can be observed that besides 2030, the scenario selection can highly impact the amount of curtailments and CO_2 emissions. Although for 2030 some considerable deviations may be observed, for instance the first vision deviates in terms of total emissions and the second vision in terms of VRES curtailments, overall all four scenarios show a relatively similar behavior with respect to the depicted variables (e.g. 20.4% standard deviation for the VRES curtailments). On the other hand, for 2040 and 2050, the differences between the corresponding scenarios increase significantly, thus reflecting the rise of uncertainty in describing future systems. For instance, these uncertainties translate to 21.1% and 35.8% standard deviation for the VRES curtailments for the years 2040 and 205 respectively. Nevertheless, for both of these years, similar scenario characteristics can be identified. The VRES curtailments for the “Small and local” scenario are considerably lower in both cases due to the less centralized generation and the lower electricity demand. Load curtailments become highest for the “100% RES” scenario due to the low availability of flexible natural gas generation and storage options. Lastly, CO_2 emissions become highest for the “Large-scale RES” scenario” due to the considerable dependency on natural gas generation as well as the high electricity consumption. Regarding VRES curtailments, the average value for all scenarios amounts to 589.4 TWh, i.e. 19.2% lower than the reference case, hence significantly higher than the impact of the weather year as well as the daily demand flexibility.

As far as the chronological evolution of the system is concerned, the total amount of curtailments shows a considerable increase from 2030 to 2050, while the corresponding CO_2 emissions are reduced. The VRES curtailments exhibit an almost exponential trend, where the total value approximately doubles every 10 years starting from 184.6 TWh and reaching 589.4 TWh, while the load curtailments rise as well but with a slower pace (from 178.5 TWh up to 320.5 TWh). Such a behavior is expected, since the increasing shares of VRES generation in this scenario are not accompanied by a corresponding increase in electricity storage or grid capacity. On the opposite side, CO_2 emissions, including bioenergy sources, gradually decrease until they reach a reduction of 73% in comparison to the 1990 levels, as shown in the second picture of figure 6-35. Further reduction of emissions may be achieved by either increasing the installed RES capacities for 2050 or by considering additional measures for a higher integration of VRES.

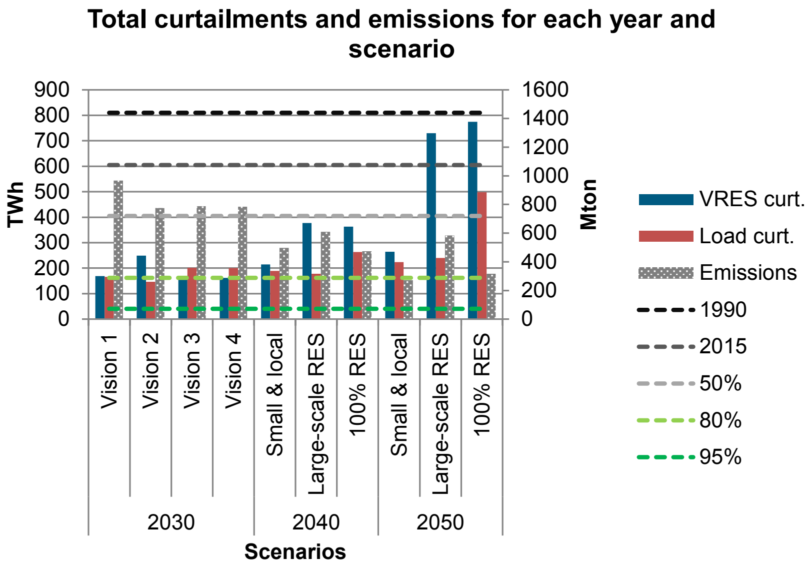

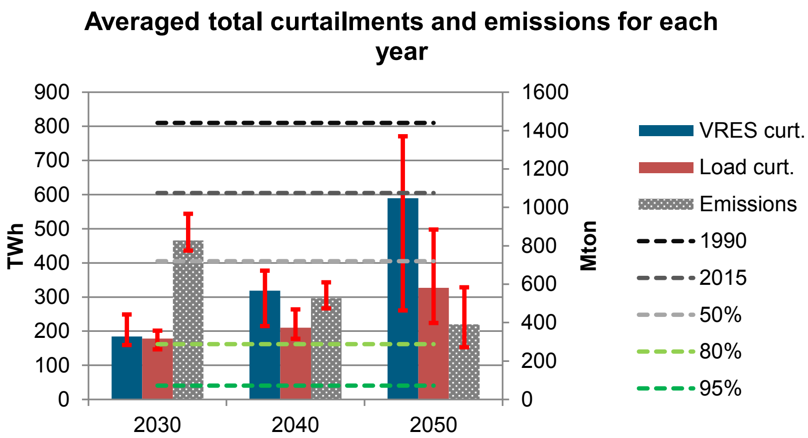

Figure 6-35 Total curtailments and emissions for 2030, 2040 and 2050 including all the investigated scenarios. The first picture shows all values in detail, whereas in the second picture the same values are averaged for each with the scenario variation shown in the form of error bars. The dotted lines indicate the total emissions for the years 1990 and 2015 as well as the values that correspond to various reduction targets with respect to 1990 values. All emission values refer to the right axis.

Regarding the spatial distribution of the VRES curtailments, figure 6-36 depicts the total respective amount of each transmission node for the years 2030, 2040 and 2050 along with the corresponding scenarios. It can be observed that high spatial concentrations of curtailments become more prominent primarily for the “Large-scale RES” and “100% RES” scenarios of 2040 and 2050. Moreover, these curtailments are mostly located near the North and Baltic seas, therefore associated with wind generation. Furthermore, it becomes apparent that the scenario definition not only determines the total amount of curtailments to a significant degree, but it also dictates the spatial distribution of these curtailments. In contrast to the “Large-scale RES” and “100% RES” scenarios, which show similar distribution patterns, the “Small and local” scenario exhibits a considerably different spatial distribution which may also lead to significant changes in the potential for power-to-X applications that would rely on these curtailments. The main reason for this behavior stems from the different rationale of this scenario which promotes a more distributed approach for the future power system and a higher reliance on solar generation.

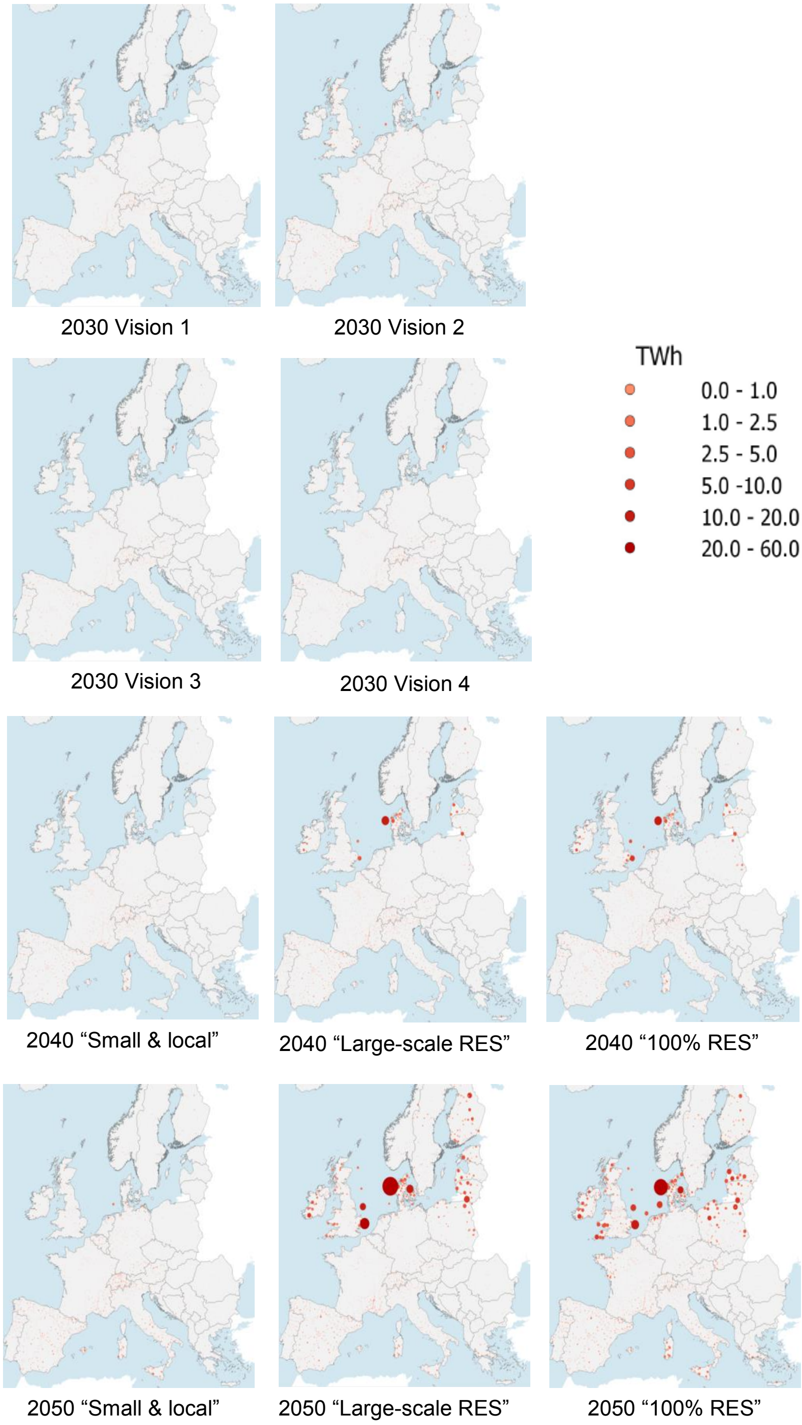

Figure 6-36 Evolution of the spatial distribution of VRES curtailments for the years 2030, 2040 and 2050 along with their corresponding scenarios.

In figure 6-24 the impact of shifting demand in both time and space is depicted for the reference case, nevertheless the investigation of the impact over the rest of the scenarios for 2050 as well may provide a more complete picture for the year 2050. Similarly to the reference case, a substantial decrease in curtailments can be observed for all scenarios, as depicted in figure 6-37. The average amount of VRES curtailments drops to 428 TWh, i.e. a 41% reduction in comparison to the reference case and a 27% reduction in comparison to the initial scenario average for 2050. Thereby, shifting demand in space and consequently, the original spatial distribution of the electricity load as well can pose a considerable impact on the total VRES curtailments. In contrast to the curtailments however, the total CO_2 emissions do not decrease to a similar degree since demand shifting prioritizes the replacement of load curtailments with RES generation rather than the replacement of conventional generation.

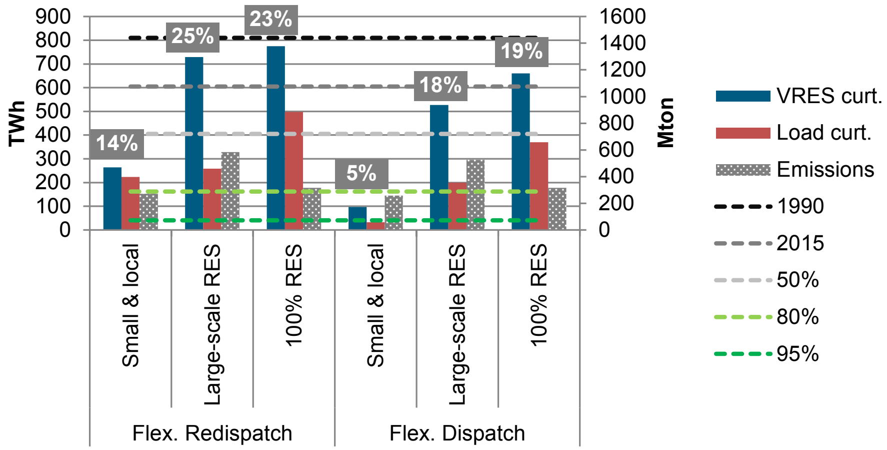

Figure 6-37 VRES and load curtailments for the three scenarios of 2050 when applying demand flexibility in a redispatch and a dispatch formulation correspondingly. The relative values correspond to the VRES curtailments in relation to the total VRES generation available. The dotted lines indicate the total emissions for the years 1990 and 2015 as well as the values that correspond to various reduction targets with respect to 1990 values. All emission values refer to the right axis.

6.2.4 Comparison with literature

The presented analysis focuses on the VRES curtailments of the future European power system as well as the impact of demand flexibility based on original calculations. Nevertheless, it is worth investigating whether similar conclusions can also be found in the literature. Since dispatch models are not typically applied for future years as far as 2050, the relative literature is extended to include investment models as well, which may include either generation or grid expansion or both. Moreover, since it is unlikely for such studies to refer to identical scenarios or system conditions, the models selected for comparison are chosen such that they cover the same investigated geographical region as well while also referring to the same year in the future.

Regarding curtailments from VRES, few studies only focus on their analysis, where frequently corresponding results are omitted entirely. Nevertheless, total values for Europe can be found for 2030 in Huber [317] and Tröster et al. [318] and for 2050 in Haller et al. [132], Bertsch et al. [319], Tröster et al. [318] and Zappa et al. [320]. Figure 6-38 shows the total VRES curtailments as reported by these studies as well as the corresponding values presented in section 6.2.3. Moreover, the total number of nodes representing the European transmission grid is depicted as well in logarithmic scale. It can be observed that the current study involves a network size that is one order of magnitude higher than that of the literature study with the highest number of nodes. Although not all studies agree on the amount of total curtailments, all the reported values are significantly lower, approximately half, than the corresponding values derived by this thesis. This discrepancy resembles the respective differences shown in figure 6-24 for the four modeling levels with different levels of spatial resolution and probably originates thereof. Hence, very high resolution models are required for accurately estimating VRES integration. Moreover, comparing the results of this study to literature values not only does not question their validity but also further reinforces the general conclusion that even models with relatively high resolution (e.g. 200 nodes) can significantly underestimate the amount of VRES curtailments.

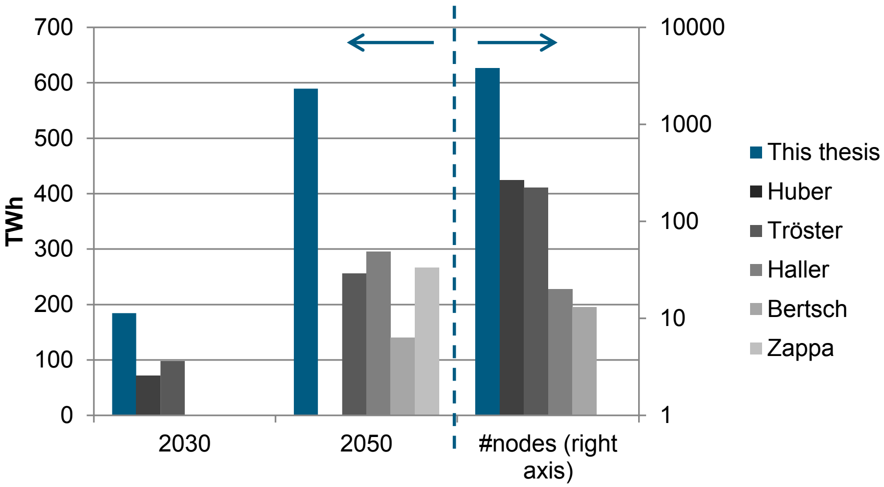

Figure 6-38 Total VRES curtailments in Europe for 2030 and 2050 in comparison to literature values [132, 317-320] and the corresponding number of nodes representing the transmission grid.

As far as the impact of demand flexibility is concerned, only Tröster et al. [318] report respective values for the year 2030, as shown in figure 6-39. Although the increasing rate of curtailments reduction for increasing available flexibility is slightly higher than the corresponding results of section 6.2.2, the discrepancy in the values between the studies is deemed negligible. What is more, the overall conclusion that higher available demand flexibility only bears minor curtailments reduction is further confirmed.

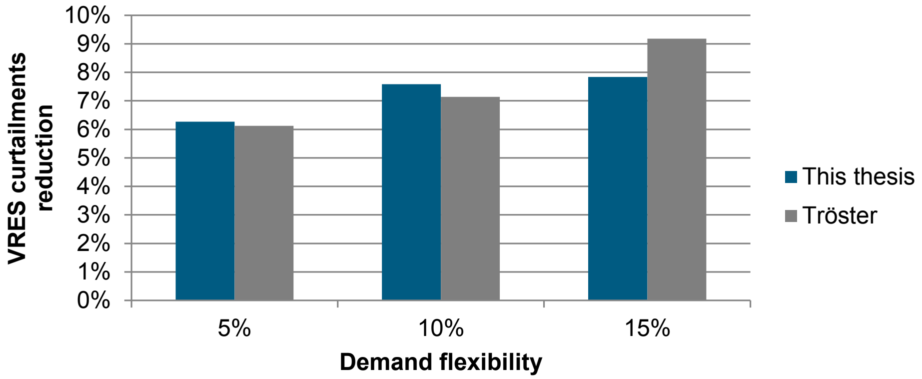

Figure 6-39 Relative reduction in VRES curtailments for different amounts of demand flexibility.

6.3 Chapter summary and discussion

In this chapter, the future European power system is investigated with respect to VRES curtailments. Moreover, several critical modeling factors and their corresponding impact on the integration of VRES are additionally examined. Such factors include the level of demand flexibility, the selected weather year and the scenario framework.

Before introducing the results of the pan-European model, the selection of the modeling approach for demand shifting as well as an adequate number of nodes for the "clusters" level need to be determined. In section 6.1, the different methodologies described in section 3.5 are evaluated in terms of total VRES curtailments and execution time for a different number of clusters. It is concluded that despite the poorer accuracy, the decoupled virtual storage method is selected due to its computational performance.

In section 6.2, the pan-European multi-level model is applied under various settings and the corresponding results are analyzed and compared to the literature. Section 6.2.1 introduces the reference case which consists of the system state for 2050 according to the "Large-scale RES" scenario, using the weather year of 2011 and demand flexibility of 10%, deferrable by 24 hours and examines the results of all four modeling levels. Moreover, the final results are also compared to the same system conditions but with demand flexibility being applied directly at the "country" level and allowing spatial shifting within the national borders. Section 6.2.2 evaluates the impact of demand flexibility by measuring the curtailments reduction for different levels of available flexibility and maximum shifting duration. In section 6.2.3, the impact of the weather year is discussed, while also the system states for the years 2030, 2040 and 2050 along with the corresponding scenarios are analyzed. Finally, the results regarding VRES curtailments and the respective impact of demand flexibility are compared to literature values in section 6.2.4.

Examining the reference case for all modeling levels provides a consistent picture of the European power system regarding grid congestion, curtailments and flexibility requirements. The most significant congestions are identified between the northern and central Europe as well as between the coast of the North and Baltic seas and the mainland, thus related to wind and hydro generation that cannot reach the demand centers in central Europe. Moreover, further congestion can be noticed at the landing points of the African interconnections. These congestions, which also show low dependency on the applied weather year, appear to constitute the most significant factors for the corresponding VRES curtailments that are primarily located close to the North and Baltic seas, hence related to wind generation as well. Examining the German power system shows that although Germany is designed with lower VRES capacities than respective values from the literature, considering the transmission grid in high resolution results in VRES curtailments that match corresponding values found in the literature regarding both the total amount and spatial distribution. Moreover, it is found that considering each node separately and after the application of demand flexibility, the best locations for power-to-X applications relying exclusively on VRES curtailments are identified in western Ireland and western Denmark.

Comparing the results of the different modeling levels which use different resolutions for representing the transmission grid shows that the corresponding resolution can significantly affect the resulting amount of VRES curtailments, which again justifies the causation relationship between these two components. It is found that for the reference scenario a pan-European copper plate case results in merely 13.4 TWh, a zonal market representation (i.e. 33 nodes) in 328.5 TWh, an equivalent grid reduced to 150 nodes in 452.4 TWh, whereas a detailed transmission grid with 3790 nodes in 729.5 TWh. This discrepancy is in agreement with the results of the e-Highway study, and highlights the significance of considering highly resolved models when analyzing VRES integration.

Regarding the impact of demand flexibility, besides analyzing the reference case, various levels of available flexibility and shifting duration are tested as well, while also demand shifting in space is further examined. It is shown that load shifting is primarily driven by reducing the expensive load curtailments and exploiting the solar generation whose capacity factor peaks during noon. Consequently the highest curtailments reduction occurs in the Iberian Peninsula. Moreover, it is shown that such curtailments reduction is more sensitive to the maximum shifting duration rather than the available flexibility whose influence quickly reaches a threshold. Maximum, i.e. yearly, shifting can attain 27% reduction in VRES curtailments whereas maximum available flexibility, i.e. 25%, reaches merely 7.6%. An additional factor with significant impact on reducing curtailments consists of allowing demand shifting in space, which can lead up to 27.7% of VRES curtailments reduction (527.5 TWh in total) and further highlights the importance of the initial spatial distribution of electricity demand as well. Overall, it is shown that demand flexibility can play only a minor role in the integration of VRES, since it can merely reduce VRES curtailments by 5-10% under realistic assumptions. Therefore, alternative methods should be considered as well, such as grid expansion, chemical storage or different spatial allocation of generation and demand, where the latter can primarily be considered for energy-intensive industries.

Applying sensitivity analysis with regard to scenarios shows a significant impact on the total amount and distribution of VRES curtailments, whereas the sensitivity to different weather years is lesser. The variation in curtailments for the different weather years is primarily driven by wind generation which fluctuates more highly than solar generation. Overall, the discrepancy between the average of all weather years and the reference case reaches 7.7% (i.e. 674 TWh in total), which is comparable to the influence of allowing demand flexibility. Regarding the variation of scenarios, it is shown that systems relying more on wind and on centralized generation exhibit a considerably higher rate of curtailments, which tend to become more centralized as well. On average, the total VRES curtailments in Europe almost double every ten years from 2030 to 2050 until they reach 592 TWh for 2050. Comparing this value to the literature as well as to the modeling levels with reduced spatial resolution shows a significant discrepancy of around a factor of 2, even for models with relatively high spatial resolution (150-250 nodes). Thereby, the importance of the spatial resolution when VRES integration is concerned should not be underestimated.

7 Summary

In this thesis a model for the pan-European power system has been developed and applied for future scenarios with high shares of RES. In chapter 2 the operating principles of power systems were presented for the quasi-static regime as well as the numerical methods to approach the non-linear power flow equations. Such methods include iterative approaches, the Holomorphic Embedding method and linearization techniques where the corresponding advantages and drawbacks were discussed. In addition, the determination of the power injections that govern the power flows across transmission systems is presented by describing the existing electricity market and congestion management frameworks in Europe. An additional review on the different variations of the popular optimal power flow (OPF) method is performed and discussed as well as the corresponding numerical approaches. Finally, a literature review is conducted regarding the existing approaches for modeling the European power system used by the research community.

In chapter 3 the primary modeling methodology of the thesis is described in detail. In order to tackle the challenging questions of VRES integration on the European scale, a novel multi-level dispatch model based on linear programming is developed. Solving the complete problem, where fine temporal and spatial resolutions are considered simultaneously, is limited by the existing computational resources. Hence, the developed approach attempts to simplify the problem by sequentially decoupling the spatial and temporal dimensions while still capturing the main system dynamics. Overall, the main assumptions of the selected approach include perfect competition conditions for the electricity market, a centralized congestion management scheme, the use of linear approximations for the unit commitment and power flow problems as well as perfect foresight for the yearly dispatch scheduling. The main limitations of the model are associated with the involved linearization assumptions and market operation conditions that may overestimate the system's flexibility and efficiency. Regarding the modeling of flexible demand, various methodologies are reviewed with respect to the system perspective, while two selected approaches are implemented. The DIETER approach can accurately describe load shifting, however with a high computational cost, whereas the virtual storage approach sacrifices modeling accuracy for the sake of performance and is therefore selected for the purposes of this thesis.

In chapter 4 the selected assumptions as well as the necessary system data are verified against historical conditions for the investigated European area. It is shown that due to the lack of publicly available data, verification attempts can only be rarely found in the literature, while also such attempts may result in significant deviations even for averaged values. This research gap is filled by this thesis, where it is found that with a two-level linear model an adequate representation of the European power system can be achieved. The presented verification process is conducted in multiple steps. In the first verification step, the fundamental assumptions regarding market operation and congestion management as well as the corresponding linearization assumptions are tested for the case of Germany. Unlike previous verification attempts, the underestimation of natural gas generation could be significantly improved by the inclusion of the special conditions of CHP plants operation. Despite any shortcomings, the desired system quantities could be adequately reproduced. In the second verification step, various pan-European models, mainly differentiating in terms of spatial resolution, were verified for the year 2015. In contrast to the German case, hydro scheduling and cross-border flows were also verified since they no longer constituted exogenous variables of the system.

Regarding the pan-European case, the modeling of all power system components are described in detail as well as evaluated independently. The transmission grid is modeled based on geographical data from open street map (OSM). The conventional power plants are modeled using various public sources and their parameters are calibrated while also a novel method to estimate their efficiencies is developed. The hydro power plants data are obtained from public sources as well, while their variable energy inflow related to water runoff is modeled based on river discharge data. Wind and PV generation profiles are considered in high spatial resolution from a validated model in the literature. Finally, the spatial disaggregation of electricity demand was investigated via a novel methodology based on multivariate, non-linear regression analysis. The resulting pan-European model can form the basis for analyzing the existing system under different angles, for comparing different methodologies as well as for developing future scenarios with high spatiotemporal resolution.

In chapter 5, the scenarios of the European power system for 2030, 2040 and 2050 are implemented. Due to the significant uncertainties involved into describing the shape of the future European power system, multiple scenarios are implemented and investigated for each year. The selected scenarios originate from the ten year network development plan (TYNDP) 2016 and e-Highway studies, whose results constitute the primary policy drivers for developing the European transmission grid of the future. However, further assumptions were deployed in order to translate the scenario guidelines to the desired spatial resolution.

The application of the developed and verified model is conducted in chapter 6. In section 6.1, the two implemented methodologies for modeling load shifting are compared with respect to computational performance and impact on VRES curtailments. The decoupled virtual storage method is selected for the purposes of this thesis.

In section 6.2, the pan-European multi-level model is applied under various settings and the corresponding results are analyzed and compared to the literature for both the pan-European and German cases. The selected reference case corresponds to the year 2050, the “Large-scale RES” scenario, the weather year 2011 and 10% demand flexibility, deferrable by 24 hours. The results of all four modeling levels were examined with respect to identifying grid bottlenecks, the behavior of load shifting and the spatio-temporal analysis of VRES curtailments, with a focus on the potential of exploiting such curtailments using Power-to-X applications. Moreover, the application of load shifting directly at the dispatch level and the consequent permission of spatial load shifting within each country was further examined. Besides the reference case, the impact of the demand flexibility parameters on reducing curtailments was investigated as well as the impact of modeling different weather years and considering different scenarios. Finally, the obtained results were compared to literature values referring to future European systems of 2030 and 2050.

8 Conclusions

The goal of this thesis consists of analyzing the future European power system with regard to VRES integration, thus quantifying and investigating VRES curtailments, as well as examining the corresponding impact of load shifting. In addition, the main grid bottlenecks should be identified such that appropriate grid reinforcement requirements can be considered.

The application of the verified model for the future European power systems showed that:

- Grid bottlenecks for the reference scenario (i.e. 2050 “Large-scale RES”) appear primarily at the interconnections between the northern and central Europe as well as the grid lines connecting the northern coastal region of continental Europe with the inland, thus related to wind generation. Moreover, congestion is also observed at the connection points with North Africa. This picture is not altered significantly by considering different weather years, therefore it may be neglected when the analysis is not focused on single elements.
- Grid congestion shows high spatial correlation with VRES curtailments, hence it can be concluded that it constitutes the primary cause for these curtailments. Similarly to the grid bottlenecks, it is found that the majority of the VRES curtailments are located near the North and Baltic seas, thus related to wind generation. The countries with the highest curtailments are Great Britain, Denmark and Germany with 101, 98 and 88 TWh respectively. Regarding the German power system, comparison with the corresponding literature shows that although the system is designed with lower VRES, representing the transmission grid in high resolution results in VRES curtailments that match corresponding values with respect to both the total amount and spatial distribution. By analyzing the curtailment profiles on each node, it is concluded that the best locations for exploiting the corresponding energy via conversion or transportation are found in western Denmark and western Ireland.
- Representing the transmission grid in different resolutions can significantly affect the resulting amount of VRES curtailments, which again justifies the causation relationship between these two components. It is found that for the reference scenario a pan-European copper plate case results in merely 13.4 TWh, a zonal market representation (i.e. 33 nodes) in 328.5 TWh, an equivalent grid reduced to 150 nodes in 452.4 TWh, whereas a detailed transmission grid with 3790 nodes in 729.5 TWh. This discrepancy appears consistent with literature values, including the results of the e-Highway study, and clearly illustrates the significance of considering highly resolved models when analyzing VRES integration.
- Applying demand flexibility under realistic assumptions can only have minor impacts on VRES integration. It is found that by allowing 10% demand flexibility, deferrable by 24 hours, can lead up to merely 7.6% of VRES curtailments reduction, a value that is consistent with the literature as well. It is also found that the benefits of such flexibility are mostly capitalized by solar generation. Varying the amount of available flexibility does not significantly improve VRES integration, however varying the available shifting duration can lead to a considerable reduction in curtailments (up to 27% for VRES and 92% for load when yearly shifting is assumed). Moreover, if load is allowed to be shifted in space as well (e.g. relocating industry) but within national borders, it is

found that the total VRES curtailments can be reduced to 527.5 TWh in total (i.e. a 27.7% reduction).

- Similarly to the effects on congestion, considering different weather years does not significantly impact the overall integration of VRES but may lead to more substantial discrepancies on individual locations. The total curtailments when considering 10 weather years instead of only one are found to be 674 TWh (i.e. 7.7% lower than the reference scenario).
- The parameter with the highest influence on VRES integration, both in terms of average behavior and spatial distribution, consists of the scenario framework, which becomes increasingly more important for the more distant years due to the higher uncertainties involved. The average of all scenarios for 2050 amounts to 592 TWh of VRES curtailments (i.e. 18.8% lower than the reference case).
- VRES curtailments constantly increase from 2030 to 2050, where it is found that the average of all scenarios approximately doubles every ten years (starting from 184.6 TWh in 2030 and reaching 589.4 TWh in 2050).

Overall, the results show significant amounts of VRES curtailments for 2050, which indicates that there could be economically viable solutions to exploit this energy by transforming it such that it can be used by other energy sectors or by improving its integration into the power system. Such an option for higher integration could be demand flexibility, where it was shown however that it cannot constitute the only solution for a higher VRES integration but further alternatives may be required as well, e.g. grid expansion.

Appendix

A Nodal admittance matrix

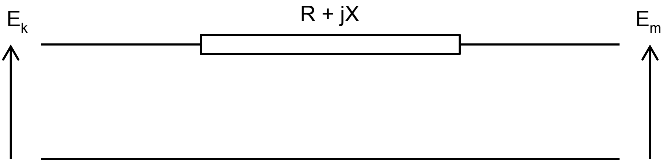

Figure A-1 Model of an overhead transmission line as two-port circuit, consisting of a single lumped element of impedance *R+jX*. The model is valid for short transmission lines.

Bulk electrical energy is traditionally transferred via the high voltage transmission grid, i.e., higher than 220 kV, which mostly consists of overhead power lines. The construction of the nodal admittance matrix is based on several assumptions for the mathematical description of a transmission line and applies only to steady state and symmetric operation.

- **Steady state operation** implies that for a single state of the system, no transient phenomena are considered and therefore all the quantities involved (power, current, voltage, etc.) can be simply represented by a complex number (phasor).
- **Symmetric operation** means that all three phases operate only in the positive sequence, while the anti-symmetrical and zero components are 0. This allows the use of a single-phase equivalent for the grid and therefore single line diagrams.
- **Short-line approximation** is required for the use of lumped elements for the electrical parameters (e.g. line impedance) instead of distributed elements. The validity of this assumption increases for lower frequencies which affect the propagating wavelength.

Under these assumptions, a power line that connects buses k and m can be modeled as a simple two-port network with an equivalent series impedance $\boldsymbol{Z} = R + jX$ as depicted in figure A-1. For the derivation of the admittance matrix, however, the inverse of the impedance, i.e., the admittance, $\boldsymbol{Y}$ of the line is used.

A power system can be described as a linear system $\boldsymbol{I} = \boldsymbol{Y} \cdot \boldsymbol{E}$, where $\boldsymbol{I}$ represents the injection/withdrawal currents, $\boldsymbol{E}$ the nodal voltages ($E = Ue^{j\theta}$) and $\boldsymbol{Y}$ the nodal admittance matrix. $\boldsymbol{Y}$ elements depend on the transmission line characteristics as well as the existence of phase-shift transformers or FACTS devices on the line, which can be cumulatively modeled by a $t = \alpha e^{j\varphi}$ expression.

The elements of the nodal admittance matrix can be expressed by

$$Y_{km} = -t^*{}_{km} t_{km} y_{km} \tag{A-1}$$

$$Y_{kk} = y_k{}^{sh} + \sum_{m \in \Omega_k} \alpha_{km}{}^2 \left(y_{km}{}^{sh} + y_{km} \right) \tag{A-2}$$

where y_{km} is the line series admittance, $y_{km}{}^{sh}$ is the line shunt admittance with the shunt conductance usually ignored, $y_k{}^{sh}$ the bus shunt admittance and Ω_k the set of all nodes adjacent to k [55].

B Passive nature of AC networks

The passive nature of the AC electrical networks and the difference to the classical transportation model description can be illustrated be the three-node example in figures B-1 and B-2. The system state in both networks can be derived directly by the network and generator properties. In the initial network, all lines are equivalent with 1 ohm reactance and 500 MW thermal capacity. The cheap generator is located on node A, whereas the expensive generator is located on node B, while both hold adequate capacity to supply the 300 MW load on node C. Since no power transfer restrictions are essentially posed by the network, all of the demand can be supplied by the cheap generator. Nevertheless, due to the passive nature of the network elements, constraining one line to 50 MW affects the maximum power flows to the rest of the network as well, as it can be seen in figure B-2. In this configuration the cheaper generator cannot inject more than 150 MW, hence the remaining power needs to be supplied by the expensive generator and thus the operational cost is increased. It can also be seen that, although counter-intuitive, by dropping the constraining line, power from the cheaper generator can be transferred with less restrictions to the load bus, thus resulting in lower operational costs.

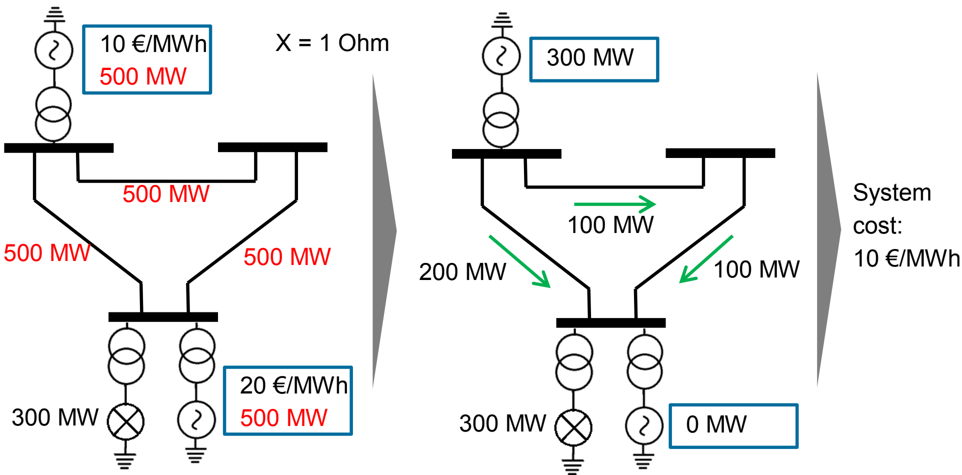

Figure B-1 Three node system before

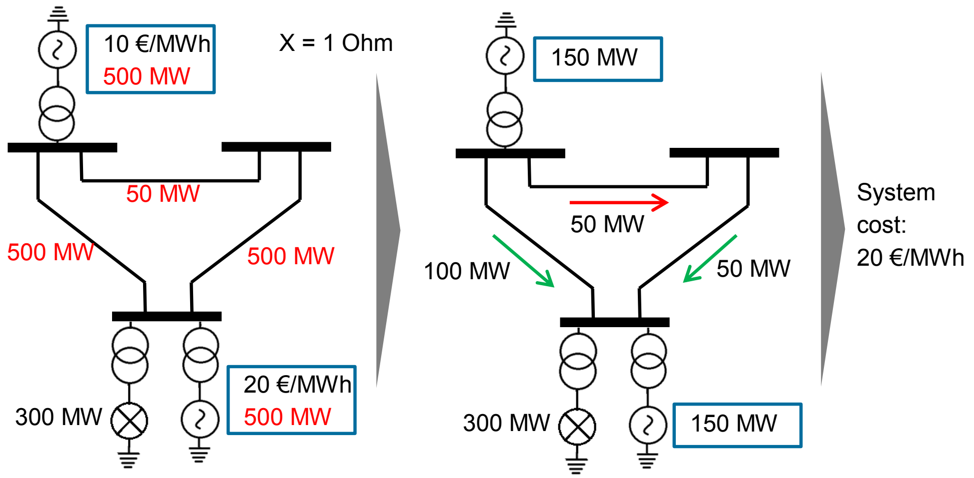

Figure B-2 Three node system after

C Impact of neighboring systems

In chapter 4, the operation of the German power system was verified by using two separate approaches with regard to modeling interconnections and the coupling with the neighboring systems. In the first approach, the interactions were assigned as fixed inflows and outflows from historical data, while in the second approach the power system of the neighboring countries was additionally modeled as well, hence the power exchanges could be obtained endogenously. Aside from historical conditions however, the behavior of the neighboring systems and the respective exchanges cannot be neglected or assumed unaffected, especially when highly meshed regions, such as central Europe, are considered. Therefore, it is worth examining the impact of both of these components onto VRES integration.

The German power system is selected as the test case for evaluating the influence of neighboring systems due to its central location and high number of neighbors. Since VRES integration is investigated, a future scenario with high shares of PV and wind are implemented. Moreover, considering that the variability of wind renders it the most challenging source with respect to system integration, the rest of the generation and demand conditions are selected to be maintained at the same level while different onshore capacities are tested. Since future scenarios are examined, potential grid extensions may be considered as well. To this end, a 2025 grid version of the German transmission grid is considered as well, which includes all projects proposed by the “B2 2025” scenario of the German network development plant [154] and the PCI list. Regarding conventional power plants, the total installed capacities follow the guidelines from the “B2 2020” scenario as well, while the residual load besides wind and PV is modeled via the methodology of section 4.1.3. As for PV and wind, generation data from Robinius [32] are considered, where the total installed PV and offshore wind capacities are selected to be 47 GW and 12.7 respectively.

Different onshore wind capacities along with the remaining boundary conditions of the system are applied for the transmission grids of 2015 and 2025 and different behavior of the neighboring systems and the corresponding impact on RES integration is assessed. Figure

C-1 shows the total negative residual load in Germany for the different onshore wind capacities for 2015 and 2025 grids as well as when interactions with the neighboring countries are modeled either by using historical data or by assuming unlimited willingness to import any available generation. By these means, the imposed error of not considering the transmission grid or ignoring the neighboring countries can be estimated. It can be observed that the impact of the grid can become rather significant, especially for low wind shares where the “copper plate” model shows considerably lower values than the models that incorporate grid constraints. However, this impact is reduced for high wind capacities where further reduction in curtailments can only be achieved via storage and additional electricity demand. Moreover, it can be seen that if the neighboring countries can absorb any amount of the negative residual load allowed by the interconnections, thus behaving as “perfect neighbors”, the integration of RES can be improved substantially. The corresponding impact becomes even more prominent for higher onshore wind shares and stronger transmission grids which can allow better access to the neighboring consumers.

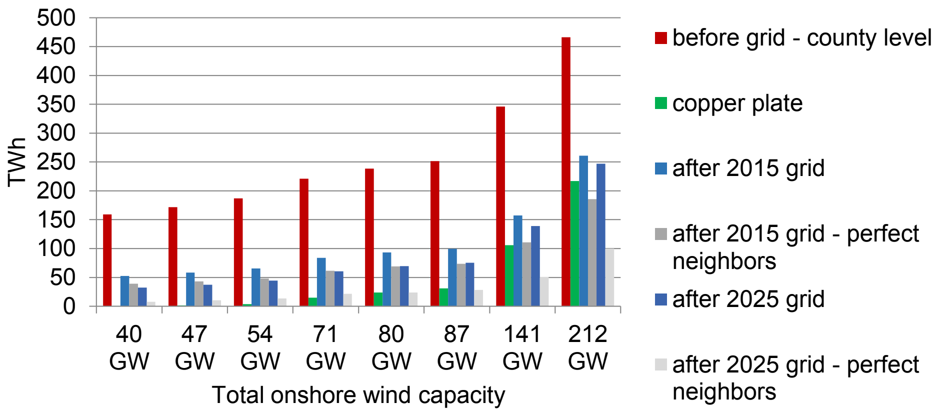

Figure C-1 Total negative residual load of the German power system for different onshore wind installed capacities, grid scenarios and behavior of neighboring countries.

In addition to assuming perfect absorbing behavior for all countries, the contribution of individual countries is also examined in figure C-2. For each onshore wind scenario the total negative residual load for Germany is shown, where all neighboring countries are assumed to behave as perfect absorbers except for the depicted country. This country’s behavior is instead varied by assuming different withdrawal levels spanning no interaction (0 GW) to perfect absorption (10 GW). It can be observed that only few countries can effectively contribute in mitigating VRES curtailments, where the majority of them are related to the higher wind generation in Northern Germany, i.e. Denmark, Netherlands and Poland. Moreover, it can be seen that in almost all cases even a mere level of 1 GW absorption level essentially reaches the absorption limit posed by the transmission grid capacity. Nevertheless, even by assuming such extreme willingness from all neighboring countries to import excess RES generation from Germany, the corresponding amount of curtailments remains considerable.

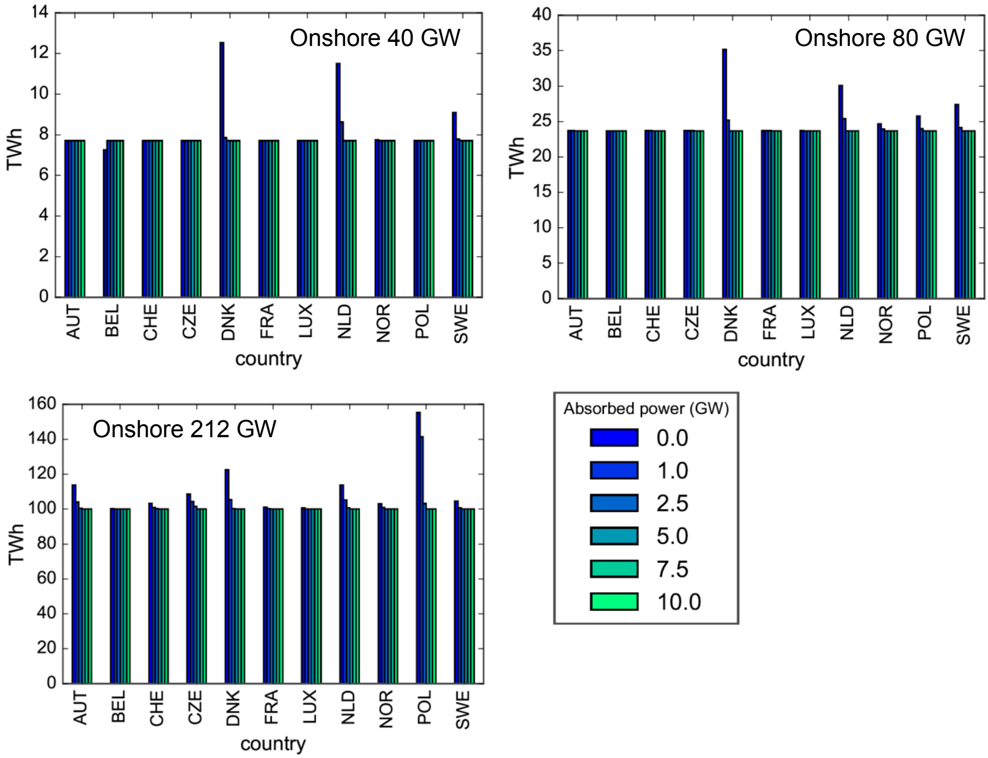

Figure C-2 Total negative residual load of the 2025 German power system for different onshore wind installed capacities and absorbed power level of neighboring countries.

D Hydro inflow profiles

The catchment areas (or drainage basins) represent specific areas of land where all the precipitation drains off into a common outlet. Drainage basins are generally divided by their surrounding topography and limited by water dividers[4]. The major element of a catchment area is represented by a stream where typically most of the precipitation, surface and subsurface runoff is collected. The streamflow and the magnitude of the river depend highly on the size of the related catchment area. In contrast to small rivers with small catchment areas, large rivers have large catchment areas and therefore more surface area available where water can be gathered [321].

Accordingly, the size of the catchment area differs due to the point selected as outlet. Typically, outlet points refer to connections on the river network. From there, different drainage basins can easily be delineated or combined. For organising drainage basins, coding systems like the “Pfafstetter Coding System” have been developed. The methodology invented by Otto Pfafstetter in 1989 is used to assign unique IDs to catchment areas based on the topology of the land surface [258].

For each catchment area a specific number is given based on the location within the overall drainage system. The first level, respectively the first number of the ID, corresponds to a continental scale catchment area. Higher levels, represented by the second, the third and following ID numbers, typify the same area but divided into smaller catchments [322]. Figure D-1 gives a schematic example of the application of the Pfafstetter Coding system. It can be observed that the drainage basin (2) is split into different subsystems. Depending on the existence of a river branch, these subsystems are either called inter- (see uneven ID’s 23, 25, 27) or sub-basins (see even ID’s 22, 26, 28).

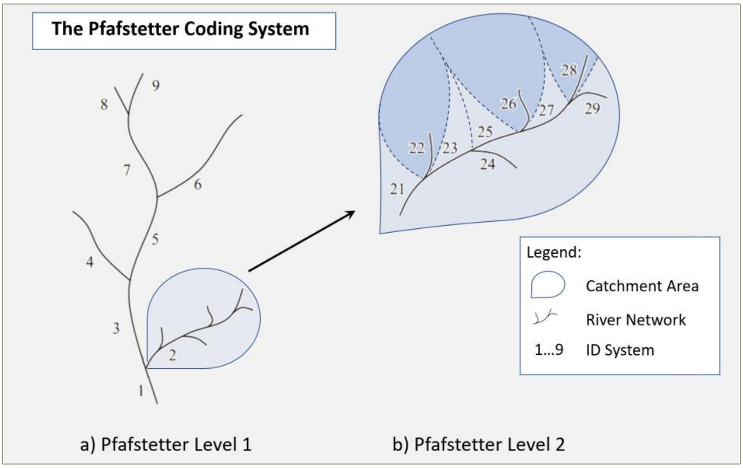

Figure D-1 Explanation of the Pfafstetter Coding System: a) Pfafstetter Level 1 with different river branches (1-9); b) Pfafstetter Level 2 of a selected river branch (2) partly split into inter- and sub-basins. (Own illustration according to Linke et al. [323])

[4] Topographic boundaries apply to surface flows and do not necessarily overlap with subsurface flows. For overall considerations, both kinds of flow have to be taken into account.

Figure D-2 shows the GRDC measurement stations with the corresponding of data availability. In order to favor better spatial representation, stations with data within the period 1956-2005 are selected and equivalent reference year streamflows are composed respectively. A lack of stations can be observed in the Balkans, whereas a lack of measurement data is observed in the Iberian peninsula.

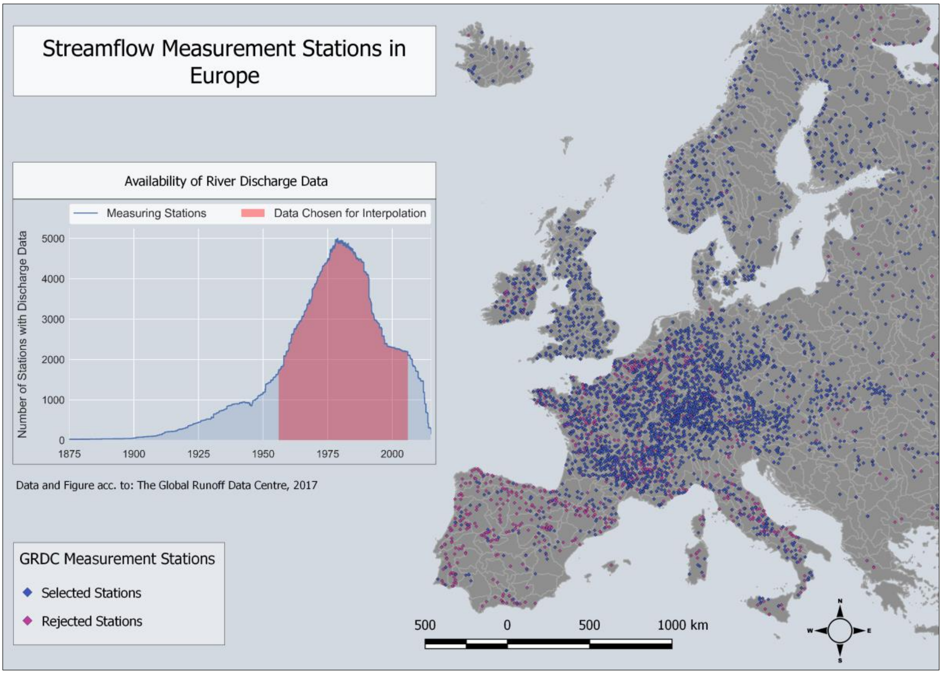

Figure D-2 GRDC measurement stations based on their data availability. The period from 1955 to 2005 is selected to construct the equivalent profiles.

Figure D-3 shows the three ways to interpolate river flow time series data from measurement stations to power plants. Catchment areas are used as groupers since the measurement stations constitute an unstructured dataset and an interpolation methodology using all available points may result to unrealistic flow contributions from measurement stations unrelated to the point of interest. When no station is present within the same catchment area, a larger basin with a higher Pfafstetter level is used until at least one station is found. Table D-1 summarizes the statistics of hydro plants using these levels as well as the aforementioned interpolation methodologies.

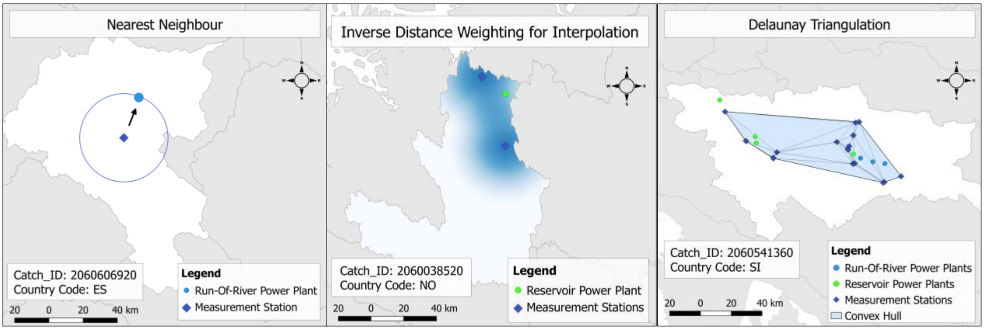

Figure D-3 Interpolation rules for streamflow data. For one measurement station, the profile is used directly. For two stations, the Inverse Distance Weighting (IDW) method is applied. For more than two stations, the points inside the formed convex hull are linearly interpolated using Delaunay triangulation [324], whereas for the points outside, profiles are extrapolated using the IDW method.

Table D-1 Applied interpolation/extrapolation methodologies per catchment level. When no measurements stations exist in the same level with a power station, a higher catchment level is considered.

Applied Method	Stations per Catchment x	Catchment Level			
		6	**5**	**4**	**3**
Nearest Neighbour	x =1	*101*	*0*	*0*	*0*
Inverse Distance Weighting	x = 2	*154*	*17*	*0*	*0*
Linear Interpolation (Delaunay)	x > 2	*737*	*44*	*6*	*0*
Inverse Distance Weighting		*614*	*102*	*31*	*6*
Total		**1606**	**163**	**37**	**6**

E Regional historical demand

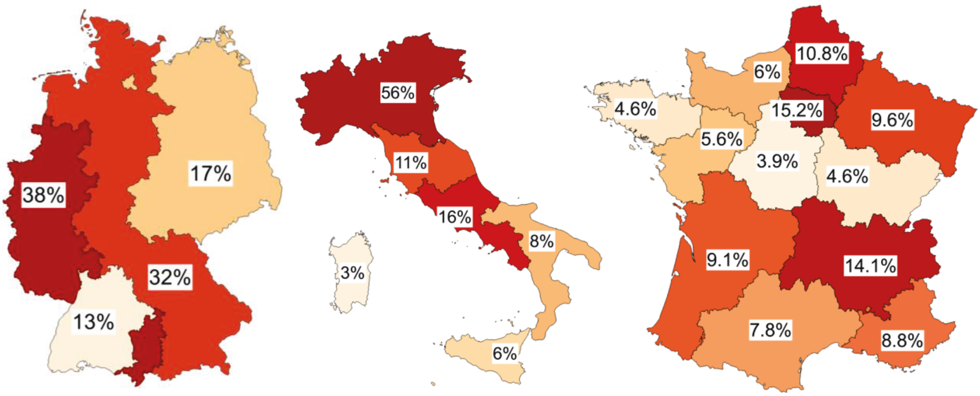

Figure 4 Spatial distribution of the annual demand according to the load profiles of the German TSOs [195], the Italian bidding zones [284] and the 12 French RTE regions [283] respectively. Own illustration.

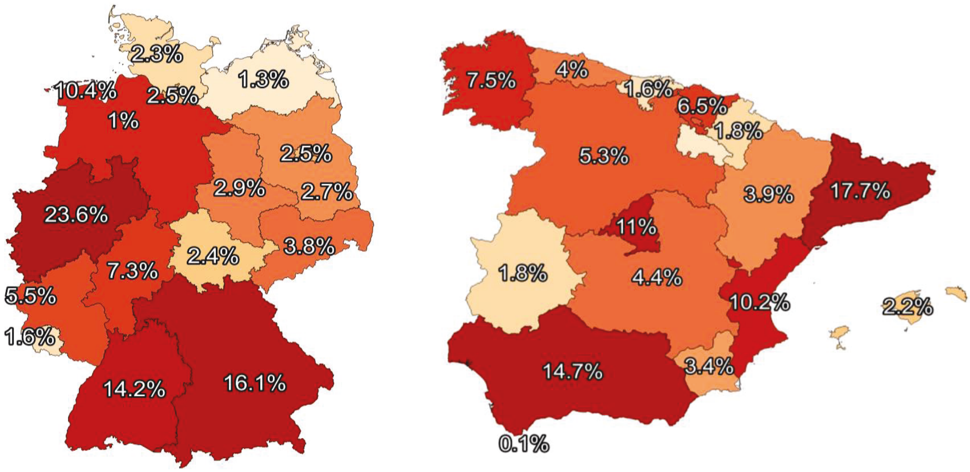

Figure 5 Spatial distribution of the annual demand for the German [206] and Spanish [325] administrative regions respectively. Own illustration.

F European verification

Figure F-1 shows the German energy mix in detail for four of the models shown in table 4-9 excluding the “grid – NTC constraints” scenario, while also including the linear OPF version of section 4.1 and the reference values from the German Federal Network Agency [210]. It can be observed that the “grid” model with historical hydro generation shows the best performance among all European models, nevertheless the “hybrid” and “two-level” models show adequate agreement as well. Moreover, it can be seen that the models with the more simplified grid representation tend to overestimate the cheap generation from coal and nuclear, which in turn result in higher exports. Except for the isolated German case however, all pan-European simulations tend to underestimate the generation from natural gas.

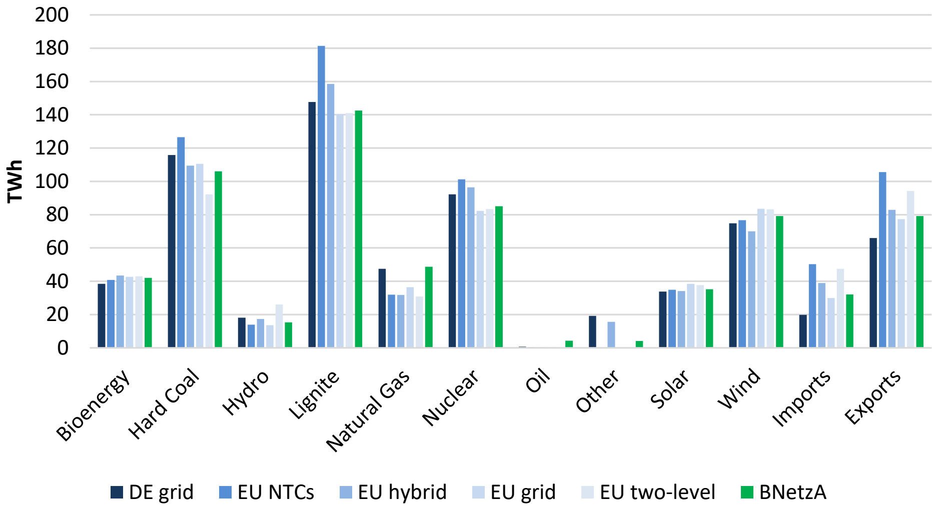

Figure F-1 The German mix for 2015 as predicted by different models as well as reported by the German Federal Network Agency [210].

The European mix is also shown in detail for the afore-mentioned scenarios, both in absolute and relative values in figures F-2 and F-3, including the values reported by ENTSOE [326] as reference case. Despite the significant differences in the grid representation between the models, no substantial difference can be observed regarding the countries’ energy mix. Thereby, a better modeling of the power plants operation or the corresponding dataset is probably required for better agreement with the reference mix. As expected from cost minimization nature of the model, generation from natural gas is systematically underestimated, although not to the same degree for all countries. Moreover, it can be observed that smaller countries are more difficult to predict, since the model becomes increasingly sensitive to the input data.

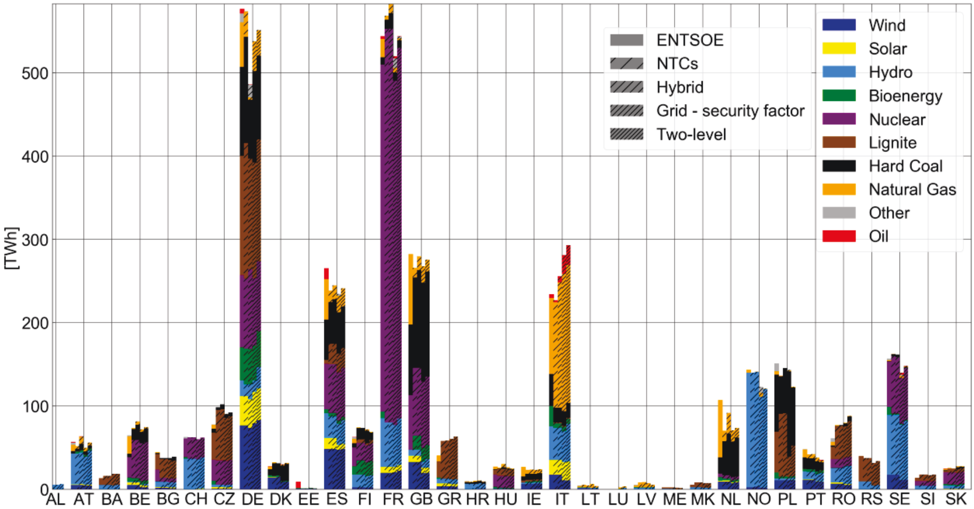

Figure F-2 European energy mix in absolute values for 2015 as predicted by different pan-European models as well as reported by ENTSO-E [326].

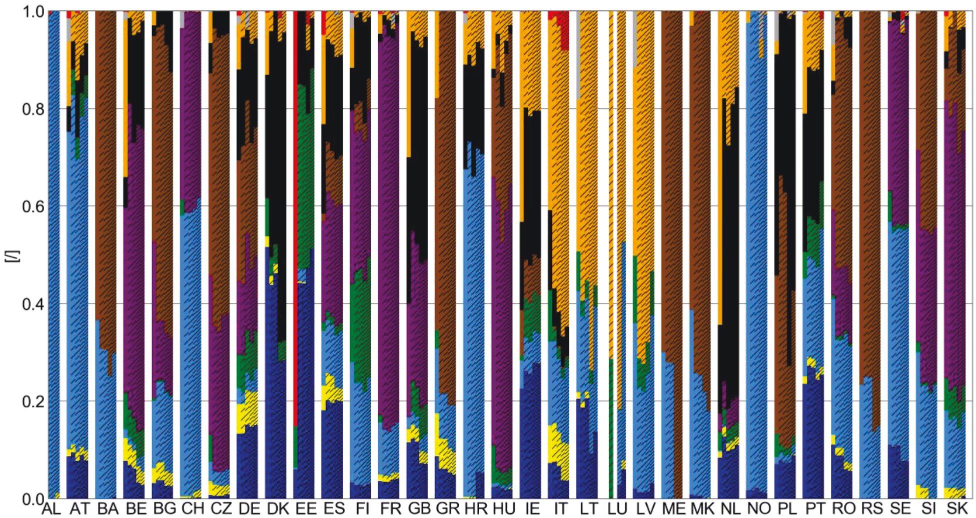

Figure F-3 European energy mix in relative values for 2015 as predicted by different pan-European models as well as reported by ENTSO-E [326].

Finally, some insightful plots for the “two-level” model, which constitutes the one used for the rest of the thesis as well, are depicted in the following figures. Figure F-4 shows the energy mix in comparison to the corresponding demand, whereas figure F-5 shows the total inter-regional flows for the same regionalization. Hence, the existing decentralization of power generation at regional level can be visualized. Moreover, figure F-6 depicts the frequency of individual line loadings beyond 70% of the corresponding, “secure” capacity, thus suggesting potential grid bottlenecks. A clearer understanding of such bottlenecks is given by figure F-7, where the average nodal prices are depicted. It can be seen that the individual countries tend to have almost uniform distributions over their territories, thus suggesting that the current market zone configuration constitutes a reasonable approximation.

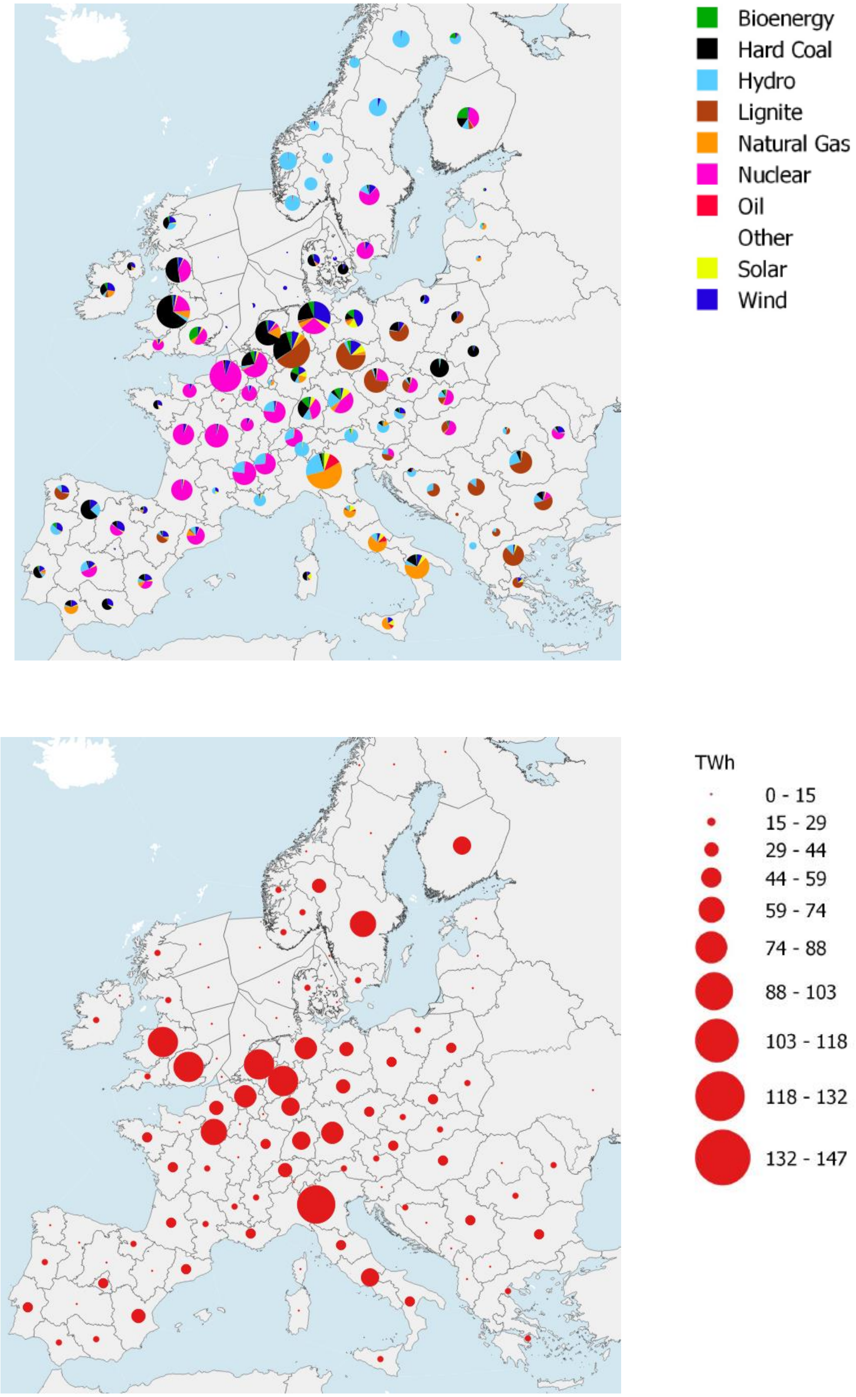

Figure F-4 Regional energy mix and electricity demand for 2015.

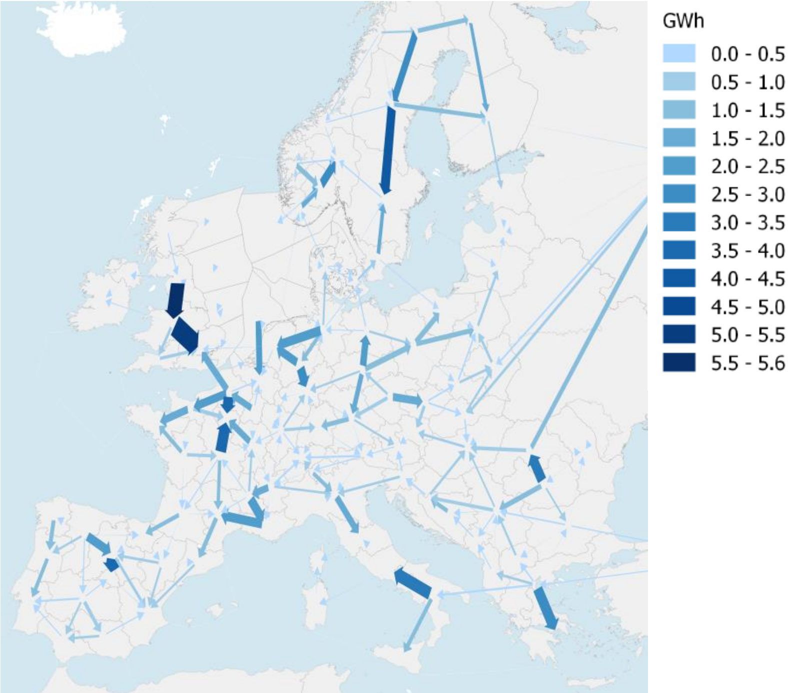

Figure F-5 Net flows over the year 2015.

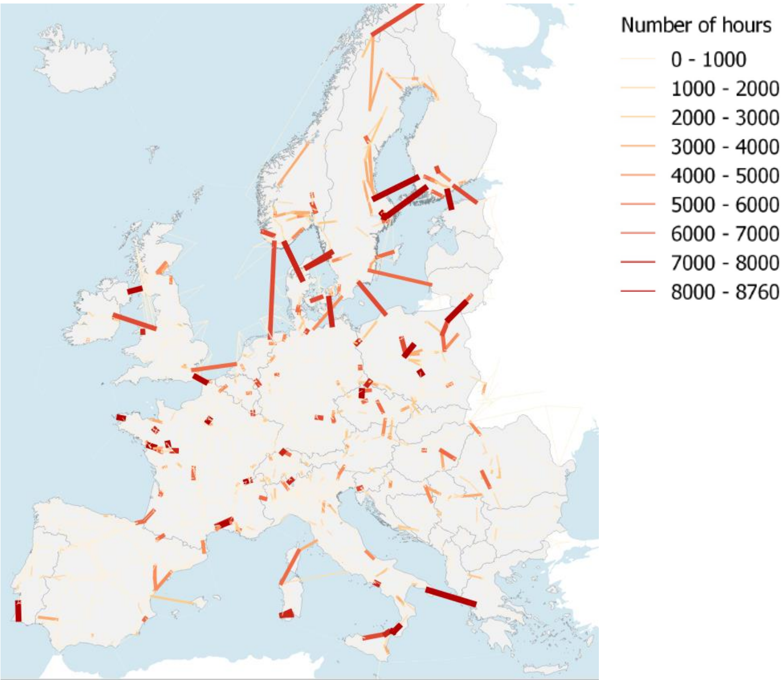

Figure F-6 Frequency of line loadings beyond 49% of their nominal capacity for 2015.

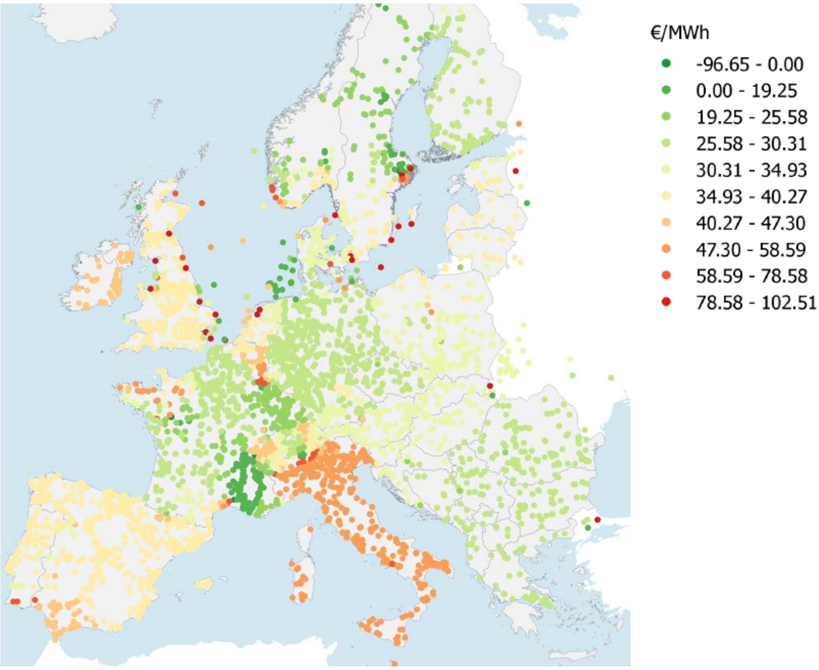

Figure F-7 Average nodal prices for 2015.

G The TYNDP and e-highway 2050 scenarios

The investigation of the future European power system follows the scenarios of 2030, 2040 and 2050 as described in chapter 5. Due to their longer horizon, the e-highway scenarios for 2040 and 2050 must consider further technological developments than the TYNDP, although all the scenarios have their origins to one of the TYNDP visions. Such developments may include the electrification of transport and heating, carbon capture and storage (CCS) technology or generation from CSP plants. A more elaborate description of each scenario's rationale is shown in table G-1, where the key characteristics for each case are highlighted.

Table G-1 Description of the e-highway 2050 scenarios [315].

Scenario name	Description
X5 – Large-scale RES	The scenario focuses on the deployment of **Large-scale RES** such as projects in the North Sea and North Africa. GDP growth is high and electrification of transport and heating is very significant. The public attitude is passive resulting in low energy efficiency and limited DSM. Thus, the **electricity demand is very high**.
X7 – 100% RES	This scenario relies only on **RES**, thus nuclear and fossil energy generation are excluded. High GDP, high electrification and high energy efficiency are assumed. **Storage technologies and DSM** are widespread.
X10 – Big & market	In this scenario, the electricity sector is assumed to be **market-driven**. A preference is thus given to centralized projects (renewable and non-renewable) and no source of energy is excluded. **CCS** is assumed to be mature. GDP growth is high. Electrification of transport and heating is significant but energy efficiency is limited.
X13 – Fossil & nuclear	In this scenario, decarbonization is achieved mainly through **nuclear and CCS**. RES plays a less significant role and centralized projects are preferred. GDP growth is high. Electrification of transport and heating is significant and energy efficiency is low.
X16 – Small & local	The *Small & local* scenario focuses on local solutions dealing with **de-centralized generation**. GDP and population growth are low. Electrification of transport and heating is limited but energy efficiency is significant, resulting in a **low electricity demand**.

In figures G-1 and G-2 all future scenarios are classified in three pathways based on the progress of deploying RES power plants, where the relative capacity mix evolution and total annual electricity demand for the investigated European region are shown correspondingly. The first category consists of the vision 1 and X13 scenarios where the demand is assumed to grow significantly and the RES share is only slightly increased. Coal plants are primarily replaced by gas plants, hence CCS technology is considered mandatory to achieve the climate targets. The second category includes the vision 2 and X10 scenarios and assumes a predominantly market-driven system evolution with a moderate increase in demand and a gradual replacement of coal plants by RES. Finally, all other scenarios fall into the renewables category where the generation mix focuses heavily on low-emission technologies, thus gradually replace all coal power plants. Nevertheless, various scenarios are investigated based on the collaboration between the European countries as well as the focus on more centralized or distributed solutions.

Moreover, tables G-2 to G-11 show the installed capacities for all investigated scenarios by country.

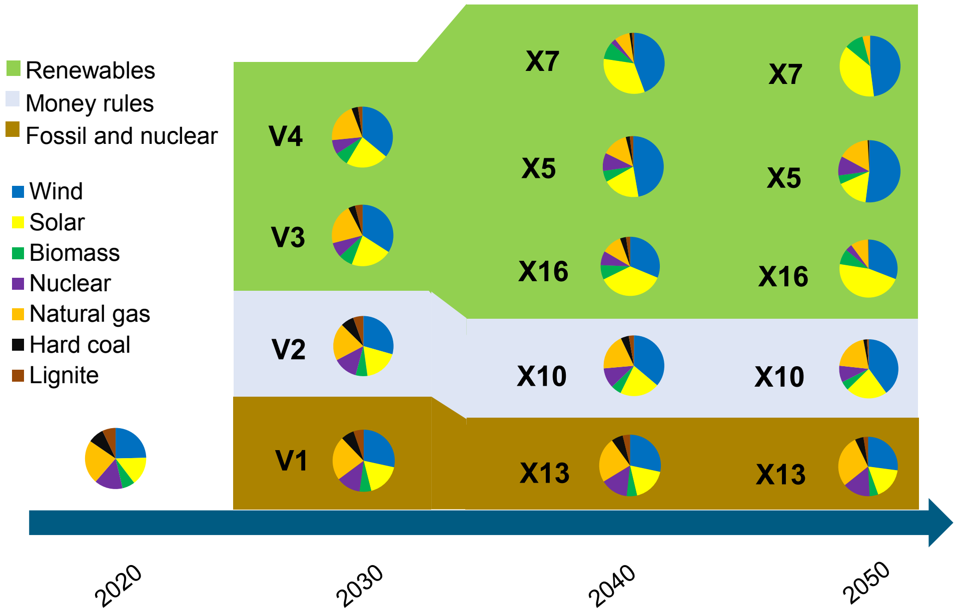

Figure G-1 Capacity mix evolution based on the selected scenarios for 2030, 2040 and 2050 excluding hydro capacity which considered constant.

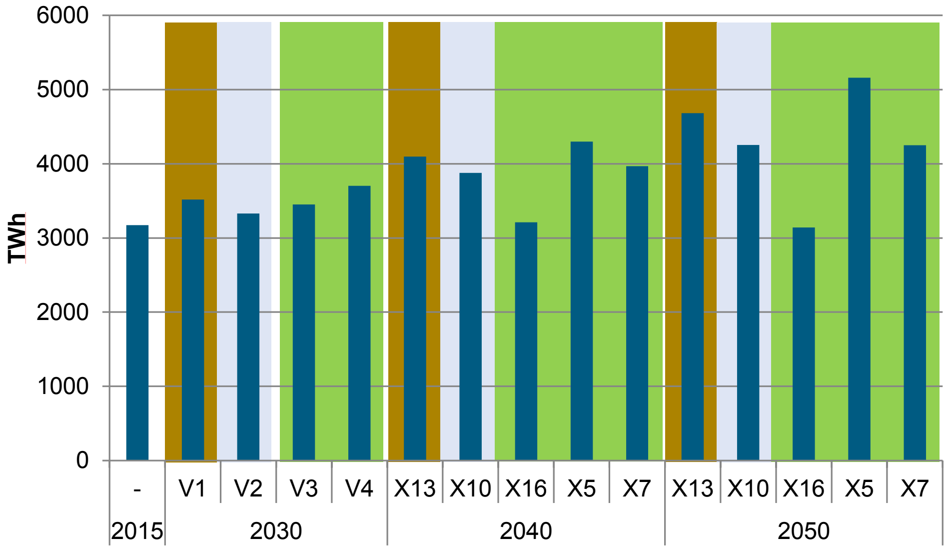

Figure G-2 Total annual electricity demand in TWh for the various future scenarios of the European power system in comparison to the historical demand of 2015.

Table G-2 Installed capacities by country for vision 1 2030 in MW.

	Bioener-gy	Natural Gas	Hard Coal	Hydro	Lignite	Nuclear	Oil	Other	Others RES	Solar	Wind
AL	0	500	0	3152	0	0	0	0	0	50	150
AT	0	4271	598	16418	0	0	196	990	800	2500	4000
BA	0	0	0	2107	2158	0	0	300	0	100	640
BE	0	7370	0	1438	0	0	0	3200	1700	4050	4900
BG	0	810	710	3150	4000	2000	0	0	0	1800	1200
CH	0	0	0	18510	0	2115	0	850	600	2550	220
CZ	0	2020	310	2170	5330	4140	0	0	1110	3690	880
DE	0	21138	23365	13257	12610	0	1026	8650	6960	57240	74050
DK	1460	2604	410	9	0	0	735	0	260	840	6190
EE	656	94	0	10	0	0	413	160	230	0	400
ES	0	24948	5900	23450	0	7120	0	10480	2400	16800	35750
FI	580	0	805	3400	0	5550	1360	1770	3760	100	2500
FR	0	6051	1740	25200	0	57644	819	5400	1400	12300	21700
GB	0	45017	2897	4754	0	4552	309	4070	5560	8470	23320
GR	0	6252	0	4259	2876	0	0	0	480	4250	6200
HR	0	1700	1200	2700	0	0	200	300	300	200	1300
HU	210	4185	0	56	470	4108	407	720	550	60	750
IE	0	3575	750	508	0	0	260	210	250	200	4420
IT	0	38974	7926	22635	0	0	1394	10160	7240	24580	13400
LT	0	740	0	1265	0	1303	0	270	310	80	650
LU	0	375	0	1344	0	0	0	90	70	150	130
LV	0	1036	0	1621	0	0	0	150	250	10	800
ME	0	0	0	1215	450	0	0	0	0	0	120
MK	0	440	530	716	410	0	0	0	30	30	150
NL	0	8757	4610	38	0	486	0	5080	300	4000	7000
NO	0	425	0	38900	0	0	0	0	0	0	2080
PL	5867	2804	5492	2426	7031	3000	0	7550	1210	1500	8900
PT	0	4156	0	7858	0	0	0	1340	720	720	5300
RO	0	4757	786	7737	4014	2630	0	0	500	2500	5000
RS	0	593	0	4308	4965	0	0	0	0	20	530
SE	0	0	0	16203	0	7992	0	470	5340	0	7840
SI	45	505	0	1929	545	696	0	120	60	290	30
SK	204	843	0	3140	223	4004	0	990	310	610	90

Table G-3 Installed capacities by country for vision 2 2030 in MW.

	Bioener-gy	Natural Gas	Hard Coal	Hydro	Lignite	Nuclear	Oil	Other	Others RES	Solar	Wind
AL	0	400	0	3152	0	0	0	0	0	0	0
AT	0	3915	598	16418	0	0	196	990	800	2000	3880
BA	0	0	0	2107	2158	0	0	300	0	0	350
BE	0	7370	0	1438	0	0	0	3200	1700	4050	4900
BG	0	760	710	3150	4000	2000	0	0	0	1250	900
CH	0	0	0	18510	0	2115	0	850	600	1750	120
CZ	0	915	310	2170	5330	4140	0	0	1110	2560	580
DE	0	15463	23365	13257	12610	0	1026	8650	6960	46860	61200
DK	1460	2604	410	9	0	0	735	0	260	840	8410
EE	656	94	0	10	0	0	413	160	230	0	400
ES	0	21572	5900	23450	0	7120	0	10480	2400	33150	27650
FI	580	0	805	3400	0	5550	1360	1770	3760	100	2500
FR	0	6051	1740	25200	0	57644	819	5400	1400	8500	13900
GB	0	37878	2897	4754	0	4552	309	4070	5560	7610	58520
GR	0	3111	0	4259	2876	0	0	0	480	4050	4880
HR	0	1200	1200	2700	0	0	200	300	300	100	700
HU	210	2980	0	56	470	4108	407	720	550	60	750
IE	0	3575	750	508	0	0	260	210	250	10	3600
IT	0	34886	7926	22635	0	0	1394	10160	7240	27140	13400
LT	0	740	0	1265	0	1303	0	270	310	70	500
LU	0	375	0	1344	0	0	0	90	70	120	90
LV	0	1036	0	1621	0	0	0	150	250	60	360
ME	0	0	0	1215	450	0	0	0	0	0	120
MK	0	440	530	716	410	0	0	0	30	30	100
NL	0	7776	4610	38	0	486	0	5080	300	5100	6160
NO	0	425	0	38900	0	0	0	0	0	0	2080
PL	5867	2804	5492	2426	7031	3000	0	7550	1210	500	6450
PT	0	3693	0	7858	0	0	0	1340	720	2010	5300
RO	0	3331	786	7737	4014	2630	0	0	500	2000	4200
RS	0	296	0	4308	4965	0	0	0	0	20	530
SE	0	0	0	16203	0	7992	0	470	5340	0	7840
SI	45	505	0	1929	545	696	0	120	60	280	40
SK	204	256	0	3140	223	4004	0	990	310	550	60

Table G-4 Installed capacities by country for vision 3 2030 in MW.

	Bioener-gy	Natural Gas	Hard Coal	Hydro	Lignite	Nuclear	Oil	Other	Others RES	Solar	Wind
AL	0	500	0	3162	0	0	0	0	0	100	200
AT	0	6030	0	18471	0	0	196	990	1200	3500	5500
BA	0	373	0	2317	2158	0	0	0	0	100	900
BE	0	6840	0	2730	0	0	0	3200	2500	5800	8500
BG	0	1500	710	3468	3300	2000	0	0	0	2300	1700
CH	0	0	0	20160	0	1145	0	990	1120	4250	370
CZ	0	1990	310	2170	5330	1880	0	0	1110	3690	880
DE	0	34429	14940	17637	10209	0	871	10630	9340	60740	10075
DK	1460	3746	410	9	0	0	735	0	260	1970	10750
EE	656	94	0	20	0	0	0	1010	300	100	650
ES	0	29208	4160	25050	0	7120	0	12210	5100	25000	39300
FI	580	970	0	4350	0	3350	2165	1390	4670	2500	5000
FR	0	14051	1740	27200	0	37646	819	5400	4800	24100	36600
GB	0	38206	0	7732	0	9022	225	4290	8740	15860	52820
GR	0	6252	0	4699	2212	0	0	0	650	5300	7800
HR	0	1700	1200	3000	0	0	200	300	300	200	1500
HU	210	4977	0	100	0	3000	407	720	1040	200	1000
IE	0	4270	0	558	0	0	260	710	1200	500	5500
IT	0	37993	7056	23535	0	0	1386	10160	10750	40400	18990
LT	0	923	0	1265	0	0	0	270	330	80	850
LU	0	375	0	1344	0	0	0	140	100	200	180
LV	0	1036	0	1621	0	0	0	150	400	20	1000
ME	0	0	0	1271	450	0	0	0	0	20	190
MK	0	720	330	716	410	0	0	0	30	40	200
NL	4610	9358	0	38	0	486	0	5080	470	15400	12700
NO	0	855	0	40800	0	0	0	0	0	0	2910
PL	5240	1911	5389	3176	6571	0	0	9860	1210	4000	11000
PT	0	3717	0	9717	0	0	0	1560	850	910	6400
RO	0	4757	786	8087	4014	2630	0	0	800	2800	5500
RS	0	593	0	4308	5659	0	0	0	0	50	1000
SE	0	950	0	16203	0	7142	660	0	5340	1000	11400
SI	45	425	0	2005	545	1796	0	130	70	310	70
SK	204	843	0	3266	223	2880	0	810	520	720	260

Table G-5 Installed capacities by country for vision 4 2030 in MW.

	Bioenergy	Natural Gas	Hard Coal	Hydro	Lig-nite	Nucle-ar	Oil	Other	Others RES	Solar	Wind
AL	0	500	0	3162	0	0	0	0	0	449	175
AT	0	6030	0	2224	0	0	196	990	1200	3000	4750
BA	0	373	0	2618	943	0	0	0	0	100	770
BE	0	6840	0	2226	0	0	0	3200	2500	4925	7518
BG	0	1500	710	3468	0	2000	0	0	0	2598	1450
CH	0	0	0	2016	0	1145	0	990	1120	3692	295
CZ	0	1990	310	2170	4424	1880	0	0	1110	3690	880
DE	0	34429	1494	1450	9026	0	871	1063	9340	5899	9696
DK	1460	3746	410	9	0	0	735	0	260	1405	1282
EE	656	94	0	20	0	0	0	1010	300	50	525
ES	0	29208	4160	2563	0	7120	0	1221	5100	5413	4060
FI	580	970	0	3400	0	3350	216	1390	4670	1300	4057
FR	0	14051	1740	2720	0	3764	819	5400	4800	1820	4485
GB	0	38206	0	5470	0	9022	225	4290	8740	1216	5949
GR	0	6252	0	4366	1070	0	0	0	650	8384	1233
HR	0	1700	1200	3200	0	0	200	300	300	929	1400
HU	210	4977	0	100	0	3000	407	720	1040	339	7114
IE	0	4270	0	558	0	0	260	710	1200	350	5090
IT	0	37993	5667	2353	0	0	138	1016	1075	4216	2345
LT	0	923	0	1265	0	0	0	270	330	80	750
LU	0	375	0	1344	0	0	0	140	100	175	155
LV	0	1036	0	1621	0	0	0	150	400	15	900
ME	0	0	0	1271	450	0	0	0	0	20	155
MK	0	720	330	716	0	0	0	0	30	736	175
NL	4610	9358	0	38	0	486	0	5080	470	9700	9995
NO	0	855	0	4870	0	0	0	0	0	0	2495
PL	5240	1911	5389	3176	6571	0	0	9860	1210	2750	9950
PT	0	3717	0	9717	0	0	0	1560	850	3280	8572
RO	0	4757	786	8100	465	2630	0	0	800	2650	9371
RS	0	593	0	4308	1609	0	0	0	0	512	765
SE	0	950	0	1620	0	7142	660	0	5340	500	9620
SI	45	425	0	2005	545	1796	0	130	70	444	931
SK	204	843	0	3266	0	2880	0	810	520	665	831

Table G-6 Installed capacities by country for scenario “Large-scale RES” 2040 in MW.

	Bioenergy	Natural Gas	Hard Coal	Hydro	Lignite	Nuclear	Solar	Wind
AL	0	0	0	3309	0	0	607	1729
AT	1250	4500	0	20246	0	0	5363	6187
BA	250	0	0	3618	800	0	511	1750
BE	3000	8500	0	2685	0	0	7111	10700
BG	1000	1000	0	7610	2400	1600	2798	3052
CH	1250	1000	0	18928	0	0	7375	876
CZ	750	1500	0	2466	3200	6400	3808	5579
DE	9000	27000	10400	14481	4800	0	57584	109714
DK	2250	2000	800	11	0	0	2288	30237
EE	500	500	0	379	0	0	254	4447
ES	5500	21500	2400	31367	0	8000	37848	53374
FI	4000	1500	800	5813	0	3200	2003	21099
FR	5750	11000	1600	33451	0	54400	28595	60409
GB	6500	26000	800	9768	0	17600	11123	88281
GR	1250	2500	0	7166	1600	0	6783	16831
HR	250	1000	800	4031	0	0	541	3878
HU	2000	2500	0	806	0	4800	1663	2945
IE	1000	4500	0	1184	0	0	379	10490
IT	7250	28000	4800	24019	0	0	36826	30141
LT	500	1000	0	1601	0	1600	304	7905
LU	250	500	0	1434	0	0	160	399
LV	750	1000	0	1626	0	0	223	7355
ME	0	0	0	2630	0	0	318	355
MK	0	500	0	1246	0	0	242	286
NL	4000	11000	800	0	0	1600	10787	18308
NO	0	500	0	71	0	0	240	8314
PL	5750	2000	2400	6,660	4000	4800	3904	36760
PT	1000	3000	0	4206	0	0	3227	8937
RO	2000	3000	800	10477	2400	3200	4102	5159
RS	250	1000	0	10890	3200	0	643	1215
SE	4000	500	0	4330	0	6400	1312	23879
SI	250	500	0	21406	0	1600	1025	271
SK	1000	1000	0	2030	0	3200	862	2478

Table G-7 Installed capacities by country for scenario “100% RES” 2040 in MW.

	Bioenergy	Natural Gas	Hard Coal	Hydro	Lignite	Nuclear	Solar	Wind
AL	0	0	0	3575	0	0	843	1738
AT	2250	3000	0	23027	0	0	7545	5815
BA	250	0	0	4029	800	0	695	1685
BE	3750	5000	0	2433	0	0	14506	10426
BG	2500	1000	0	7733	0	1600	4184	2927
CH	1250	0	0	18720	0	0	10329	841
CZ	3000	1500	0	2615	2400	0	8369	5557
DE	18500	18500	8000	14052	4800	0	78795	110348
DK	2750	2000	800	11	0	0	1722	27514
EE	1000	0	0	445	0	0	427	4336
ES	11250	14000	0	33582	0	3200	72591	56396
FI	4500	500	800	5692	0	1600	3567	16640
FR	16500	7000	1600	34569	0	19200	62552	88553
GB	10500	19500	0	9170	0	4800	36030	95036
GR	2000	3000	0	7560	800	0	12907	17571
HR	250	1000	800	4388	0	0	2471	3827
HU	4250	2500	0	885	0	1600	7672	3753
IE	1000	3000	0	1343	0	0	2093	9944
IT	12000	19500	2400	25400	0	0	75272	30435
LT	1000	500	0	1750	0	0	711	7956
LU	0	500	0	1572	0	0	603	449
LV	1000	500	0	1626	0	0	574	7355
ME	0	0	0	2816	0	0	255	340
MK	0	500	0	1329	0	0	912	275
NL	4500	6000	0	0	0	0	15974	22593
NO	250	500	0	71	0	0	2682	9753
PL	10250	1000	2400	68302	3200	0	13912	46079
PT	1750	1500	0	4522	0	0	8446	10090
RO	5000	2500	800	10974	800	1600	7156	5864
RS	500	500	0	11024	2400	0	2855	1101
SE	5500	500	800	4576	0	3200	4709	18951
SI	500	0	0	24181	800	1600	1496	436
SK	1750	500	0	2056	0	1600	3772	2855

Table G-8 Installed capacities by country for scenario “Small & local” 2040 in MW.

	Bioenergy	Natural Gas	Hard Coal	Hydro	Lignite	Nuclear	Solar	Wind
AL	0	500	0	1532	0	0	1680	378
AT	1000	2000	0	16425	0	0	2414	3229
BA	0	500	0	1864	800	0	508	735
BE	4000	5000	0	1553	0	0	12551	9002
BG	1250	500	0	3789	2400	1600	2527	1835
CH	1250	0	0	17679	0	0	8519	751
CZ	1250	2000	0	2110	2400	4800	3515	1864
DE	11000	13000	12800	11531	6400	0	78068	76794
DK	1750	1500	800	7	0	0	455	7509
EE	750	500	0	260	0	0	725	1231
ES	6250	13500	3200	23464	0	4800	54530	36511
FI	3750	0	800	4921	0	6400	55	2500
FR	8500	5500	1600	28311	0	36800	42799	33949
GB	5500	23000	1600	6080	0	8000	25478	46647
GR	1500	4000	0	3880	1600	0	6232	6822
HR	250	500	800	2896	0	0	2093	1371
HU	2500	2500	0	346	0	3200	2019	2642
IE	500	2500	800	942	0	0	2045	6157
IT	7500	17000	4000	21021	0	0	73094	26215
LT	500	500	0	1326	0	1600	1514	1884
LU	500	500	0	1268	0	0	512	315
LV	750	1000	0	1540	0	0	1541	1635
ME	0	0	0	956	0	0	194	152
MK	250	500	0	566	0	0	1234	236
NL	2250	6000	2400	0	0	1600	18332	11130
NO	250	0	0	28	0	0	0	2807
PL	7000	2000	3200	47931	4000	1600	10030	10624
PT	1000	2500	0	2683	0	0	6014	6143
RO	1500	2000	800	7506	2400	1600	1511	4468
RS	500	1000	0	6906	3200	0	2020	980
SE	5500	0	0	3567	0	4800	2111	7426
SI	250	500	0	18066	0	0	1604	162
SK	1000	500	0	1528	0	1600	1907	1089

Table G-9 Installed capacities by country for scenario “Large-scale RES” 2050 in MW.

	Bioenergy	Natural Gas	Hard Coal	Hydro	Lignite	Nuclear	Solar	Wind
AL	0	0	0	3994	0	0	850	2421
AT	1250	5250	0	22021	0	0	7226	6875
BA	250	0	0	4919	0	0	921	2599
BE	3500	18500	0	2640	0	0	8421	12901
BG	1750	1500	0	11752	800	1600	3296	4403
CH	1250	3500	0	17696	0	0	10500	1382
CZ	500	3000	0	2763	800	11200	3925	10279
DE	9000	41000	4000	14899	0	0	54428	118677
DK	3000	2250	0	13	0	0	2606	49723
EE	250	1000	0	738	0	0	409	8244
ES	6000	31000	800	37683	0	8000	50822	67448
FI	3000	3000	0	7475	0	3200	1505	37198
FR	6750	16500	800	39703	0	72000	33090	84219
GB	4500	32750	800	11805	0	25600	6386	123741
GR	1500	1000	0	9633	0	0	8266	25861
HR	250	1000	0	5062	0	0	882	6255
HU	2500	2000	0	1512	0	6400	3127	4889
IE	500	6250	0	1811	0	0	258	15479
IT	5500	39500	2400	24503	0	0	30252	41293
LT	750	2500	0	1938	0	1600	529	14959
LU	250	1000	0	1525	0	0	121	617
LV	750	1000	0	1631	0	0	425	13709
ME	0	0	0	3988	0	0	616	520
MK	0	500	0	1776	0	0	443	371
NL	3000	22500	800	0	0	1600	6173	23916
NO	250	500	0	104	0	0	480	13718
PL	4750	5000	0	80519	800	9600	3807	62521
PT	1000	4750	0	5237	0	0	5544	11474
RO	3250	3500	0	11237	800	4800	5404	4818
RS	250	2000	0	13693	800	0	1235	1429
SE	3000	500	0	4351	0	6400	1624	36358
SI	250	500	0	26608	0	2000	1739	472
SK	1000	1000	0	2055	0	3200	1004	4697

Table G-10 Installed capacities by country for scenario “100% RES” 2050 in MW.

	Bioenergy	Natural Gas	Hard Coal	Hydro	Lignite	Nuclear	Solar	Wind
AL	0	0	0	4367	0	0	1181	2433
AT	3500	1500	0	23810	0	0	12090	6880
BA	250	0	0	5440	0	0	1291	2599
BE	4750	2500	0	2640	0	0	24087	13903
BG	4750	0	0	11999	0	0	5395	4403
CH	1250	2000	0	17696	0	0	15000	1382
CZ	5000	1750	0	3061	0	0	13048	10234
DE	27750	13000	0	17032	0	0	98599	125526
DK	3750	1000	0	13	0	0	2038	44308
EE	1000	250	0	870	0	0	803	8141
ES	17250	8500	0	41529	0	0	102523	69383
FI	3750	1250	0	7985	0	0	5835	29531
FR	28250	16000	0	41939	0	0	106905	124197
GB	12500	6500	0	12871	0	0	59896	130312
GR	3750	0	0	10753	0	0	15068	25851
HR	0	0	0	5576	0	0	3782	6254
HU	7250	0	0	1670	0	0	13997	4897
IE	250	2000	0	2128	0	0	3836	13628
IT	14750	9000	0	27265	0	0	101044	41290
LT	1750	500	0	2235	0	0	1343	15163
LU	0	250	0	1800	0	0	1030	739
LV	1750	500	0	1631	0	0	1133	13811
ME	0	0	0	4360	0	0	490	520
MK	0	0	0	1942	0	0	1374	371
NL	4000	3000	0	0	0	0	22247	30897
NO	500	0	0	104	0	0	5364	15175
PL	14250	3000	0	87905	0	0	24220	81918
PT	2750	0	0	5869	0	0	13805	11861
RO	9250	0	0	12232	0	0	10980	4828
RS	1000	0	0	13949	0	0	4986	1431
SE	5500	0	0	4844	0	0	8919	27211
SI	750	250	0	32158	0	0	2332	472
SK	2750	500	0	2107	0	0	6880	5230

Table G-11 Installed capacities by country for scenario “Small & local” 2050 in MW

	Bioenergy	Natural Gas	Hard Coal	Hydro	Lignite	Nuclear	Solar	Wind
AL	0	1000	0	1507	0	0	2351	529
AT	1250	1000	0	16433	0	0	2827	2578
BA	0	750	0	1622	0	0	1016	1121
BE	6500	6500	0	1667	0	0	21052	13105
BG	2250	0	0	4428	0	0	3805	2771
CH	1500	250	0	16849	0	0	15000	1381
CZ	1750	5000	0	2049	0	4800	4469	3147
DE	15000	16000	1600	12261	0	0	109275	93019
DK	2500	1000	0	4	0	0	69	6668
EE	500	1000	0	511	0	0	1449	2063
ES	9750	16000	0	23478	0	3200	87300	39141
FI	3000	250	0	6443	0	6400	10	2500
FR	16000	10500	0	31422	0	14400	77098	53678
GB	5500	17000	0	7406	0	11200	43347	41935
GR	2250	7000	0	3502	0	0	8414	9085
HR	250	500	0	3091	0	0	4085	2042
HU	4000	3500	0	636	0	1600	3979	4534
IE	500	4000	0	1377	0	0	4080	6635
IT	7750	8500	0	19408	0	0	108833	39031
LT	750	1000	0	1386	0	1600	2959	3267
LU	500	1000	0	1192	0	0	904	540
LV	1250	2500	0	1460	0	0	3071	2910
ME	0	0	0	697	0	0	388	183
MK	250	500	0	415	0	0	2438	372
NL	4500	7000	0	0	0	1600	31565	14731
NO	500	0	0	18	0	0	0	3535
PL	7000	2500	0	56962	0	1600	19561	14798
PT	1500	3000	0	2939	0	0	9098	6875
RO	3000	3000	0	7154	0	1600	1022	4737
RS	750	3000	0	6074	800	0	4021	1430
SE	5500	0	0	2827	0	0	4222	7013
SI	500	500	0	19928	0	0	2928	283
SK	1500	500	0	1126	0	0	3263	2118

In section 5.3 the spatial distribution of the generation capacity for the years 2030, 2040 and 2050 is described. Regarding the conventional power plants, figure G-3 depicts the dataset that is used for the pan-European model verification in section 4.2 that also forms the basis for the corresponding power plant dataset of the future scenarios. Figures G-4, G-5 and G-6 show conventional power plants for each scenario of the years 2030, 2040 and 2050, where all figures refer to the legend of figure G-3. It can be observed that significant disparities in the generation capacity mix exist among the different scenarios of the same year.

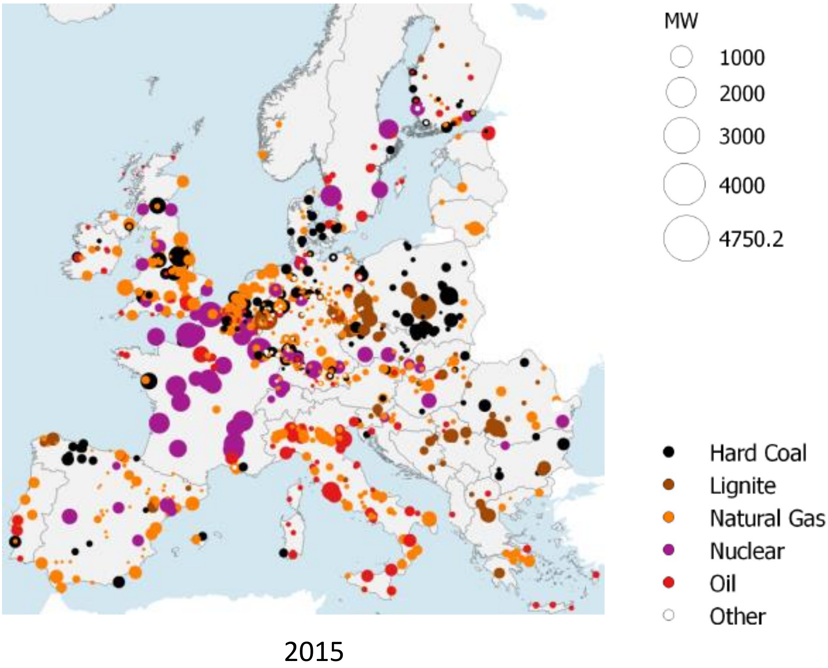

Figure G-3 Conventional power plants for the year 2015 classified by fuel type.

.

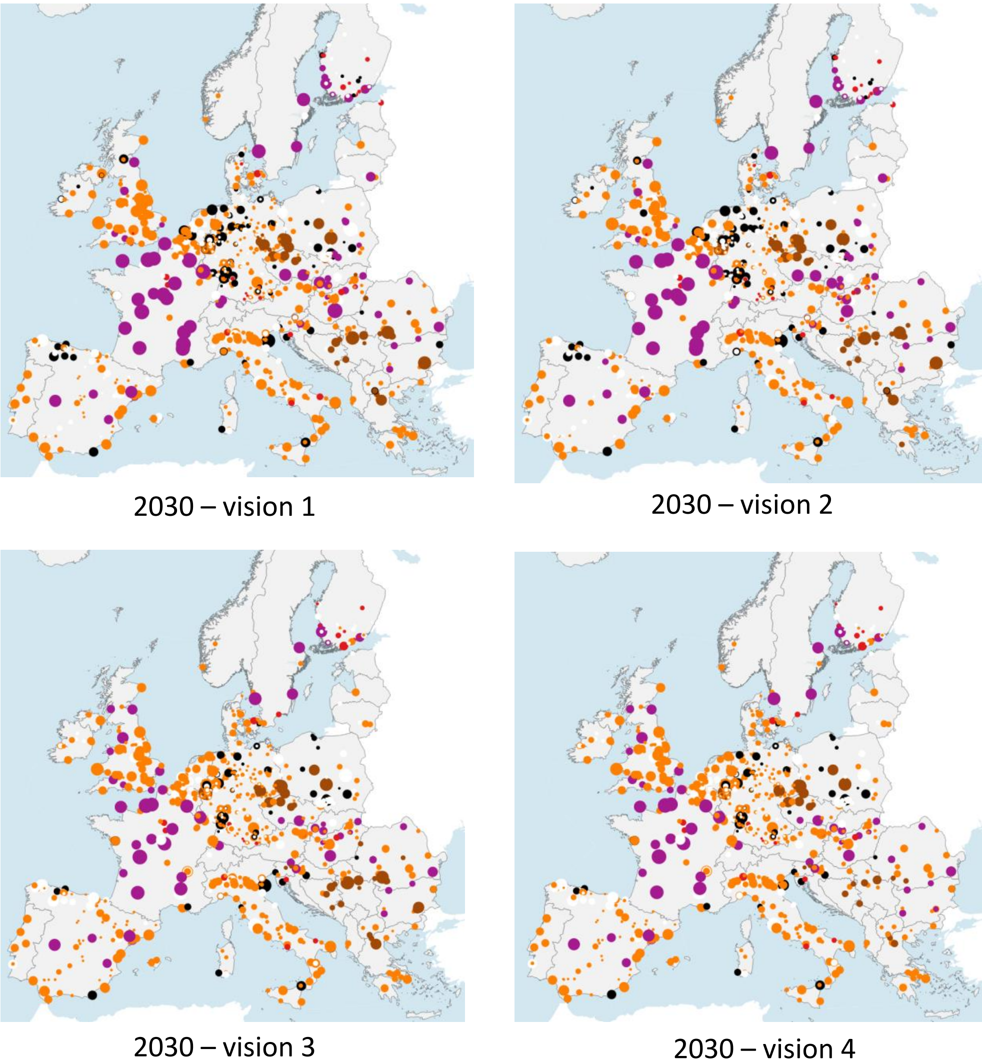

Figure G-4 Projection of the European conventional power plants for the year 2030 following the targets of the 4 TYNDP visions.

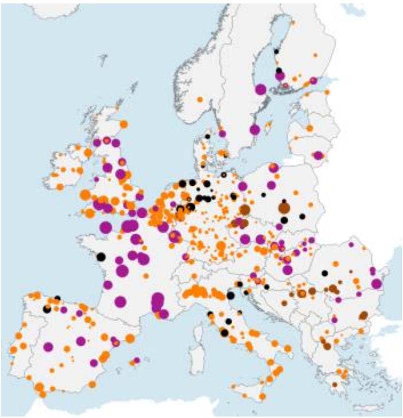

2040 – Large-scale RES

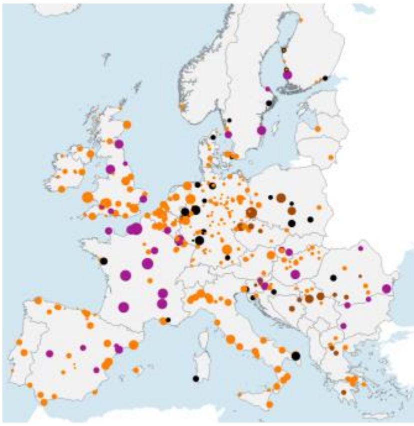

2040 – 100% RES

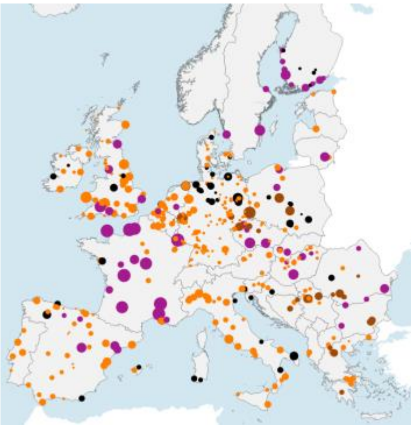

2040 – Small & Local

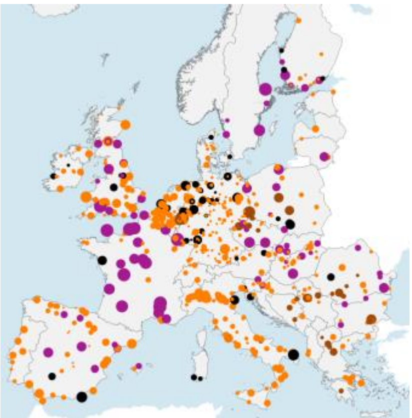

2040 – Big & Market

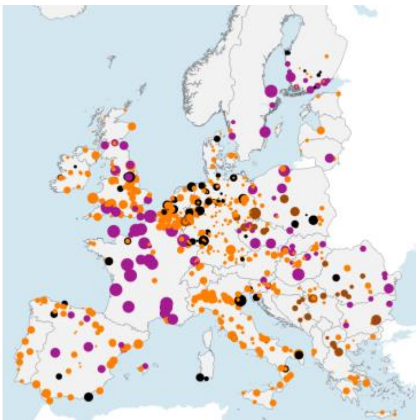

2040 – Fossil & Nuclear

Figure G-5 Projection of the European conventional power plants for the year 2040 following the targets of the 5 e-highway scenarios.

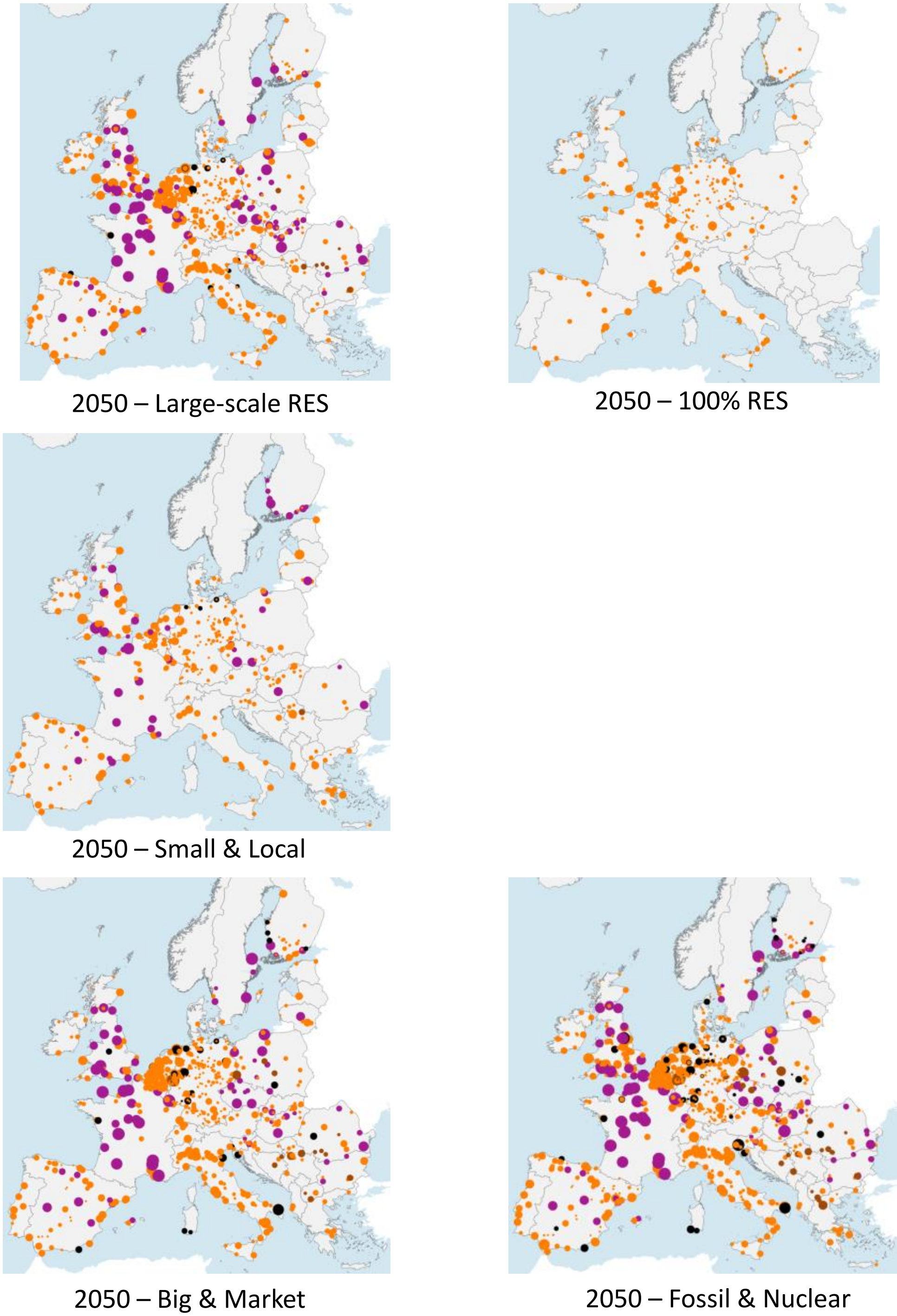

Figure G-6 Projection of the European conventional power plants for the year 2050 following the targets of the 5 e-highway scenarios.

Similarly to the conventional power plants, the generation from wind and solar energy is also depicted in order to provide a better intuition of the system conditions. Figure G-7 illustrates the total available wind energy and figure G-11 the total available solar energy per transmission grid node as modeled in section 4.2. Furthermore, figures G-8, G-9 and G-10 depict the available wind energy and figures G-12, G-13 and G-14 the available solar energy per transmission grid for the years 2030, 2040 and 2050 correspondingly, including all relative scenarios. Showing the available energy instead of merely the installed capacity provides a better insight regarding the operating conditions of the systems, since different locations may have different average capacity factors. Moreover, the values are shown at the transmission grid node level which may highlight regions with sparser grid nodes, e.g. the offshore or northern Africa regions that are merely represented by a single node with regard to allocating generation. Nevertheless the selected depiction serves the better reflection of the operational conditions for each power system scenario.

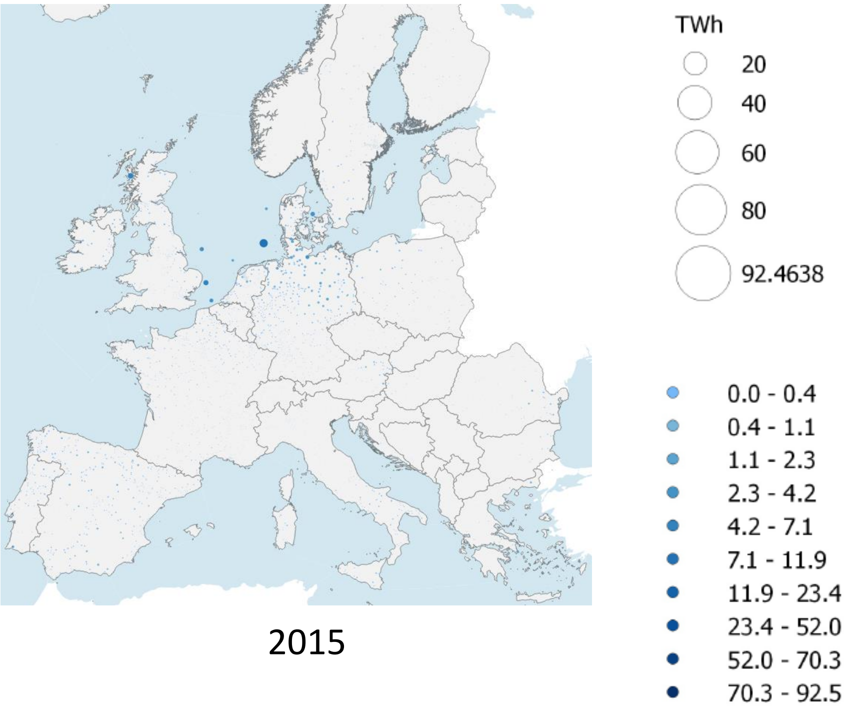

Figure G-7 Total available wind energy per transmission grid node for the year 2015 and wind year 2015.

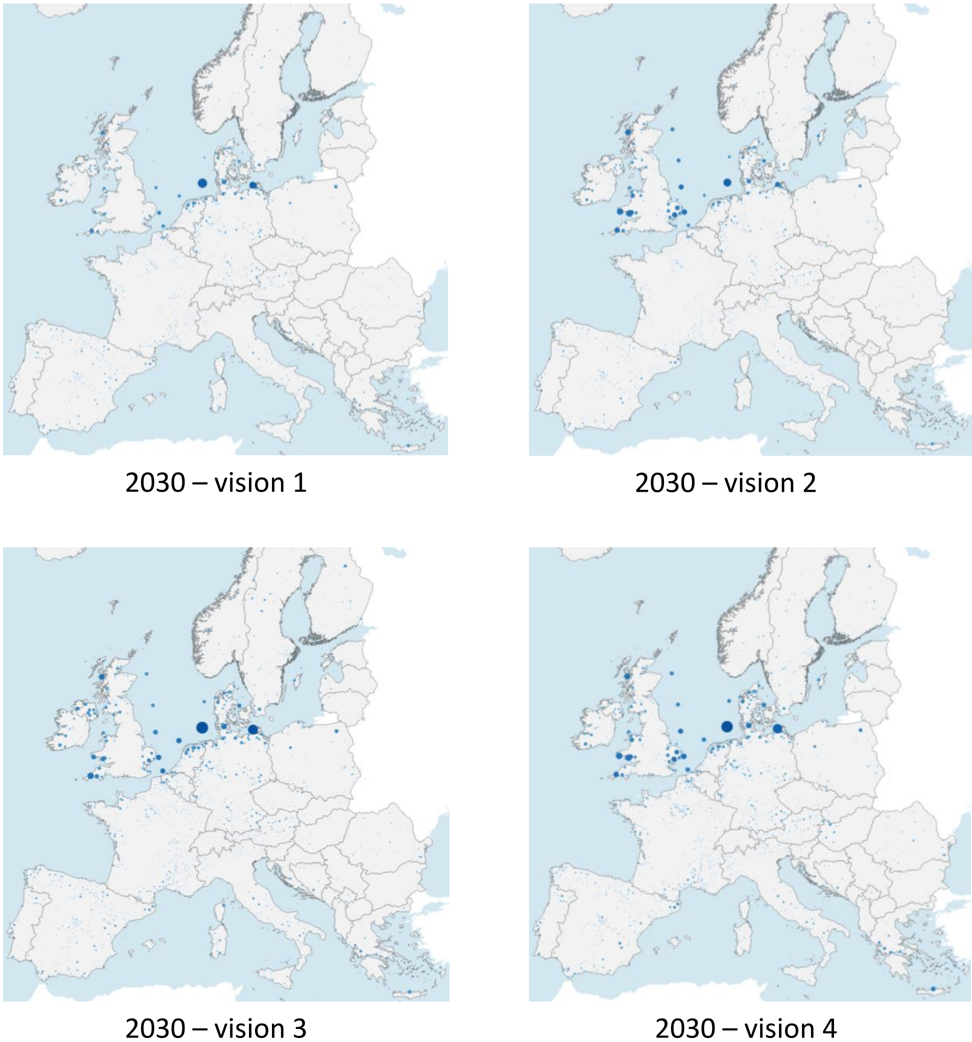

Figure G-8 Total available wind energy per transmission grid node for the 4 visions of the 2030 system and wind year 2011.

2040 – Large-scale RES

2040 – 100% RES

2040 – Small & Local

2040 – Big & Market

2040 – Fossil & Nuclear

Figure G-9 Total available wind energy per transmission grid node for the 5 scenarios of the 2040 system and wind year 2011.

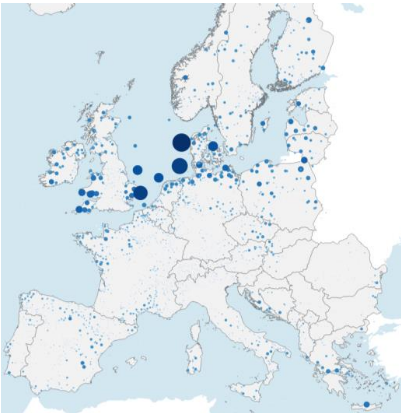

2050 – Large-scale RES

2050 – 100% RES

2050 – Small & Local

2050 – Big & Market

2050 – Fossil & Nuclear

Figure G-10 Total available wind energy per transmission grid node for the 5 scenarios of the 2050 system and wind year 2011.

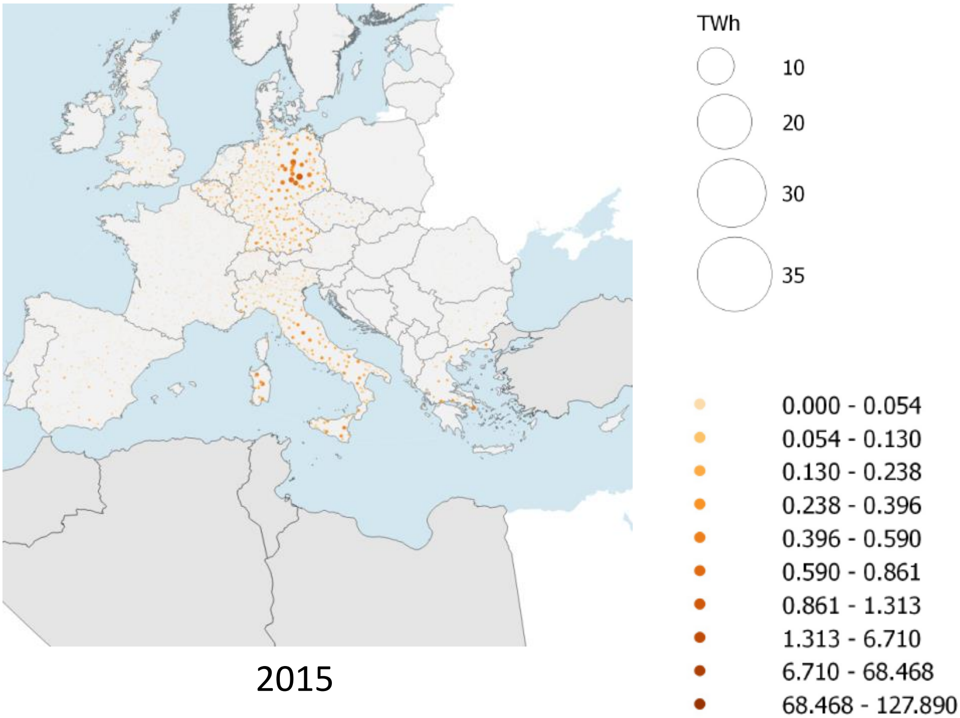

Figure G-11 Total available solar energy per transmission grid node for the year 2015 and solar year 2015.

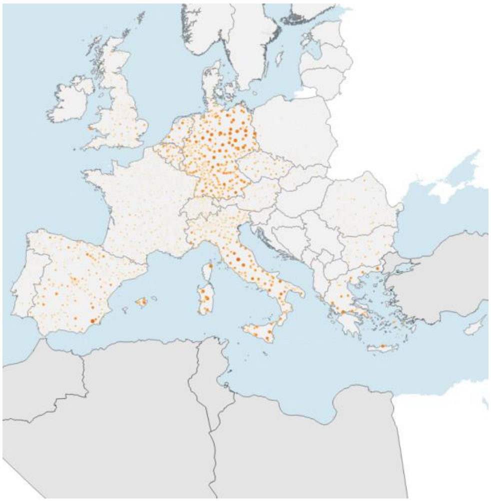

2030 – vision 1

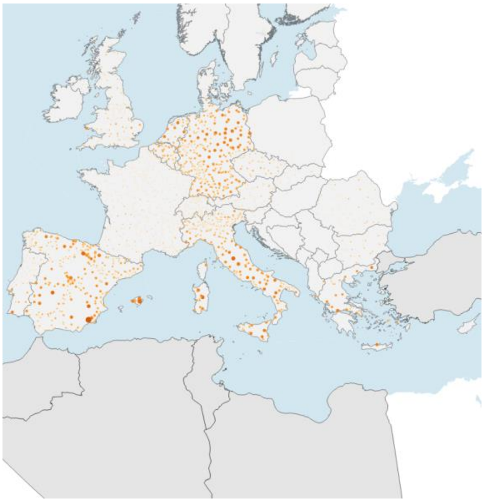

2030 – vision 2

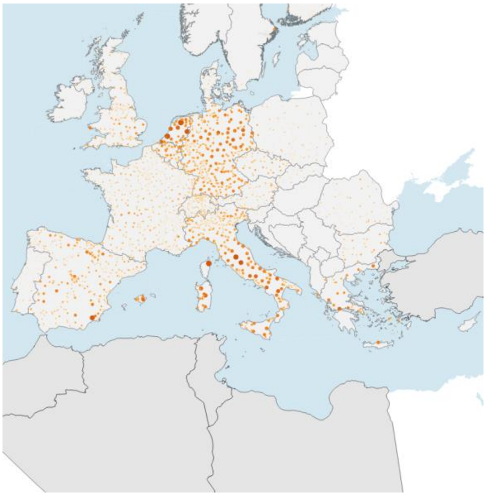

2030 – vision 3

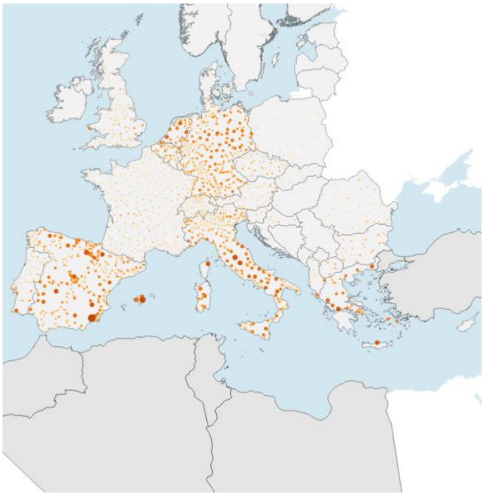

2030 – vision 4

Figure G-12 Total available solar energy per transmission grid node for the 4 visions of the 2030 system and solar year 2011.

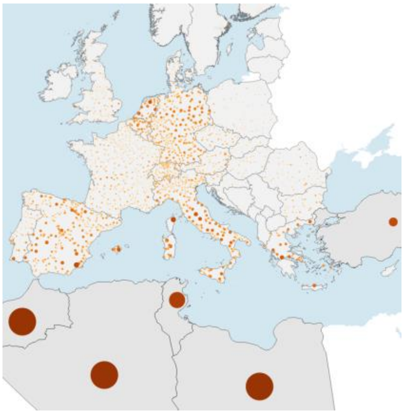

2040 – Large-scale RES

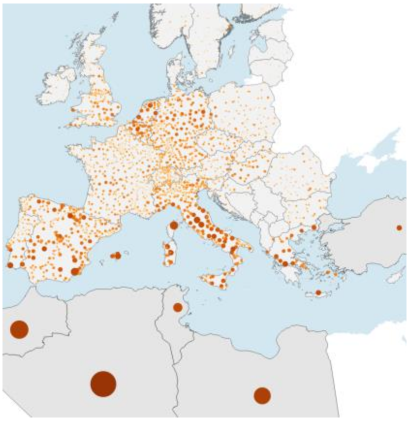

2040 – 100% RES

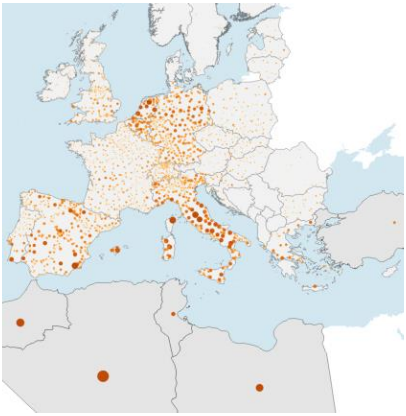

2040 – Small & Local

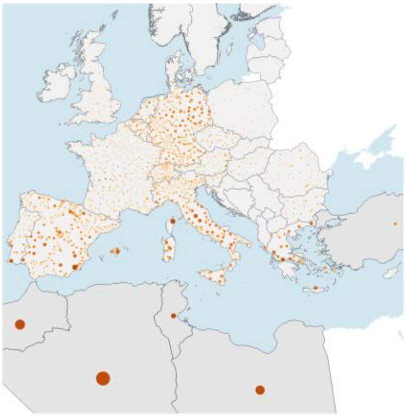

2040 – Big & Market

2040 – Fossil & Nuclear

Figure G-13 Total available solar energy per transmission grid node for the 5 scenarios of the 2040 system and solar year 2011.

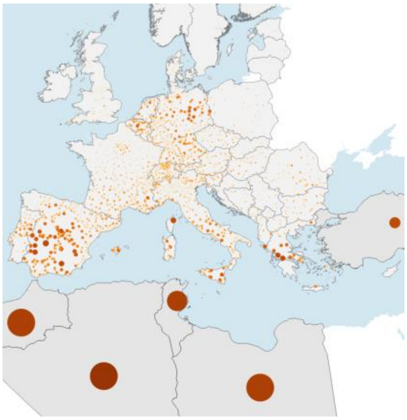

2050 – Large-scale RES

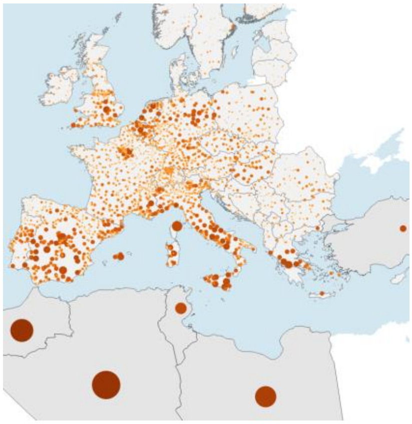

2050 – 100% RES

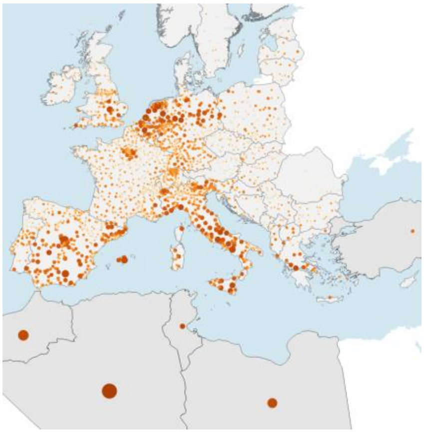

2050 – Small & Local

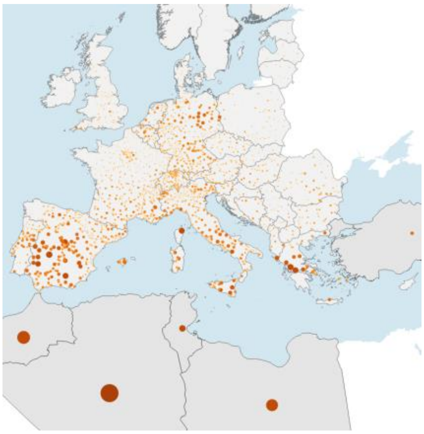

2050 – Big & Market

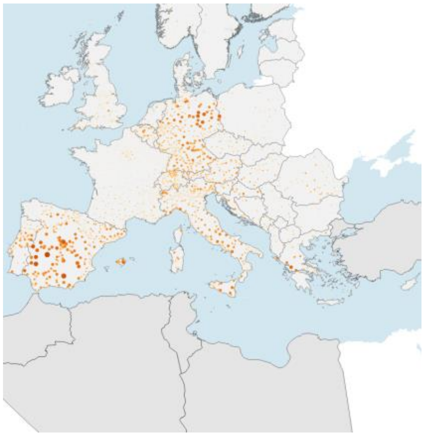

2050 – Fossil & Nuclear

Figure G-14 Total available solar energy per transmission grid node for the 5 scenarios of the 2050 system and solar year 2011.

H The market value factor of wind

One of the advantages of the "grid" modeling level consists of its high spatial resolution which allows the estimation of the market value of VRES generation assets including transmission grid constraints. The market value metric, expressed as the relative price of a source with respect to the base market price, measures the impact of the variability of a source in comparison to an equivalent source with a flat profile. Unlike other metrics, the market value also considers the effects of the whole system operation. As described by Hirth [327], two opposing forces influence this value, namely correlation with demand and the merit-order effect. The first force can be observed at low penetration rates, where the source cannot significantly influence the outcome of the market itself and therefore the corresponding generation can benefit from supply shortages. However, as the share in the market increases, the clearing price may reduce significantly due to the low variable operational costs of VRES, hence reducing the profits of the corresponding source as well.

For a single market zone, the market value of the variable source, e.g. wind, can be derived by eq. (H-3), where $\bar{p}$ corresponds to the average base price and $\bar{p}^w$ to the average revenue of wind power, both measured in $^{€}/_{MWh}$. The extension of this formulation to include the spatial dimension is further introduced by Hirth [327] and expressed by eq. (H-4) and (H-5), where however the spatial averaging is introduced in eq. (H-5) instead of (H-4) as proposed by the author. The market value can be expressed again by eq. (H-3).

$$\bar{p} = \frac{\boldsymbol{p}'\boldsymbol{t}}{\boldsymbol{t}'\boldsymbol{t}} \tag{H-1}$$

$$\bar{p}^w = \frac{\boldsymbol{p}'\boldsymbol{g}}{\boldsymbol{g}'\boldsymbol{t}} \tag{H-2}$$

$$v^w = \frac{\bar{p}^w}{\bar{p}} \tag{H-3}$$

$$\bar{p} = \frac{(\boldsymbol{P}\boldsymbol{d})'\boldsymbol{t}}{\boldsymbol{t}'\boldsymbol{t}} \tag{H-4}$$

$$\bar{p}^w = \frac{[(\boldsymbol{P}'\boldsymbol{G})\boldsymbol{n}]'\boldsymbol{n}}{(\boldsymbol{G}\boldsymbol{n})'\boldsymbol{t}(\boldsymbol{n}'\boldsymbol{n})} \tag{H-5}$$

where $\boldsymbol{p}'$ is the vector of zonal prices

$\boldsymbol{g}$ is the vector of wind generation

$\boldsymbol{d}$ is the vector of demand weights on the system's nodes

$\boldsymbol{P}$ is the matrix of nodal prices

$\boldsymbol{G}$ is the matrix of wind generation for each system's node

$\boldsymbol{t}$ and $\boldsymbol{n}$ are unit vectors referring to the temporal and nodal size of the investigated system correspondingly

Figure H-1 shows the market value of wind for all countries with both of the described formulations as well as for the investigated European area as a whole. By the term zonal, the corresponding results refer to the "country" modeling level partitioning, i.e. each country is considered as a single zone, whereas by nodal the results refer to the “grid” level where the whole transmission grid is considered. Regarding Europe as a whole, it can be seen that the difference in the market value is only marginal despite the difference in the operation of hydro plants. Similarly, each country is evaluated with both the zonal and nodal formulations. Although for many countries analogous conclusions can be drawn as well, a few countries experience a significant increase in the market value of wind when the transmission grid is considered. This behavior can be attributed to internal grid congestion that may prohibit importing cheaper generation from neighboring nodes, thus increasing local prices and the revenues of the corresponding wind turbines. In principle, if zonal prices are used in eq. (H-5) instead of nodal prices, hence disregarding grid constraints, wind generation located in rich wind areas is benefited, whereas in poor wind regions the corresponding revenues are reduced. This behavior is further supported by the local merit-order effect that may limit the revenue of generation in rich wind areas when nodal prices are considered. From figure H-1 it can further be observed that countries with high shares of wind generation show the lowest market values due to this merit-order effect.

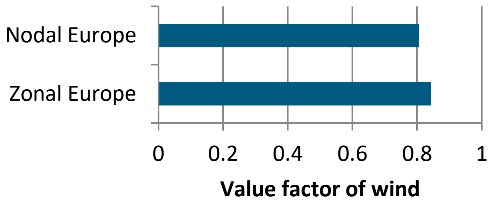

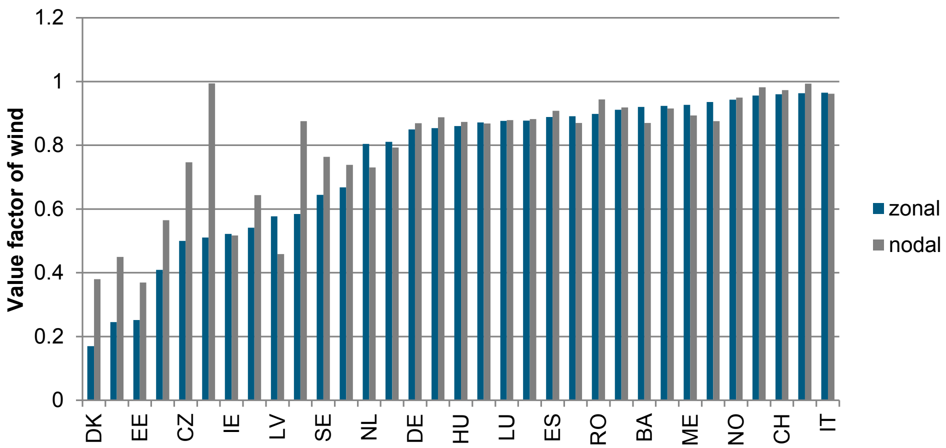

Figure H-1 Market value factor of wind for the 2050 “Large scale RES” scenario and 2011 weather year. On the top picture the values correspond to all of Europe, where zonal considers each country as copper plate whereas nodal considers the whole European transmission grid. On the bottom picture each country is evaluated separately, where zonal refers to copper plate conditions and nodal considers any transmission grid constraints.

I Figures

J Tables

K Abbreviations

4MMC	4M Market Coupling
AAC	Already Allocated Capacity
AC	Alternating Current
ACCC	Aluminum Conductors Composite Core
ACER	Agency for the Cooperation of Energy Regulators
ACOPF	Alternating Current Optimal Power Flow
ACSR	Aluminum Conductor Steel Reinforced
ATC	Available Transfer Capacity
AVR	Automatic Voltage Regulator
BEV	Battery Electric Vehicle
BNetzA	Bundesnetzagentur (Federal Network Agency)
CARMA	Carbon Monitoring for Action
CB	Critical Branches
CBA	Cost-Benefit Analysis
CCGT	Closed or Combined Cycle Gas Turbine
CHP	Cogeneration or Combined Heat and Power
CM	Congestion Management
CO	Critical Outages
CPF	Continuation Power Flow
CSP	Concentrated Solar Power
CWE	Central Western European area
DC	Direct Current
DCOPF	Direct Current Optimal Power Flow
DSM	Demand Side Management
ED	Economic Dispatch
EEA	European Environmental Agency
EEG	Erneuerbare Energien Gesetz (Renewable Energy Act)
ENS	Energy Not Served
ENTSOE	European Network of Transmission System Operators for Electricity
ENTSOG	European Network of Transmission System Operators for Gas
ETS	Emission Trading System

EU	European Union
EV	Electric Vehicle
FACTS	Flexible AC Transmission Systems
FMBC	Flow Based Market Coupling
FPSB	First-Price Sealed Bid
FRM	Flow Reliability Margin
GA	Genetic Algorithm
GDP	Gross Domestic Product
GEO	Global Energy Observatory
GEP	Generation Expansion Planning
GHG	Greenhouse Gas
GRDC	Global Runoff Data Center
GSK	Generation Shift Key
GVA	Gross Value Added
HTLS	High Temperature Low Sag
HV	High Voltage
HVDC	High Voltage DC
IAEA	International Atomic Energy Agency
IFMBC	Intuitive Flow Based Market Coupling
ISO	Independent System Operator
LMP	Locational Marginal Price
LODF	Line Outage Distribution Factor
LOPF	Linear Optimal Power Flow
LP	Linear Programming
MILP	Mixed Integer Linear Programming
MPI	Message Passing Interface
MRC	Multi-Regional Coupling
NEP	Netzentwicklungsplan (Network Development Plan)
NGO	Non-Governmental Organization
NTC	Net Transfer Capacity
NUTS	Nomenclature des Unités Territoriales Statistiques (Classification of Territorial Units for Statistics)
O&M	Operation & Maintenance

OCGT	Open Cycle Gas Turbine
OLTC	On-Load Tap Changer
OPF	Optimal Power Flow
OPSD	Open Power System Data
OSM	Open Street Map
OTC	Over The Counter
PCI	Projects of Common Interest
PCR	Price Coupling of Regions
PDF	Probability Density Function
PHS	Pumped Hydro Storage
POPF	Probabilistic Optimal Power Flow
PPM	Powerplantmatching
PSO	Particle Swarm Optimization
PTDF	Power Transfer Distribution Factor
PV	Photovoltaics
PX	Power Exchange
PyPSA	Python for Power System Analysis
RAM	Remaining Available Margin
RCM	Regional Climate Model
RES	Renewable Energy Sources
RMSE	Root Mean Square Error
ROR	Run Of River
RPF	Repeated Power Flow
SCOPF	Security Constraint Optimal Power Flow
ST	Steam Turbine
TEP	Transmission Expansion Planning
TRL	Technology Readiness Level
TRM	Transmission Reliability Margin
TSO	Transmission System Operator
TTC	Total Transfer Capacity
TUT	Transmission Usage Tariff
TYNDP	Ten Year Network Development Plant

UBA	Umweltbundesamt (Federal Environmental Office)
UC	Unit Commitment
UCTE	Union for the Co-ordination of the Transmission of Electricity
VDE	Verband der Elektrotechnik, Elektronik und Informationstechnik
VRES	Variable Renewable Energy Sources
VS	Virtual Storage
WGS	World Geodetic System
WRI	World Resources Institute

L References

[1] European Environment Agency (EEA). (2018). *GHG emissions by sector in the EU-28, 1990-2016*. Available: https://www.eea.europa.eu/data-and-maps/daviz/ghg-emissions-by-sector-in#tab-chart_1

[2] K. Syranidis, M. Robinius, and D. Stolten, "Control techniques and the modeling of electrical power flow across transmission networks," *Renewable and Sustainable Energy Reviews,* vol. 82, pp. 3452-3467, 2018/02/01/ 2018.

[3] F. D. Galiana, F. Bouffard, J. M. Arroyo, and J. F. Restrepo, "Scheduling and Pricing of Coupled Energy and Primary, Secondary, and Tertiary Reserves," *Proceedings of the IEEE,* vol. 93, pp. 1970-1983, Nov 2005.

[4] H. Vu, P. Pruvot, C. Launay, and Y. Harmand, "An improved voltage control on large-scale power system," *Power Systems, IEEE Transactions on,* vol. 11, pp. 1295-1303, Aug 1996.

[5] European Network of Transmission System Operators for Electricity (ENTSO-E), "Continental Europe Operation Handbook," ed, 2009.

[6] European Network of Transmission System Operators for Electricity (ENTSO-E), "Cost benefit analysis methodology CBA 1.0 for TYNDP project assessment," ed.

[7] S. Hagspiel, C. Jägemann, D. Lindenberger, T. Brown, S. Cherevatskiy, and E. Tröster, "Cost-optimal power system extension under flow-based market coupling," *Energy,* vol. 66, pp. 654 - 666, 2014.

[8] S. Lumbreras and A. s. Ramos, "The new challenges to transmission expansion planning. Survey of recent practice and literature review," *Electric Power Systems Research,* vol. 134, pp. 19 - 29, 2016.

[9] A. Wood, *Power generation, operation, and control*. Hoboken, New Jersey: Wiley-Interscience, 2014.

[10] A. C. Z. de Souza, C. B. R. Junior, I. B. Lima Lopes, R. C. Leme, and O. A. S. Carpinteiro, "Non-iterative load-flow method as a tool for voltage stability studies," *Generation, Transmission Distribution, IET,* vol. 1, pp. 499-505, May 2007.

[11] A. Trias, "The Holomorphic Embedding Load Flow method," in *Power and Energy Society General Meeting, 2012 IEEE*, 2012, pp. 1-8.

[12] J. Zhu, *Optimization of Power System Operation (IEEE Press Series on Power Engineering)*: Wiley-IEEE Press, 2015.

[13] V. E. Shamanskii, "A modification of Newton's method," *Ukrainian Mathematical Journal,* vol. 19, pp. 118-122, 1967.

[14] L. Freris and D. Infield, *Renewable Energy in Power Systems*, 1. Auflage ed. New York: Wiley, 2008.

[15] K. Van den Bergh and E. Delarue, "DC power flow in unit commitment models," University of Leuven (KU Leuven)2014.

[16] B. Stott, J. Jardim, and O. Alsac, "DC Power Flow Revisited," *Power Systems, IEEE Transactions on,* vol. 24, pp. 1290-1300, Aug 2009.

[17] Y. Qi, D. Shi, and D. Tylavsky, "Impact of assumptions on DC power flow model accuracy," in *North American Power Symposium (NAPS), 2012*, 2012, pp. 1-6.

[18] C. Coffrin, P. Van Hentenryck, and R. Bent, "Approximating line losses and apparent power in AC power flow linearizations," in *Power and Energy Society General Meeting, 2012 IEEE*, 2012, pp. 1-8.

[19] C. Duthaler, M. Emery, G. Andersson, and M. Kurzidem, "Analysis of the Use of Power Transfer Distribution Factors (PTDF) in the UCTE Transmission Grid," in *Power System Computation Conference*, Glasgow, 2008.

[20] M. Liu and G. Gross, "Role of distribution factors in congestion revenue rights applications," *Power Systems, IEEE Transactions on,* vol. 19, pp. 802-810, May 2004.

[21] X. Cheng and T. J. Overbye, "PTDF-based power system equivalents," *Power Systems, IEEE Transactions on,* vol. 20, pp. 1868-1876, Nov 2005.

[22] V. D. Krsman, A. T. Sarić, and N. V. Kovački, "Including of branch resistances in linear power transmission distribution factors for fast contingency analysis," *European Transactions on Electrical Power,* vol. 22, pp. 961-975, 2012.

[23] D. Waniek, C. Rehtanz, and E. Handschin, "Flow-based evaluation of congestions in the electric power transmission system," in *2010 7th International Conference on the European Energy Market*, 2010, pp. 1-6.

[24] R. Baldick, "Variation of distribution factors with loading," *IEEE Transactions on Power Systems,* vol. 18, pp. 1316-1323, Nov 2003.

[25] M. Liu and G. Gross, "Effectiveness of the distribution factor approximations used in congestion modeling," in *Proceedings of the 14th Power Systems Computation Conference, Seville, 24--28 June 2002*, 2002.

[26] S. Alexey, R. Steffen, M. P. Panos, A. Iliadis, and V. F. Pereira, *Handbook of networks in power systems I*. Berlin New York: Springer, 2012.

[27] M. Kłos, K. Wawrzyniak, M. Jakubek, and G. Oryńczak, "The scheme of a novel methodology for zonal division based on power transfer distribution factors," in *IECON 2014 - 40th Annual Conference of the IEEE Industrial Electronics Society*, 2014, pp. 3598-3604.

[28] T. Güler, G. Gross, and M. Liu, "Generalized Line Outage Distribution Factors," *Power Systems, IEEE Transactions on,* vol. 22, pp. 879-881, May 2007.

[29] J. Guo, Y. Fu, Z. Li, and M. Shahidehpour, "Direct Calculation of Line Outage Distribution Factors," *Power Systems, IEEE Transactions on,* vol. 24, pp. 1633-1634, Aug 2009.

[30] H. Ronellenfitsch, D. Manik, J. Hörsch, T. Brown, and D. Witthaut, "Dual theory of transmission line outages," *ArXiv e-prints,* June 2016.

[31] J. Hossain and A. Mahmud, *Large Scale Renewable Power Generation: Advances in Technologies for Generation, Transmission and Storage*: Springer Science & Business Media, 2014.

[32] M. Robinius, "Strom- und Gasmarktdesign zur Versorgung des deutschen Straßenverkehrs mit Wasserstoff," Dr., RWTH Aachen University, Jülich, 2015.

[33] M. Ventosa, Á. Baíllo, A. Ramos, and M. Rivier, "Electricity market modeling trends," *Energy Policy,* vol. 33, pp. 897 - 913, 2005.

[34] European Energy Exchange, "Rules and Regulation," ed.

[35] Official Journal of the European Union, "Regulation (EU) No 1227/2011 of the European parliament and of the council of 25 October 2011 on wholesale energy market integrity and transparency," ed, 2011.

[36] Federal Ministry for Economic Affairs and Energy, "An electricity market for Germany's energy transition (Green Paper)," ed, 2014.

[37] S. Rebennack, P. M. Pardalos, M. V. F. Pereira, and N. A. Iliadis, *Handbook of power systems*: Springer, 2010.

[38] H. Y. Yamin, "Review on methods of generation scheduling in electric power systems," *Electric Power Systems Research,* vol. 69, pp. 227 - 248, 2004.

[39] F. Ofgem, "Bidding zones literature review," Technical report, July2014.

[40] D. Chatterjee, J. Webb, Q. Gao, M. Y. Vaiman, M. M. Vaiman, and M. Povolotskiy, "N-1-1 AC contingency analysis as a part of NERC compliance studies at midwest ISO," in *Proc. 2010 IEEE PES Transmission and Distribution Conf. Expo*, 2010, pp. 1-7.

[41] A. Nüßler, "Congestion and Redispatch in Germany. A model-based analysis of the development of redispatch," Universität zu Köln, 2012.

[42] A. F. Meyabadi, H. Barati, and M. Ehsan, "Simultaneous congestion management and cost allocation in a short-run market model," *Iranian Journal of Science and Technology,* vol. 31, p. 617, 2007.

[43] R. M. Hermans, P. P. J. V. den Bosch, A. Jokić, P. Giesbertz, P. Boonekamp, and A. Virag, "Congestion management in the deregulated electricity market: An assessment of locational pricing, redispatch and regulation," in *2011 8th International Conference on the European Energy Market (EEM)*, 2011, pp. 8-13.

[44] A. Kumar, S. C. Srivastava, and S. N. Singh, "Congestion management in competitive power market: A bibliographical survey," *Electric Power Systems Research,* vol. 76, pp. 153 - 164, 2005.

[45] M. J. van Blijswijk and L. J. de Vries, "Managing congestion in the Dutch transmission grid," *TU Berlin,* 2011.

[46] B. Burstedde, "From nodal to zonal pricing: A bottom-up approach to the second-best," in *2012 9th International Conference on the European Energy Market*, 2012, pp. 1-8.

[47] J. Bertsch, "Is an inefficient transmission market better than none at all? On zonal and nodal pricing in electricity systems," Energiewirtschaftliches Institut (EWI), Universität Köln, Köln, EWI Working Paper 15/05, 2015.

[48] C. Breuer and A. Moser, "Optimized bidding area delimitations and their impact on electricity markets and congestion management," in *11th International Conference on the European Energy Market (EEM14)*, 2014, pp. 1-5.

[49] C. Duthaler, "Europe nodal: a simulation of the European electricity market based on the full network model," in *Second annual conference on competition and regulation in network industries, Center for European Studies*, 2009.

[50] T. Kristiansen, "Cross-border transmission capacity allocation mechanisms in South East Europe," *Energy Policy,* vol. 35, pp. 4611 - 4622, 2007.

[51] G. EPEX SPOT, Nord Pool, OMIE, OPCOM, OTE, TGE,, "Euphemia public desctription, PCR market coupling algorithm," ed, 2016.

[52] G. EPEX SPOT, HEnEx, Nord Pool, OMIE, OPCOM, OTE, TGE,, "PCR Project Main features," ed, 2018.

[53] R. D. Christie, B. F. Wollenberg, and I. Wangensteen, "Transmission management in the deregulated environment," *Proceedings of the IEEE,* vol. 88, pp. 170-195, Feb 2000.

[54] Belpex, apX Group, and Powernext, "Trilateral market coupling algorithm," ed, 2006.

[55] A. R. Bergen and V. Vittal, *Power Systems Analysis (2nd Edition)*: Prentice Hall, 1999.

[56] M. Schäfer, S. Hempel, J. Hörsch, B. Tranberg, S. Schramm, and M. Greiner, "Power Flow Tracing in Complex Networks," in *New Horizons in Fundamental Physics*, S.

Schramm and S. Mirko, Eds., ed Cham: Springer International Publishing, 2017, pp. 357-373.

[57] K. V. den Bergh, D. Couckuyt, E. Delarue, and W. D'haeseleer, "Redispatching in an interconnected electricity system with high renewables penetration," *Electric Power Systems Research,* vol. 127, pp. 64 - 72, 2015.

[58] H. S. Martin Strohmaier, "Implikationen von NTC, Zonal Pricing, Nodal Pricing, PTDF und ENTSO-E Leitungsausbauverfahren," ed, 2016.

[59] European Network of Transmission System Operators for Electricity (ENTSO-E), "Procedures for cross-border transmission capacity assessments," ed, 2001.

[60] "Berechnung von regelblockuberschreitenden Ubertragungskapatzitaten zu internationalen Partnernetzen," ed: Amprion GmbH.

[61] "Determination of transfer capacity at trade relevant cross-border interconnections of TenneT TSO GmbH," ed: TenneT GmbH, 2012.

[62] A. Amprion, BELPEX, Creos, Elia, Transnet BW, Epex spot, RTE, Tennet, "CWE Enhanced Flow-Based MC intuitiveness report," ed, 2013.

[63] Energy Institute KU Leuven, "Cross-border electricity trading: towards flow-based market coupling," 2015.

[64] M. Aguado, R. Bourgeois, J. Bourmaud, J. Van Casteren, M. Ceratto, M. Jakel*, et al.*, "Flow-based market coupling in the central western european region-on the eve of implementation," *CIGRE, C5-204,* 2012.

[65] European Network of Transmission System Operators for Electricity (ENTSO-E), "ENTSO-E Capacity Allocation and Nomination System (ECAN) Implementation Guide, Version 6," ed, 2018.

[66] K. Van den Bergh, J. Boury, and E. Delarue, "The Flow-Based Market Coupling in Central Western Europe: concepts and definitions," *Electr. J.,* 2016.

[67] A. M. Erik van der Hoofd, "Market Review 2015," TenneT, IAEW RWTH Aachen2016.

[68] S. Frank, I. Steponavice, and S. Rebennack, "Optimal power flow: a bibliographic survey I," *Energy Systems,* vol. 3, pp. 221-258, 2012.

[69] H. W. Dommel and W. F. Tinney, "Optimal Power Flow Solutions," *Power Apparatus and Systems, IEEE Transactions on,* vol. PAS-87, pp. 1866-1876, Oct 1968.

[70] M. M. Bhaskar and S. MuthyalaSrinivas, "Security constraint optimal power flow (SCOPF)--A comprehensive survey," *Global Journal of Technology and Optimization,* vol. 2, 2011.

[71] K. S. Pandya and S. K. Joshi, "A Survey of Optimal Power Flow Methods," *Journal of Theoretical & Applied Information Technology,* vol. 4, pp. 450 - 458, 2008.

[72] S. Frank, I. Steponavice, and S. Rebennack, "Optimal power flow: a bibliographic survey II," *Energy Systems,* vol. 3, pp. 259-289, 2012.

[73] D. H. Wolpert and W. G. Macready, "No free lunch theorems for optimization," *Evolutionary Computation, IEEE Transactions on,* vol. 1, pp. 67-82, Apr 1997.

[74] N. S. Rau, *Optimization principles: practical applications to the operation and markets of the electric power industry* vol. 16: John Wiley & Sons, 2003.

[75] N. S. Rau, "Issues in the path toward an RTO and standard markets," *Power Systems, IEEE Transactions on,* vol. 18, pp. 435-443, May 2003.

[76] E. Lobato, R. Rouco, M. I. Navarrete, R. Casanova, and G. Lopez, "An LP-based optimal power flow for transmission losses and generator reactive margins minimization," in *Power Tech Proceedings, 2001 IEEE Porto*, 2001, pp. 5 pp. vol.3-.

[77] P. T. Boggs and J. W. Tolle, "Sequential Quadratic Programming," *Acta Numerica,* vol. 4, pp. 1-51, 1 1995.

[78] S.-D. Chen and J.-F. Chen, "A direct Newton-Raphson economic emission dispatch," *International Journal of Electrical Power & Energy Systems,* vol. 25, pp. 411 - 417, 2003.

[79] J. Peschon, D. W. Bree, and L. P. Hajdu, "Optimal power-flow solutions for power system planning," *Proceedings of the IEEE,* vol. 60, pp. 64-70, Jan 1972.

[80] S. Granville, J. C. O. Mello, and A. C. G. Melo, "Application of interior point methods to power flow unsolvability," *Power Systems, IEEE Transactions on,* vol. 11, pp. 1096-1103, May 1996.

[81] G. L. Torres and V. H. Quintana, "An interior-point method for nonlinear optimal power flow using voltage rectangular coordinates," *Power Systems, IEEE Transactions on,* vol. 13, pp. 1211-1218, Nov 1998.

[82] Y.-X. Yuan, "Recent Advances in Trust Region Algorithms," *Math. Program.,* vol. 151, pp. 249-281, June 2015.

[83] A. J. Conejo, F. J. Nogales, and F. J. Prieto, "A decomposition procedure based on approximate Newton directions," *Mathematical Programming,* vol. 93, pp. 495-515, 2002.

[84] H. Y. Yamin, K. Al-Tallaq, and S. M. Shahidehpour, "New approach for dynamic optimal power flow using Benders decomposition in a deregulated power market," *Electric Power Systems Research,* vol. 65, pp. 101 - 107, 2003.

[85] A. G. Bakirtzis and P. N. Biskas, "A decentralized solution to the DC-OPF of interconnected power systems," *Power Systems, IEEE Transactions on,* vol. 18, pp. 1007-1013, Aug 2003.

[86] X. Bai, H. Wei, K. Fujisawa, and Y. Wang, "Semidefinite programming for optimal power flow problems," *International Journal of Electrical Power & Energy Systems,* vol. 30, pp. 383 - 392, 2008.

[87] Y. Xia and K. W. Chan, "Dynamic constrained optimal power flow using semi-infinite programming," *IEEE Transactions on Power Systems,* vol. 21, pp. 1455 - 1457, 2006.

[88] V. K. Suganthi and R. Meenakumari, "Hybrid imperialist competitive algorithm x2014; A meta-heuristic approach to solve security constrained optimal power flow," in *Cognitive Computing and Information Processing (CCIP), 2015 International Conference on*, 2015, pp. 1-6.

[89] S. Duman, U. Güvenç, Y. Sönmez, and N. Yörükeren, "Optimal power flow using gravitational search algorithm," *Energy Conversion and Management,* vol. 59, pp. 86 - 95, 2012.

[90] H. R. E. H. Bouchekara, "Optimal power flow using black-hole-based optimization approach," *Applied Soft Computing,* vol. 24, pp. 879 - 888, 2014.

[91] A. Bhattacharya and P. K. Chattopadhyay, "Application of biogeography-based optimisation to solve different optimal power flow problems," *IET Generation, Transmission Distribution,* vol. 5, pp. 70-80, Jan 2011.

[92] U. Leeton and T. Kulworawanichpong, "Multi-Agent Based Optimal Power Flow Solution," in *2012 Asia-Pacific Power and Energy Engineering Conference*, 2012, pp. 1-4.

[93] O. Alsac and B. Stott, "Optimal Load Flow with Steady-State Security," *IEEE Transactions on Power Apparatus and Systems,* vol. PAS-93, pp. 745-751, May 1974.

[94] F. Capitanescu, J. L. M. Ramos, P. Panciatici, D. Kirschen, A. M. Marcolini, L. Platbrood*, et al.*, "State-of-the-art, challenges, and future trends in security constrained optimal power flow," *Electric Power Systems Research,* vol. 81, pp. 1731 - 1741, 2011.

[95] L. Platbrood, F. Capitanescu, C. Merckx, H. Crisciu, and L. Wehenkel, "A Generic Approach for Solving Nonlinear-Discrete Security-Constrained Optimal Power Flow Problems in Large-Scale Systems," *IEEE Transactions on Power Systems,* vol. 29, pp. 1194-1203, May 2014.

[96] S. Mei, Y. Ni, G. Wang, and S. Wu, "A Study of Self-Organized Criticality of Power System Under Cascading Failures Based on AC-OPF With Voltage Stability Margin," *Power Systems, IEEE Transactions on,* vol. 23, pp. 1719-1726, Nov 2008.

[97] M. Madrigal, K. Ponnambalam, and V. H. Quintana, "Probabilistic optimal power flow," ed, 1998, pp. 385-388.

[98] H. Yu and W. D. Rosehart, "An optimal power flow algorithm to achieve robust operation considering load and renewable generation uncertainties," *IEEE Transactions on Power Systems,* vol. 27, pp. 1808-1817, 2012.

[99] S. Shargh, B. K. ghazani, B. Mohammadi-ivatloo, H. Seyedi, and M. Abapour, "Probabilistic multi-objective optimal power flow considering correlated wind power and load uncertainties," *Renewable Energy,* vol. 94, pp. 10 - 21, 2016.

[100] M. Aien, M. Rashidinejad, and M. F. Firuz-Abad, "Probabilistic optimal power flow in correlated hybrid wind-PV power systems: A review and a new approach," *Renewable and Sustainable Energy Reviews,* vol. 41, pp. 1437-1446, 2015.

[101] J. Schwippe, A. Seack, and C. Rehtanz, "Pan-European market and network simulation model," in *PowerTech (POWERTECH), 2013 IEEE Grenoble*, 2013, pp. 1-6.

[102] University of Duisburg-Essen, "Study on the impact of price zones in different configurations in Europe," Commission for energy and gas regulation2016.

[103] F. Sensfuß, M. Ragwitz, M. Genoese, and D. Möst, "Agent-based simulation of electricity markets: a literature review," Fraunhofer Institute for Systems and Innovation Research (ISI), Working Papers "Sustainability and Innovation" S5/2007, 2007.

[104] C. Budischak, D. Sewell, H. Thomson, L. Mach, D. E. Veron, and W. Kempton, "Cost-minimized combinations of wind power, solar power and electrochemical storage, powering the grid up to 99.9% of the time," *Journal of Power Sources,* vol. 225, pp. 60 - 74, 2013.

[105] B. Steffen and C. Weber, "Efficient storage capacity in power systems with thermal and renewable generation," *Energy Economics,* vol. 36, pp. 556 - 567, 2013.

[106] J. F. DeCarolis, K. Hunter, and S. Sreepathi, "The case for repeatable analysis with energy economy optimization models," *Energy Economics,* vol. 34, pp. 1845 - 1853, 2012.

[107] S. Pfenninger, "Energy scientists must show their workings," *Nature,* vol. 542, pp. 393-393, feb 2017.

[108] M. Koch, D. Bauknecht, C. Heinemann, D. Ritter, M. Vogel, and E. Tröster, "Modell based analysis of grid-development within the European grid and options providing flexibility within the German electricity system from 2020 to 2050," *Zeitschrift für Energiewirtschaft,* vol. 39, pp. 1-17, 2015.

[109] G. Blanco, D. Waniek, F. Olsina, F. Garcés, and C. Rehtanz, "Flexible investment decisions in the European interconnected transmission system," *Electric Power Systems Research,* vol. 81, pp. 984 - 994, 2011.

[110] M. Fürsch, S. Hagspiel, C. Jagemann, S. Nagl, D. Lindenberger, and E. Tröster, "The role of grid extensions in a cost-efficient transformation of the European electricity system until 2050," *Applied Energy,* vol. 104, pp. 642 - 652, 2013.

[111] M. Gorner, T. Hahnemann, T. Hess, and H. Weigt, "Electricity transmission modeling economic impact of technical characteristics," in *Electricity Market, 2008. EEM 2008. 5th International Conference on European*, 2008, pp. 1-7.

[112] R. Green, "Nodal pricing of electricity: how much does it cost to get it wrong?," *Journal of Regulatory Economics,* vol. 31, pp. 125-149, 2007.

[113] I. Fuchs, S. Voller, and T. Gjengedal, "Improved method for integrating renewable energy sources into the power system of Northern Europe: Transmission expansion planning for wind power integration," in *Environment and Electrical Engineering (EEEIC), 2011 10th International Conference on*, 2011, pp. 1-4.

[114] D. Couckuyt, D. Orlic, K. Bruninx, A. Zani, A.-C. Leger, E. Momot*, et al.*, "System simulations analysis and overlay-grid development," e-HIGHWAY 20502015.

[115] H. Farahmand, S. Jaehnert, T. Aigner, and D. Huertas-Hernando, "Nordic hydropower flexibility and transmission expansion to support integration of North European wind power," *Wind Energy,* vol. 18, pp. 1075-1103, 2015.

[116] A. Kanevce, I. Mishkovski, and L. Kocarev, "Modeling long-term dynamical evolution of Southeast European power transmission system," *Energy,* vol. 57, pp. 116 - 124, 2013.

[117] F. U. Leuthold, H. Weigt, and C. von Hirschhausen, "A Large-Scale Spatial Optimization Model of the European Electricity Market," *Networks and Spatial Economics,* vol. 12, pp. 75-107, 2012.

[118] N. Hutcheon and J. W. Bialek, "Updated and validated power flow model of the main continental European transmission network," in *PowerTech (POWERTECH), 2013 IEEE Grenoble*, 2013, pp. 1-5.

[119] A. Ø. Lie, E. A. Rye, H. G. Svendsen, H. Farahman, and M. Korpås, "Validation study of an approximate 2014 European power-flow model using PowerGAMA," *IET Generation, Transmission Distribution,* vol. 11, pp. 392-400, 2017.

[120] A. Maffei, D. Meola, G. Marafioti, G. Palmieri, L. Iannelli, G. Mathisen*, et al.*, "Optimal Power Flow model with energy storage, an extension towards large integration of renewable energy sources," *\{IFAC\} Proceedings Volumes,* vol. 47, pp. 9456 - 9461, 2014.

[121] A. Roehder, H. Natemeyer, S. Winter, and A. Schnettler, "Coordinated control of active devices in an overlay grid to facilitate the integration of renewable energy sources in Europe," in *PowerTech (POWERTECH), 2013 IEEE Grenoble*, 2013, pp. 1-6.

[122] G. Celli, S. Mocci, N. Natale, and F. Pilo, "The effect of massive renewable deployment on the Sardinian power system," in *Renewable Power Generation Conference (RPG 2013), 2nd IET*, 2013, pp. 1-4.

[123] H. Lund and P. A. Østergaard, "Electric grid and heat planning scenarios with centralised and distributed sources of conventional, CHP} and wind generation," *Energy,* vol. 25, pp. 299 - 312, 2000.

[124] U. P. Müller, I. Cussmann, C. Wingenbach, and J. Wendiggensen, "AC Power Flow Simulations within an Open Data Model of a High Voltage Grid," in *Advances and*

New Trends in Environmental Informatics: Stability, Continuity, Innovation, V. Wohlgemuth, F. Fuchs-Kittowski, and J. Wittmann, Eds., ed Cham: Springer International Publishing, 2017, pp. 181-193.

[125] P. Eser, A. Singh, N. Chokani, and R. S. Abhari, "High resolution simulations of increased renewable penetration on Central European transmission grid," in *Power Energy Society General Meeting, 2015 IEEE*, 2015, pp. 1-5.

[126] M. K. Kim and D. Hur, "An optimal pricing scheme in electricity markets by parallelizing security constrained optimal power flow based market-clearing model," *International Journal of Electrical Power & Energy Systems,* vol. 48, pp. 161 - 171, 2013.

[127] J. Bertsch, S. Hagspiel, and L. Just, "Congestion management in power systems: Long-term modeling framework and large-scale application," Energiewirtschaftliches Institut (EWI), Universität Köln, Köln, EWI Working Paper 15/03, 2015.

[128] F. Kunz and A. Zerrahn, "The benefit of coordinating congestion management in Germany," in *2013 10th International Conference on the European Energy Market (EEM)*, 2013, pp. 1-8.

[129] R. Barth, J. Apfelbeck, P. Vogel, P. Meibom, and C. Weber, "Load-flow based market coupling with large-scale wind power in Europe," in *8th International Workshop on Large-Scale Integration of Wind Power into Power Systems as well as on Transmission Networks for Offshore Wind Farms*, 2009, pp. 296-303.

[130] G. Oggioni and Y. Smeers, "Market failures of Market Coupling and counter-trading in Europe: An illustrative model based discussion," *Energy Economics,* vol. 35, pp. 74 - 87, 2013.

[131] K. Schaber, F. Steinke, and T. Hamacher, "Transmission grid extensions for the integration of variable renewable energies in Europe: Who benefits where?," *Energy Policy,* vol. 43, pp. 123 - 135, 2012.

[132] M. Haller, S. Ludig, and N. Bauer, "Decarbonization scenarios for the EU and MENA power system: Considering spatial distribution and short term dynamics of renewable generation," *Energy Policy,* vol. 47, pp. 282 - 290, 2012.

[133] S. Pfenninger and J. Keirstead, "Renewables, nuclear, or fossil fuels? Scenarios for Great Britain's power system considering costs, emissions and energy security," *Applied Energy,* vol. 152, pp. 83 - 93, 2015.

[134] F. Van Hulle, J. O. Tande, K. Uhlen, L. Warland, s. Korp\aa, Magnus, P. Meibom*, et al.*, "Integrating wind: Developing Europe's power market for the large-scale integration of wind power," European Wind Energy Association (EWEA)2009.

[135] F. Steinke, P. Wolfrum, and C. Hoffmann, "Grid vs. storage in a 100% renewable Europe," *Renewable Energy,* vol. 50, pp. 826 - 832, 2013.

[136] S. Becker, R. A. Rodriguez, G. B. Andresen, M. O. W. Greiner, and S. Schramm, "What can transmission do for a fully renewable Europe?," *arXiv preprint arXiv:1401.4298,* 2014.

[137] C. Bussar, P. Stöcker, Z. Cai, L. M. Jr., D. Magnor, P. Wiernes*, et al.*, "Large-scale integration of renewable energies and impact on storage demand in a European renewable power system of 2050—Sensitivity study," *Journal of Energy Storage,* vol. 6, pp. 1 - 10, 2016.

[138] Y. Scholz, "Renewable energy based electricity supply at low costs : development of the REMix model and application for Europe," University of Stuttgart, 2012.

[139] L. Kotzur, P. Markewitz, M. Robinius, and D. Stolten, "Time series aggregation for energy system design: Modeling seasonal storage," *Applied Energy,* vol. 213, pp. 123-135, 2018/03/01/ 2018.

[140] European Commission, "State aid: Commission approves six electricity capacity mechanisms to ensure security of supply in Belgium, France, Germany, Greece, Italy and Poland," ed, 2018.

[141] C. Weber, *Uncertainty in the electric power industry: methods and models for decision support* vol. 77: Springer Science & Business Media, 2006.

[142] L. Göransson, "The impact of wind power variability on the least-cost dispatch of units in the electricity generation system " Doctoral, Chalmers, Energy and Environment, Energy Technology Chalmers University of Technology, GOTHENBURG, SWEDEN, 2014.

[143] L. Göransson, J. Goop, T. Unger, M. Odenberger, and F. Johnsson, "Linkages between demand-side management and congestion in the European electricity transmission system," *Energy,* vol. 69, pp. 860-872, 2014/05/01/ 2014.

[144] P. E. Grohnheit, "Modelling CHP within a national power system," *Energy Policy,* vol. 21, pp. 418-429, 1993/04/01/ 1993.

[145] H. G. Svendsen and O. C. Spro, "PowerGAMA: A new simplified modelling approach for analyses of large interconnected power systems, applied to a 2030 Western Mediterranean case study," *Journal of Renewable and Sustainable Energy,* vol. 8, 2016.

[146] W. Lise, V. Linderhof, O. Kuik, C. Kemfert, R. Östling, and T. Heinzow, "A game theoretic model of the Northwestern European electricity market—market power and the environment," *Energy Policy,* vol. 34, pp. 2123-2136, 2006/10/01/ 2006.

[147] Egerer J., "Open Source Electricity Model for Germany (ELMOD-DE), DIW Data Documentation," DIW, Ed., ed, 2016.

[148] Single Electricity Market (SEM) Ireland, "Validation of Market Simulation Software in SEM to end 2012," 2011.

[149] B. Barbara, "The NEULING Model," 2012.

[150] L. Hirth, "The European Electricity Market Model EMMA, Model documentation," ed, 2012.

[151] J. Šumbera and M. Dlouhý, "A Model of German Spot Power Market," *Prague Economic Papers,* 2015.

[152] M. Koch, D. Bauknecht, C. Heinemann, D. Ritter, M. Vogel, and E. Tröster, "Modellgestützte Bewertung von Netzausbau im europäischen Netzverbund und Flexibilitätsoptionen im deutschen Stromsystem im Zeitraum 2020–2050," *Zeitschrift für Energiewirtschaft,* vol. 39, pp. 1-17, 2015/03/01 2015.

[153] C. Pape, N. Gerhardt, P. Härtel, A. Scholz, R. Schwinn, T. Drees*, et al.*, "ROADMAP SPEICHER SPEICHERBEDARF FÜR ERNEUERBARE ENERGIEN–SPEICHERALTERNATIVEN–SPEICHERANREIZ–ÜBERWINDUNG RECHTLICHER HEMMNISSE," *Kassel,* vol. 49, 2014.

[154] G. Bundesnetzagentur für Elektrizität, Telekommunikation, Post und Eisenbahnen,, "Netzentwicklungspläne Strom 2025, Erster Entwrurf der Übertragungsnetzbetreiber," Bonn2015.

[155] M. Beer, "Regionalisiertes Energiemodell zur Analyse der flexiblen Betriebsweise von Kraft-Wärme-Kopplungsanlagen," Technische Universität München, 2012.

[156] C. Kail and G. Haberberger, "Technik und Kosten der Kraft-Wärme-Kopplung bei GUD-und Dampfkraftwerken," *VDI BERICHTE,* vol. 1495, pp. 95-112, 1999.

[157] EURO-CORDEX, C. community, and B. U. o. T. B. C. Chair of Environmental Meteorolog. cordex-reklies.output.EUR-11.CLMcom-BTU.MPI-M-MPI-ESM-LR.rcp26.r1i1p1.CCLM4-8-17.v1.3hr.tas [Online]. Available: https://euro-cordex.net/060378/index.php.en

[158] EURO-CORDEX, "CORDEX domains for model integrations," 2015.

[159] S. Funder, "Rotated grid transform," ed, 2013.

[160] Arbeitsgemeinschaft Energiebilanzen e.V. (AGEB). Auswertungstabellen zur Energiebilanz Deutschland [Online]. Available: https://ag-energiebilanzen.de/10-0-Auswertungstabellen.html

[161] Gurobi Optimization LLC. (2018). *Gurobi Optimizer Reference Manual*. Available: http://www.gurobi.com/

[162] W. E. Hart, C. D. Laird, J.-P. Watson, D. L. Woodruff, G. A. Hackebeil, B. L. Nicholson*, et al.*, *Pyomo - Optimization Modeling in Python*, Second ed. vol. 67: Springer Science & Business Media, 2017.

[163] T. Brown, J. Hörsch, and D. Schlachtberger, "PyPSA: Python for Power System Analysis," *Journal of Open Research Software,* vol. 6(1), 2018.

[164] Lisandro Dalcin, "MPI for Python 3.0.0," ed, 2017.

[165] J. Hörsch and T. Brown, "The role of spatial scale in joint optimisations of generation and transmission for European highly renewable scenarios," in *2017 14th International Conference on the European Energy Market (EEM)*, 2017, pp. 1-7.

[166] T. Anderski, Y. Surmann, S. Stemmer, N. Grisey, E. Momot, A.-C. Leger*, et al.*, "European cluster model of the Pan-European transmission grid," e-HIGHWAY 20502015.

[167] J. Amme, G. Pleßmann, J. Bühler, L. Hülk, E. Kötter, and P. Schwaegerl, "The eGo grid model: An open-source and open-data based synthetic medium-voltage grid model for distribution power supply systems," *Journal of Physics: Conference Series,* vol. 977, p. 012007, 2018.

[168] P. D. Lund, J. Lindgren, J. Mikkola, and J. Salpakari, "Review of energy system flexibility measures to enable high levels of variable renewable electricity," *Renewable and Sustainable Energy Reviews,* vol. 45, pp. 785-807, 2015/05/01/ 2015.

[169] H. C. Gils, "Economic potential for future demand response in Germany – Modeling approach and case study," *Applied Energy,* vol. 162, pp. 401-415, 2016/01/15/ 2016.

[170] M. A. Ortega-Vazquez and D. S. Kirschen, "Estimating the Spinning Reserve Requirements in Systems With Significant Wind Power Generation Penetration," *IEEE Transactions on Power Systems,* vol. 24, pp. 114-124, 2009.

[171] S. M. Krause, S. Börries, and S. Bornholdt, "Econophysics of adaptive power markets: When a market does not dampen fluctuations but amplifies them," *Physical Review E,* vol. 92, p. 012815, 07/22/ 2015.

[172] A. Schroeder, "Modeling storage and demand management in power distribution grids," *Applied Energy,* vol. 88, pp. 4700-4712, 2011/12/01/ 2011.

[173] A. Keane, A. Tuohy, P. Meibom, E. Denny, D. Flynn, A. Mullane*, et al.*, "Demand side resource operation on the Irish power system with high wind power penetration," *Energy Policy,* vol. 39, pp. 2925-2934, 2011/05/01/ 2011.

[174] D. Kleinhans, "Towards a systematic characterization of the potential of demand side management," *arXiv preprint arXiv:1401.4121,* 2014.

[175] A. Kies, U. B. Schyska, and L. von Bremen, "The Demand Side Management Potential to Balance a Highly Renewable European Power System," *Energies,* vol. 9, 2016.

[176] A. Zerrahn and W.-P. Schill, "On the representation of demand-side management in power system models," *Energy,* vol. 84, pp. 840-845, 2015/05/01/ 2015.

[177] W.-P. Schill and A. Zerrahn, "A Dispatch and Investment Evaluation Tool with Endogenous Renewables "DIETER"," ed.

[178] S. Dehmel, "Modeling of the pan-European power generation mix based on open data sources," Institure of Electrochemical Process Engineering (IEK-3), Jülich Research Center, 2017.

[179] L. Hirth, J. Mühlenpfordt, and M. Bulkeley, "The ENTSO-E Transparency Platform – A review of Europe’s most ambitious electricity data platform," *Applied Energy,* vol. 225, pp. 1054-1067, 9/1/ 2018.

[180] T. Grittith and B. Christian, *Algorithms to live by : the computer science of human decisions*. London: William Collins, 2017.

[181] E. Trutnevyte, "Does cost optimization approximate the real-world energy transition?," *Energy,* vol. 106, pp. 182-193, 2016/07/01/ 2016.

[182] P. Eser, A. Singh, N. Chokani, and R. S. Abhari, "Effect of increased renewables generation on operation of thermal power plants," *Applied Energy,* vol. 164, pp. 723-732, 2016/02/15/ 2016.

[183] OpenStreetMap Contributors, "OpenStreetMap," *URL www. openstreetmap. org,* 2012.

[184] Matke C., Medjroubi W., and Kleinhans D. SciGRID - An Open Source Reference Model for the European Transmission Network (v0.2) [Online]. Available: http://www.scigrid.de

[185] Google maps street view [Online]. Available: maps.google.com

[186] T. Brown and J. Hörsch, "Pypsa examples: Script to add load, generators, missing lines and transformers to SciGRID," ed.

[187] L. L. Grigsby, *The electric power engineering handbook. [v. 1], : Electric power generation, transmission, and distribution [E-Book]*, Third edition. ed. Boca Raton, FL: CRC Press, 2012.

[188] Deutsche Energieagentur, "dena-Verteilnetzstudie," *Ausbau-und Innovationsbedarf der Stromverteilnetze in Deutschland bis,* vol. 2030, p. 138, 2012.

[189] J. Hörsch, F. Hofmann, D. Schlachtberger, and T. Brown, "PyPSA-Eur: An Open Optimisation Model of the European Transmission System," *ArXiv e-prints,* vol. 1806.01613, 2018.

[190] M. Scharf and A. Nebel. (2017). *osmTGmod: Open source German transmission grid model based on OpenStreetMap v0.1.3*. Available: https://github.com/wupperinst/osmTGmod

[191] B. Wiegmans. GridKit extract of ENTSO-E interactive map (Jun. 2016) [Online].

[192] European Network of Transmission System Operators for Electricity (ENTSO-E). (2017). *ENTSO-E Interactive Transmission System Map*. Available: https://www.entsoe.eu/map/

[193] Forum Netztechnik/ Netzbetrieb im VDE, "Deutsches Höchstspannungsnetz," ed, 2016.

[194] Federal Network Agency (Bundesnetzagentur). Power plant list [Online]. Available: https://www.bundesnetzagentur.de/EN/Areas/Energy/Companies/SecurityOfSupply/GeneratingCapacity/PowerPlantList/PubliPowerPlantList_node.html

[195] Open Power System Data data platform [Online]. Available: https://open-power-system-data.org/

[196] Umweltbundesamt. Datenbank "Kraftwerke in Deutschland" [Online]. Available: https://www.umweltbundesamt.de/dokument/datenbank-kraftwerke-in-deutschland

[197] Postleitzahlen Deutschland [Online]. Available: https://www.suche-postleitzahl.org/downloads

[198] G. Bundesnetzagentur für Elektrizität, Telekommunikation, Post und Eisenbahnen ,, "Genehmigung des Szenariorahmens für die Netzentwicklungspläne Strom 2017-2030," Bonn2016.

[199] K. Juhrich, "CO_2-Emissionsfaktoren für fossile Brennstoffe," Umweltbundesamt, 2016.

[200] Ragnar Frisch Centre for Economic Research and R. D. a. S. Norway, "Liberalization Model for the European Energy Markets (LIBEMOD)," ed.

[201] European Network of Transmission System Operators for Electricity (ENTSO-E). ENTSO-E transparency platform [Online]. Available: https://transparency.entsoe.eu/

[202] "Gesetz für den Ausbau erneuerbarer Energien (Erneuerbare-Energien-Gesetz - EEG 2017)," ed, 2014.

[203] "Gesetz zur Neuregelung des Kraft-Wärme-Kopplungsgesetzes," ed, 2015.

[204] S. M. Omohundro, *Five balltree construction algorithms*: International Computer Science Institute Berkeley, 1989.

[205] F. Pedregosa, G. Varoquaux, A. Gramfort, V. Michel, B. Thirion, O. Grisel*, et al.*, "Scikit-learn: Machine learning in Python," *Journal of machine learning research,* vol. 12, pp. 2825-2830, 2011.

[206] M. Robinius, F. t. Stein, A. Schwane, and D. Stolten, "A Top-Down Spatially Resolved Electrical Load Model," *Energies,* vol. 10, 2017.

[207] Bundesamt für Kartographie und Geodäsie. Verwaltungsgebiete von Deutschland [Online]. Available: https://www.bkg.bund.de/DE/Produkte-und-Services/Shop-und-Downloads/Digitale-Geodaten/Verwaltungsgebiete-Verwaltungsgrenzen/verwaltungsgebiete_cont.html

[208] EnergyMap.info. EEG-Anlagenregister [Online]. Available: http://www.energymap.info/download.html

[209] F. Hofmann and J. Hörsch. (2016). *powerplantmatching*. Available: https://github.com/FRESNA/powerplantmatching

[210] G. Bundesnetzagentur für Elektrizität, Telekommunikation, Post und Eisenbahnen,, "Monitoring report 2016," 2016.

[211] European network of Transmission System Operators for Electricity (ENTSO-E), "ENTSO-E TYNDP Dataset," ed.

[212] european Network of Transmission System Operators for Electricity (ENTSO-E). (11.04.2018). *ENTSO-E Transmission System Map*. Available: https://www.entsoe.eu/data/map/

[213] European network of Transmission System Operators for Electricity (ENTSO-E), "Interconnected network of ENTSO-E Map," ed.

[214] Q. Zhou and J. W. Bialek, "Approximate model of European interconnected system as a benchmark system to study effects of cross-border trades," *Power Systems, IEEE Transactions on,* vol. 20, pp. 782-788, May 2005.

[215] T. V. Jensen and P. Pinson, "RE-Europe, a large-scale dataset for modeling a highly renewable European electricity system," *Scientific Data,* vol. 4, p. 170175, 11/28/online 2017.

[216] B. Wiegmans. *GridKit*. Available: https://github.com/bdw/GridKit

[217] D. B. Vincent, G. Jean-Loup, L. Renaud, and L. Etienne, "Fast unfolding of communities in large networks," *Journal of Statistical Mechanics: Theory and Experiment,* vol. 2008, p. P10008, 2008.

[218] European network of Transmission System Operators for Electricity (ENTSO-E), "TYNDP 2016 Projects Map," ed.

[219] *List of HVDC projects*. Available: https://en.wikipedia.org/wiki/List_of_HVDC_projects#Europe

[220] TenneT B.V. *Offshore projects in Germany*. Available: https://www.tennet.eu/our-grid/offshore-projects-germany-2/?tx_kesearch_pi1%5Bfilter%5D%5B-2%5D%5B%5D=syscat70&tx_kesearch_pi1%5Bfilter%5D%5B-2%5D%5B%5D=syscat65

[221] 4COffshore limited. *Offshore Transmission Systems*. Available: https://www.4coffshore.com/transmission/

[222] Nordel, "The transmission grid in the Nordic countries," ed, 2005.

[223] S&P Global Platts. Platts World Electric Power Plants Database [Online]. Available: https://www.spglobal.com/platts/en/products-services/electric-power

[224] World Resource Institute. Global Power Plant Database [Online]. Available: http://datasets.wri.org/dataset/globalpowerplantdatabase

[225] *Duke*. Available: https://github.com/larsga/Duke

[226] Global Energy Observatory. [Online]. Available: http://globalenergyobservatory.org/

[227] Carbon Monitoring for Action. [Online]. Available: http://carma.org/plant

[228] E. Meller, G. Milojcic, F. J. Wodopia, and G. Schöning, "Jahrbuch der europäischen Energie- und Rohstoffwirtschaft 2010," ed: VGE Verlag GmbH, 2009, p. 1092.

[229] European Environment Agency. (2017). *Reported data on large combustion plants covered by Directive 2001/80/EC*. Available: https://www.eea.europa.eu/data-and-maps/data/lcp-4

[230] J. Schröter, *Auswirkungen des europäischen Emissionshandelssystems auf den Kraftwerkseinsatz in Deutschland*: diplom. de, 2004.

[231] B. Hintermann, "Pass-through of CO2 emission costs to hourly electricity prices in Germany," *Journal of the Association of Environmental and Resource Economists,* vol. 3, pp. 857-891, 2016.

[232] European Energy Exchange (EEX). (2015). *European Emission Allowances (EUA)*. Available: https://www.eex.com/en/market-data#/market-data

[233] F. Ueckerdt, L. Hirth, G. Luderer, and O. Edenhofer, "System LCOE: What are the costs of variable renewables?," *Energy,* vol. 63, pp. 61-75, 2013/12/15/ 2013.

[234] J. De Decker, P. Kreutzkamp, S. Cowdroy, L. Warland, J. Völker, and J. Tambke, "Offshore electricity grid infrastructure in Europe," *OffshoreGrid Final Report,* 2011.

[235] European Climate Foundation, "Roadmap 2050: a practical guide to a prosperous, low-carbon Europe, Volume I: technical and economic assessment," 2010.

[236] S. Wissel, U. Fahl, M. Blesl, and A. Voß, "Erzeugungskosten zur Bereitstellung elektrischer Energie von Kraftwerksoptionen in 2015," *Institut für Energiewirtschaft und Rationelle Energieanwendung, Stuttgart,* 2010.

[237] International Energy Agency, "World Energy Outlook 2016," 2016.

[238] A. Schröder, F. Kunz, J. Meiss, R. Mendelevitch, and C. Von Hirschhausen, "Current and prospective costs of electricity generation until 2050," Data Documentation, DIW2013.

[239] eurostat. Combined Heat and Power (CHP) data 2005-2015 [Online]. Available: http://ec.europa.eu/eurostat/web/energy/data

[240] Eurostat. Supply, transformation and consumption of electricity - annual data (nrg_105a) [Online]. Available: http://ec.europa.eu/eurostat/web/energy/data/database#

[241] european network of Transmission System Operators for Electricity (ENTSO-E). Indicative values for Net Transfer Capacities (NTC) in Continental Europe [Online]. Available: https://www.entsoe.eu/fileadmin/user_upload/_library/ntc/archive/NTC-Values-Winter-2010-2011.pdf

[242] European Network of Transmission System Operators for Electricity (ENTSO-E), "The ten year network development plan," 2016.

[243] European Network of Transmission System Operators for Electricity (ENTSO-E). Data Portal [Online]. Available: https://www.entsoe.eu/data/data-portal/

[244] S. Rehman, L. M. Al-Hadhrami, and M. M. Alam, "Pumped hydro energy storage system: A technological review," *Renewable and Sustainable Energy Reviews,* vol. 44, pp. 586-598, 2015.

[245] Réseau de Transport d'Électricité (RTE), Syndicat des énergies renouvelables (SER), Enedis, and A. d. D. d. É. e. F. (ADEeF), "Panorama de l'électricité renouvelable en 2017," 2017.

[246] F. Geth, T. Brijs, J. Kathan, J. Driesen, and R. Belmans, "An overview of large-scale stationary electricity storage plants in Europe: Current status and new developments," *Renewable and Sustainable Energy Reviews,* vol. 52, pp. 1212-1227, 2015.

[247] M. Gimeno-Gutiérrez and R. Lacal-Arántegui, *Assessment of the European potential for pumped hydropower energy storage: A GIS-based assessment of pumped hydropower storage potential* vol. 25940. Luxembourg: {Publications Office of the European Union}, 2013.

[248] T. Brown, D. Schlachtberger, A. Kies, S. Schramm, and M. Greiner, "Synergies of sector coupling and transmission extension in a cost-optimised, highly renewable European energy system," *arXiv preprint arXiv:1801.05290,* 2018.

[249] C. Pfister, "Modelling of the pan-European Power Generation from Hydroelectric Power Plants," Institute of Electrochemical Process Engineering (IEK-3), Jüliche Research Center, 2017.

[250] EURO-CORDEX, "About EURO-CORDEX," ed, 2017.

[251] The Global Runoff Data Centre 56068 Koblenz Germany, "River Discharge Data," ed, 2017.

[252] Eurostat, "Energy from Renewable Sources: SHARES 2015 detailed results," ed, 2017.

[253] European Network of Transmission System Operators for Electricity (ENTSO-E), "Yearly Statistics & Adequacy Retrospect 2015: European Electricity System Data - Background Data," ed, 2017.

[254] Bundesamt für Energie (BFE), "Gesamte Erzeugung und Abgabe Elektrischer Energie in der Schweiz 2015," ed, 2016.

[255] Réseau de Transport d'Électricité (RTE). Operational data - Generation in France - Actual generation per production type [Online]. Available: http://clients.rte-france.com/lang/an/visiteurs/vie/prod/realisation_production.jsp

[256] T. Brown, M. Greiner, D. P. Schlachtberger, and S. Schramm, "The Benefits of Cooperation in a Highly Renewable European Electricity Network - Preprint," 2017.

[257] D. Heinemann, T. Vogt, F. Merten, and D. Kleinhans, "RESTORE2050: 2. Fortschrittsbericht des BMBF-Forschungsvorhabens," ed, 2014.

[258] A. L. de Jager and J. V. Vogt, "Development and demonstration of a structured hydrological feature coding system for Europe," *Hydrological Sciences Journal,* vol. 55, pp. 661-675, 2010.

[259] I. G. Aparicio, A. Zucker, F. Careri, F. Monforti-Ferrario, T. Huld, and J. Badger, "EMHIRES dataset: Part I: wind power generation," in *Tech. Rep.*, ed, 2016.

[260] Wikipedia. Lists of offshore wind farms by country [Online]. Available: https://en.wikipedia.org/wiki/Lists_of_offshore_wind_farms_by_country

[261] Eurostat. NUTS (Nomenclature des unités territoriales statistiques) administrative units [Online]. Available: http://ec.europa.eu/eurostat/web/gisco/geodata/reference-data/administrative-units-statistical-units/nuts

[262] I. G. Aparicio, T. Huld, F. Careri, F. Monforti, and A. Zucker, "EMHIRES dataset Part II: Solar power generation," in *Tech. Rep.*, ed, 2017.

[263] S. Pfenninger and I. Staffell, "Long-term patterns of European PV output using 30 years of validated hourly reanalysis and satellite data," *Energy,* vol. 114, pp. 1251-1265, 2016/11/01/ 2016.

[264] A. Singh, P. Eser, N. Chokani, and R. S. Abhari, "Improved modelling of demand and generation in high resolution simulations of interconnected power systems," in *European Energy Market (EEM), 2015 12th International Conference on the*, 2015, pp. 1-5.

[265] R. Elsland, T. Boßmann, A.-L. Klingler, A. Herbst, M. Klobasa, and M. Wietschel, "Netzentwicklungsplan Strom, Entwicklung der regionalen Stromnachfrage und Lastprofile," 2016.

[266] L. Kotzur, "Future Grid Load of the Residential Building Sector," Doctoral, Institute for Electrochemical Process Engineering, RWTH Aachen, 2018.

[267] D. Waniek, U. Hager, C. Rehtanz, and E. Handschin, "Influences of wind energy on the operation of transmission systems," in *2008 IEEE Power and Energy Society General Meeting - Conversion and Delivery of Electrical Energy in the 21st Century*, 2008, pp. 1-8.

[268] F. Leuthold, H. Weigt, and C. Hirschhausen, "ELMOD - A Model of the European Electricity Market," *Electricity Markets Working Paper No. WP-EM-00,* 2008.

[269] A. A. Singh, D. D. Willi, N. N. Chokani, and R. S. Abhari, "Increasing On-Shore Wind Generated Electricity in Germany's Transmission Grid," *ASME. J. Eng. Gas Turbines Power,* vol. 137(2), 2014.

[270] D. Hewes, R. Witzmann, and P. Espinosa, "Influence of energy mix on the future grid integration of PV and wind in Europe," in *2015 Modern Electric Power Systems (MEPS)*, 2015, pp. 1-6.

[271] D. Hewes, S. Altschaeffl, I. Boiarchuk, and R. Witzmann, "Development of a dynamic model of the European transmission system using publicly available data," in *2016 IEEE International Energy Conference (ENERGYCON)*, 2016, pp. 1-6.

[272] Eurostat. Population on 1 January by age group, sex and NUTS3 region (demo_r_pjanaggr3) [Online]. Available: http://ec.europa.eu/eurostat/web/population-demography-migration-projections/population-data/database

[273] Agency for Statistics of Bosnia and Herzegovina, "Preliminary results of the 2013 census of population, households and dwellings in Bosnia and Herzegovina," 2013.

[274] Statistical Office of the Republic of Serbia, "Statistical release SN70, Statistics of population," 2016.

[275] Kosovo Agency for Statistics. Estimated data by municipality 2012-2014 [Online]. Available: http://askdata.rks-gov.net/PXWeb/pxweb/en/askdata/askdata__09%20Population__Population%20Structure/Estimated%20data%20by%20municipality%202012-2014.px/?rxid=95b5a9f7-0931-4f3c-a132-15073e923257

[276] Eurostat. Gross domestic product at market prices (tec00001) [Online]. Available: http://ec.europa.eu/eurostat/web/national-accounts/data/main-tables

[277] Federal Statistical Office of Switzerland. Gross domestic product (GDP) per region and canton [Online]. Available: https://www.bfs.admin.ch/bfs/en/home/statistics/national-economy/national-accounts/gross-domestic-product-canton.assetdetail.1180568.html

[278] Statistical Office of the Republic of Serbia, "Regional gross domestic product, Regions and areas of the Republic of Serbia 2014 (Preliminary results)," 2014.

[279] Kosovo Agency for Statistics. Gross Domestic Product (GDP) according to economic activity and expenditure approach, 2015 [Online]. Available: http://ask.rks-gov.net/en/kosovo-agency-of-statistics/add-news/gross-domestic-product-gdp-according-to-economic-activity-and-expenditure-approach-2015

[280] Agency for Statistics of Bosnia and Herzegovina, "Gross domestic product by production, income and expenditure approach 2015," 2017.

[281] Eurostat. Gross value added at basic prices by NUTS3 regions (nama_10r_3gva) [Online]. Available: http://appsso.eurostat.ec.europa.eu/nui/show.do?dataset=nama_10r_3gva&lang=en

[282] National Aeronautics and Space Administration (NASA). Modern-Era Retrospective analysis for Research and Applications, Version 2 (MERRA-2) [Online]. Available: https://gmao.gsfc.nasa.gov/reanalysis/MERRA-2/data_access/

[283] Réseau de Transport d'Électricité (RTE), *eCO2mix - Regional electricity consumption estimates*.

[284] Terna. Transparency Report - Actual Load [Online]. Available: https://www.terna.it/SistemaElettrico/TransparencyReport/Load/ActualLoad.aspx

[285] Eurostat. Electricity consumption by households (tsdpc310) [Online]. Available: http://ec.europa.eu/eurostat/data/database?node_code=tsdpc310

[286] SciPy. *scipy.optimize.curve_fit*. Available: https://docs.scipy.org/doc/scipy/reference/generated/scipy.optimize.curve_fit.html

[287] National Aeronautics and Space Administration (NASA) - Socioeconomic Data and Applications Center (SEDAC). Population Density, v4 [Online]. Available: http://sedac.ciesin.columbia.edu/data/set/gpw-v4-population-density/data-download

[288] S. Charlotte, B. Wolfgang, S. Shivenes, and L. Sven, "Evaluation of load flow and grid expansion in a unit-commitment and expansion optimization model SciGRID International Conference on Power Grid Modelling," *Journal of Physics: Conference Series,* vol. 977, p. 012008, 2018.

[289] G. Bundesnetzagentur für Elektrizität, Telekommunikation, Post und Eisenbahnen,, "Genehmigung des Szenariorahmens 2019-2030," 2018.

[290] European Commission, "Projects of common interest - Interactive map," ed.

[291] "e-Highway 2050, Modular Development Plan of the Pan-European Transmission System 2050," ed, 2015.

[292] K. Bruninx, D. Orlic, D. Couckuyt, N. Grisey, T. Anderski, Y. Surmann*, et al.*, "e-Highway 2050, D2.1 Data sets of scenarios for 2050," 2015.

[293] European Network of Transmission System Operators for Electricity (ENTSO-E). Monthly Hourly Load Values [Online]. Available: https://www.entsoe.eu/data/power-stats/hourly_load/

[294] European Network of Transmission System Operators for Electricity (ENTSO-E), "Specific national considerations - Data Expert Group," 2016.

[295] S. Schmitt, "Pan-European Modeling of Wind Energy," Master, Institute for Electrochemical Process Engineering (IEK-3), Jülich Research Center, Jülich, 2017.

[296] wind-turbine-models. (2018). *Vestas V136-3.45*. Available: https://en.wind-turbine-models.com/turbines/1282-vestas-v136-3.45

[297] D. Ryberg, M. Robinius, and D. Stolten, "Evaluating Land Eligibility Constraints of Renewable Energy Sources in Europe," *Energies,* vol. 11, p. 1246, 2018.

[298] Gurobi Optimization LLC. (2018). *Gurobi v8.0 parameters*. Available: http://www.gurobi.com/documentation/8.0/refman/parameters.html

[299] N. Gerhardt, D. Böttger, T. Trost, A. Scholz, C. Pape, A. Gerlach*, et al.*, "Analyse eines europäischen 95%-Klimazielszenarios über mehrere Wetterjahre," Tech. rep., Fraunhofer IWES2017.

[300] M. Thema, M. Sterner, T. Lenck, and P. Götz, "Necessity and Impact of Power-to-gas on Energy Transition in Germany," *Energy Procedia,* vol. 99, pp. 392-400, 2016/11/01/ 2016.

[301] J. Nitsch and B. Wenzel, *Langfristszenarien und Strategien für den Ausbau erneuerbarer Energien in Deutschland unter Berücksichtigung der europäischen und globalen Entwicklung: Untersuchung i. A. des Bundesministeriums für Umwelt, Naturschutz und Reaktorsicherheit*: BMU, 2009.

[302] T. Klaus, C. Vollmer, K. Werner, H. Lehmann, and K. Müschen, "Energieziel 2050: 100% strom aus erneuerbaren quellen," *Dessau: Umweltbundesamt,* 2010.

[303] J. Nitsch, T. Pregger, T. Naegler, D. Heide, D. L. de Tena, F. Trieb*, et al.*, "Langfristszenarien und Strategien für den Ausbau der erneuerbaren Energien in Deutschland bei Berücksichtigung der Entwicklung in Europa und global," *Schlussbericht im Auftrag des BMU, bearbeitet von DLR (Stuttgart), Fraunhofer IWES (Kassel) und IfNE (Teltow),* vol. 345, 2012.

[304] M. Schlesinger, P. Hofer, A. Kemmler, A. Kirchner, S. Koziel, A. Ley*, et al.*, "Entwicklung der Energiemärkte–Energiereferenzprognose," *Projekt Nr. 57/12. Studie im Auftrag des Bundesministeriums für Wirtschaft und Technologie. Basel/Köln/Osnabrück: ewi/gws/prognos,* 2014.

[305] N. Gerhardt, F. Sandau, B. Zimmermann, C. Papa, S. Bofinger, and C. Hoffmann, "Geschäftsmodell Energiewende: Eine Antwort auf das "Die-Kosten-der-

Energiewende" -Argument.," *Fraunhofer Institut für Windenergie und Energiesystemtechnik (IWES). Kassel,* 2014.

[306] J. Repenning, L. Emele, R. Blanck, H. Böttcher, G. Dehoust, H. Förster*, et al.*, "Klimaschutzszenario 2050− 2. Endbericht," *Öko-Institut e.V., Fraunhofer ISI,* 2015.

[307] H.-M. Henning and A. Palzer, "Energiesystem Deutschland 2050. Sektor-und Energieträgerübergreifende, modellbasierte, ganzheitliche Untersuchung zur langfristigen Reduktion energiebedingter CO2-Emissionen durch Energieeffizienz und den Einsatz Erneuerbarer Energien," *FhG-ISE, Studie im Rahmen eines BMWi-Projektes, Freiburg,* 2013.

[308] P. Gerbert, P. Herhold, J. Burchardt, S. Schönberger, F. Rechenmacher, A. Kirchner*, et al.*, "Klimapfade für Deutschland," *The Boston Consulting Group und Prognos,* 2018.

[309] S. Lorenczik, M. Gierkink, L. Schmidt, O. Hennes, C. Rehtanz, M. Greve*, et al.*, "Kosteneffiziente Umsetzung der Sektorenkopplung," EWI Energy, EF.RUHR2018.

[310] I. Fraunhofer, "Langfristszenarien für die Transformation des Energiesystems in Deutschland," *Studie im Auftrag des Bundesministeriums für Wirtschaft und Energie,* 2017.

[311] K. Purr, U. Strenge, M. Will, G. Knoche, and A. Volkens, "Treibhausgasneutrales Deutschland im Jahr 2050," *Climate Change, Umweltsbundesamt,* vol. 7, 2014.

[312] T. Bründlinger, J. E. König, O. Frank, D. Gründig, C. Jugel, P. Kraft*, et al.*, "dena-Leitstudie Integrierte Energiewende - Impulse für die Gestaltung des Energiesystems bis 2050," 2018.

[313] M. Robinius, A. Otto, K. Syranidis, D. S. Ryberg, P. Heuser, L. Welder*, et al.*, "Linking the Power and Transport Sectors—Part 2: Modelling a Sector Coupling Scenario for Germany," *Energies,* vol. 10, 2017.

[314] M. Jentsch, T. Trost, and M. Sterner, "Optimal Use of Power-to-Gas Energy Storage Systems in an 85% Renewable Energy Scenario," *Energy Procedia,* vol. 46, pp. 254-261, 2014/01/01/ 2014.

[315] G. Sanchis, "Europe's future secure and sustainable electricity infrastructure. e-Highway 2050 project results.," 2015.

[316] European Environment Agency (EEA). EEA greenhouse gas - data viewer [Online]. Available: https://www.eea.europa.eu/data-and-maps/data/data-viewers/greenhouse-gases-viewer

[317] M. Huber, "Flexibility in Power Systems - Requirements, Modeling, and Evaluation," Doctoral, Fakultät für Elektrotechnik und Informationstechnik, Technische Universität München, Germany, 2017.

[318] E. Tröster, R. Kuwahata, and T. Ackermann, "European grid study 2030/2050," energynautics GmbH, commissioned by Greenpeace International2011.

[319] J. Bertsch, C. Growitsch, S. Lorenczik, and S. Nagl, "Flexibility options in European electricity markets in high RES-E scenarios, Study on behalf of the Iternational Energy Agency (IEA)," Institute of Energy Economics at the University of Cologne2012.

[320] W. Zappa and M. van den Broek, "Analysing the potential of integrating wind and solar power in Europe using spatial optimisation under various scenarios," *Renewable and Sustainable Energy Reviews,* vol. 94, pp. 1192-1216, 2018/10/01/ 2018.

[321] *Environmental geology: Handbook of field methods and case studies*. Berlin, Heidelberg: Springer, 2007.

[322] B. Lehner and G. Grill, "Global river hydrography and network routing: baseline data and new approaches to study the world's large river systems," *Hydrological Processes,* pp. 2171-2186, 2013.

[323] S. Linke, M. J. Kennard, V. Hermoso, J. D. Olden, J. Stein, B. J. Pusey*, et al.*, "Merging connectivity rules and large-scale condition assessment improves conservation adequacy in river systems," *Journal of Applied Ecology,* vol. 49, pp. 1036-1045, 2012.

[324] SciPy, "scipy.interpolate.griddata (Interpolate unstructured D-dimensional data)," ed.

[325] R. E. d. España, "Estadisticas," ed, 2016.

[326] European Network of Transmission System Operators for Electricity (ENTSO-E). Data Portal, Production Data - Detailed monthly production [Online]. Available: https://www.entsoe.eu/data/data-portal/

[327] L. Hirth, "The market value of variable renewables: The effect of solar wind power variability on their relative price," *Energy Economics,* vol. 38, pp. 218-236, 2013/07/01/ 2013.

Band / Volume 495
Measurements of Atmospheric OH and HO_2 Radicals by Laser-Induced Fluorescence on the HALO Aircraft during the OMO-ASIA 2015 Campaign
C. Künstler (2020), 156 pp
ISBN: 978-3-95806-477-5

Band / Volume 496
Tomographic observations of gravity waves with the infrared limb imager GLORIA
I. Krisch (2020), vii, 187 pp
ISBN: 978-3-95806-481-2

Band / Volume 497
Aquisition of temporally and spatially highly resolved data sets of relevant trace substances for model development and model evaluation purposes using a mobile measuring laboratory
D. Klemp, R. Wegener, R. Dubus, U. Javed (2020), 110 pp
ISBN: 978-3-95806-465-2

Band / Volume 498
Charakterisierung des Werkstoffverhaltens während des Kosinterns einer neuartigen, inert gestützten Festoxidbrennstoffzelle
F. Grimm (2020), ix, 168 pp
ISBN: 978-3-95806-482-9

Band / Volume 499
WEGE FÜR DIE ENERGIEWENDE
Kosteneffiziente und klimagerechte Transformationsstrategien für das deutsche Energiesystem bis zum Jahr 2050
M. Robinius et al (2020), VIII, 141 pp
ISBN: 978-3-95806-483-6

Band / Volume 500
Mechanical Behavior of Solid Electrolyte Materials for Lithium-ion Batteries
G. Yan (2020), x, 139 pp
ISBN: 978-3-95806-484-3

Band / Volume 501
Retrieval of atmospheric quantities from remote sensing measurements of nightglow emissions in the MLT region
Q. Chen (2020), 208 pp
ISBN: 978-3-95806-485-0

Band / Volume 502
Auswirkungen der Energiewende auf das deutsche Gastransportsystem
B. Gillessen (2020), XVII, 186
ISBN: 978-3-95806-487-4

Band / Volume 503
Lagrangian Simulation of Stratospheric Water Vapour: Impact of Large-Scale Circulation and Small-Scale Transport Processes
L. Poshyvailo (2020), 126 pp
ISBN: 978-3-95806-488-1

Band / Volume 504
Water Management in Automotive Polymer-Electrolyte-Membrane Fuel Cell Stacks
S. Asanin (2020), XVIII, 172 pp
ISBN: 978-3-95806-491-1

Band / Volume 505
Towards a new real-time irrigation scheduling method: observation, modelling and their integration by data assimilation
D. Li (2020), viii, 94 pp
ISBN: 978-3-95806-492-8

Band / Volume 506
Modellgestützte Analyse kosteneffizienter CO_2-Reduktionsstrategien
P. M. Lopion (2020), XIV, 269 pp
ISBN: 978-3-95806-493-5

Band / Volume 507
Integration of Renewable Energy Sources into the Future European Power System Using a Verified Dispatch Model with High Spatiotemporal Resolution
C. Syranidou (2020), VIII, 242 pp
ISBN: 978-3-95806-494-2

Weitere ***Schriften des Verlags im Forschungszentrum Jülich*** unter
http://wwwzb1.fz-juelich.de/verlagextern1/index.asp

Energie & Umwelt / Energy & Environment
Band / Volume 507
ISBN 978-3-95806-494-2

Mitglied der Helmholtz-Gemeinschaft

JÜLICH
Forschungszentrum